Insights into the molecular interaction between the *Schistosoma mansoni* egg-secreted glycoprotein IPSE/alpha-1 and the host cell

Dissertation

Zur Erlangung des Doktorgrades der Naturwissenschaften

(Dr. rer. nat.)

vorgelegt von

Pia Franziska Marie Naujack

angefertigt am

Institut für Parasitologie und Zoonosen

Justus-Liebig Universität, Gießen

2024

Die Ihnen vorliegende Arbeit wurde am Institut für Parasitologie, des Fachbereichs Veterinärmedizin der Justus-Liebig-Universität Gießen im Rahmen eines LOEWE-Zentrum-geförderten Projekts, DRUID angefertigt.

Dekan:

Prof. Dr. Holger Zorn

Institut für Lebensmittelchemie und Lebensmittelbiotechnologie,

Justus-Liebig Universität Gießen

1. Gutachterin:

Prof. Dr. Katja Sträßer

Institut für Biochemie, Justus-Liebig Universität, Gießen

2. Gutachter

Prof. Dr. Franco Falcone

Institut für Parasitologie, Justus-Liebig Universität, Gießen

Eidesstattliche Versicherung

Hiermit erkläre ich, dass ich die vorgelegte Dissertation selbstständig und ohne unerlaubte, fremde Hilfe und nur mit den Hilfen angefertigt, die ich in der Dissertation angegeben habe. Alle Textstellen, die wörtlich oder sinngemäß aus veröffentlichten Schriften entnommen sind, und alle Angaben, die auf mündlichen Auskünften beruhen, sindals solche kenntlich gemacht. Ich stimme einer evtl. Überprüfung meiner Dissertation durch eine Antiplagiat-Software zu. Bei den von mir durchgeführten und in der Dissertation erwähnten Untersuchungen habe ich die Grundsätze guter wissenschaftlicher Praxis, wie sie in der „Satzung der Justus-Liebig-Universität Gießen zur Sicherung guter wissenschaftlicher Praxis“ niedergelegt sind, eingehalten.

Statement of authorship

I hereby declare that I have completed this dissertation single-handedly without the unauthorized help of a second party and only with the assistance acknowledged therein. I have appropriately acknowledged and cited all text passages that are derived verbatim from or are based on the content of published work of others, and all information relating to verbal communications. I consent to the use of an anti-plagiarism software to check my thesis. I have abided by the principles of good scientific conduct laid down in the charter of the Justus Liebig University Giessen „SatzungderJustus-Liebig-Universität Gießen zur Sicherung guter wissenschaftlicher Praxis“ in carrying out the investigations described in the dissertation.

_____ _____

Ort, Datum Pia F. M.Naujack

Danksagung

An dieser Stelle möchte ich mich von ganzem Herzen bei all den Personen bedanken, die mich während meiner Doktorarbeit tatkräftig unterstützt haben.

Prof. Dr. Falcone danke ich vorallem dafür, dass er mir es ermöglicht hat meine Arbeit innerhalb seiner Arbeitsgruppe anzufertigen und mir immer mit wertvollen Ratschlägen und weiteren Ideen zu Seite stand.

Auch möchte ich mich bei meiner gesamten AG und der AG Grevelding bedanken, vorallem Prema, Bernardo und Georgette, die mir besonders angfangs viel gezeigt und geholfen haben.

Ted, Javaria, Anthony, Yao und Svetlana bin ich sehr dankbar, dass sie mich alle herzlich in Stanford willkommen geheißen haben und allesamt die vollen drei Monate bei jeder Kleinigkeit alles für mich stehen und liegen lassen haben. Dies war eine sehr einprägsame und wertvolle Zeit für mich. Ich konnte viel durch alle lernen und freue mich nach wie vor mit ihnen im Kontakt zu stehen.

Ein besonderer Dank gilt natürlich auch Olli und Max, die sich nie zu schade waren mit mir wissenschaftliche Diskussionen zu führen, Probleme zu lösen oder mich beim Sport mitzuziehen.

Der AG Bartkuhn, insbesondere Tobi und Marek, danke ich vorallem dafür, dass sie mich mit offenen Armen in ihrer Gruppe aufgenommen haben und genug Geduld hatten, mir RNA-seq von Grundauf zu erklären.

Natürlich möchte ich mich auch bei meiner Familie bedanken, die mich während meines gesamtes Lebens, dort wo sie konnten, immer unterstützt haben und auch als Nicht-Naturwissenschaftler alles geben, um meine Welt zu verstehen.

Der allergrößte Dank gebührt Minna, Vanda, David, Lina und Taylor. Ohne euren täglichen Beistand wäre ich wohl nie soweit gekommen.

Abstract

IPSE/alpha-1 (IL-4 inducing principle of *S. mansoni* eggs) is a dimeric glycoprotein secreted by the eggs of the blood-trematode *S. mansoni*, the causative agent of schistosomiasis, an important neglected tropical disease. Natural IPSE has been shown to bind to IgE, resulting in the release of IL-4 and IL-13 from basophils and mast cells. The classical mechanism of IgE-dependent activation consists of cross-linking IgE by allergen binding to the antigen-recognition variable region of the corresponding immunoglobulin. Homodimeric IPSE appears to activate basophils by binding to IgE without any typical cross-linking. The aim of this study is to investigate the molecular details underlying this unique interaction between IPSE/alpha-1 and IgE. Using site-directed mutagenesis, we created six mutants, based on the knowledge that neither IPSE monomers nor the T92Y/R127L mutant, are able to activate basophils. Proteins were expressed in HEK293-6E suspension cells, followed by affinity chromatography for purification. The ability of all IPSE forms to activate basophils by binding IgE was evaluated using humanized RS-ATL8 rat basophilic leukemia (RBL) IgE reporter cells. Cells were sensitized with either IgE-containing serum or different IgE truncates and luciferase expression was measured after stimulation with IPSE. Ancillary ELISAs using similar truncated IgE forms and IPSE were performed to further determine the binding region. Our results show that all the mutations have an impact on IPSE's capability to interact with IgE, thus lowering the activation of the reporter cells. Only the double mutant T92Y/R127L inhibits cell activation completely, leading us to the conclusion that both amino acids must be key residues involved in IgE interaction. Furthermore, we show that IPSE does not bind to all truncated forms of IgE, but also only activates basophils sensitized with IgEλ, suggesting that IgE-IPSE interaction is highly dependent by IgE's light chain.

Besides its name giving property of inducing IL-4, Sm IPSE possesses the ability to enter the host cell where it exhibits unknown functions. To further investigate host cell interactions with the parasite's protein, we conducted endocytosis-assays in different cell lines, as well as bulk RNA-seq analysis after IPSE treatment. Here we show that IPSE-uptake occurs via endocytosis and its cytosolic accumulation is cell type-dependent. Moreover, it appears that Sm IPSE infiltration might enable pathways associated with cell organization. Future experiments, should include cryo-EM of the IgE-IPSE complex to reveal a detailed model of interaction, as well as further RNA-seq and ChIP-seq experiments, validated by protein level work.

Zusammenfassung

IPSE/alpha-1 (IL-4 inducing principle of *Schstisoma mansoni* eggs) ist ein dimeres Glykoprotein, das von den Eiern der Bluttrematode S. mansoni, dem Erreger der Bilharziose, einer wichtigen vernachlässigten Tropenkrankheit, ausgeschieden wird. Es hat sich gezeigt, dass natürliches IPSE an IgE bindet, was zur Freisetzung von IL-4 und IL-13 aus Basophilen und Mastzellen führt. Der klassische Mechanismus der IgE-abhängigen Aktivierung besteht in der *cross-linking* von IgE durch Bindung des Allergens an die variable Antigenerkennungsregion des entsprechenden Immunglobulins. Homodimeres IPSE scheint Basophile durch Bindung an IgE zu aktivieren, ohne dass es zu einer typischen *cross-linking* kommt. Ziel dieser Studie ist es, die molekularen Details dieser einzigartigen Interaktion zwischen IPSE/alpha-1 und IgE zu untersuchen. Auf der Erkenntnis beruhend, dass weder IPSE-Monomere, noch die Mutante T92Y/R127L, in der Lage sind Basophile zu aktivieren, haben wir mit Hilfe der zielgerichteten Mutagenese sechs Mutanten erstellt. Die Proteine wurden in HEK293-6E-Suspensionszellen exprimiert und anschließend durch Affinitätschromatographie aufgereinigt. Die Fähigkeit aller IPSE-Formen, Basophile durch Bindung von IgE zu aktivieren, wurde mit humanisierten RS-ATL8 *rat basophilic leukemia* (RBL) IgE-Reporterzellen untersucht. Die Zellen wurden entweder mit IgE-haltigem Serum oder verschiedenen IgE-Formen sensibilisiert, und die Luziferase-Expression wurde nach Stimulation mit IPSE gemessen. Zur weiteren Bestimmung der Bindungsregion wurden ergänzende ELISAs mit den gleichen (verkürzten) IgE-Formen und IPSE durchgeführt. Unsere Ergebnisse zeigen, dass sich alle Mutationen auf die Fähigkeit von IPSE auswirken, mit IgE zu interagieren, und somit die Aktivierung der Reporterzellen verringern. Nur die Doppelmutante T92Y/R127L hemmt die Zellaktivierung vollständig, was uns zu dem Schluss führt, dass beide Aminosäuren Schlüsselfiguren sein müssen, die an der IgE-Interaktion beteiligt sind. Darüber hinaus zeigen wir, dass IPSE nicht an alle verkürzten Formen von IgE bindet, sondern auch nur mit IgEλ sensibilisierte Basophile aktiviert, was darauf hindeutet, dass die IgE-IPSE-Interaktion in hohem Maße von der leichten Kette des IgE abhängig ist.

Neben seiner namensgebenden Eigenschaft, IL-4 zu induzieren, besitzt Sm IPSE die Fähigkeit, in die Wirtszelle einzudringen, wo es unbekannte Funktionen ausübt. Um die Interaktionen der Wirtszelle mit dem Parasitenprotein weiter zu untersuchen, haben wir Endozytose-Assays in verschiedenen Zelllinien sowie RNA-seq-Analysen nach IPSE-Behandlung durchgeführt. Wir zeigen, dass die Aufnahme von IPSE über Endozytose erfolgt und die zytosolische Akkumulation zelltypabhängig ist. Darüber

hinaus hat es den Anschein, dass die Infiltration von Sm IPSE mit der Zellorganisation verbundene Signalwege aktivieren könnte. Zukünftige Experimente sollten Cryo-EM des IgE-IPSE-Komplexes umfassen, um ein detailliertes Modell der Interaktion aufzuzeigen, sowie weitere RNA-seq- und ChIP-seq-Experimente, die durch Arbeiten auf Proteinebene validiert werden.

Table of content

Eidesstattliche Versicherung II
Danksagung III
Abstract IV
Zusammenfassung V
List of Tables XI
List of Figures XIII
List of abbreviations XVI
1. Introduction 1
1.1 Schistosomiasis 1
1.2 Egg-translocation and the human immune system 4
1.3 Sm IPSE/alpha-1 (IL-4 inducing principle of *Schistosoma mansoni* eggs) 7
1.4 Immunoglobulin E 12
1.5 Sm IPSE/alpha-1 induces basophil degranulation by binding IgE 16
1.6 Sm IPSE as chemokine binding protein 19
1.7 Sm IPSE/alpha-1 acts as "infiltrin" in human host cells 20
1.8 Aim of the study 21
2. Materials & Methods 23
2.1 Establishment of basic experimental conditions 23
2.1.1 Cell culture 23
2.1.2 HEK (human embryonic kidney) 293-6E suspension cells 23
2.1.3 RS-ATL8 RBL (humanized rat basophilic leukemia) cells 23
2.1.4 HCT-116 (human colorectal carcinoma) cells and CHO-Trvb- (Chinese hamster ovary) cells 24
2.1.5 HepG2 (Hepatoblastoma) cells 24
2.1.6 Species identification of cells via PCR 24
2.1.7 Agarose gel electrophoresis 25
2.1.8 Site-directed mutagenesis of Sm IPSE mutants and 6x-His tagged IgEλ 25
2.1.9 Bacterial transformation via Heat Shock 28
2.1.10 Plasmid amplification and purification from cell culture 28
2.1.11 Missense3D prediction – ChimeraX 28
2.1.12 Protein structure prediction in AlphaFold2 – ChimeraX 29
2.1.13 SDS-PAGE and Western Blot 29
2.1.14 Anti-IPSE antibody production 31
2.1.15 Anti-IPSE antibody testing via western blot 31

2.1.16 Test of hybridoma cell line supernatants 32
2.1.17 Small scale transfection of HEK293-6E cells to determine best transfection conditions 32
2.1.18 Trichloroacetic acid (TCA)-precipitation 33
2.1.19 Sm IPSE (and mutants) as well as IgE form recombinant protein expression and purification from HEK293-6E cells 33
2.1.20 Protein purification with Immobilized Metal Affinity Chromatography (IMAC) 34
2.1.21 Stripping and Recharging the Hi Trap Column HP (1 mL, Cytiva) 35
2.1.22 Size exclusion chromatography 35
2.1.23 Bicinchoninic acid (BCA) Assay 36
2.1.24 Thermal Shift Assay 36
2.1.25 6x His-tag insertion into IgE λ via site-directed mutagenesis 36
2.1.26 IgE λ expression and purification 37
2.2 Functional assays for IPSE - IgE interaction 38
2.2.1 Fast Protein Liquid Chromatography (FPLC) for binding stoichiometry 38
2.2.2 Negative Staining to identify binding Sm IPSE domains in IgE via electron microscopy 38
2.2.3 Protein-Protein Interaction measurements with ELISA 38
2.2.3 Biolayer Interferometry (BLI) with Sm IPSE and IgE motavizumab to ascertain the bimolecular interaction kinetics 39
2.2.4 Reporter Cell Assay with RS-ATL8 humanized basophilic rat leukemia cells to test for IgE binding capacity of IPSE (mutants) 40
2.3 Functional assays for IPSE-host cell interaction 43
2.3.1 Immunofluorescence microscopy to determine cellular uptake dynamics of Sm IPSE 43
2.3.2 Confocal microscopy using fluorogenic biarsenical dye FlAsH-EDT2-conjugated Sm IPSE for localization in the host cell 43
2.3.3 Flow cytometry-based internalization assay to measure the cellular uptake of fluoro-labelled Sm IPSE 44
2.3.4 Bulk RNA sequencing of Sm IPSE treated HepG2 cells 46
2.3.5 Electrophoretic Mobility Shift Assay (EMSA) to determine DNA binding capacity of IPSE 48
2.3.6 Fluorescence microscopy assays of Sm IPSE binding to importin-alpha 50
3. Results 52
3.1 Establishment of basic experimental conditions 52
3.1.1 Optimal transfection conditions of HEK293-6Esuspension cells with (TC-)Sm IPSE pTT5 for Sm-IPSE expression 52
3.1.2 Generation of a specific antibody against Sm IPSE and Sh IPSE 53

3.1.2 Generation of Sm IPSE mutants using site-directed mutagenesis ...55

3.1.3 Recombinant expression of Sm IPSE mutants in the HEK293-6E expression system ...58

3.1.4 Thermal Shift Assay with (mutated) Sm IPSE is inhibited by mammalian glycosylation ...59

3.1.5 Prediction of the impact of the different mutations inserted in Sm IPSE using Missense 3D reveals conformational conservedness for the Sm IPSE mutants and impaired dimer formation in C132A Sm IPSE...60

3.1.6 Immunoglobulin E (IgE) variants and human FCERIα$_{Val26\text{-}Gln205}$ can be expressed in the HEK293-6Eexpression system...61

3.1.7 Expression of IgE λ is limited to small scale expression and lack of release into the supernatant ...63

3.2 IPSE - IgE interaction ...67

3.2.1 IgE mota is able to form a stable complex with huFcεRIα, but not with Sm IPSE in FPLC ...67

3.2.2 Sm IPSE forms oligomers at designated protein concentrations and does not form a stable complex with IgE-motavizumab (IgE-mota)...70

3.2.3 Determination of the IPSE-IgE binding affinity using ELISA ...75

3.2.4 No detectable interaction of Sm IPSE with IgE-motavizumab with Biolayer Interferometry ...77

3.2.5 Basophil degranulation reporter assay of Sm IPSE, Sh06 IPSE und Sh03 IPSE reveals strong stimulation capacity of all orthologues ...78

3.2.6 Basophil degranulation reporter cell assay with Sm IPSE mutants reveals differential loss of basophil stimulation capacity ...81

3.2.7 Sm IPSE requires IgE λ sensitization to activate basophiles ...88

3.3 IPSE - host cell interaction ...93

3.3.1 Recombinantly expressed Sm IPSE differentially enters host cells, but not the nucleus...93

3.3.2 Flash-TC IPSE ...95

3.3.3 Different cell types temperature-dependently take up DyLight488 labelled Sm IPSE at different extents ...97

3.3.4 Analysis of transcriptome of HepG2 cells with RNA-seq...108

3.3.5 Sm IPSE WT has the fundamental ability to bind to DNA ...116

3.3.6 Sm IPSE does not lead to an obvious change of subcellular distribution of importinα ...118

3.3.7 Species Identification via PCR reveals that pDsRed-Importinα cells originate from rat – not from human ...121

4. Discussion ...122

4.1 Establishment of basic experimental conditions...122

4.1.1 Expression of Sm IPSE and mutants in HEK293-6Ecells is successful ...122

4.1.2 HEK cell expression of IgE forms was successful, except for IgEλ123

4.1.3 Thermal Shift Assay and Missense 3D 124
4.2 IPSE - IgE interaction 125
4.2.1 IgE Reporter Cell Assay (Rs-ATL8) with IPSE mutants 125
4.2.2 ELISA 127
4.3 IPSE - host cell interaction 130
4.3.1 Analysis of the transcriptome (Bulk RNAseq) 130
4.3.2 Uptake and nuclear localization of Sm IPSE in different host cells 135
4.3.3 IPSE only selectively binds to DNA 142
4.4 Final Conclusion 143
5. References 145
6. APPENDIX 171

List of Tables

1) List of aimed mutations and the original amino acids, including their triplet
2) Primer pairs used to either change desired amino acids in Sm IPSE pTT5, insert a His-tag into pVITRO-102.1F10-IgE/λ or for sequencing.
3) List of oligonucleotides used for hybridisation
4) Evaluation of Reporter Cell Assay including different IPSE orthologues. Statistical analysis with ordinary one-way ANOVA
5) Unpaired T-test of Sm IPSE tested against Sh03 and Sh06 IPSE tested in a reporter cell system
6) IPSE Wild type and IPSE mutants evaluated after conduction of the reporter cell assay.
7) Unpaired T-test of basophil activation evaluated in the reporter cell system after stimulation with IPSE mutants
8) Reporter Assay evaluation after IPSE-stimulation of IgE-motavizumab (κ)-sensitized RS-ATL8 cells.
9) Reporter Assay evaluation after IPSE-stimulation of IgEλ (Bio-Rad)-sensitized RS-ATL8 cells.
10) Reporter Assay evaluation after IPSE-stimulation of IgE Cε2-4 -sensitized RS-ATL8 cells
11) Reporter Assay evaluation after IPSE-stimulation of IgE Cε3-4 -sensitized RS-ATL8 cells.
12) Ratios of quenched and unquenched geometric means (fluorescent signal BB515-A measured at 420V) of tested cell lines for IPSE-internalization
13) T-Test analyses of HCT-116 cells treated with either Sm IPSE DyLight488 or human transferrin-FITC at 37°C in comparison with untreated cells and with respect to unquenched (PBS) and quenched (TB) signals
14) T-Test analyses of HCT-116 cells treated with either Sm IPSE DyLight488 or human transferrin-FITC at 4°C in comparison with untreated cells and with respect to unquenched (PBS) and quenched (TB) signals
15) T-Test analyses of CHO-Trvb cells treated with either Sm IPSE DyLight488 or human transferrin-FITC at 37°C in comparison with untreated cells and with respect to unquenched (PBS) and quenched (TB) signals
16) T-Test analyses of HepG2 cells treated with either Sm IPSE DyLight488 or human transferrin-FITC at 37°C in comparison with untreated cells and with respect to unquenched (PBS) and quenched (TB) signals

17) Sequencing and alignment statistics of analyses of the transcriptome of cell treated with IPSE
18) List of statistically significantly deregulated genes

List of Figures

1) Worldwide distribution of *Schistosoma spp*.
2) *Schistosoma mansoni* life cycle
3) Immunohistological detection of Sm IPSE/alpha-1 performed in mice liver tissue
4) Display of the 3D-structure of a Sm IPSE monomer
5) Sequence of Sm IPSE extracted from Schramm et al., (2003)
6) Structure of monomeric IPSE lacking NLS (NMR and crystal structure)
7) Sequences of IPSE orthologues
8) General structure of IgE
9) Structure of CDR (complementary determining regions) of an antibody
10) Schematic mechanism of IgE cross-linking
11) Proposed model of interaction between Sm IPSE and IgE (Schramm et al., 2015)
12) Immunolocalization of Sm IPSE in liver and intestine sections of a mouse infected with *S. mansoni*
13) Strucute of different IgE forms
14) Schematic diagram showing the main principle underlying the RBL reporter systems (Falcone et al., 2015)
15) Expression of recombinant proteins after transfection with different DNA:PEI ratios
16) Testing of different mouse sera potentially containing monoclonal anti-IPSE antibody
17) Western blots of Sh03 IPSE and Sm IPSE to detect Anti-IPSE-antibodies within the respective hybridoma cell line supernatant
18) Relevant sections of chromatograms of sequences of Sm IPSE pTT5 after the insertion of the respective mutation via site-directed mutagenesis
19) Expression and purification of different IPSE forms
20) Expression and purification of Sm IPSE NLS-AAA
21) Chromatogram of Thermal Shift Assay conducted with either HEK293-6Eexpressed Sm IPSE (+ mutants) or E. coli expressed Sm IPSE
22) Structural analysis for IPSE Wild type and the following mutants: T92Y, C132A, R127L, R128A and R129A
23) Expression of different IgE variants
24) Attempts to insert a 8x-His-tag into pVITRO1-102.1F10-IgE/λ and sequence alignment

25) Full plasmid sequencing of the “new” batch of pVITRO1-102-1F10-IgE/λ
26) Sequence alignments, PCR-products and small scale protein expression of IgEλ
27) Size exclusion chromatography of recombinantly expressed IgE-motavizumab
28) Size exclusion chromatography of recombinantly expressed Sm IPSE
29) Chromatogram of the recombinantly expressed high affinity receptor huFcεRIα
30) Overlay of FPLC curves of IgE-motativzumab uncomplexed and the IgE-motavizumab-FcεRIα complex (molar ratio 1:1)
31) Chromatogram (SEC) of IgE-mota incubated with Sm IPSE in a 1:2 molar ratio
32) SDS-PAGE and Western Blot of FPLC fractions (IgE: IPSE 1:2)
33) Negative Staining of IPSE in different concentrations and buffers
34) Negative staining of IPSE pre-incubated with IgE-mota or IgE-mota/huFCεRIα
35) Determination of the binding affininty of IPSE to IgE-mota (huFCεRIα) and IgEλ in ELISA
36) ELISA with different IPSE variants and mutants using IgE-mota as binding partner
37) ELISA of recombinantly expressed IPSE immobilized on plates and incubated with different concentrations of the two truncated IgE forms
38) Diagram of BLI using Streptavidin-Tips pre-incubated in multi-biotinylated IgE-mota
39) Diagram of BLI conducted with Ni-NTA Tips treated with recombinantly expressed His-tagged Sm IPSE and IgE-mota
40) Evaluation of reporter assay using sensitized (human sera) RS-ATL8 cells that have been stimulated with IPSE and its orthologues
41) Evaluation of reporter assay conductes with Sm IPSE and its mutants with (human serum) sensitized RS-ATL8 cells
42) Prediction model of IPSE (T92) and its mutant form T92Y
43) Prediction model of IPSE (R127) and the two mutations: R127L and R127A
44) Reporter assay with RS-ATL8 cells sensitized with different IgE forms over night and stimulated with IPSE
45) Non-specific binding of anti-His antibody visualized by confocal microscopy in CHO-Trvb cells
46) Subcellular localization of recombinantly expressed Sm IPSE in different cell lines
47) Confocal Images of HCT-116 cells preincubated 3h with 1.5 µg/mL Sm C-TC IPSE and subsequently treated with FlAsH-EDT_2

48) Examples for gating strategy adapted to every cell line and experiment in FACS experiment
49) Analyses of HCT-116 pre-incubated with either Sm IPSE DyLight488 or human Transferrin-FITC at 37°C with FACS
50) Analyses of HCT-116 cells pre-incubated with either Sm IPSE DyLight488 or human Transferrin-FITC at 4°C with FACS measuring BB515-A
51) Analyses of CHO-Trvb cells pre-incubated with either Sm IPSE DyLight488 or human Transferrin-FITC at 37°C with FACS measuring BB515-A
52) Analyses of HepG2 cells pre-incubated with either Sm IPSE DyLight488 or human Transferrin-FITC at 37°C with FACS measuring BB515-A
53) Isolated RNA of HepG2 samples either treated with Sm IPSE for 4h or with no added stimulus
54) Effects of Sm IPSE on transcription of top 100 differentially expressed genes, displayed in a heat map showing levels of expression of these genes
55) Dendrogram of the top 40 deregulated pathways after 4h Sm IPSE treatment of HepG2 cells according to Gene Ontology.
56) Top 40 deregulated GO biological processes identified with GSEA
57) Top 40 deregulated Reactome pathways identified with GSEA
58) GSEA plot enrichment plot representing the GO biological process term cell-substrate junction organization
59) Hybridization of oligonucleotides and Native PAGEs after EMSA conducted with IPSE forms
60) Subcellular localization of DsRed-importinα expressed in RS-ATL8 cells after exogenous incubation of cells with IPSE
61) 51 Localization of DsRed-importinα in the cytoplasm with and without exogenous treatment of the Rs-ATL8 cells with recombinant IPSE, including a nuclear stain
62) Results of species identification by PCR
63) Immunolocalization of IPSE in mouse liver infected with *S. mansoni*

List of abbreviations

aa	Amino acid
AIDS	Acquired immunodeficiency syndrome
ANOVA	Analysis of variance (statistical method)
AS	Acute Schistosomiasis
BCA	Bicinchoninic acid
BLI	Biolayer Interferometry
bp	base pairs
cDNA	complementary DNA
CDR	Complementary determining regions
CDR-H3	Complementary determining regions Heavy chain
CDR-L3	Complementary determining regions Light chain
ChIP-seq	Chromatin ImmunoPrecipitation DNA-Sequencing
CHO-Trvb	Chinese Hamster Ovary cells lacking Transferrin recpotor (b)
CLR	C-type lectin receptor
Cryo-EM	Cryo-electron microscopy
CS	Chronic Schistosomiasis
Cε1-4	Constant domains of heavy chain
DNA	Deoxyriboncleic acid
DC	Dendritic cell
DC-SIGN	Dendritic Cell-Specific Intercellular adhesion molecule-3-Grabbing Non-integrin
DEG	Differentially expressed genes
E. coli	*Eschericha coli*
EDTA	Ethylen diamin tetra acetate
ELISA	Enzyme linked immunosorbent assay
EMSA	Electrophoretic mobility shift assay
Fab	Fragment antigen-binding region
FACS	Fluorescence activated cell sorting
FBS	Fetal bovine serum
Fc	Fragment crystallizable region
FCεRI	High affinity IgE receptor
FlAsH	fluorogenic biarsenical dye fluorescein arsenical hairpin binder–ethanedithiol
FPLC	Fast protein liquid chromatography
G418	Geneticin (antiobiotic)
GFP	Green fluorescent prtein
GO	Gene Onthology
GSEA	Gene set enrichment analysis
HCT-116	Human colorectal carcinoma cell line
HEK293-6E	Human embryonal kidney cell line
HepG2	Hepatocellular carcinoma cell line
His-tag	Histidin-tag
HIV	Human Immunodeficiency virus
HRP	Horse reddish peroxidase
huFCεRIα	human hihg-affinity receptor for IgE (alpha chain)

HygrB	Hygromycin B
IFN	Interfon gamma
Ig	Immunoglobulin
IL-	Interleukin
IMAC	Immobilized-metal affininty chromatography
IPSE	Interleukin-4-inducing principle of Schistosoma mansoni eggs
KEGG	Kyoto Encyclopedia of Genes and Genomes
LB	Lysogeny Broth
M2	Macrophages of M2 phenotype
MR	Mannose receptor
mRNA	messenger RNA
n.c.	Negative control
NFAT	Nuclear factor of activated T-cells
NTD	Neclected tropical disease
ORA	Over representation analysis
PAGE	Polyacrylamide gel electrophoresis
PBE	Phosphate buffered saline with 0.1 % BSA, 2.5 M EDTA
PBS	Phosphate buffered saline
PCR	Polymerase chain reaction
PEI	Polyethylenimin
PNGase	Peptide-N-Glycosidase
RBL	Rat basophilic leucemia cells
RNA	Ribonucleic acid
RNA-seq	RNA sequencing
rpm	Revolutions per minute
RS-ATL8	Humanised rat basophilic leukaemia cell line
RT	Room temperature
S.	*Schistosoma*
SDS	Sodium dodecyl sulfate
Sh IPSE	*Schistosoma haematobium* IPSE
Sm IPSE	*Schistosoma mansoni* IPSE
SmCKBP	*Schistosoma mansoni* Chemokine binding protein
SmEA	*Schistosoma mansoni* egg antigens
TBS (-T)	Tris-buffered saline (0.01% vol/vol Tween 20)
TCA	Trichloroacetic acid
TC-IPSE	Tetracysteine tagged IPSE
Th1	T-helper 1 immune response
Th2	T-helper 2 immune response
Tm	Melting temperature
xg	relative centrifugal force

1. Introduction

1.1 Schistosomiasis

Schistosomiasis is a tropical disease, caused by parasitic trematodes of the species *Schistosoma*. They include seven human-pathogenic species, the two best-characterized representatives are *Schistosoma haematobium (S. haematobium)* (urogenital Schistosomiasis) and *S. mansoni* (intestinal Schistosomiasis). With 240 million people affected worldwide, Schistosomiasis is one of the most important neglected tropical diseases (NTD) (World Health Organization, Schistosomiasis Facts, 2024). Its geographical spread range includes the tropical and subtropical areas of East Asia, Africa, South America but it has also more recently been described in France, Spain and Portugal (Gabrielli & Garba Djirmay, 2023; World Health Organization, Schistosomiasis Facts, 2024). Above all, Schistosomiasis is mostly associated with poverty leading to the lack of sanitation (World Health Organization, Schistosomiasis Facts, 2024). The disease was first described in the 19th century by Theodore Bilharz and is therefore known as Bilharzia. Without treatment, Schistosomiasis may lead to severe pathology, such as hepatic fibrosis, hepatosplenomegaly, portal hypertension and in the worst case to fatality. As chronic disease, Schistosomiasis can also result in urogenital or intestinal/bowel cancer (Lucius et al., 2018; Santos et al., 2021; von Bülow et al., 2021). Chronical Schistosomiasis (CS) is caused by neither the adult worm, nor the infective stage (cercariae), but by unreleased eggs (Colley et al., 2014; Gobbi et al., 2020; Goebel, 1905). Acute Schistosomiasis (AS) is believed to be triggered by the migrating and maturing larval stage (Gobbi et al., 2020; Jauréguiberry et al., 2010; Ross et al., 2007). No protective vaccination is available against the parasite and the currently used Schistosomiasis drug (praziquantel) is not uniformly effective (Andrews, 1985). Consequently, further research effort in *Schistosoma* biology is necessary to reveal future targets for the development of preventive measures such as a suitable vaccination and reduction of disease burden in affected individuals.

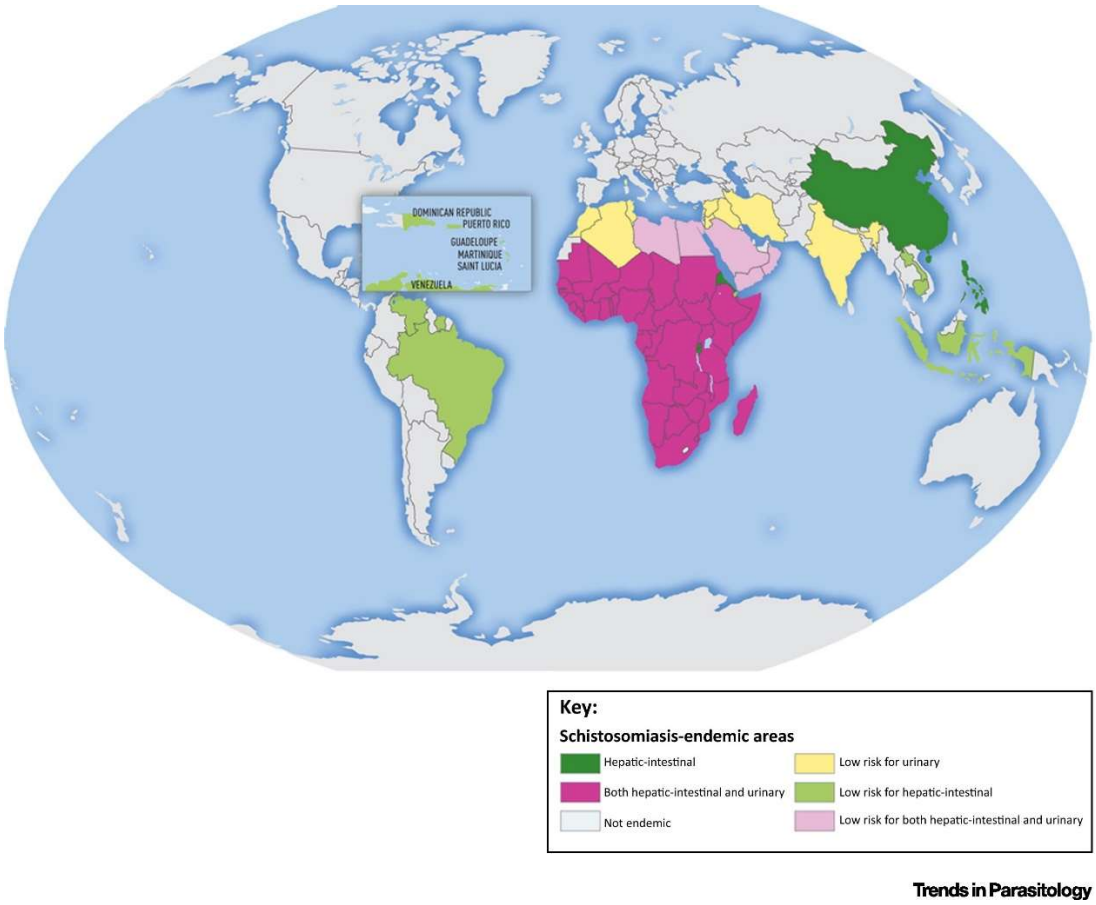

Figure 1 Worldwide distribution of *Schistosoma spp*. (Sm-p80-Based Schistosomiasis Vaccine: Preparation for Human Clinical Trials: Trends in Parasitology (cell.com)).

The typical life cycle of *Schistosoma spp.* (Figure 2) starts with the release of the parasite's eggs by the human host via urine (*S. haematobium*) or faeces (*S. mansoni* and other schistsome species) into fresh water. Here, triggered by temperature, the muscular activity of the larva and a change in osmotic pressure, as well as the influx of fresh water into the egg, and the influence of light exposure ,eggs hatch immediately, liberating the miracidium (larvae), which subsequently infect their intermediate host – aquatic snails of the family of *Biomphalaria*, in which they reproduce asexually (Candido et al., 2017; Mason & Fripp, 1977; Xu & Dresden, 1990). After several weeks, cercariae will egress from their intermediate host, exiting into fresh water where they localize their final mammalian host in maximum 6 h (in case of *S. mansoni* and *S. haematobium* - the human). While penetrating the human skin, cercariae cleave off their tail, which was previously needed for swimming. Here, they penetrate to the epidermal basal membrane, breaking through the Corium and finally end up in the blood- and lymphatic system. This process usually takes around 2-3 days.

Locally, the cercariae transform to the migrating and maturing larval stage known as Schistosomula. Subsequently, these schistosomula first migrate within 3-4 days towards the lungs and the left heart, where they reach the arterial circulation and can thus head for the site of its sexual reproduction – the hepatic portal vein. 2-12 weeks post-infection the host might develop symptoms of acute schistosomiasis such as “Katayama Fever”, which includes fatigue, dry cough and fever and is triggered by a systemic reaction against the schistosomula migrating through the host (Gobbi et al., 2020; Jauréguiberry et al., 2010; Lucius et al., 2018; Ross et al., 2007). In the hepatic portal veins, male worms are already completely sexually matured, whereas the later arriving female worms reach their sexual matureness only if engulfed in the males’ abdominal cavity known as gynaecophoric canal (Grevelding, 2004; Loverde et al., 2011; Popiel & Basch, 1984). Within a permanent copula, the paired *Schistosoma* adults migrate to their final destination in the mesenterial vessels. In the case of *S. mansoni*, the adult couple inhabit the intestinal vessels where they reach a life-span between 5 and 10 years. After one month, the fertile female starts to deposit up to 300 eggs per day in the veins, which migrate through several tissues into the intestine (Moore & Sandground, 1956). In order to close the parasite‘s life cycle, these eggs need to migrate from the vessels into the intestinal lumen, to be finally released with the faeces. During chronic *Schistosoma* infection, at least half of the laid eggs fail to be excreted, resulting with them being swept back to other organs by circulation (Moore & Sandground, 1956). Notably, most eggs accumulate in the liver where they are trapped and are the main cause of the immunopathology. Here, granulomatous inflammation around the eggs eventually resulting in fibrosis is the main cause for severe pathology associated to Schistosomiasis. The immunopathology may eventually cause obstructive portal lesions and portal hypertension and subsequent hepatic encephalopathy, liver failure and gastrointestinal bleeding (Colley et al., 2014; Lucius et al., 2018).

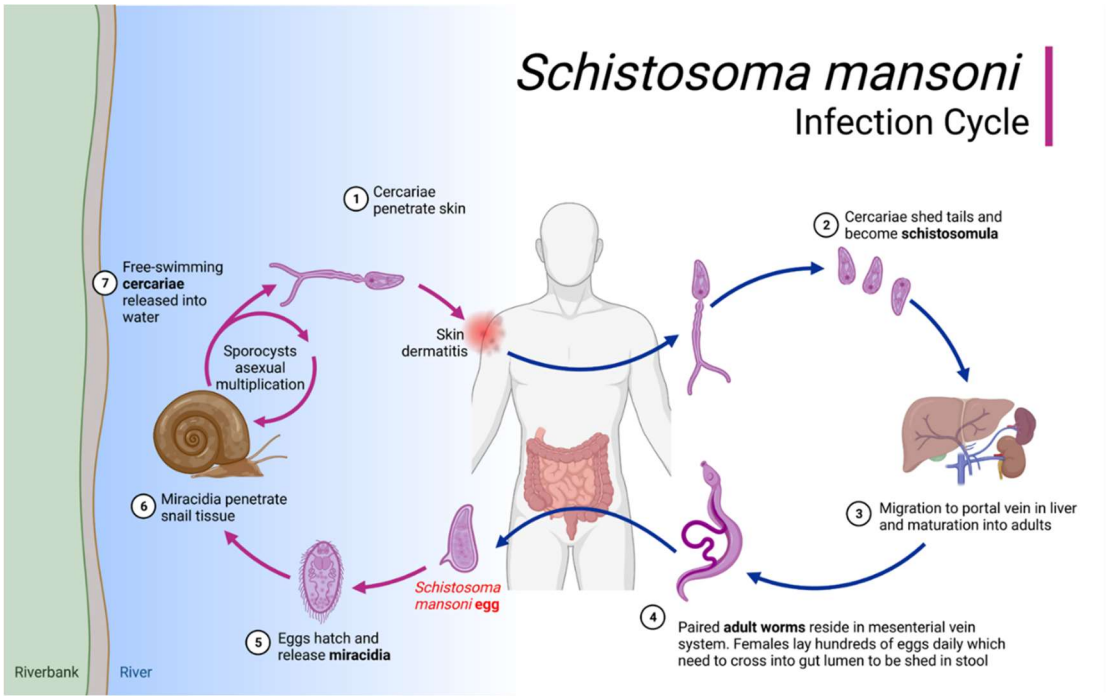

Figure 2 *Schistosoma mansoni* life cycle (created by F. H. Falcone with Biorender)

1.2 Egg-translocation and the human immune system

In general, the translocation from the mesenterial vessels through different tissues into the intestinal can be divided into four different steps. First, the eggs are deposited by the female worm into the mesenterial vessel in close proximity to the endothelium, but without active penetration (deWalick et al., 2012; Schwartz & Fallon, 2018). The process of egg attachment to the endothelium itself, is facilitated by different egg secretions. Due to the fact that the bloodstream flows in the opposite direction than the intestine, a rapid attachment of the eggs to the endothelium is crucial. Next, triggering the host inflammatory response for the formation of granulomas consisting of immune cells. This is followed by egg transition between the endothelium and the epithelium and finally the release of the eggs into the intestinal lumen (Schwartz & Fallon, 2018). This intended journey of a *S. mansoni* egg, including the extravasation of the vessel wall and penetration of the gut wall, usually takes at least six days up to several weeks (deWalick et al., 2012; Jourdane and Théron, 1987).

A newly produced egg of *Schistosoma mansoni*, only consisting of cross-linked eggshell proteins surrounding the ovum and vitelline cells, takes around one week to be fully mature. After oviposition, a fully formed egg is still undeveloped and matures within the host tissue (Jurberg et al., 2009). Freshly laid eggs are lacking the complex subshell structures between the eggshell (von Lichtenberg´s envelope) and the

embryo (Ashton et al., 2001; Neill et al., 1988). These structures early start appearing and differentiating during the progressing development of the egg (Ashton et al., 2001; Neill et al., 1988). In the early stage of the egg development, a few cells detach from the embryo and form the “von Lichtenberg’s envelope”, a thin syncytial layer which is situated between the eggshell and the miracidium (Ashton et al., 2001; Neill et al., 1988). As the egg is fully maturated, a new layer of extracellular material develops between the von Lichtenberg’s envelope (inner envelope) and the eggshell that is mainly composed of granulated material, known as “Reynolds’ layer”. (Ashton et al., 2001; Jurberg et al., 2009; Neill et al., 1988). During the last developmental step, the eggs produce and secrete different egg antigens, such as IPSE/alpha-1, omega-1 and kappa-5, which were shown to be exclusively accumulated in the subshell area, presumably the von Lichtenberg’s and Reynold’s layer (Ashton et al., 2001; Dunne et al., 1991; Jurberg et al., 2009; Schramm et al., 2006, 2009). These secretions were shown to be only secreted by the mature, not the immature egg (Ashton et al., 2001). *Schistosoma mansoni* eggs possess a relatively short life-time, with remaining viable for mere 2-3 weeks after oviposition (Ashton et al., 2001; Costain et al., 2018).

For a successful migration, the survival of the egg and the protection of the host tissues to prevent overbearing pathology, an adaptation and modulation of the immune system is indispensable. Indeed, the presence of the eggs modulates both pro- and anti-inflammatory responses, especially in respective to the adaptive immunity that includes the differentiation of an unspecific T-helper-0-cell after the antigen-presentation by cells of the innate immune system, to either the T-helper-1 (Th1) or T-helper-2 (Th2) (Pezzutto et al., 2007). Here, a switch from the highly pro-inflammatory Th1 response to a less inflammatory Th2 response takes place. A Th1 phenotype with elevated interferon (IFN) γ and Interleukin-12 release initially impedes the migrating schistosomulae whereby the Th2 profile will allow granuloma formation favouring the egg translocation (Abbas et al., 1996; Doenhoff, 1997; Fallon, 2000; Lucius et al., 2018; Wuhrer et al., 2006). Underlining the important role of the immune system for egg transition, it was shown that severe immunodeficient mice were nearly unable of passaging *Schistosome* eggs (Amiri et al., 1992; Cheever et al., 1999). These findings are supported by the fact that in Human Immunodeficiency virus (HIV)-positive individuals suffering from acquired immunodeficiency syndrome (AIDS), as well as intestinal schistosomiasis, excrete fewer eggs with their faeces compared to HIV-negative patients with similar *S. mansoni* load (Colombe et al., 2018; Karanja et al., 1997).

In general, a Th2 switch includes a decrease of IFN-gamma release and the polarization of CD4+ helper cells. Additionally, a Th2 switch is followed by the polarization of macrophages towards the classically less inflammatory M2 phenotype and an increase of eosinophils. This is accompanied by increased production of IL-4, IL-5 and IL-13, as well as a change of the immunoglobulin isotype from IgG1 to IgE in a mouse model and IgG4 to IgE in adult Schistosomiasis patients (Pearce & MacDonald, 2002; Schwartz, Oeser, et al., 2014). In an experimental setup with mice injected with *Schistosome* eggs, the switch to a more protective Th2 response was shown to be induced during the chronical phase of the infection. Here, the switch and subsequent IgE production was only observed when eggs were deposited by the worms or treatment with eggs or its extracts occurred (Okano et al., 1999; Pearce et al., 1991; Vella & Pearce, 1992). The Th2 immune response is marked by high IgE production and eosinophilia and was shown to be orchestrated by IL-4 release as its key-inducer cytokine. Eventually, by recruiting of eosinophils and triggering the differentiation of alternatively activates macrophages, IL-4 also facilitates several anti-inflammatory mechanisms in order to restrict host tissue damage, which is favourable for the granuloma formation and further downregulates the Th2 response (Maizels et al., 2009; Schramm & Haas, 2010; Seder et al., 1992; Wiedemann & Voehringer, 2020). These findings were supported by studies showing that genetically engineered mice with abrogated IL-4 (IL-4 -/-) production or inactive IL-4 receptor activity (IL-4 receptor alpha-chain -/-), once infected with *Schistosoma*, manifested massively impaired granuloma formation and overbearing intestinal inflammation which was followed by their death (Brunet et al., 1997; Fallon, 2000; Fallon et al., 2000; Herbert et al., 2008). Fallon et al., (2000) also reported that in IL-4 and IL-13 double knock out mice granuloma formation as well as eosinophil infiltration were abolished, whereby IL-4 application alone rescued against liver damage and played an important role in the function of the intestine.

It should be noted that pathology differs with the localization of the granuloma. For instance, intestinal and hepatic granuloma differ from each other. Hepatic granulomas form during chronic infection when the eggs are washed back into the liver when not excreted from the host. They bear more macrophages than the granulomas in the colon which contain more eosinophils, B and T cells (Amaral et al., 2017; Weinstock & Boros, 1983). Nevertheless, it should not be ignored that most of the studies were carried out on hepatic granulomas and due to that, the lack of experimental data concerning intestinal granuloma formation should not be neglected. Moreover, most of the in vivo studies include mouse models, whereas the mouse itself is not the

natural host for *Schistosomes*. As mice do not display the exact pathology as humans, data should always be treated cautiously (Fallon, 2000).

Irrespective of their localization, freshly deposited eggs are immature and progressively increase in size and mature in their morphology during the week after oviposition in the tissue. Thereafter, mature eggs produce large amounts of antigens that modulate parasite pathogenicity and host response. These proteins are unique to *Schistosome* eggs, with the best studied being k-5, omega-1 and IPSE/alpha-1 (Dunne et al., 1981, 1991). Even though it was believed for many years that these egg antigens (SmEA) are equally expressed and secreted irrespective the eggs' localization, a most recent study was showing that gene expression in general, but especially regarding the antigens, was critically dependent on tissue localization. With the help of transcriptomic analysis and immunolocalization of eggs in liver and intestinal tissue of a murine model, they were able to demonstrate that egg antigen expression and secretion, such as omega-1 and IPSE/alpha-1, differs tremendously and is mostly restricted to liver-eggs. It was therefore suggested that these differences might reflect a two-way communication between eggs and the host (Peterková et al., 2024).

1.3 Sm IPSE/alpha-1 (IL-4 inducing principle of *Schistosoma mansoni* eggs)

The homodimeric glycoprotein IPSE/alpha-1 was first described as alpha-1 and later identified as IPSE (Genbank-accession# AY028436) (Dunne et al., 1984, 1991; Schramm et al., 2003, 2006)**.** IPSE (IL-4-inducing principle of *Schistosoma mansoni* eggs) is synthesized in the second half of egg development, after the complete development of all layers. Its translation is restricted to the egg state, even though female worms also express mRNA for IPSE (Schramm et al., 2006). As it is enriched in the subshell (Figure 3), non miracidial tissue of the egg, which was identified with the help of immunohistological localization and in situ hybridisation with labelled antisense transcripts of full-length IPSE cDNA in liver sections of schistosome-infected mice, IPSE secretion occurs via microchannels of the eggshell (Schramm et al., 2003, 2006). Previously, it was shown that expression of IPSE by the egg differed tremendously depending on their localization, as transcriptomic and immunolocalization experiments revelead. The study showed that all 13 (in V9 *S. mansoni* genome) IPSE-encoding genes were notably upregulated in liver-derived mature eggs, but not in intestinal-derived eggs. This was further confirmed with

immunofluorescence microscopy of murine liver and intestinal sections containing mature *S. mansoni* eggs. Sections were treated with a monoclonal anti-IPSE antibody, confirming that IPSE was highly abundant in and around liver-eggs, but only sporadically (and in lower intestity) found in intestinal-eggs (Peterková et al., 2024).

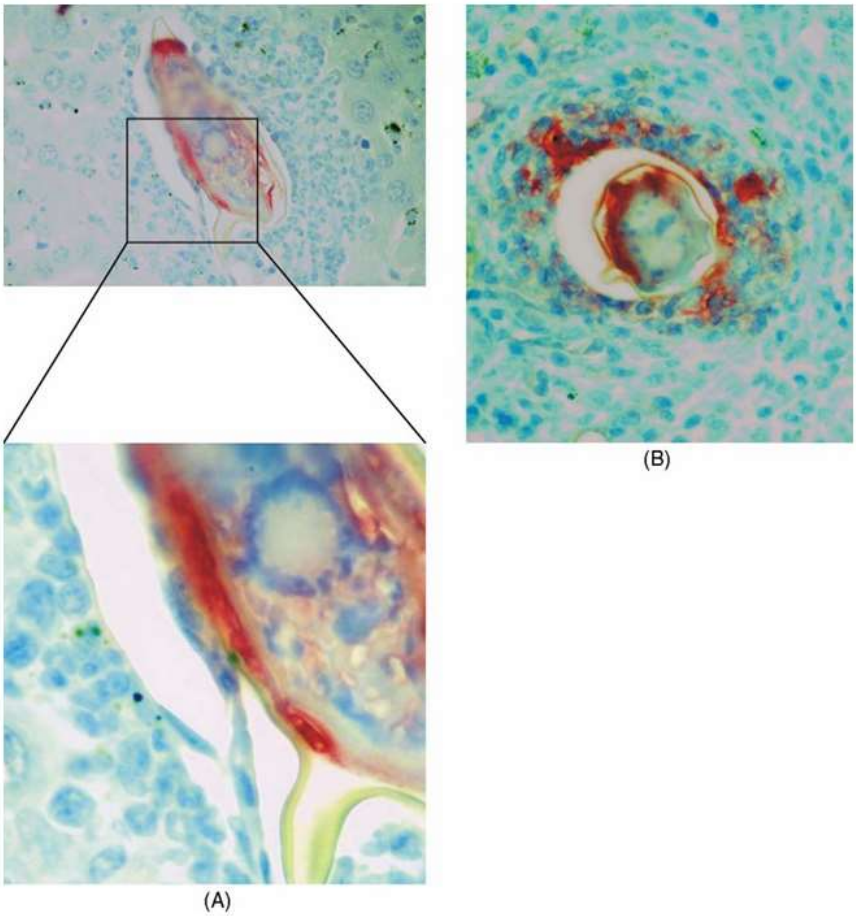

Figure 3 Immunohistological detection of Sm IPSE/alpha-1 performed in mice liver tissue. (A) Picture of Longitudinal section and (B) transverse section of *S. mansoni* eggs. Figure was taken from (Wuhrer et al., 2006, S. 200).

Pre-mature full-length IPSE/alpha-1 consists of 134 amino acids, from which the first 20 amino acids function as secretion signal and are cleaved after the release of the mature protein, resulting in a molecular weight of ca. 40 kDa when containing an an α-linked fucose (N. H. Meyer et al., 2015; Schramm et al., 2003). Notably, numbering refers to pre-mature IPSE (Figure 5).

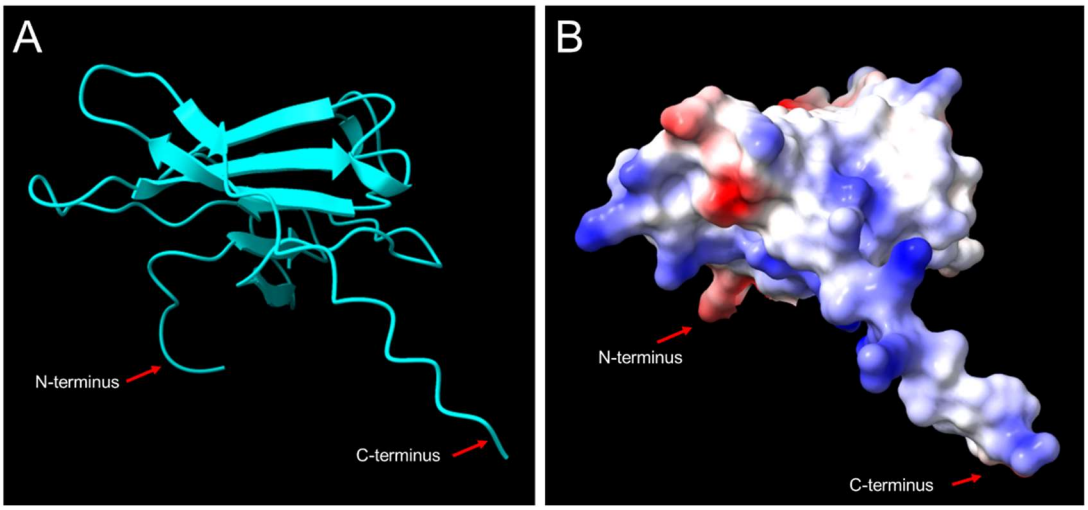

Figure 4 Display of the 3D-structure of a Sm IPSE monomer. (A) Tertiary structure (B) electrostatic map. Created with ChimeraX using the AF-Q869D4-F1 3D (secretion signal was deleted for display) extracted from www.uniprot.org.

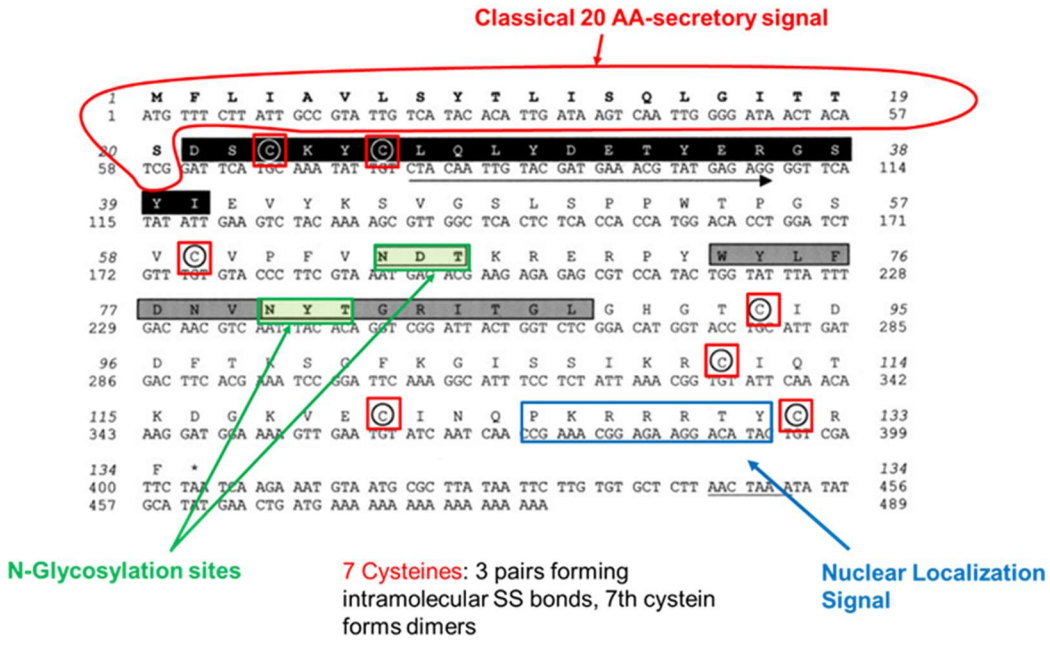

Figure 5 Sequence of Sm IPSE extracted from Schramm et al., (2003). The first 20 amino acids represent a secretory signal that is cleaved of. A monomer bears two N-glycosylation sites (64-66 and 80-82), 7 cysteines from which the 7th (132) is responsible for dimerization and a predicted Nuclear Localization Signal (PKRRRTY, 125-131).

IPSE bears a compact globular structure that consists mostly of beta-sheets, but also two N-glycosylation-sites (at amino acid position 64 and 80) (Schramm et al., 2003). Due to its crystalline beta/gamma “greek key motif” (Figure 6), IPSE belongs to the gamma crystallin-like superfamily (N. H. Meyer et al., 2015; Wuhrer et al., 2006). Proteins of this family share a similar structure, usually consisting of two domains with

four Greek key motifs, two per domain forming the crystalline fold (Serebryany & King, 2014). A crystalline fold is further characterized by a highly consereved signature sequence (Y/F)XXXX(Y/F)XG that can also be found in case of IPSE/alpha-1. IPSE bears two putative greek key motifs, which are surrounding a long flexible loop, as revealed in NMR spectroscopy and crystallographic analysis of monomeric IPSE (21-124), is unique for IPSE and its orthologues. (N. H. Meyer et al., 2015). Natural IPSE/alpha-1 occurs as a dimer, in which the unpaired C-terminal cysteine (C132) is responsible for intermolecular homodimerization, while six other cysteines provide three intramolecular disulfide bonds, aiding stability. By removing the putative Nuclear Localization Signal (NLS)-sequence (PKRRRTY) that is situated close to the C-terminus, plus the entire C-terminus and with it the 7th Cysteine (C132), Meyer et al., obtained monomeric IPSE, standing in line with the assumption that this cysteine mediates covalent dimerization. The NLS itself is thought to guide the protein in the host cell nucleus (Kaur et al., 2011; Pennington et al., 2017).

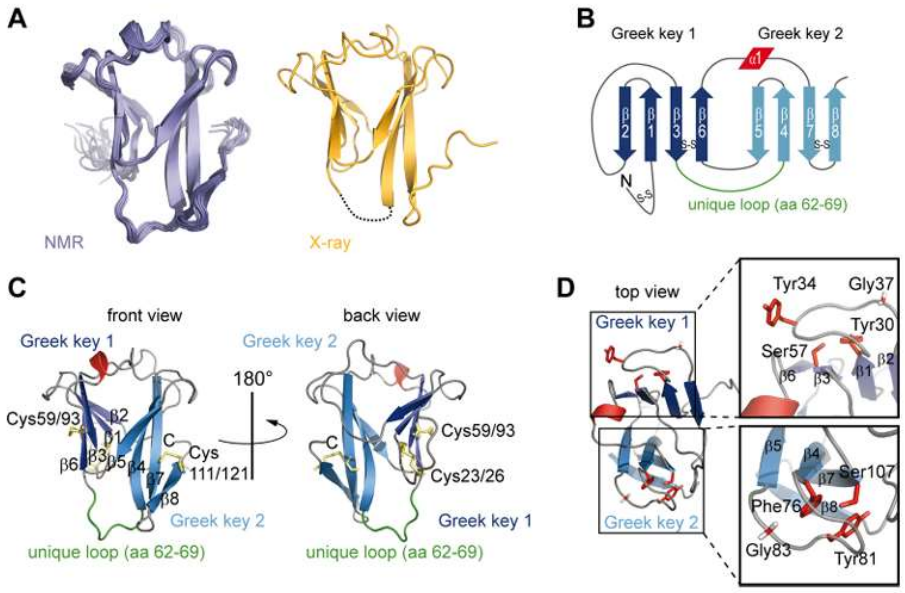

Figure 6 Structure of monomeric IPSE lacking the NLS. (A) NMR (left) and crystal (right) structure. (B) secondary structure topology of monomeric IPSE (ΔNLS). (C) ribbon representation of thr NMR-derived structure of IPSEΔNLS (monomeric) with indications of the unique loop of the crystalline fold and Cysteine residues responsible for disulphide bonds. (D) Highlighted amino acids bind part of the greek key signature sequence in red. Extracted from (N. H. Meyer et al., 2015)

Pennington et al., 2017 also described two orthologues of *Schistosoma mansoni* IPSE (Sm IPSE) derived from *Schistosoma heamatobium* (Sh03 and Sh06 IPSE). These possess a similar sequence, but with a few amino acid exchanges (Figure 7)

(Pennington et al., 2017). The here presented study mainly focuses on the *S. mansoni* Sm IPSE and the term “IPSE” therefore refers to Sm IPSE.

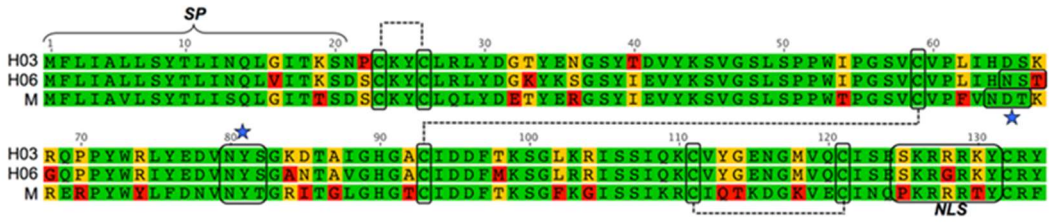

Figure 7 Sequences of IPSE orthologues Sh03 and Sh06 from *S. haematobium* aligned to Sm IPSE Figure derived from (Pennington et al., 2017).

In the past, it has been shown that Sm IPSE/alpha-1 possesses many different modes of action.

IPSE’s name is derived from **I**nterleukin-4-inducing **p**rinciple of ***S****. mansoni* **e**ggs for its ability to induce IL-4 release from basophils of immunological naïve donors. Here, binding of Sm IPSE to IgE induces downstream activation of basophils triggering the production of IL-4 and IL-13, as well as degranulation of mediators such as histamine. Therewith, IPSE/alpha-1 is the principal bioactive component in ***S****. **m**ansoni* **E**gg **A**ntigens (SmEA) inducing the activation of basophils and therefore the expression of IL-4 and IL-13 (Schramm et al., 2003). This was shown in experiments using different pools of SmEA either containing or devoid IPSE, as well as recombinant IPSE, to incubate basophils. These assays revealed that only basophils treated with IPSE and IPSE-containing pools were able to induce basophil degranulation (histamine release) and the release of IL-4 and IL-13 (Schramm et al., 2003). Despite these findings, intravenous injection of IPSE into mice, was leading to IL-4 release of basophils in the liver tissue (Schramm et al., 2007). It was also shown that IL-4 production by basophils was dose-dependently inhibited by the addition of a murine anti-IPSE serum, when cells were previously stimulated with SmEA containing IPSE or simply recombinant IPSE (Schramm et al., 2003). As another attempt, Schramm et al., (2003) performed immunodepletion, by using the IgG fraction of the murine anti-IPSE antiserum bound to a protein G-Sepharose, they revealed a complete lack of IL-4 inducing capacity from SmEA, once again supporting IPSE as sole IL-4 inducing principle in SmEA. In the scope of this study, they also showed that Sm IPSE is an IgE binding factor, as it was biding in various concentrations of human IgE in blotting experiments (Schramm et al., 2003). Standing in line with the previous findings, IPSE was found to be able to dampen inflammatory cytokine responses by its capability to

trigger basophil release of IL-4 and -13, especially in the context of TLR activation and thereby turning inflammatory monocytes to rather anti-inflammatory AAMs. Additionally, IPSE inhibits pro-inflammatory cytokine release from monocytes which have been activated by LPS (in context of whole PBMC) (Knuhr et al., 2018).

Furthermore, IPSE harbours more immune modulatory functions, serving as IL-10 inducer in naïve B cells and thus orchestrating their switch to regulatory B cells. These trigger T cell development and IL-10 production in human CD1d+ B cells (Haeberlein et al., 2017). Another immunomodulatory function of IPSE is the capacity of Sh06 IPSE to dampen pro-inflammatory responses of previous chemical insults in a mice model, resulting in the amelioration of pain, although the mechanism governing this reaction remains to be elucidated (Ishida et al., 2020).

1.4 Immunoglobulin E

One way in which IPSE mediates its immunomodulatory function is by engagement of host IgE (Immunoglobulin E) which triggers basophil activation (Schramm et al., 2003). IgE is in particular associated with a critical role in allergic responses (Gould & Sutton, 2008). Furthermore, high serum levels of IgE have also been attributed to helminthic infections in humans, including *S. mansoni* infection. Elevated IgE levels in *S. mansoni* infections have been reported already in 1973 (Kellermeyer et al., 1973). Indeed, Dessaint et al., (1975) were able to show that IgE levels in *S. mansoni* patients were increased in 77.5% of all cases.

IgE is the least abundant antibody in human serum. Its synthesis is triggered by two signals from T cells i) IL-4 or IL-13 abundance and ii) ligation of CD40 on B cells resulting in a DNA switch recombination (Prussin & Metcalfe, 2006). IgE comprises of two identical light and heavy chains and two antigen-binding sites that are formed by the pairing of the variable regions of the heavy and light chains (Figure 8).

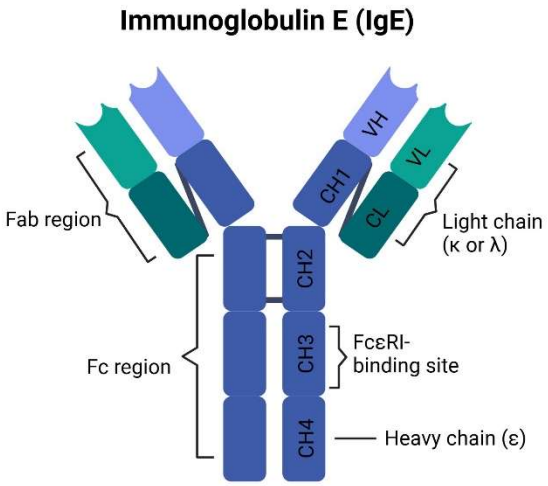

Figure 8 General structure of IgE. CH= constant heavy domains, part of heavy chain (ε), CL = constant light domain, part of light chain, VL= variable domain of light chain, VH= variable domain of heavy chain.

The heavy and the light chain are covalently linked by disulphide bonds (Shamji et al., 2021; Sutton & Gould, 1993). Light chains appear either as κ or λ form and are swapped during antigen receptor editing on B-cells to change the specifity of the antibody (Halverson et al., 2004; Yachimovich et al., 2002). In general, there are more κ than λ antibodies in human peripheral blood (Bräuninger et al., 2001; Molé et al., 1994; Montaño & Morrison, 2002). λ and K light chain bearing antibodies differ in structure and properties, as it has been shown that they display a broad range of phenotypic differences in terms of conformational flexibility led back to its larger elbow angle and half-life (Montaño & Morrison, 2002a; Stanfield et al., 2006; Townsend et al., 2016). The elbow angle is the angle between the variable and constant domain in Fab and light-chain fragments (Schiffer et al., 1973). Moreover, it was shown that κ and λ significantly differ in thephysicochemical properties of their CDR-L3 (complementary-determining regions of Light chain) (Townsend et al., 2016). CDR loops (canonical structures) (Figure 9) are hypervariable regions, of which are three found on each variable region of the immunoglobulin, evenly distributed between four less variable framework regions (E. Gabrielli et al., 2009; Kabat, 1978; Kabat et al., 1977; Morea et al., 2000). The strucutural beta-sheet framework regions help to keep them in place (Chothia & Lesk, 1987). CDRs provide a specific recognition-site on the antibody's surface, enabling the antigen recognition and binding, which is facilitated by their hypervariability (Kabat, 1978; Kabat et al., 1977; Morea et al., 2000). CDRs, most importantly the CDR-H3 loop, are as well involved in antigen-binding itself (Kabat, 1978; Kabat et al., 1977; Tsuchiya & Mizuguchi, 2016). Comparing CDR-L3

regions in λ to κ, it was shown that in case of λ, CDR-L3 regions appear longer, are more hydrophobic and display a higher aliphatic index than the corresponging region in κ antibodies (DeKosky et al., 2016; Townsend et al., 2016). Due to their differences, it was proposed by Townsend et al., (2016) that κ and λ light chains may be involved in different roles in the humoral immune response.

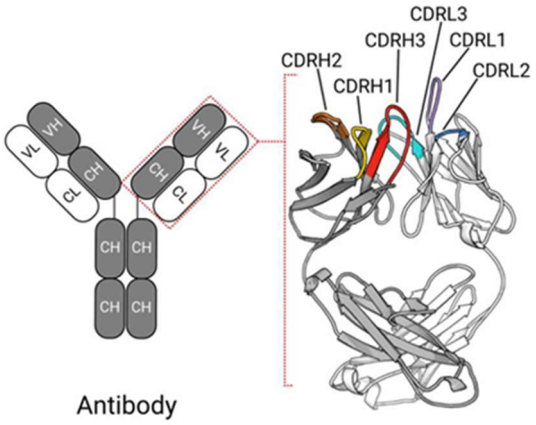

Figure 9 Structure of CDR (complementary determining regions) of an antibody. A variable region bears a total of six hypervariable CDRs which are evenly distributed between four less variable framework regions (Wong et al., 2019).

IgE includes four constant heavy domains (Cε1-4) with Cε2 replacing the hinge region which is usually found in other antibody classes (e.g. IgG). Another special attribute of IgE is the high flexibility in its Fc region. These unique features result in the extremely high-affinity binding to the FcεRrI receptor (Harwood & McDonnell, 2007; McDonnell et al., 2023). Free serum IgE classically binds with a 1:1 stoichiometry to its high affinity receptor FcεRI. The receptor binds to the Fc region, in particular the Cε3 domain, of IgE. It is present on basophils or mast cells as a tetramer comprised of an α chain (the extracellular antibody-binding site), as well as one β chain and two γ chains which act as intracellular immune-receptor for activating the cellular response on antigen binding and aid the receptor's stability (Gould et al., 2003; Kinet, 1999; McDonnell et al., 2023). FcεRI can also be found on other cells, such as mucosal epithelial cells, but here the receptor appears either as αγ2 trimer or tetramer. Notably, basophils and mast cells express high levels of FcεRI, which are mostly occupied by IgE *in vivo*. Therefore, minute concentrations of multivalent antigen can cross-link the binary antibody-receptor complex and thus trigger rapid cellular activation (Kinet, 1999; McDonnell et al., 2023). The classical mechanism of IgE-dependent activation consists of cross-linking of receptor-bound IgE by multivalent

cognate allergen binding to the antigen-recognition variable region of the corresponding immunoglobulin (Figure 10). This mechanism subsequently triggers cell activation and degranulation of basophils or mast cells, resulting in the release of IL-4, IL-13, leukotrienes and histamines, which further play a crucial role in immune responses (Dvorak, 1998; Gibbs et al., 1996; Li et al., 1996; Ochensberger et al., 1995; Shamji et al., 2021; Sutton & Gould, 1993).

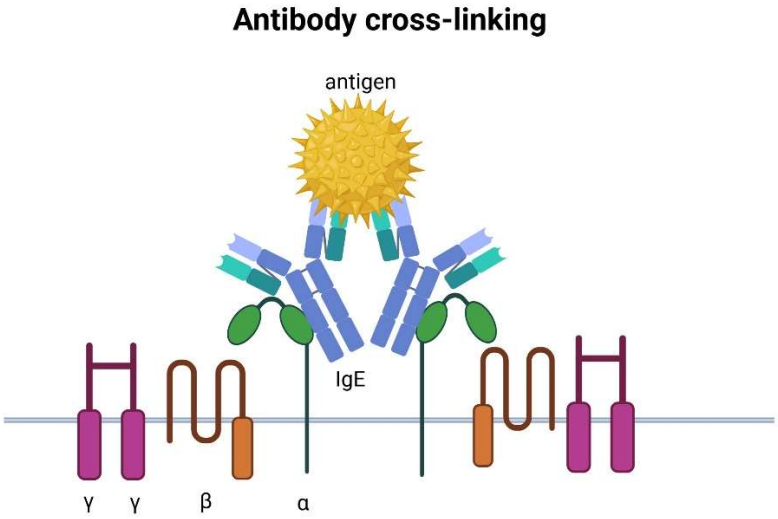

Figure 10 Schematic mechanism of IgE cross-linking. The antigen binds to the Fab region of IgE and the alpha chain of FcεRI binds to the Cε3 of IgE.

One group of basophil-activating molecules are lectins, substantial constituents of edible plant products, which bear the capacity to induce mediator release in a time- and dose dependent manner by binding to IgE without antigen-specificity. It was shown that the binding of lectins, such as Concanavalin A (derived from the Jack bean *Canavalia ensiformis*), was rather mediated via their glycosylation (Haas et al., 1999; Lallès & Peltre, 2009). Haas et. al (1999) furthermore suggested that lectins directly cross-link FcεRI resulting in basophil activation and degranulation. That mechanism was suggested to be dependent on the different carbohydrate specifies of each lectin that also lead to different activation capacities (Haas et al., 1999). Another group of antigen-independent basophil activators are B-cell super antigens, which bind directly to IgE's backbone of the Fab or Fc region (Patella et al., 2000).

1.5 Sm IPSE/alpha-1 induces basophil degranulation by binding IgE

Sm IPSE was previously identified as general immunoglobulin binding factor to all human serum immunoglobulins, in a non-antigen specific manner (N. H. Meyer et al., 2015). Nevertheless, Sm IPSE was attributed to bind with the highest affinity to FcεRI-bound IgE on the surface of basophils, which subsequently leads to basophil activation and degranulation (Schramm et al., 2003). Moreover, it was shown that basophil activation by IPSE depends on the presence of IgE on the surface of the cell irrespective IgE's antigen specifity (Falcone et al., 1996; Schramm et al., 2003, 2007).

Because basophils produce large amounts of IL-4 and IL-13, once they have been activated, they are seen as potent Th2-type effector cells (Eglite et al., 2000; Voehringer, 2017). Additionally, it was stated that basophils might play a crucial role in anti-helminth immunity, since it has been shown that these cells target parasite-infested tissues and become completely active, thus also providing an important source of IL-4 (Sullivan et al., 2011; van Panhuys et al., 2011). This stands in line with the finding that basophils accumulate in helminth-infected tissues, such as the intestine, where they promote rapid expansion of Th2 cells and protection against different parasitic helminths during secondary infection by IgE-induced secretion of IL-4/IL-13 (Schwartz et al., 2014).

As IPSE binds indiscriminately to all isotypes of immunoglobulins (IgE, IgG, IgA and IgM) in western blot experiments, conducted with human serum samples, IPSE was declared as general immunoglobulin binding factor (N. H. Meyer et al., 2015). Here, it became obvious that IPSE binds with the highest affinity to IgE. This finding was further supported with size exclusion chromatography and dot blots conducted with IPSE and IgE or IgG, showing a much higher affinity to IgE than to IgG. Standing in line with that, surface plasmon resonance experiments, which included *E. coli* -expressed mature IPSE (21-134) and monomeric IPSE lacking NLS (21-124) and IgG or IgE, revealed a four-fold higher binding affinity to IgE in case of monomeric IPSE and no calculable affinity for the dimeric form (N. H. Meyer et al., 2015).

By investigating the binding mechanism, Meyer et al., (2015) were able to rule out the possibility of IPSE cross-linking to receptor-bound IgE. With the help of sandwich dot blots using unlabelled membrane bound IgE, IPSE and labelled soluble IgE, as well as double immunodiffusion (Ouchterlony) assay showing immunoprecipitation in all positive controls but not with IPSE, they established a cross-linking independent mechanism. Moreover, they were interested whether the IPSE/IgE complex occurs

via binding in a lectin or B-cell superantigen like manner. Lectin-like binding was ruled out when comparing western blotting experiments carried out with native IPSE to PNGase F-deglycosylated Fc fragments of IgG. IPSE was able to recognize both, glycosylated and deglycosylated Fc of IgG. A B-cell super antigen-like binding could also be excluded due to the fact that IPSE binds to both, the Fc and Fab region in blotting experiments (N. H. Meyer et al., 2015).

To analyse the interaction site of IPSE and IgE, especially to map the binding interface of IPSE to IgE, Meyer et al., carried out studies of IPSE lacking the NLS (21-124) with IgE in NMR (nuclear magnetic resonance) chemical shift studies. A large positively charged binding surface, including a flexible loop connecting two greek motifs, that is unique for IPSE's aforementioned crystalline fold, was identified. The flexible loop (62-96) comprises positively charged and aromatic amino acids, which were shown in peptide scan and NMR titration to be critical for effective IgE binding. Peptide scan analysis of the sequence requirements in the peptide compromising residues 62-76 revealed that when exchanging positively charged amino acids to either glutamate or alanine, the binding affinity to IgE is decreased. Furthermore, swapping aromatic residues in this region to alanine, leads to lower binding as well. The finding that binding interference involves aromatic side chains in NMR, once more supports the idea of electrostatic and charged interactions play an essential role in IgE/IPSE interaction. To get more details of IPSE's interaction interface, Meyer et al., (2015) also conducted mutational analysis of amino acids situated in the predicted binding surface. Here the mutations were introduced in both, dimeric and monomeric IPSE, which in case of monomeric led to improper folding in some cases. Monomeric IPSE, in general showed lower binding capacities, compared to the dimeric form, when analysed for immunoglobulin binding (IgG and IgE) in western blot and for basophil IL-4 releasing capacities. This underlines the fact, that IPSE requires its dimeric form to function. In the scope of these experiments, the authors were able to show that mutations located outside of the binding interface assessed via NMR show same capacities, but the mutations inside the flexible loop, showed remarkably reduced binding and basophil activation properties (N. H. Meyer et al., 2015). Interestingly, a *Schistosoma* egg secreted protein termed SmCKBP, seemingly being very similar to IPSE but bearing T92Y/R127L mutations were reported to display markedly reduced immunoglobulin binding and complete impairment of basophil activation, in line with previous findings (N. H. Meyer et al., 2015; Smith et al., 2005).

In the scope of their study, the authors therefore proposed an *in silico* model of Sm IPSEΔNLS binding to the Cε2 domain of IgE, probably mediated via the negatively

charged region of IgE binding to the positively charged IPSE. Furhtermore, the authors propsed a model of dimeric IPSE interacting with FcεRI-bound IgE on the basophil surface. The model includes an initial binding of the first IPSE monomer to the Cε2 domain, facilitating the binding of the second monomer to the Fab region. This eventually might induce structural rearrangement in the IgE moleculare that triggers the activation of the receptor-signalling cascade (Figure 11). Furthermore, they suggested, based on the complexes formed at equivalence, as assessed by size exclusion chromatography, a binding stoichiometry of one dimeric IPSE/alpha-1 to one IgE molecule (1:1). This would further support the proposed cross-linking-independent mechanism (N. H. Meyer et al., 2015).

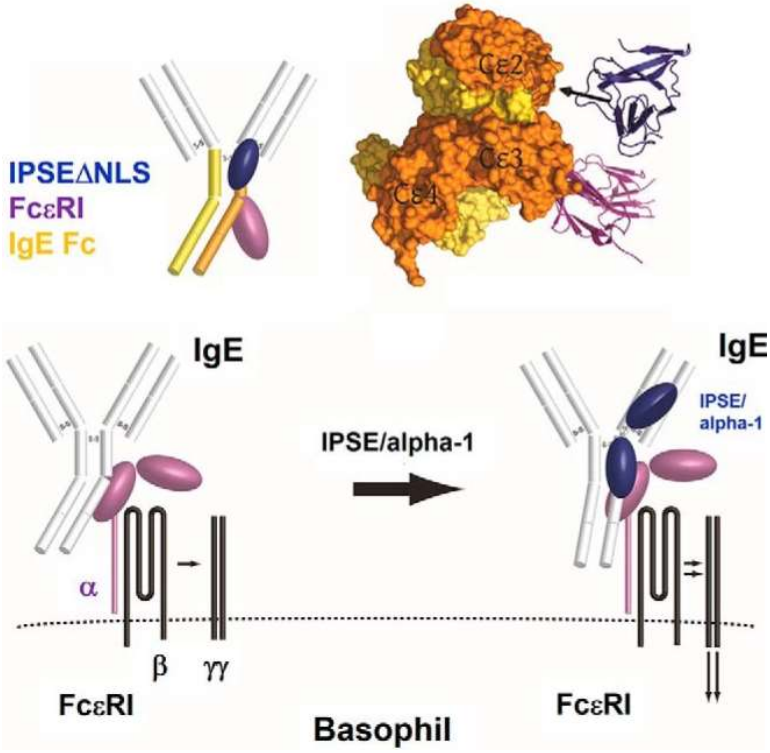

Figure 11 Proposed model of interaction between Sm IPSE and IgE by Meyer et al., (2015). Display of proposed model of interaction of monomeric IPSEΔNLS to IgE Fc (yellow) /FcεRI (pink) (PDB accession code 2WQR). Hereby, the positively charged binding interface of monomeric IPSE (mapped by NMR) and mutational analysis presumably interacts with a negatively charged surface of the IgE Cε2 domain of the receptor bound (Cε3) IgE. The other model includes dimeric IPSE/alpha-1 binding to full-length IgE bound by its high affinity receptor on the suface of the basophil. This binding might induce structural rearrangement in the IgE moleculare that eventually triggers the activation of the receptor-signalling cascade (Meyer et al., 2015).

Considering all the findings in the work of Meyer et al., (2015) further studies are still necessary to elucidate the binding mechanism behind the IgE/IPSE interaction.

Notably, it should not be underestimated that IPSE naturally occurs as a dimeric protein and that especially here; most analysis of NMR spectroscopy was predominantly conducted using the monomeric IPSE NLS mutant. Therefore, it would be important to further analyse the interaction of IgE with dimeric IPSE, since Kaur et al., (2011) were also able to show that monomeric IPSE does not lead to basophil activation.

Above that, Meyer et al., were only able to limit an area of interaction, but not definitively determine the exact mechanism of IPSE's interaction, with IgE. Here, it would be important to investigate which exact domain of IgE mediates binding, and which amino acid residues within these domains are essential. So far, it is not known if the light chain, meaning λ or κ, plays a crucial role. Since most of the work was also carried out in biochemical assays, it would be useful to use in vitro assays including more experiments with basophils.

1.6 Sm IPSE as chemokine binding protein

As mentioned above, Smith et al., (2005) were describing a SmEA derived protein, which is identical to Sm IPSE bearing the mutations T92Y/R127L. So far, it is not clear whether SmCKBP is derived from *ipse* coding genes, or not. Another unsolved question is, if *Schistosoma* eggs are producing a mixture of IPSE and SmCKBP or only one them. This particular egg secreted protein, also termed as *Schistosoma mansoni* Chemokine Binding Protein (SmCKBP), possesses the ability to bind to chemokines and neutralize them. SmCKBP is the only *Schistosoma* egg protein which was shown to display this particular activity (Smith et al., 2005). Smith et al., (2005) were able to recombinantly express and purify this protein, and subsequently show that it bears the capacity of suppressing inflammation in several murine disease models. Above that, they figured that it manifested markedly reduced immunoglobulin binding together with complete lack of IL-4 releasing capacity. The latter is in accordance with findings of Meyer et al., 2015 for Sm IPSE T92Y/R127L displaying a markedly reduced IgE-binding capacity, as well as a complete lack of IL-4 release by basophils.

The SmCKBP, therefore, seemingly possesses immune-regulatory properties. This is underlined by the fact that it has been attributed specific *in vivo* activity in suppressing the immediate or local inflammation, such as significantly reducing CXCL-8-induced neutrophil infiltration in an murine air pouch model and in general resulting in a

modulation of the differential recruitment of cells and size of the egg granuloma (Smith et al., 2005).

1.7 Sm IPSE/alpha-1 acts as “infiltrin” in human host cells

Previous studies demonstrated for IPSE/alpha-1 (and its orthologues) not only an interaction with immune associated cells, rather it was also shown to infiltrate different types of host cells (Kaur et al., 2011; Pennington et al., 2017). IPSE/alpha-1 can be detected in liver granulomas surrounding the intact *S. mansoni* egg (Figure 12), but was rarely detected in intestinal granulomas (Peterková et al., 2024; Wuhrer et al., 2006).

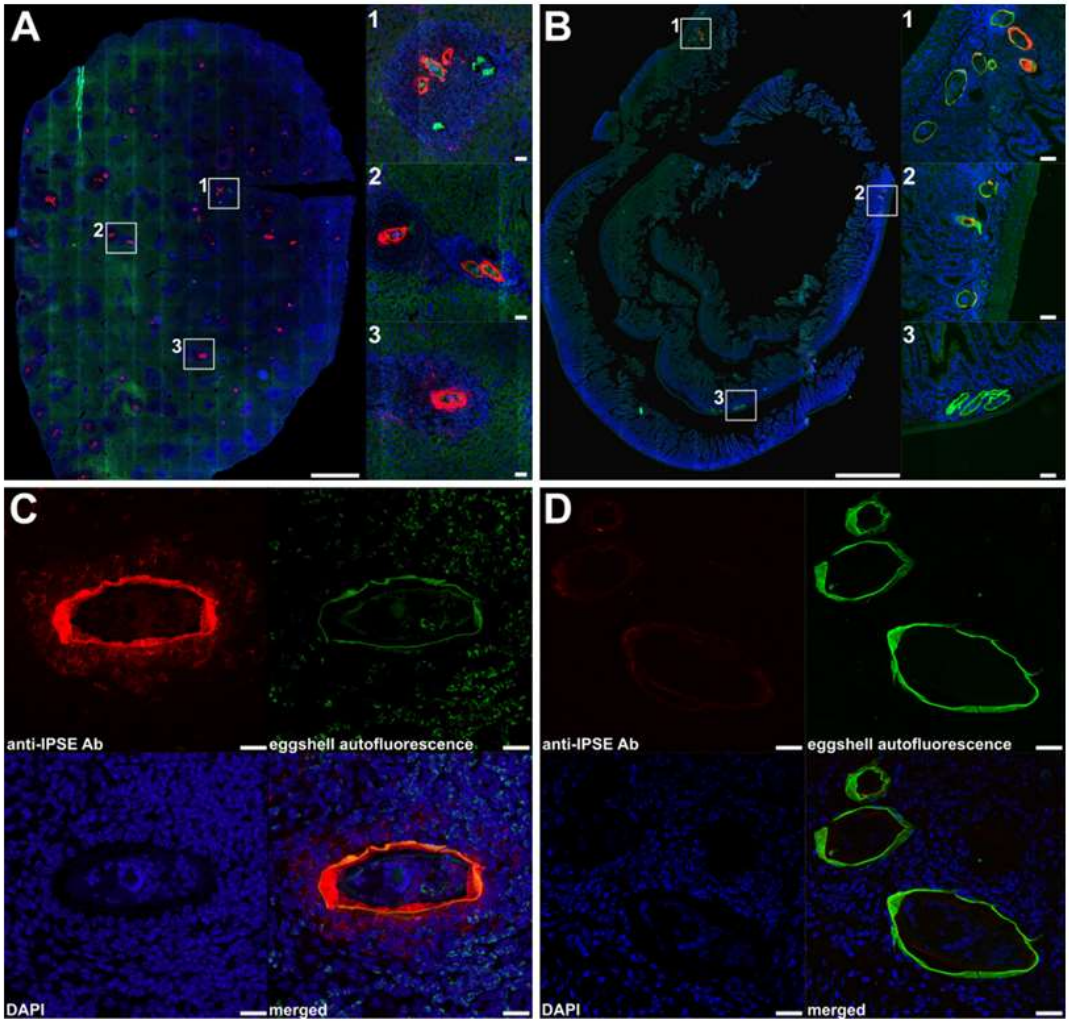

Figure 12 Immunolocalization of *Schistosoma mansoni* IPSE. (A,C) Images of liver sections and (B,D) intestine sections of mouse infected with *S. mansoni*. (A,B) Overview axioscan images showing the whole sections of *S. mansoni* infected tissues including zoomed areas. (C,D) Confocal images of mature eggs, labelled with anti-IPSE antibody (red), autofluorescence (green) and blue for DAPI-labelled cell

nuclei. The subshell area in liver sections displayed an intensive red anti-IPSE signal, as well as the surrounding tissue, while the signal is weaker or absent in intestinal eggs. Extractraced from (Peterková et al., 2024).

To this date, the consequences of the incorporation of IPSE into a host cell remain unexplored. IPSE and its orthologues bear a putative Nuclear Localization Signal (NLS) (Figure 5 and 7), which was shown to guide the protein into the cell nucleus. Previous works on IPSE stated DNA-binding properties of IPSE and a putative role as transcription factor (Kaur et al., 2011; Pennington et al., 2017). This hypothesis was indirectly confirmed by Mbanefo et al, by showing that IPSE bearing the NLS increases the proliferation of endothelial and urothelial cells, an effect which was not observed upon penetration of IPSE mutants lacking the NLS.

Besides its internalization in and interaction with tissue cells, IPSE (as part of SmEA) was also shown to bind to C-type lectin-receptors (CLR) and subsequently be taken up by the host dendritic cells (DC). It is therefore believed that aspects of egg-induced immune processes are partially driven by protein glycosylation of SmEAs (Hokke & Yazdanbakhsh, 2005).

It was demonstrated that IPSE's glycosylation (antennae fucoses) plays a crucial role in binding to DC-SIGN (DC-specific ICAM3-grabbing non-integrin) and MRs (Mannose receptors) in a cellular context with dendritic cells and single CLR (C-type lectin-receptors)-cell lines. IPSE binds in its natural form preferentially DC's via the Mannose receptor (Meevissen et al., 2012).

Interestingly, besides the fact that IPSE interacts with the host cell with via its glycosylation/carbohydrates, studies using *E. coli* - recombinatly expressed IPSE, lacking glycosylation, has the capacity to enter human cells in vitro (Kaur et al., 2011). This suggests that there must be multiple mechanism involved in IPSE uptake.

1.8 Aim of the study

This study intends to elucidate molecular interactions of the *Schistosoma mansoni* egg-secreted glycoprotein IPSE with the host cells.

The two objectives within the study are IPSE's interaction with IgE and its internalization in different host cells.

To investigate the underlying mechanism of the interaction between Sm IPSE and IgE, known to enable basophil activation, IPSE's IgE-binding capacity, as well as basophil activation was tested using different IPSE mutants and multiple IgE variants.

Furthermore, on the basis that IPSE has been known to exert further functions that are not immunomodulatory and encodes a putative NLS, its DNA binding capacity and uptake in diverse cell types comprise another objective of this thesis. We also aimed to assess the influence of internalized IPSE on the transcriptome of host cells and the cellular processes.

2. Materials & Methods

2.1 Establishment of basic experimental conditions

2.1.1 Cell culture

All adherent cell lines were split 1:6 by trypsinization using 1x Trypsin-EDTA in DPBS. Trypsinization was stopped using cell culture medium containing FCS.

2.1.2 HEK (human embryonic kidney) 293-6E suspension cells

HEK293-6E cells were used as pTT5 HEK293-6E expression model (National Research Council Canada file 11565), licensed from the Canadian Research Council. Cells were grown in suspension under constant shaking at a rate of 120 rpm in an incubator at 37 °C (5 % CO_2 humidified atmosphere). For this purpose, serum-free Freestyle F17 medium (Gibco, Rockville, MD) was supplemented with 0.1% (wt/vol) Kolliphor P-188 (Sigma-Aldrich/Merck, Germany), 4 mM L-Glutamine (Sigma-Aldrich), 0.5 % P/S (10000 units/ml; 10000 µg/ml) and 25 µg/mL G418 (50 mg/mL) (ThermoFisher Scientific, Germany). Density of 2 mio cells/mio was never exceeded during cultivation.

2.1.3 RS-ATL8 RBL (humanized rat basophilic leukemia) cells

RS-ATL8 RBL cells were cultured in T75 flasks using Eagle minimum essential medium (MEM; Sigma-Aldrich), supplemented with 10 % heat-inactivated fetal bovine serum (FBS; Serana Europe GmbH, Pessin, Germany), 1 % P/S (10000 units/mL; 10000 µg/mL) (Gibco, ThermoFisher Scientific, Germany), 1 % L-Glutamine (200 mM) (Sigma-Aldrich/Merck, Germany), 0.5 mg/mL Hygromycin (600 µg/mL) (Gibco, ThermoFisher Scientific, Germany) and 0.5 mg/mL G418 (ThermoFisher Scientific, Germany). Cells were used for the basophil-activation based reporter assay.

2.1.4 HCT-116 (human colorectal carcinoma) cells and CHO-Trvb- (Chinese hamster ovary) cells

HCT-116 cells, kindly provided by Michael Kracht (Justus Liebig University, Giessen, Germany) and CHO-Trvb- cells, a kind gift from Timothy E. McGraw and Frederick R. Maxfield (Weill Cornell Medical College, NY) were cultivated in T25 flasks using Eagle minimum essential medium (MEM; Sigma-Aldrich/Merck, Germany). The medium was supplemented with 10 % heat-inactivated fetal bovine serum (FBS; Serana Europe GmbH, Pessin, Germany), 1 % P/S (10000 units/mL; 10000 µg/mL) (Gibco, ThermoFisher Scientific, Germany) and 1 % L-Glutamine (200 mM) (Sigma-Aldrich/Merck, Germany). CHO-TrvB cells lack the endogenous Transferrin receptor (McGraw et al., 1987).

2.1.5 HepG2 (Hepatoblastoma) cells

HepG2 cells, kindly provided by Dieter Glebe (Justus Liebig University, Gießen) were cultivated in collagen-coated T25 cell flasks. Cells were grown in DMEM High Glucose including L-Glutamine (Gibco, ThermoFisher Scientific, Germany) (supplemented with 10 % heat-inactivated fetal bovine serum (Serana Europe GmbH, Pessin, Germany), 1 % P/S (10000 units/mL; 10000 µg/mL) (Gibco, ThermoFisher Scientific, Germany).

2.1.6 Species identification of cells via PCR

To ensure the identity and quality of cell lines, a PCR for species identification of cells was performed according to Holder and Cooper, 2011(Holder & Cooper, 2011). DNA of the different cell lines was extracted with the DNeasy® Blood & Tissue Kit (50) (Qiagen, Germany). For PCR, 25 µL reactions were prepared with 12.5 µL GoTaq Green Master Mix 2x (Promega GmbH, Germany), 1 µL DNA template (50 ng), 1 µL forward and 1 µL reverse Primer, filled up with molecular grade water. Samples were applied in a 1% agarose gel (see section 2.1.7). The cycling conditions were as follows: initial denaturation 5 min at 95°C, followed by 32 cycles of DNA amplification for 20 min at 94°C, primer annealing for 20 sec at either 66.5°C (rat), 66°C (mouse) or 67.5°C (human), extension 68°C for 20 sec and a final extension at 72°C for 10 min.

2.1.7 Agarose gel electrophoresis

Standard DNA or RNA gel electrophoresis was performed using a 0.8–1.5% (w/v) agarose (ThermoFisher Scientific, Germany) gel in 0.1% TBE buffer (ThermoFisher Scientific, Germany) containing 10 mg/ml ethidium bromide (10 mg/mL). Gels were imaged via the Bio-Rad ChemiDoc™ Imaging System.

2.1.8 Site-directed mutagenesis of Sm IPSE mutants and 6x-His tagged IgEλ

In order to create different mutant forms of IPSE (Table 1), site-directed mutagenesis was conducted. For that, forward and reverse oligonucleotide primer (Table 2) pairs were designed with the help of NEBaseChanger™, whereas Sm IPSE wild type pTT5 vector (AmpR, hVEGF Signal Peptide, 8xHis-Tag, TEV site) or pVITRO-102.1F10-IgEλ (HygR, FMDV IRES, EF-1α polyA, SV40 polyA) served as template DNA. Primers were ordered from IDT and reconstituted with nuclease-free water to 100 µM.

Q5® Site-Directed Mutagenesis Kit (New England BioLabs®, USA) was used to obtain the wanted mutations. Steps of exponential amplification in Polymerase Chain Reaction (PCR) was conducted according to manufacturer's instructions using matching primer pairs (12.5 µL Q5 Hot Start High-Fidelity 2X master mix, 1.25 µl 10 µM forward and reverse primer each, 1 µL 25 ng/µL template DNA and 9 µL Nuclease free water). The cycling conditions were as follows: initial denaturation 98°C for 30 sec, followed by 25 cycles of i) DNA denaturation at 98°C for 10 sec, ii) annealing depending on primer set for 30 sec, and iii) elongation at 72°C for 20-30 sec/kbp and a final extension step at 72°C for 2 min. The PCR product was then used for KLD reaction (1 µL PCR product, 5 µL 2X KLD reaction buffer, 1 µL 10X KLD enzyme mix and 3 µL nuclease free water), an enzyme mix consisting of Kinase, Ligase and DpnI enzymes allowing efficient phosphorylation, intramolecular ligation/circularization and template removal (see (New England BioLabs® product information), and incubated 5 min at RT.

Bacterial transformation was performed with NEB 5-alpha competent *E. coli* cells (New England BioLabs®, USA). Purified plasmids were sequenced by Microsynth Seqlab using pTT5, SV-40 and specific pVITRO-102.1F10-IgE/λ primer (table 1) combination, respectively. The obtained sequencing chromatograms were aligned to the original template vector in SnapGene and visually inspected.

Table 1 List of aimed mutations and the original amino acids, including their triplett.

Amino Acid	Desired amino acid	Original nucleotides	Final nucleotides
Threonine 92	Tyrosine	ACC	TAC
Cysteine 132	Alanine	TGC	GCC
Arginine 127	Alanine	CGG	GCC
Arginine 127	Leucine	CGG	CTG
Arginine 127-129 (NLS)	Alanine	CGGCGGAGG	GCCGCCGCG

Table 2 Primer pairs used to either change desired amino acids in Sm IPSE pTT5, insert a His-tag into pVITRO-102.1F10-IgE/λ or for sequencing.

Name	Description	Primer Name	Sequence
Sm IPSE C132A	Mutation of Cysteine 132 to Alanine	Sm IPSE C132A pTT5 FW	5'-GCGGAGGACCTACGCCCGGTTCTAGT-3'
Sm IPSE C132A	Mutation of Cysteine 132 to Alanine	Sm IPSE C132A RV	5'-CGCTTGGGCTGGTTGATGC-3'
Sm IPSE T92Y	Mutation of Threonine 92 to Tyrosine	Sm IPSE T92Y FW	5'-CCTGGGCCACGGCTACTGTATCGACG-3
Sm IPSE T92Y	Mutation of Threonine 92 to Tyrosine	Sm IPSE T92Y RV	5'-CCGGTGATCCGGCCGGTGTA-3'
Sm IPSE R127L	Mutation of Argnine 127 to Leucine	Sm IPSE R127L FW	5'-CAGCCCAAGCtGCGGAGGACC-3'
Sm IPSE R127L	Mutation of Arginine127 to Leucine	Sm IPSE R127L RV	5'-GTTGATGCATTCCACCTTGCC-3'
Sm IPSE R127A	Mutation of Arginine 127 to Alanine	Sm IPSE R127A FW	5'-CCAGCCCAAGgccCGGAGGACCT-3'

Sm IPSE R127A	Mutation of Arginine 127 to Alanine	Sm IPSE R127A RV	5'-TTGATGCATTCCACCTTG-3'
Sm IPSE NLS-AAA	Mutation of Arginine 127-129 to Alanine	Sm IPSE NLS-AAA FW	5'-CGCCACCTACTGCCGGTTCTAG-3'
Sm IPSE NLS-AAA	Mutation of Arginine 127-129 to Alanine	Sm IPSE NLS-AAA RV	5'-GCGGCCTTGGGCTGGTTGATGCA-3'
pVITRO mEF	Sequencing Primer pVITRO-102.1F10-IgE/λ	pVitro mEF fw	5'-CTCGGGCTTCTTAGCGGTTCAAAGGTATC-3'
pVITRO IgE λ gene	Sequencing Primer pVITRO-102.1F10-IgE/λ	pVITRO IgE FW	5'-AGGAGGAGAAGCAGCGCAATGGCAC-3'
SV 40	Sequencing primer for plasmids with SV 40	SV 40 FW	5'-CCGGACTCAGATCTCCGAAGAAG-3'
Octahis pVITRO.IgEλ	introduction of 8xHis Tag in pVITRO1-102.1F10-IgE λ	Octahis pVITRO FW	5'-caccaccaccatTGATTAGCTGGCCAGACA-3'
Octahis pVITRO.IgEλ	introduction of 8xHis Tag in pVITRO1-102.1F10-IgE λ	Octahis pVITRO RV	5'-gtgatgatgatgTTTACCGGGATTTACAGAC-3'
6xHis pVITRO.IgEλ	introduction of 6xHis Tag in pVITRO1-102.1F10-IgE λ	Hexahis pVITRO FW	5'-accaccactagATTAGCTGGCCAGACATG-3'
6xHis pVITRO.IgEλ	introduction of 6xHis Tag in pVITRO1-102.1F10-IgE λ	Hexahis pVITRO RV	5'-accaccactagATTAGCTGGCCAGACATG-3'

2.1.9 Bacterial transformation via Heat Shock

To produce plasmid and to have a bacterial glycerol-stock, bacterial transformation via Heat Shock with chemically potent *Escherichia coli (E. coli)* NEB-5 alpha cells (New England BioLabs®, USA) was performed. To that end, a tube containing 50 µL *E. coli* was thawed on ice and 1-5 µL plasmid was added and mixed by gently tapping the tube. Cells were left on ice for 30 min and afterwards shocked by holding them for 45 sec in 42°C warm water. The tube was placed back on ice for another 5 min. Next, 950 µL Lysogeny Broth (LB) (CHEMSOLUTE Th. Geyer GmbH & co. KG, Germany) medium was added and incubated for 1h, 37°C 300 rpm. Eventually, 200 µL cells were spread on an agar plate containing the respective antibiotic, which was placed O/N at 37°C. The next day, colonies were picked and cultivated in 5 mL LB + antibiotic for glycerol stocks (250 µL glycerol and 750 µL bacterial culture) and further experiments such as Mini-preps (New England BioLabs®, USA).

2.1.10 Plasmid amplification and purification from cell culture

Neb 5 alpha *E. coli* cells bearing the wanted plasmid were grown over night in LB-medium supplemented with the respective antibiotic. Depending on the needed amount of plasmid, either Monarch Plasmid Mini-Prep Kit (New England BioLabs®, USA), PureYield™ Plasmid Midi-Prep (Promega GmbH, Germany) or PureYield™ Plasmid Maxi-Prep System (Promega GmbH, Germany) were performed according to the manufacturers' descriptions. In case of Midi- and Maxi-Prep, the vacuum-protocol was usually conducted.

2.1.11 Missense3D prediction – ChimeraX

To predict the potential destabilizing effect of a substation on the structure of Sm IPSE/alpha-1 introduced by of the mutants was evaluated with the Missense 3D prediction tool (Missense3D | Structural Bioinformatics Group | Imperial College London) (Ittisoponpisan et al., 2019) (Imperial College London). For that, the PDB 4AKA structural sequence was downloaded from the UniProt database (www.uniprot.com) and subsequently used for analysis with Missense3D. Figures were created with ChimeraX (Pettersen et al., 2021).

2.1.12 Protein structure prediction in AlphaFold2 – ChimeraX

To predicit the threedimensional protein structure of Sm IPSE wild type and chosen mutants (T92Y, R127L, R127A) with the use of the ColabFold tool (Mirdita et al., 2022). For that the IPSE sequence (Q869D4) was downloaded from the UniProt data base. The first 20 aa (secretion signal) were deleted and the respective mutations were inserted manually. The subsequent molecular display was created with ChimeraX (Pettersen et al., 2021).

2.1.13 SDS-PAGE and Western Blot

To identify the purity and presence of a protein, SDS-Polyacrylamide-Gel-electrophoresis was performed. To that end, either 4–20% Mini-PROTEAN® TGX™ Precast Protein Gels (Bio-Rad Laboratories GmbH, Germany) or self-made gels were used. Gels were prepared by firstly casting the separating gel (Separating Buffer) (12% polyacrylamide) and secondly pouring the stacking gel (SDS Stacking Buffer) of the gel containing the combs. Each part was solidified for around 20 min before continuing. After application of the different samples, which were prepared by mixing them with Laemmli-Buffer (5X reducing or 4X unreducing Bio-Rad Laboratories GmbH, Germany) and boiling them 7 min at 95°C, the gel was run 10 min at 80 mV, followed by 1h at 135 mV in Running Buffer. Usually either Color Prestained Protein Standard, Broad Range ladder or Blue Prestained Protein Standard, Broad Range ladder (New England BioLabs®, USA) were used.

For subsequent SDS-PAGE, Coomassie staining was performed by incubating for one hour in PageBlue Protein Staining Solution (ThermoFisher Scientific, Germany) followed by 3 washing steps in deionized water. For western blotting, the polyacrylamide gel was transferred onto a 0.2 µm nitrocellulose membrane using the Bio Rad Turbo Blot system. Here, the membrane was pre-soaked in Bio Rad Transfer Buffer (ethanol and H_2O added, Bio-Rad Laboratories GmbH, Germany). After blotting, the membrane was blocked 45 min at RT with 5 % dried skim milk (Carl Roth GmbH + Co. KG, Germany) in TBS-T (Tris-buffered saline, 0.01 % (vol/vol) Tween-20 (Merck, Germany) before incubating 2-3 h at RT with the respective primary antibody in TBS-T (5% skimmed milk powder). Then, the blots were washed 3x 5 min each in TBS-T, followed by 1-2 h incubation (RT) with the respective secondary antibody in TBS-T (5 % dried skim milk, Carl Roth GmbH + Co. KG, Germany).

For chemiluminescent detection, the western blot was first washed again 3x with TBS-T and then incubated with Clarity™ Western ECL Substrate kit (Bio-Rad Laboratories GmbH, Germany) and analyzed with Bio-Rad ChemiDoc™ Imaging System.

Western blot buffers/solutions:

5X Laemmli/Loading Buffer reducing

5%(v/v) β-mercaptoethanol

0.025% (w/v) Bromophenol blue

30% (v/v) Glycerol

10% (w/v) SDS (Sodium dodecyl sulphate) (Fisher# BP166-5, LOT# 183025)

250 mM Tris-HCl pH 6.8

Filled up to 100% with ddH_2O

Separating Buffer (pH 8.8)

1.5 M Tris-HCl

0.4% (w/v) SDS

ddH2O to 100%

Stacking Buffer (pH 6.8)

0.5 M Tris-HCl

0.4% (w/v) SDS

ddH2O to 100%

10X Running Buffer (pH 8.3)

0.025 M Tris base

0.192 M glycine

1% (w/v) SDS

ddH_2O to 100%

1X TBS-T

25 mM Tris-HCl

140 mM NaCl

2.5 mM KCl

0.01% Tween-20

2.1.14 Anti-IPSE antibody production

For downstream functional assay, a monoclonal Antibody against IPSE able to require the protein from both species was required. This was outsourced to GenScript.

Mice were immunized against a peptide with the sequence

This process initially required the repeated immunizations of mice with the antigenic peptide CVYKSVGSLSP, a sequence which is shared between IPSE from *S. mansoni* and *S. haematobium*, is accessible on the surface based on AlphaFold2 structural predictions and is predicted to be a B cell immunogen (work performed by the project supervisor).

Mouse sera were screened for the presence of anti IPSE antibodies in order to generate specific B-cells for hybridoma fusion and finally antibody production.

2.1.15 Anti-IPSE antibody testing via western blot

To determine which mouse was the best choice for producing the anti-IPSE antibody, GenScript serum from five mice, containing serum identified as a control (“pre-bleeder”) and post-immunization polyclonal serum (“after 3rd immunization”) for each. The capacity to detect IPSE was subsequently tested using western blot (see section .2.1.13) against the following antigens: Sm IPSE, Sh03 IPSE and Sh06 IPSE. Here, the respective mouse sera (“pre-bleeder” sera 1:1000 or “after 3rd immunization”

1:2000) were incubated over night at 4°C, before adding the secondary goat anti-mouse IgG HRP-conjugated antibody (1:10000, Invitrogen, ThermoFisher Scientific, Germany) for 2h. Chemiluminescence was detected with Clarity™ Western ECL Substrate kit (Bio-Rad Laboratories, Germany) and images taken on a Bio-Rad ChemiDoc™ Imaging System. The mouse, whose serum led to the strongest signal detected in Western Blot was subsequently chosen for hybridoma cell line production.

2.1.16 Test of hybridoma cell line supernatants

The final step before committing to an anti-IPSE antibody was to test the different hybridoma cell line supernatants provided by GenScript. Therefore, once again western blots with the different supernatants were performed as described above with recombinantly expressed Sm IPSE and Sh03 IPSE. For that purpose, the 9 different hybridoma supernatants (Clone IDs: 1E4-1, 1E4-2, 3F11-1, 3F11-2, 11D2-1, 11D2-2, 12E4-1, 12E4-2 and Anti-Na as negative control (GenScript, LOT#DF0001) were diluted 1:5 with 5% skimmed milk in TBS-T to be used as primary antibody. Then, the secondary goat anti-mouse IgG HRP-conjugated antibody (1:10000, Invitrogen, ThermoFisher Scientific, Germany) was added for 2h. After washing with PBS, Chemiluminescence was detected with Clarity™ Western ECL Substrate kit (Bio-Rad Laboratories, Germany) and images taken on a Bio-Rad ChemiDoc™ Imaging System.

2.1.17 Small scale transfection of HEK293-6E cells to determine best transfection conditions

To determine the optimal conditions for transfection HEK293-6E suspension cells with N-terminal and C-terminal tetracysteine-tagged Sm IPSE pTT5 plasmid (kindly provided and created by Jude Akinwale), a preliminary assay was conducted which included different plasmid and PEI-Max concentrations and ratios. For that, cells were grown in supplemented F17 medium until they reached 97-100% viability and a density of 1.8-2 x10^6 cells/mL. To begin, two tubes for each condition were prepared from which each contained 100 µL cultivation medium. DNA or PEI-Max (Polyscience Inc., USA) was then added to the tubes, respectively. The PEI mix and the respective plasmid mix were blended together by pipetting up and down three times. Mixtures were incubated for 5-10 min at RT. Subsequently, the PEI DNA mix (200 µL) was added dropwise to the respective cell suspension prepared in a 6-well plate (1.8 mL

per well). Chosen conditions were either DNA:PEI ratio of 1:2 or 1:3 and plasmid concentrations of either 2.5 or 5 µg/mL. Cell viability was checked after one day of incubation on a shaker (120 rpm, 37°C, 5% CO_2) and TN1 was added to a total concentration of 5 mg/mL per well . Transfected cells were incubated for 120h.

Since the proteins are expected to be secreted in the supernatant, cell suspension was centrifuged for 3 min, 8000xg. Supernatant was then used for TCA-precipitation, followed by SDS-PAGE and Western Blot.

2.1.18 Trichloroacetic acid (TCA)-precipitation

To detect proteins present at low concentration in a solution, TCA-precipitation was performed. For that purpose, 250 µL of TCA (Merck, Germany) was added to 1 mL of HEK293-6E cell supernatant. After 10 min on ice, the tube was centrifuged for 5 min, 14.000 rpm. Supernatant was discarded and the protein pellet was washed with 200 µL ice-cold acetone (ThermoFisher Scientific, Germany) and centrifuged again. This step was repeated and the supernatant was discarded again. Pellet was then dried by placing the tube with an opened cap on heat block for 2 min at 95°C. For subsequent protein analysis via SDS-PAGE and Western Blot, the protein pellet was resuspended in 50 µL Laemmli-buffer and heated for 7 min, 95°C.

2.1.19 Sm IPSE (and mutants) as well as IgE form recombinant protein expression and purification from HEK293-6E cells

IPSE/alpha-1 (*S. mansoni* and *S. haematobium*), its mutants and different IgE forms were recombinantly expressed for further experiments using the HEK293-6E expression system licensed from the NRC (National Research Council Canada, file 11565) (Plasmid Maps see Appendix). For medium and large-scale transfection, either 250 mL or 1 L vented flasks were used, placed on a shaker, respectively. For transient transfection, 45 - 400 mL HEK293-6E suspension cells were grown to a density of ca. 2 x10^6 cells/mL, viability was checked prior transfection and usually was about 97-99 %. To the cells, 5 mL medium containing 1 or 2.5 µg/mL plasmid (total volume of flask), previously mixed with medium containing 3 or 5 µg/mL PEI Max (1 mg/mL, Polyscience Inc., USA), respectively, was added. 24 h post transfection, tryptone N1 (TN1, TekniScience Inc., Canada) in culture medium (20% w/v) was added to a total concentration of 0.5 % (v/v), i.e. 5 g/L final concentration.

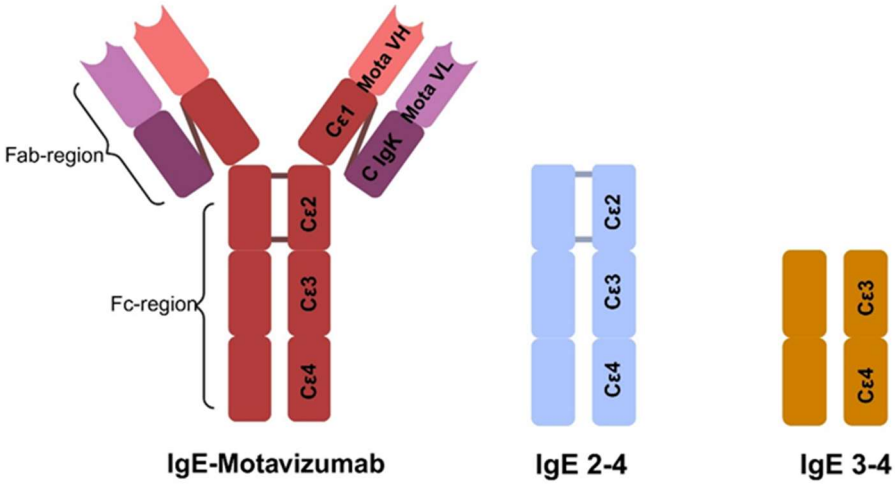

Figure 13 Strucure of different IgE forms. IgE-Motavizumab consists of the Cε 1-4 derived from human IgE, Ig κ light chain and the variable domain of motavizumab a humanized monoclonal IgG1 antibody targeting an antigenic site A on the fusion (F) glycoprotein of respiratory syncitial virus (RSV) (Cingoz, 2009). The truncated IgE forms IgE 2-4 and IgE 3-4 only comprise of the Cε2-4 and Cε3-4, respectively.

2.1.20 Protein purification with Immobilized Metal Affinity Chromatography (IMAC)

His-tagged recombinant proteins were harvested from cell-culture medium by centrifuging the supernatant at 3200 xg for 25 min, RT, followed by sterile filtration using a 0.22 µm filter. Subsequently, protein was purified by IMAC using 1 mL HiTrap (Ni^{2+}) column (Cytiva, USA) using an ÄKTA Start system. System was set to either concentration gradient with final concentration of 100% Elution Buffer or set to isocratic elution with 60% of Elution Buffer. Elution fractions were collected and further analyzed on SDS-PAGEs and Western Blot.

1X Binding Buffer (pH 7.4)

20 mM Sodium Phosphate

500 mM NaCl

20 mM Imidazole (≥99.5 %)

1X Elution Buffer (pH 7.4)

20 mM Sodium Phosphate

500 mM NaCl

500 mM Imidazole (≥99.5 %)

2.1.21 Stripping and Recharging the Hi Trap Column HP (1 mL, Cytiva)

When purifying different proteins, the Hi-Trap Column HP (1 mL, Cytiva, USA) was stripped and recharged between the purifications. This was done by washing the column once with ddH_2O (5 mL), followed by stripping it with Stripping Buffer (5 mL). The column was then washed with 5 mL Binding Buffer and 5 mL ddH_2O. To recharge the column, it was loaded with 1 mL 0.1 M $NiSO_4$ (Thermo Fisher Scientific, Germany). Residual Nickel was rinsed out with 5 mL ddH_2O. Eventually 5 mL Binding Buffer run through the column which was then ready to use.

Stripping Buffer (pH 7.4)

20 mM Sodium phosphate

0.5 M NaCl

0.05 M EDTA

2.1.22 Size exclusion chromatography

Size exclusion chromatography with a Hi Prep™ 26/60 S-100R (Cytiva, USA; recommended MW range 10-100 kDa) attached to the ÄKTA device was used to remove contaminants in the Sm IPSE (variant) samples. Before starting with this extra purification step, the column was pre-run with 160 mL ddH_2O, followed by two column volumes of PBS (640 mL). Then, marker proteins (Gel Filtration Marker Kit, Sigma/Merck , Germany) were diluted accordingly to the manufactures' advice and applied to the column to have peaks to compare protein sizes with. Subsequently, 1 mL filtered protein samples with concentrations between 0.5-1 mg/mL were applied using a 1 mL syringe. For the run, PBS pH 7.4 was used as running buffer. Only peak fractions were collected and afterwards concentrated with Pierce™ Protein Concentrator PES, 30K MWCO (ThermoFisher Scientific, Germany).

2.1.23 Bicinchoninic acid (BCA) Assay

To measure the concentration of the recombinantly expressed proteins, BCA-Assays using the Pierce™ BCA Protein Assay Kit (ThermoFisher Scientific, Germany) were preformed frequently. The assay was conducted according to the kit's instructions. For every single measurement, a standard curve with the attached BSA diluted in PBS (protein buffer) was recorded. Concentrations were calculated with the help of GraphPadPrism8.

2.1.24 Thermal Shift Assay

Thermal shift assay according to Bio-Rad ("Protein Thermal Shift Assays Made Easy with the Bio-Rad™ Family of CFX Real-Time PCR Systems – Protocol" Bulletin_7180.pdf (bio-rad.com)) was performed in order to provide information about the protein conformation of each IPSE mutant. This assay relies on SYPRO-Orange's ability to bind to the exposed hydrophobic core of proteins, once they are denatured. The dye emits a fluorescent signal when interacting with the temperature-induced unfolding of the protein. This then helps to estimate the proteins' melting point as it starts to unfold (see Bio-Rad protocol).

In this experimental setup, PBS and Lysozyme (1 mg/mL stock in ddH_2O) functioned as control. First, a stock solution of 50x SYPRO Orange (Merck, Germany) in ddH_2O was prepared, from which 8.2 µL was pipetted into a 1.5 ml Eppendorf tube. Then, 32.5 µL protein solution (0.15-0.45 µg/ml, in PBS pH 7.4) and 40.6 µL PBS pH 7.4 were added and properly mixed. 25 µL of each mix was pipetted in triplicates into a 96-well multiwell PCR plate (low profile, unskirted, clear) (ThermoFisher Scientific, Germany) and sealed with a microseal sealing film (adhesive, optical). Program: Bio-Rad C 1000 Touch™, Thermal Cycler CFX96™ Real Time System. Melt Curve, 10 - 95 °C in increments of 0.5 °C/10 secs. Assay was repeated at least three times. For data analysis the mean of every melt peak was used and values of the respective mutants were tested for significance using a T-Test against wild type data.

2.1.25 6x His-tag insertion into IgE λ via site-directed mutagenesis

To express and purify IgE λ via immobilized-metal affinity chromatography (IMAC) the plasmid pVITRO-102.1F10-IgE/λ (Addgene #50365 (Dodev et al., 2014) was used.

However, IMAC requires the insertion of a 6x His-Tag, performed via Q5 site-directed mutagenesis using the 6X His primers shown in table 2. In brief, Primer annealing was performed at 55°C, 57°C or 59°C for 30 sec and elongation was set to 7°C for 4 min. PCR products were applied onto an agarose gel and the expected band at 9000 bp was cut out and DNA was extracted with Monarch Gel Extraction Kit (New England BioLabs, USA). Neb5alpha *E. coli* cells (New England BioLabs, USA) were used for bacterial transformation. Transformed Neb5α cells were spread onto LB- agat plates containing 200 µg/mL HygrB and incubated over night at 37°C. Colonies were picked the next day and grown for Mini-prep, and purified plasmid was send in for confirmatory sequencing by MicroSynth Seqlab

2.1.26 IgE λ expression and purification

To express IgE λ, as described in section 2.1.19, HEK293-6E cells were transfected with pVITRO-102.1F10-IgE/λ 6x His.

Initially, a small-scale transfection was carried out using 3 µg plasmid with 9 µg PEI max in 2 mL cells (2 mio cells/mL). Subsequently, since the protein was expected to be secreted in the supernatant (secretion signal included in the IgE gene cassette) as described by Dodev et al., 2014, TCA-precipitation (see: 2.1.18.) was performed, followed by Western Blot for confirmation.

After realizing that the protein was expressed in the pellet, expression was scaled up to a 60 mL cell suspension. After the incubation of 4 days, the pellet was lysed via ultrasound (50%, 6x 5 sec, 1 min pause). Both, pellet lysate and supernatant were applied on the Hi trap column. A final attempt for expression was made by selecting for transfected HEK cells with 50 µg/mL HygrB for 14 days.

2.2 Functional assays for IPSE - IgE interaction

2.2.1 Fast Protein Liquid Chromatography (FPLC) for binding stoichiometry

To gain more insights into the binding stoichiometry of Sm IPSE to IgE and complexed IgE to FcεRIα, Fast Protein Liquid Chromatography (FPLC), in particular seize exclusion chromatography, was performed using a Superdex tm 200 10/300 GL (Cytiva, USA) column attached to the ÄKTA device. For that purpose, Sm IPSE and IgE or IgE-FcεRIα were incubated in the molar ratio 1:1 (same molarity) in PBS for 1h at 37°C. The samples were applied with a syringe, whereas PBS served as running buffer. The proteins were previously run on that same column, to be able to overlay the different curves.

2.2.2 Negative Staining to identify binding Sm IPSE domains in IgE via electron microscopy

To gain a better understanding of which domain in IgE is required for binding IPSE, negative staining technique was performed. In this method a heavy metal salt is used to enhance the contrast between the background and the protein's image, making the protein visible under the microscope. To that end, 5-8 µL of Sm IPSE, Sm IPSE-IgE mota, or Sm IPSE-IgE mota-FcεRIα (in TBS) were adsorbed on glow-discharged (30 sec), carbon-coated Electron Microscopy grids. After one minute, residual sample was rinsed off by holding the grids into a drop of mQ water. With the help of lint free paper, the grids were dried. Eventually, grids were incubated face down in 2 drops of 2% Uranyl aceteate and residual liquid was removed again with a lint free paper towel. EM images were obtained on JEOL 1400 electron microscope at 120 keV and recorded on a GATAN Ultrascan 4000 CCD camera with no binning.

2.2.3 Protein-Protein Interaction measurements with ELISA

To investigate the binding interaction of IPSE/alpha-1 to different IgE forms 15 µg/mL (75 µl per well) of different IPSE variants were immobilized on the surface of a 96-well-plate (ThermoFisher Scientific, USA) and incubated for 3h at 37 °C or O/N 4°C. Plates were blocked with 3 % BSA in PBST for one hour. Plates were then incubated for two hours with the respective IgE form in different concentrations (0.25, 0.5, 1, 2,

4, 8, 16, 32, 64,128, 256 and 512 nM). Tested IgEs were recombinantly expressed IgE motavizumab (consisting of the Cε 1-4 derived from IgE, Ig κ light chain and the variable domain of motavizumab an synthetical antibody originally IgG-motavizumabd IgG) form), 3-4 IgE and 2-4 IgE and Bio-Rad IgE λ (Bio-Rad Laboratories, Germany). After three washing steps with PBS, the plate was incubated for 1h with anti-human IgE Mouse mAB conjugated to HRP [B3102E8] (Abcam, USA) at 37 °C. 70 µL TMB substrate (BioLegend®, USA) was used to develop and reaction was stopped with 70 µL 2M sulforic acid (Thermo Fisher Scietific Inc., Germany). Finally, absorbance was measured at 450 nm in a CLARIOstar Plus plate reader system (BMG LABTECH GmbH, Germany).

2.2.3 Biolayer Interferometry (BLI) with Sm IPSE and IgE motavizumab to ascertain the bimolecular interaction kinetics

In order to gain more knowledge about the kinetics and bimolecular interactions on a basis of wave interference between Sm IPSE and IgE, Biolayer Interferometry (BLI) was carried out in two different setups. The BLI is based on the idea that the one of the binding partners (ligand) is immobilized on the biosensor, while the other interaction partner is kept in solution (Müller-Esparza et al., 2020). To start the measurement, the biosensor is immersed into the protein-containing solution for a certain period of time, whereupon the other binding partner starts to associate with the immobilized protein, which eventually leads to the generation of specific layer at the tip of the biosensor. Hereby, two separated surfaces are created. One of them contains the protein itself and the other one the protein interacting with the ligand immobilized on the sensor tip (Schasfoort, 2017). That, in turn, leads to the creation of a thin-film interference in which the generated layer appears as a thin film being bound by these two surfaces. Ultimately, an external light source shines at the biosensor tip and the light reflected off the surfaces, thus resulting in two reflection patterns displaying different intensities (Müller-Esparza et al., 2020; Schasfoort, 2017).

For the first set-up, streptavidin Octet® SA Biosensors (Sartorius AG, Germany) were incubated with 20 nM biotinylated recombinant IgE motavizumab (provided by the group of Prof. Dr. T. Jardetzky) in PBE (PBS with 0.1% BSA, 2.5 mM EDTA 0.05 % Tween-20). For the assay, different dilutions of Sm IPSE WT and Sm IPSE T92Y/R127L (32, 64, 128, 256, 512 and 1024 nM or 256, 512, 1024, 2048 and 4096 nM) in PBE were used. The Biacore™ system, (Surface Plasmon Resonance/ BLI

tools, Cytiva, MA, USA) setup included a 100 sec association and a 100 sec dissociation time or 200 sec association and 200 sec dissociation, respectively.

For the second set-up, Octet® Ni-NTA Biosensors (Sartorius AG, Germany) were loaded with 50 µg/mL Sm IPSE. Previously TEV-cleaved IgE mota (TEV-cleavage of 2.2 mg igE mota O/N with 50 µL of 1.2 mg/mL TEV-protease plus 0.6 µL β-mercaptoethanol) was used as interaction partner in different dilutions, namely 32, 64, 128, 256, 512 or 1024 nM. Samples were prepared in filtered PBS supplemented with 0.1% BSA and 0.05% Tween-20. Biacore™ system settings were set to Baseline 120s, association 360 sec, dissociation 600 sec, loading 600 sec and association 360 sec (shake speed 1000).

2.2.4 Reporter Cell Assay with RS-ATL8 humanized basophilic rat leukemia cells to test for IgE binding capacity of IPSE (mutants)

A reporter cell assay with RS-ATL8 humanized basophilic rat leukemia cells was performed to detect basophil activation enabled by binding of Sm IPSE variants to IgE.

Originally, these humanized rat basophilic leukemia cells (RBL) were established for monitoring of specific allergen (allergen-specific IgE) sensitization in human patient serum (Nakamura et al., 2010; Wan et al., 2014). RBL cells are humanized with at least the human alpha chain of the IgE high affinity receptor FcεRI and further stably transfected with a nuclear factor of activated T cells (NFAT)-responsive luciferase gene construct (Falcone et al., 2015; Hogan et al., 2003; Hutchinson & McCloskey, 1995; Taudou et al., 2009). This method relies on IgE crosslinking-induced, NFAT-dependend expression of firefly luciferase, leading to a measureable luminescence after adding a specific luciferase substrate (Figure 14) (Falcone et al., 2015; Nakamura et al., 2010). The detailed underlying mechanism is, that following FcεRI-depending activation of the cells, NFAT translocates to the nucleus (Hutchinson & McCloskey, 1995). The translocation itself is a consequence of the elevated calcium influx from the extracellular environment and the subsequent activation of calmodulin-dependent enzymes which lead to calcineurin activation and dephosphorylation of NFAT (Hogan et al., 2003). The process of dephosphorylation eventually results in unmasking of a hidden NLS and masking of a nuclear export signal, guiding NFAT to the nucleus, where it binds to specific promoters. This leads to the activation of the reporter gene, hence in the transcription of luciferase mRNA and the synthesis of luciferase after reching the cytosol (Falcone et al., 2015).

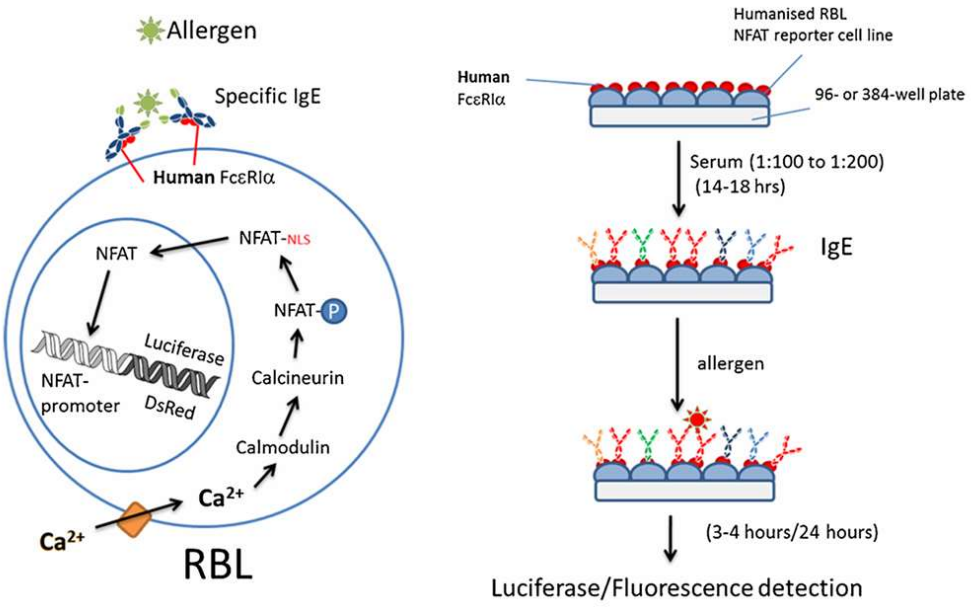

Figure 14 Schematic diagram showing the main principle underlying the RBL reporter systems. Different reporter cell lines (this case RS-ATL8) are incubated over night either with human sera containing high levels of IgE, or recombinantly expressed IgE. The next day, they are stimulated with suspected allergens (in this case IPSE forms). In the presence of intact IgE, FcεRI crosslinking by the allergens/antigens will result in activating a signal transduction cascade ultimately resulting in the nuclear translocation of NFAT, which activates the reporter gene such as luciferase. Activation can be measured after 3 h in the case of luciferase (or after 16–24 h in the case of DsRed fluorescent protein) as reporter (Falcone et al., 2015).

To that end, the density of RS-ATL8 humanized basophilic rat leukemia cells was adjusted to $1x10^6$ cells/mL in cell-culture medium. They were subsequently sensitized over-night using 1:100 heat-inactivated (5 min, 56 °C) patient serum containing IgE or 70 ng/mL of recombinantly expressed IgE form or IgE λ (Bio-Rad# HCA 171), respectively. Thereafter, 50 µL/well were seeded in white 96-well Lumitrac 600 plate and incubated (at 37 °C and 5% CO_2) for 18 h.

The next day, different stimuli (IPSE wild type and mutants) and positive controls, concanavalin A (1 mg/mL, Type VI, Sigma) and Goat anti-Human IgE polyclonal antibody (Chemicon, Merck, Germany), were prepared in phenol-red free medium (supplemented with standard concentrations of L-Glut, P/S, FCS). The following concentrations, 10/1/0.1/0.01 µg/mL, were used in case of the wild type IPSE *S. mansoni* and *haematobium*), the mutants and the control α-IgE. For concanavalin A (Sigma-Alderich/Merck , Germany) only 10 µg/mL were used. Prior to the addition of the stimuli, the cells were washed 1x with PBS to remove unbound IgE, then, stimuli as well as controls were added in 50 µL/well in quadruplicates. Phenol-red free MEME

medium (Gibco) without any stimulus served as negative control. After 3 h of incubation, plates were taken out of incubator for another 15 min in order to equilibrate to room temperature. Then, 50 µl ONE-Glo® Luciferase Assay System substrate (Promega GmbH, Germany) was added to each well. Luminescence (580 nm) was directly measured with the help of Clario-Star^{Plus} (BMG LABTECH GmbH, Germany).

Obtained values were evaluated with the help of Graph Pad Prism 8. Significance was tested/Different stimuli were analyzed with One-way Anova against negative control (non-stimulated cells). Additionally, significance between Sm IPSE and the other variants, was determined using an ordinary T-Test.

Reporter Cell assay was repeated at least three times for each IPSE mutant and IgE form.

2.3 Functional assays for IPSE-host cell interaction

2.3.1 Immunofluorescence microscopy to determine cellular uptake dynamics of Sm IPSE

To determine the dynamics of IPSE uptake in the host cell, immunofluorescence microscopy with different cell lines and incubation times was conducted. For that purpose, HepG2, HCT-116 and CHO-Trvb cells were seeded in 12-well plates (0.2 x 10^6 cells per well) onto Poly-L-Lysine coated coverslips (Corning GmbH, Germany) and grown to 90-100% confluence. Samples were then treated for 3 h with 2.5 µg/well recombinant Sm IPSE. Cells, either treated with the primary or the secondary antibody after IPSE incubation, as well as a sample treated with both antibodies but no IPSE, served as controls. After incubation, coverslips were washed once with PBS and subsequently fixed for 20 min with 4% Paraformaldehyde (ThermoFisher Scientific, Germany). Thereafter, samples were washed twice with PBS and permeabilized in 0.2% (v/v) Triton-X 100 (Merck, Germany) in PBS for 30 min. After another washing step and blocking in 3% BSA (in PBS) for 40 min at room temperature, the coverslips were placed upside-down onto 100 µL drops of either a monoclonal Anti-6xHis tag antibody produced in mouse (1:200, Merck) or anti-IPSE antibody (1:100, 0.5 mg/mL, kindly provided by Gabriele Schramm) in 3% BSA in PBS over night at 4°C. The next day, coverslips were again washed 3 x and incubated with the second goat-anti mouse IgG-Alexa Fluor 488 (1:200, Invitrogen, ThermoFisher Scientific Germany) antibody for 2h, RT. Lastly, coverslips were washed again 3 x and nuclei were counterstained for 20 min staining using Hoechst 33342 (1:1000, Invitrogen, ThermoFisher Scientific, Germany). Concluding one final washing step with ddH2O, the coverslips were mounted with one drop of ROTI®Mount FluorCare mounting-medium (Carl Roth, Germany) sealed with nail polish. Confocal images of the different samples were acquired with a Leica TCS SP5 confocal microscope (software LasX1.4.6). As staining controls, Sm IPSE treated cells just stained with secondary antibody were used.

2.3.2 Confocal microscopy using fluorogenic biarsenical dye FlAsH-EDT2-conjugated Sm IPSE for localization in the host cell

To localize Sm IPSE in the host cell, recombinant Sm IPSE bearing a specific tetracysteine tag – termed Sm TC-IPSE - was expressed and purified as described in section 2.1.19 and made visible using fluorogenic biarsenical dye FlAsH-EDT2. The

method is based on the binding of a tetracysteine tag-containing peptide (CCXXCC) binding to a small fluorescein derivative, known as fluorescein arsenical hairpin binder (FlAsH). Here, the non-fluorescent FlAsH is complexed to ethaneditiol (EDT) and only becomes fluorescent when binding to the aforementioned amino acid sequence (Griffin et al., 1998; Hoffmann et al., 2010). The benefit of this method is, that labelling of proteins can be achieved in intact cells and that the the dye is stable and might last for hours (Hoffmann et al., 2010). The small size of the tag makes it less likely to interfere with the protein's binding properties.

For the labelling purpose, the protocol of Hoffmann et al. 2010 was used as guideline. HCT-116 cells were seeded onto coverslips (0.2 x 10^6 cells per well) in a 12-well plate and grown to confluence. First, cells were treated with 2.5 µg Sm TC-IPSE in culture medium for 3 h (37°C, 5% CO_2), followed by two washing steps with DPBS (Corning, Germany). Meanwhile, a 25 mM 1,2-Ethanedithiol (EDT_2; Merck, Germany) stock solution (dissolved in DMSO ThermoFisher Scientific, Germany) was freshly prepared, from which 1 µL was taken and added to 1 µL FlAsH (1.5 mM) (Cayman Chemical, USA) for each sample to be labelled and incubated 5 min RT. Next, from 1 mL PBS (per sample), an aliquot of 100 µL was taken, added to the FlAsH-EDT_2 suspension and vortexed. The solution was then added onto the washed cells and incubated for 1h (37°C, 5% CO_2). To get rid of any residual dye, cells were washed twice à 5 min (37°C) with 2 mL of washing solution consisting of 12.5 µL 500 mM EDT_2 (dissolved in DMSO) in 25 mL PBS. Samples were washed again with PBS and fixed with 4% PFA for 20 mins, followed by 20 min counterstaining with Hoechst 33342 (1:1000). Coverslips were mounted with one drop mounting medium on slides and fluorescence microscopy pictures were taken with the confocal microscope. Cells treated with only Sm TC-IPSE or FlAsH-EDT_2 served as negative control.

2.3.3 Flow cytometry-based internalization assay to measure the cellular uptake of fluoro-labelled Sm IPSE

To understand the interaction of Sm IPSE with host cells multiple functional assays were performed. Accordingly, the uptake and internalization of IPSE was initially screened via a flow cytometry-based internalization assay using fluorescently labelled Sm IPSE, as described in the following.

2.3.3.1 IPSE labelling

As a first step, recombinant IPSE, expressed and purified as described above, was fluoro-labelled with the DyLight® 488 Conjugation Kit (Fast) – Lightning-Link® (Abcam; USA) according to the manufacturer's protocol using 100 µL of 1.3 mg/mL Sm IPSE. In short, 10 µL modifier reagent was added to 100 µL protein solution and gently mixed by pipetting. Then, the mixture was added the lyophilized material of the DyLight® 488 Conjugation Mix and resuspended by pipetting up and down twice. This was followed by 15 min incubation at room temperature in the dark. Afterwards, 10 µL quencher was added to the solution. The conjugated protein was stored at 4°C. The conjugation efficiency was confirmed by Nanodrop measuring at 488 and 280 nm.

2.3.3.2 Internalization Assay

CHO-Trvb, HCT-116 and HepG2 cells were seeded one day prior the assay into 12- or 6-well plates (0.2×10^6 or 0.4×10^6 cells per well, respectively). The next day, when cells reached full confluence, medium was removed and replaced with normal cultivation medium (1 mL for 12-well plate and 2 mL for 6-well plate) containing either 1.5 µg/mL Sm IPSE- DyLight488 or hTRF-FITC (2 mg/mL, Jackson ImmunoResearch Europe) serving as internalization control. After an incubation of 3h (37°C, 5% CO_2), cells were scraped off the plates, gently transferred to tubes and centrifuged for 4 min at 350 xg. Supernatant was removed and the pellet was washed in PBS and centrifuged again. Subsequently, the supernatant was once again discarded and cells were resuspended in either 500 µL PBS (unquenched) or 500 µl 1:4 (0.4%) Trypan Blue-PBS solution (Merck, Germany) (quenched). Subsequently, fluorescent signal corresponding to IPSE internalization was detected by flow cytometry (BD FACSCelesta™, BD FacsDiva). The underlying principle for that is the ability of the flow cytometer to measure the light scattering, and the fluorescence observed when cells are passing in a stream through laser beam. Depending on their fluorescent properties, cells are subsequently "sorted" in different populations. As Sm IPSE was previously fluoro-labelled, cells internalizing IPSE should emit a higher fluorescent signal than untreated cells. Quenching of cells with Trypan Blue is intended to block the fluorescent signal of residual fluoro-labelled protein on the cell surface (i.e. protein attached to the cell membrane). As Trypan Blue does not cross the cell membrane, it cannot lead to unwanted quenching of the inner fluorescent

signal that is derived from internalized fluoro-labelled protein. Obtained values can thus be compared and used as a tool to determine protein-uptake efficiency.

For each run, the cytometer was setup and calibrated using BD FACSDiva™ CS&T Research Beads (BD Bioscience, Heidelberg). Data were analysed using FlowJo v10.

To investigate routes of protein uptake (e.g. receptor-mediated endocytosis or entry as cell penetrating peptide), further experimental set-ups using HCT-116 cells included a 15 min incubation on ice prior to conducting the assay. Here, all following steps were performed in ice-cold medium or PBS and cells were incubated and centrifuged at 4°C keeping the samples on ice throughout the entire processing.

2.3.4 Bulk RNA sequencing of Sm IPSE treated HepG2 cells

To determine the consequences of Sm IPSE on the host transcriptome Bulk RNAseq was performed. RNA-seq stands for RNA sequencing and is a highly sensitive method based on Next Generation Sequencing. This technology is the gold standard for studying gene expression and transcriptomic landscapes in biological systems. To that end, HepG2 cells were seeded into 6-well plates that was pre-treated with rat-tail collagen (0.35 mg/mL, kindly provided by the group of Dieter Glebe, Justus Liebig University Gießen) by covering the entire surface of the well, one day prior and grown until 90% confluence. Cells were harvested by scraping and total RNA was isolated using the Monarch® Total RNA Miniprep Kit (New England Biolabs®, USA), which includes an additional on-column DNase I digestion step provided by the kit. The purified RNA was eluted with 50 µl RNase-free H_2O. RNA concentration and quality was immediately checked with Nanodrop. To have an extra quality control, 1 µg of total RNA was loaded on a 1 % agarose gel for gel electrophoresis. cDNA synthesis and the following RNA-seq was performed by the group of Marek Bartkuhn, JLU-Gießen. The obtained samples were sequenced using an Illumina NovaSeq6000. Files were written out in BCL format and demultiplexed into individual FASTQ files for each sample with bcl2fastq v2.20 according to manufacturer's instructions. Primary data from RNA-seq was processed by Tobias Friedrich and Marek Bartkuhn. First, raw FASTQ files were adaptor trimmed using trimGalore v.0.6.5 (Krueger, 2019). The sequencing adaptors to trim were detected automatically, no further parameters were set. In the second step of the primary analysis reads were aligned to the human reference genome hg19 (downloaded from Illuminas' iGenome website: https://emea.support.illumina.com/sequencing/sequencing_software/igenome.html) with Hisat2 v.2.2.1 (D. Kim et al., 2019). Hisat2 was used with the parameters "-k 1 -

-min-intronlen 30 --max-intronlen 3000". The resulting SAM files were converted into BAM files with Rsamtools v2.12.0 (Morgan et al., 2017). Following that, PCR duplicates were removed with Picard tools' (v2.21.9) *MarkDuplicates* applying the parameters "REMOVE_SEQUENCING_DUPLICATES = true REMOVE_DUPLICATES = true".

Subsequent data (secondary analysis) was further analysed in R v.4.2.1 (R Core Team 2023). The alignment locations from the primary analyses were annotated using a GTF file (downloaded from Illuminas' iGenome website: link above). For the GTF to TxDb conversion the *makeTxDBfromGFF* function from the GenomicFeatures v1.48.3 package (Lawrence et al., 2013) was used. Exonic positions in the genome were extracted from the TxDb object and stored as a GRanges object (GenomicRanges v1.48.0) (Lawrence et al., 2013). The absolute numbers of reads mapped to exons were counted with the *summarizedOverlaps* function ("mode = 'Union'") (GenomicAlignments v1.32.0) and subsequently used as input for DESeq2 v1.36.0 (Love et al., 2014) to determine differentially expressed genes. For that, DESeq2 first normalizes the expression of genes across all samples. Genes with a $\log_2$fold change (FC) < -1 or > 1 and adjusted p-value (Benjamini & Hochberg, 1995) < 0.05 were determined as significantly deregulated.

Heatmaps depicting differentially expressed genes (DEGs) were plotted with ComplexHeatmap v2.20.0 (Gu, 2022).

Gene set enrichment analysis (GSEA) and over representation analysis (ORA) pathway analyses were performed with clusterProfiler v4.4.4 (Yu et al., 2012). For that, Gene Symbols were first translated into Entrez Gene IDs with *bitr*. As data bases for ORA and GSEA Gene ontology (GO) or Kyoto encyclopaedia of genes and genomes (KEGG) were used.

Over-Representation Analysis (ORA) and Gene Set Enrichment Analysis (GSEA) are both methods used to identify whether predefined sets of genes show statistically significant, concordant differences between two biological states. ORA uses a set of genes defined by specific cut-off parameters, such as the log2fc and the p-value. In contrast to that, the GSEA uses all genes for which expression information is available, but ranked for their change in expression levels between treatment and control. Gene Ontology (GO), the Kyoto Encyclopedia of Genes and Genomes (KEGG) and Reactome are databases in which pathways or "GO terms" for various biological processes, developmental mechanisms, signal transduction and much more are manually curated for multiple organisms. These pathways each comprise of multiple genes known to play key roles in the individual annotated processes. ORA

determines if a predefined set of genes is represented more than expected by chance in these pathways. GSEA, on the other hand, evaluates whether the genes from the pathway are in general up or down regulated across all measured genes. All in all the key difference is that GSEA uses all genes in contrast to ORAs gene list determined by predefined thresholds. Therefore, GSEA provides a more sensitive analysis than ORA, but both methods complement each other.

For the ORA, the universe of genes to consider were those with at least one read in one of the samples. In case of the GSEA all genes were used after being ranked by their Wald test statistic in a decreasing manner.

Bar plots depicting ORA and GSEA results were plotted with ggplot2 v3.3.6 (Wickham, 2016).

2.3.5 Electrophoretic Mobility Shift Assay (EMSA) to determine DNA binding capacity of IPSE

2.3.5.1 General binding capacity of Sm IPSE to DNA

To investigate whether Sm IPSE and its NLS-mutants bind to DNA, a simple binding experiment using EMSA was conducted using a NEB ladder as DNA template. For that purpose, a 7% Native PAGE (lacking SDS) (2.1.13) was poured and pre-run for 2h, 125 mV in 1x TBE, in order to remove all traces of APS, a constant temperature of the gel and an even distribution of buffer was pursued. Samples were prepared by mixing 5 µL 100 bp (New England BioLabs®, USA) and TriDye 10 bp DNA ladder (Promega GmbH, Germany) with 10 µL of the respective protein (1 µg, 2.5 µg or 5 µg, in PBS pH 7.4) and filled up to total volume of 20 µL with 1x TBE. The mixture was incubated for 1h at 37°C. Subsequently, samples were applied onto the PAGE and gel the gel run for 1h, 125 mV, 4°C. The gel was treated with ethidium bromide (5 µl of 10 mg/mL in 100 mL ddH_2O) 30 min shaker to be able to visualize the bands.

2.3.5.2 Hybridization of Sh IPSE-bound oligonucleotides

Since the group of Dr. Michael Hsieh (George Washington University, USA) was already able to show binding activity of Sh IPSE to specific DNA fragments (unpublished data), it was anticipated to test whether Sm IPSE also binds to these sequences.

More specifically, binding data had been obtained by the collaborating laboratory of Trevor Siggers, Boston University, using a Universal Protein Binding Microarray (UPBM) approach. These are oligonucleotide arrays designed identify transcription-factor binding site specificities. This work had identified GGGCGGGG as a target sequence for H03 and H06-IPSE (unpublished data). This is a motif known to be recognised by the transcription factor Sp1 (Vizcaíno et al., 2015).

To that end, two forward and two reverse oligonucleotides with a size of 60 nucleotides (table 3) were ordered from Genscript, including one in Sh IPSE positive and one negative tested oligonucleotide. The oligonucleotides were dissolved in 100 µM Hybridisation Buffer by mixing. Thereof, 10 µM stocks were prepared. For hybridisation, 20 µL of the respective forward and reverse oligonucleotide were mixed 1:1 and incubated in a PCR cycler (2 min 95°C, 2 min 25°C and ∞ 4°C). Samples were afterwards separated in a 2% agarose gel.

Table 3 List of oligonucleotides used for hybridisation.

Name	Sequence
Good_H03_s1 F	AGTGGGCTTAATGGTAGGGCGGGGTGGGCCATGAGAGTCTGTGTTCCGTTGTCCGTGCTG
Good_H03_s1 R	CAGCACGGACAACGGAACACAGACTCTCATGGCCCACCCCGCCCTACCATTAAGCCCACT
Bad_H03_s1 F	AGTGGGCTTAATGGTACAATCATATGGGCCATGAGAGTCTGTGTTCCGTTGTCCGTGCTG
Bad_H03_s1 R	CAGCACGGACAACGGAACACAGACTCTCATGGCCCATATGATTGTACCATTAAGCCCACT

Hybridisation Buffer

10 mM Tris-HCl (pH 7.5)

50 mM NaCl

1 mM EDTA

2.3.5.3 EMSA of Sh IPSE-bound oligonucleotides and Sm IPSE (NLS-mutants)

To see if the EMSA setup itself works, it was tested with Sh06 IPSE as positive control leaning on the results of Dr. Hsiehs' group. Therefore, the hybridized oligonucleotides were diluted to either 1 or 0.1 µM and the same molarity of Sh06 IPSE was then added 1:1 (8 µL + 8 µL) and incubated 37°C for 60 min. As described above, a 7 % native gel was pre-run at 4°C, 2h in 0.2x TBE Buffer before applying the samples and running the gel 1:45 h at 4°C, 100 mV. BSA served in these experiments as negative control. The EMSA of Sm IPSE and its NLS-mutants was subsequently performed as previously described.

5 mL native PAGE stacking gel

4.445 mL 375 mM Tris-HCl (pH 8.8)

0.5 mL Acrylamide/Bis-acrylamide (30%/0.8% w/v)

0.05 mL 10% (w/v) ammonium persulfate

5 µL TEMED

10 mL native PAGE separating gel (7%)

8.14 mL 375 mM Tris-HCl (pH 8.8)

1.75 mL Acrylamide/Bis-acrylamide (30%/0.8% w/v)

0.1 mL 10% (w/v) ammonium persulfate

10 µL TEMED

2.3.6 Fluorescence microscopy assays of Sm IPSE binding to importin-alpha

To find out whether Sm IPSE binds to importin-α to enter the host cell nucleus, co-transfections of importin-alpha and Sm IPSE were performed. To that end, RS-ATL8 rat basophilic leukemia cells were pre-transfected with pDsRed-importin-alpha (Addgene cat# 119679, (Sugimoto et al., 2002) by growing until confluence in 6 well plates and subsequent transfection via PEI as follows. After replacement of the cultivation media with 400 µL fresh medium, per well, 200 µL medium (w/o supplements) containing 2.5 µg pDsRed-importin-α or GFPq pTT0 (negative control)

and 200 µL medium (w/o supplements) with 5 µg PEI Max were prepared and then mixed together by pipetting 3 times up and down. The PEI-DNA solution was incubated for 10 min, RT. Subsequently, it was added drop per drop to the cells. After 1.5 h, 200 µL normal cultivation medium was added. 24h after transfection, medium was exchanged with normal medium mixed 1:1 with selection medium (1 mg/mL G418). The following days, fluorescence was observed on a regularly basis and medium was changed to 100% selection medium.

Finally, to determine Sm IPSE binding to importin-α, the transfected RS-ATL8 cells were seeded at $0.15x10^6$ cells per well into a 24-well plate and grown to 95% confluence. Cells were then treated with 1.25 µg recombinant Sm IPSE. To see a possible shift of the fluorescent signal of importin-α towards the perinuclear region, indicating binding, cells were observed under the microscope (Leica Model DMIL LED Fluo) at different time points (0, 10, 20, 30 and 60 min).

3. Results

3.1 Establishment of basic experimental conditions

3.1.1 Optimal transfection conditions of HEK293-6Esuspension cells with (TC-)Sm IPSE pTT5 for Sm-IPSE expression

The optimal transfection conditions of HEK293-6E suspension cells with C-terminal tetracysteine Sm IPSE (C TC-IPSE) and N-terminal tetracysteine Sm IPSE (N TC-IPSE), as representatives for pTT5 IPSE plasmids, were determined by evaluating different PEI-DNA ratios and plasmid concentrations. To obtain a relatively fast feedback, whether transfection itself was working and to exclude loss of transfection capacity due to non-functioning detergents or impaired cells, GFPq pTT0 was included as control. GFP expression can already be detected (microscope) after a few hours post transfection. 120h after transfection and subsequent TCA-precipitation of the different cell supernatants, Western Blots (Figure 15) revealed that only C TC-IPSE, and not N TC-IPSE, was successfully expressed in the conditions tested, whereas no bands were detected for N TC-IPSE. Moreover, it appears that C TC-IPSE is expressed most efficiently when using 2.5 µg/mL plasmid DNA with both PEI-Max : DNA ratios of 1:2 or 1:3 (Figure 15 A + B). In case of 5 µg/mL of plasmid, in both ratios, the protein was expressed as well, but less efficiently than at 2.5 µg/mL plasmid.

Conclusively, all following transfections with IPSE pTT5 plasmids in HEK293-6Ecells were subsequently conducted with the maximum plasmid concentration of 2.5 µg/mL.

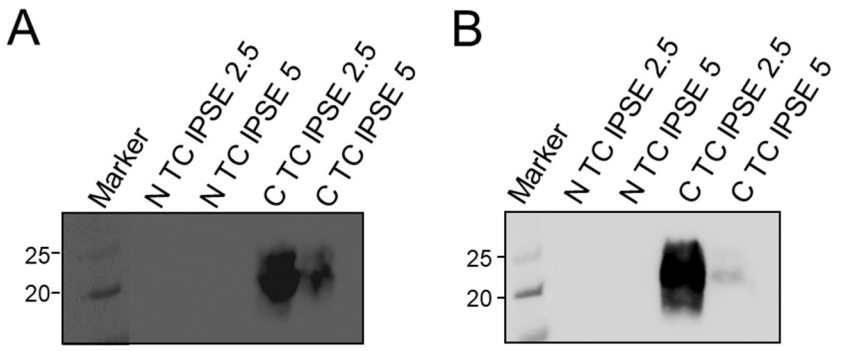

Figure 15 Expression of recombinant proteins after transfection with different DNA:PEI ratios. Western Blot images show supernatants of the transfected HEK 293-6E cells after TCA-precipitation. (A) Transfection of cell with a PEI-Max-DNA ratio of 2:1 and plasmid concentrations of 2.5 and 5 µg/mL. Supernatant was harvested after 120h. N TC IPSE = NTC- Sm IPSE and C TC IPSE = CTC-Sm IPSE. (B) Transfection of cells with a PEI-Max-DNA ratio of 3:1 and plasmid concentrations of 2.5 and 5 µg/mL. Supernatant was harvested after 120h. N TC IPSE = NTC- Sm IPSE and C TC IPSE = CTC-Sm IPSE

3.1.2 Generation of a specific antibody against Sm IPSE and Sh IPSE

3.1.2.1 Testing of pre-bleeder and after 3rd immunization serum

Since five mice were immunized for generating an antibody detecting IPSE of all Schistosoma species employed in this project – *Schistosoma mansoni* and *haematobium (Sm, Sh03,Sh06)*, sera before ("pre-bleeding") and after the third immunization were tested for the presence of specific antibodies using Western Blot.

As expected, the Western Blot (Figure 16 A) shows that "pre-bleeder" serum does not contain any IPSE-detecting antibody or residual in four out of five mice (AB2, AB6, AB8, AB10). Notably, in case of Mouse 2 (AB4), unspecific bands were detected, whereby none of the IPSE types should be detected at all. To confirm these results, the blot was repeated, verifying that the AB4 "pre-bleeder" serum was also naïve. When blotting the "after 3rd immunization" sera, it became clear that serum of Mouse 4 (AB7) was strongly positive for all three IPSE types (Sm, Sh03, Sh06), whereas Mouse 2 (AB3) serum only showed clear bands in Sh03 and Sm IPSE and a faint band for Sh06 IPSE. Mouse 1 (AB1) only recognized Sh03 IPSE (Figure 16 B). Therefore, mouse 4 (AB7) was selected for antibody and hybridoma cell line production by Genscript.

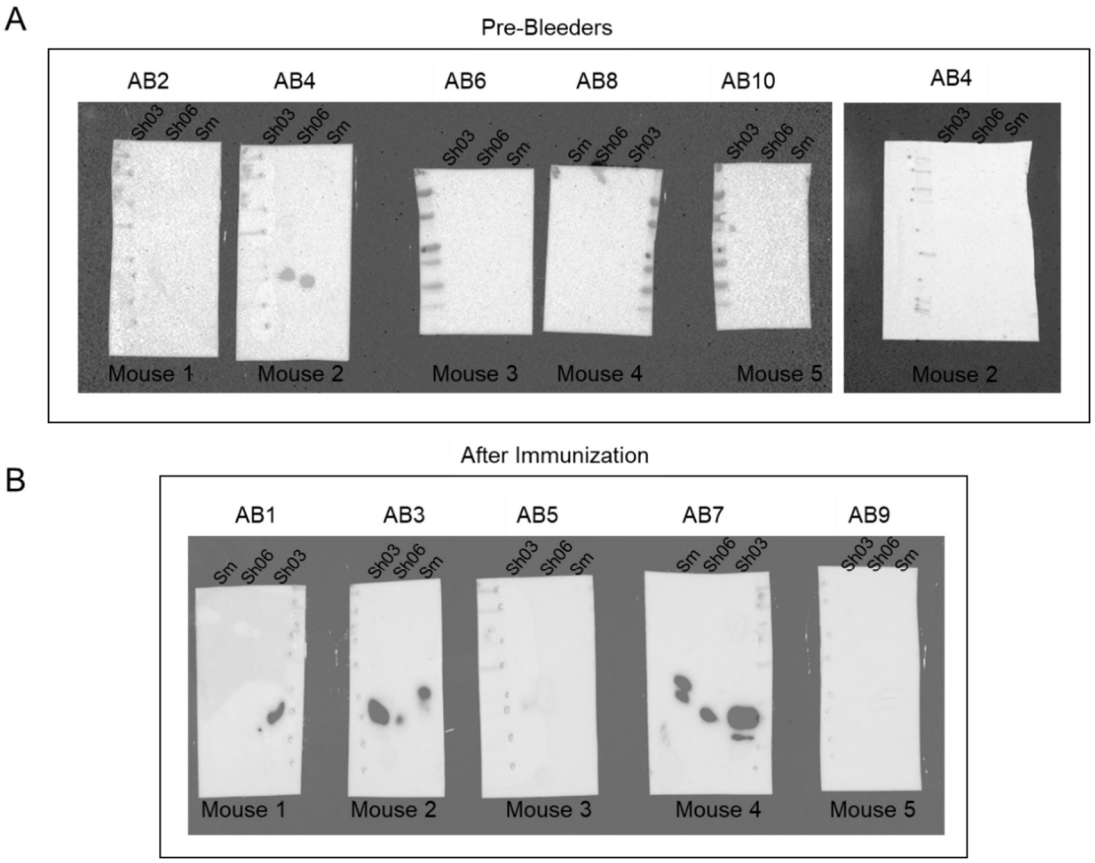

Figure 16 Testing of different mouse sera potentially containing monoclonal anti-IPSE antibody. (A) Western Blots treated with five different “pre-bleeder” sera of mice prior to antigen inoculation. (B) Western Blots showing different binding affinities sera isolated from five mice after 3 immunizations with IPSE. Samples applied in the order Sm, Sh06, Sh03. Showing that Mouse 1 AB1 serum only detects Sh03 IPSE, Mouse 2 AB3 binds to all types but with a significantly lower affinity as Mouse 4 AB7 showing the strongest bands in all three IPSE orthologues.

3.1.2.2 Testing of hybridoma cell line supernatants containing anti-IPSE antibody

Mouse 4 was used to generate hybridoma cell lines to produce monoclonal antibodies. To determine the antibody of best suitability, supernatants were tested as previously described. Here, Western Blot results revealed that in case of Sh03 IPSE all but one Clone (ID 11D2-2) failed to detect any IPSE species (Figure 17 A). All other hybridoma clones, Clone ID 12E4-1 and 2, Clone ID 3F11-2 and 2, Clone ID 11D2-1, Clone ID 1E4-1 and 2, seemed to express an anti-IPSE antibody recognizing both the Sh03 IPSE. However, hereby Clone 1E4-1 and 2 lead to the strongest signal. For Sm IPSE, only Clone 1E4-1 and 2 showed any signal (Figure 17). Beyond that, the expression of clone number 2 was strongest. All negative controls behaved as

expected. Therefore, it was decided to purify the antibody of the hybridoma cell line Clone ID-1E4-2.

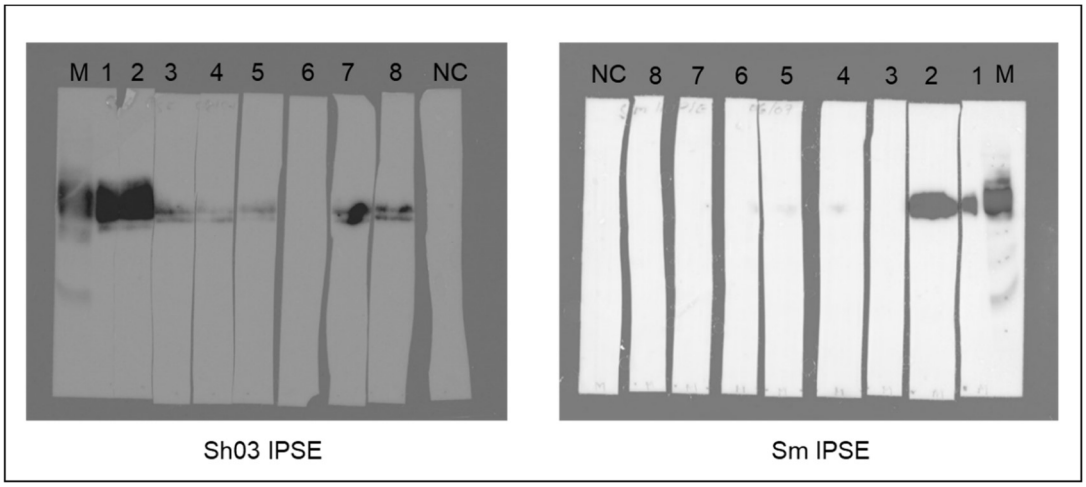

Figure 17 Western blots of Sh03 IPSE and Sm IPSE to detect Anti-IPSE-antibodies within the respective hybridoma cell line supernatant. 1 = Clone ID: 1E4-1, 2 = Clone ID: 1E4-2, 3 = Clone ID: 3F11-1, 4 = Clone ID: 3F11-2, 5 = Clone ID: 11D2-1, 6 = Clone ID: 11D2-2, 7 = Clone ID: 12E4-1, 8 = 12E4-2. M= Marker (Full Range Rainbow). Application of 1:5 supernatant dilution in 5 % (w/v) skimmed milk in TBST. Western Blot conducted with Sh03 samples showing that all clones, except for Clone ID 11D2-2 can detect the protein B Western Blot performed with Sm IPSE revealing that only Clone 1E41-1 and -2 are able to bind and detect the protein of interest.

3.1.2 Generation of Sm IPSE mutants using site-directed mutagenesis

Based on the knowledge that the SmCKBP is not able to activate basophils to degranulate and release histamine, IL-4 and IL-13 as well as the assumption that a dimeric protein is necessary for basophil activation (Smith et al. 2005; Meyer et al. 2015), six different mutants were created with the help of site-directed mutagenesis. The following mutations of the wild type were desired: single mutants C132A, T92Y, R237A, R237L, and double mutants T92Y/R237A, T92Y/R237L. Moreover, an IPSE with mutated NLS (NLS-AAA) was generated. To that end, after plasmid isolation, the pTT5 plasmids bearing the desired mutation were sent for Sanger sequencing to confirm their sequence. Here, obtained sequences were evaluated by aligning them to the template Sm IPSE pTT5 map with the help of the SnapGene software. All desired mutations were successfully generated, as depicted in Figure 18. Figure 18 A displays the chromatogram of the sequence bearing a single amino acid change from Cysteine to Alanine at position 132 (C132A, TGC > GCC). Successful mutagenesis was also achieved with changing Threonine 92 to Tyrosine (T92Y, ACC

> TAC) (Figure 18 B). Figure 18 C shows the sequence of the successfully inserted mutation from Arginine 127 Leucine (R127L, CGG > CTG), and finally Figure 18 D the chromatogram of Arginine 127 Alanine (R127A, CGG > GCC). Above that, the chromatogram represented in Figure 18 E demonstrates all the changes from triple Arginine to triple Alanine within the NLS (NLS-RRR to NLS-AAA, CGG CGG AGG > GCC GCC GCC).

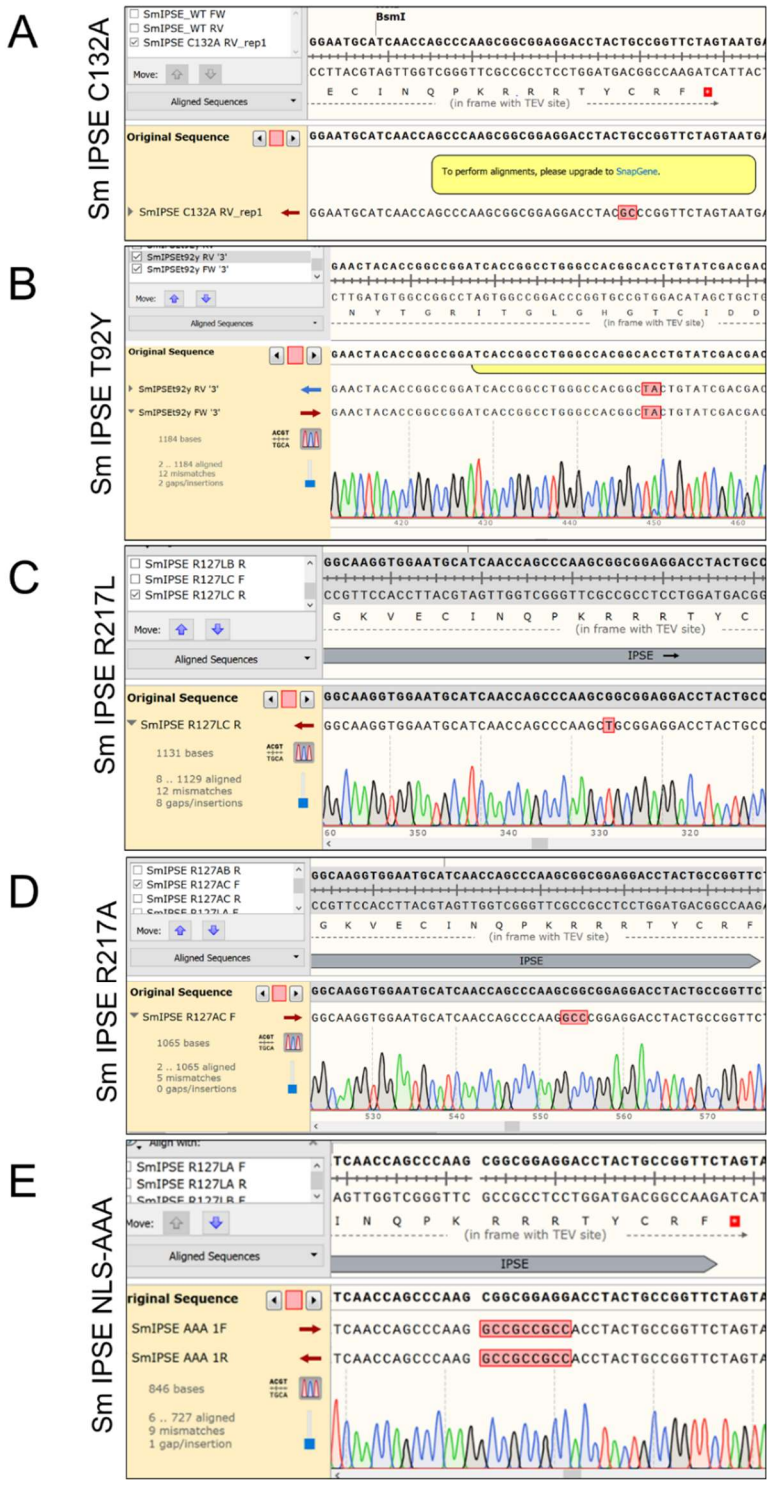

Figure 18 Relevant sections of chromatograms of sequences of Sm IPSE pTT5 after the insertion of the respective mutation via site-directed mutagenesis. (A) Chromatogram of Sm IPSE C132A showing the switch from TGC to GCC. (B) Display of succsessful base pair switch from ACC to TAC to generate the Sm IPSE T92Y mutant. (C) Chromatogram of the Sm IPSE mutant Sm IPSE R127L bearing a swith from CGG to CTG. (D) Chromatogram shows the successful mutation of Sm IPSE R127A including a change from CGG to GCC. (E) Sequence of Sm IPSE NLS-AAA triple mutant with changes in the NLS triple Arginine to Alanine (CGG CGG AGG to GCC GCC GCC).

3.1.3 Recombinant expression of Sm IPSE mutants in the HEK293-6E expression system

Based on the knowledge that the SmCKBP is not able to activate basophils to degranulate and release histamine, IL-4 and IL-13 and the assumption that a dimeric protein is necessary for IgE-dependent basophil, six different mutants of Sm IPSE were expressed to gain further insights in the IPSE-IgE interaction (Kaur et al., 2011; Smith et al., 2005). After confirming that the mutations were correctly inserted, all mutant IPSE proteins were successfully expressed and purified from HEK293-6E cells (Figure 19). The previously generated anti-IPSE mAB was hereby employed to detect the IPSE mutants, showing expected bands at the height of around 40 kDa, which corresponds to the dimeric IPSE (double bands because of glycosylation) and in case of C132A IPSE bands at 20 kDa and lower (monomeric IPSE, double bands are presumably due to glycosylation variants). Bands at the height of around 72 kDa probably represent tetramers of IPSE. Furthermore, an NLS-mutant bearing a switch from 3x Arginine to 3x Alanine in the Nuclear localization signal, was expressed and purified for subsequent DNA-interaction studies, as shown in Figure 20, displaying a similar molecular size as the wild type IPSE. To conclude, all IPSE mutants were expressed successfully and in high purity.

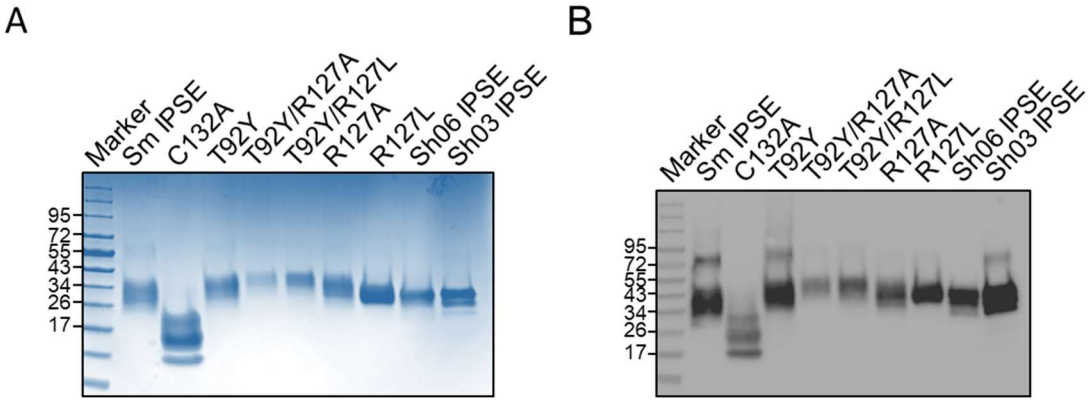

Figure 19 Expression and purification of different IPSE forms. (A) SDS-PAGE (unreduced) stained with PageBlue Protein Staining Solution showing high purity of the different proteins. (B) Western Blot blocked with anti-IPSE mAB (1:1000) and secondary antibody goat anti-mouse IgG HRP-conjugate. Wild type IPSE SmIPSE, Sh06 IPSE, Sh03 IPSE run as control.

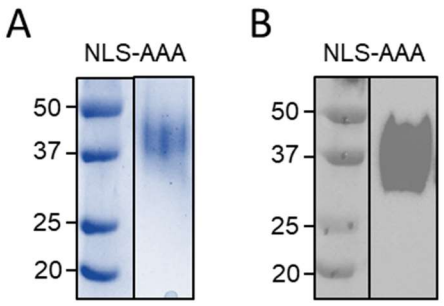

Fig 20 Expression and purification of Sm IPSE NLS-AAA (A) SDS-PAGE (unreduced) stained with PageBlue Protein Staining Solution showing high purity of the NLS-AAA mutant. (B) Western Blot of NLS-AAA blocked with anti-IPSE mAB (1:1000) and secondary antibody goat anti-mouse IgG HRP-conjugate.

3.1.4 Thermal Shift Assay with (mutated) Sm IPSE is inhibited by mammalian glycosylation

Seeking to rule out that the inserted mutations in Sm IPSE do not result in improper folding or a conformational change of each protein, a thermal shift assay detecting differences in the melting temperature was conducted.

Figure 21 A displays a chromatogram of all Sm IPSE variants recombinantly expressed in HEK293-6E cells and the positive control Lysozyme. In case of the positive control, a single peak around 78°C (melting peak) was detected and a melting temperature of 72°C, meeting the expectations and confirming the overall functionality of the assay. However, for each IPSE mutant the curves displayed more than one melting peak (Figure 21 A), as well as several peaks for melting temperature, making it impossible to determine an exact melting point of the proteins. This was further confirmed by the CFX maestro 1.1 Bio-Rad software listing for each IPSE variant various numbers of melting temperatures (data not shown). Meanwhile, the wild type IPSE melting point could not conclusively be determined, either. To investigate whether the high abundance of melting peaks in case of the IPSE mutants (and wild type) were caused by the different glycovariants of IPSE, the assay was repeated with *E. coli*-derived wild type Sm IPSE (Figure 21 B), in which the proteins are expressed without glycosylation. Indeed, the chromatogram reveals a curve with a single outstanding peak for melting temperature around 75°C, confirming our assumption of the interference from Sm IPSE's occupied glycosylation sites. Considering the relevance of the glycosylation of IPSE upon mammalian expression, as well as the enormous work standing behind it, the assay was not repeated for the variants in *E. coli*.

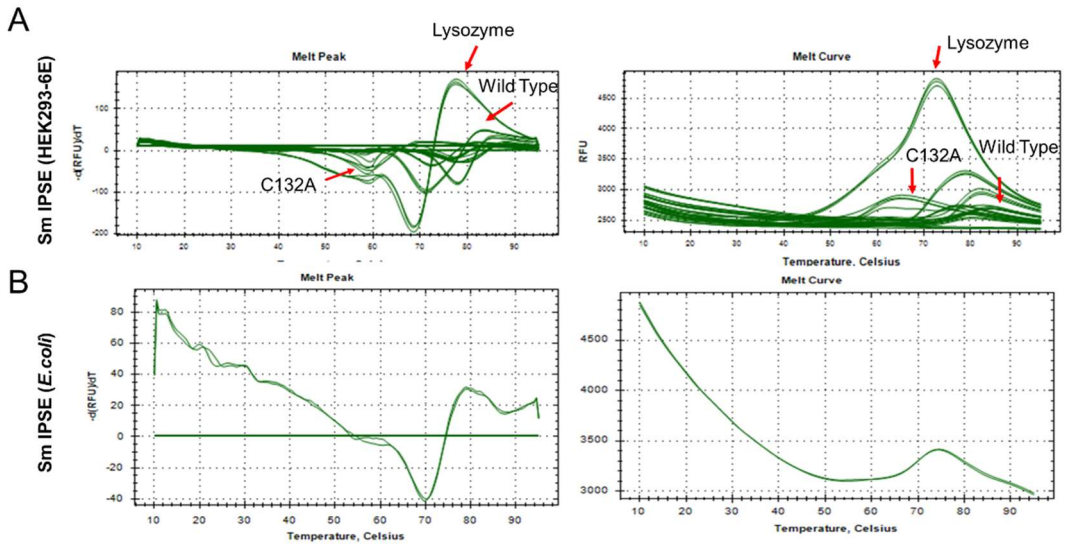

Figure 21 Chromatogram of Thermal Shift Assay conducted with either HEK293-6Eexpressed Sm IPSE (+ mutants) or E. coli expressed Sm IPSE. (A) Graph includes different IPSE mutants and the control Lysozyme. The left curve of lysozyme shows a peak around 72°C (Tm) and for IPSE mutants several peaks. The melt peak (right) for IPSE mutants and wild type cannot be detected. (B) Thermal Shift Assay performed with Sm IPSE expressed in E.coli showing one clear melt peak around 60°C (right) and a melting temperature around 75 °C, indicating as well that the glycosylation might interfere with the SYPRO Orange (NEB).

3.1.5 Prediction of the impact of the different mutations inserted in Sm IPSE using Missense 3D reveals conformational conservedness for the Sm IPSE mutants and impaired dimer formation in C132A Sm IPSE

To predict whether the introduced amino acid exchanges in Sm IPSE are likely to cause any major conformational changes within the protein, the Missense 3D tool was used. The model revealed that none of the mutations should lead to a conformational change of the protein (Figure 22). None of the tested parameters, showed an impact on proper IPSE folding. Parameters evaluated were for instance the introduction of buried hydrophobic residues, buried charge switches or replacement, buried H-bond breakage and alterations in the secondary structure. Another tested parameter within the Missense 3D prediction, was whether there was a switch in exposed/buried amino acids, which revealed that all inserted mutations, as well as the wild type amino acids are exposed. This stands in line with R127-R129 being situated in the Nuclear Localization Signal (in close proximity to the C-terminus) of IPSE, a naturally unfolded region. This also aplplies to C132, as it is part of the unfolded C-terminus of the protein. T92 is part of the estimated IgE binding site of IPSE being exposed on the proteins outer surface area (N. H. Meyer et al., 2015). However, C132A was previously observed to be incapable of forming dimers in the Western Blot (Figure

19). Cysteine is known to act as disulfide-bridge linker and thus, when mutated, the incapability of dimer-formation. Despite this, proper folding of the IPSE mutants was assumed and the possibility of interference with IgE-binding and thereby basophil activation was discarded (except for the monomeric IPSE previously shown to not induce basophil activation (Kaur et al., 2011).

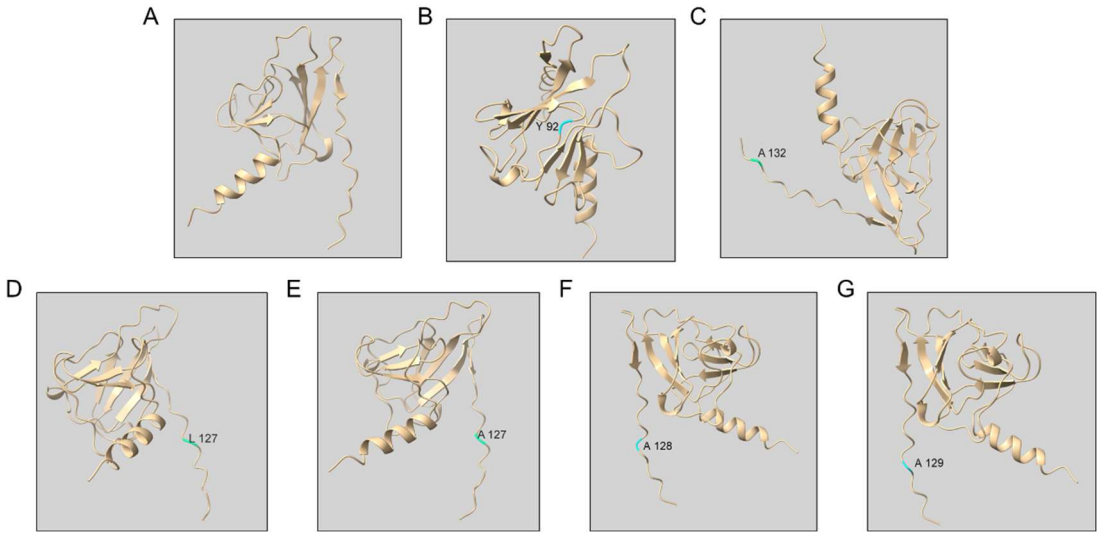

Figure 22 Structural analysis for IPSE Wild type (A) and the following mutants: (B) T92Y, (C) C132A, (D) R127L, (E) R127A, (F) R128A, and (G) R129A. De novo mutant residues are marked in turquoise. Notice: the tool is not capable of modelling double mutations; therefore, only models of single mutations were generated. The 3D structure shows that the modeled missense mutations are very unlikely to disrupt protein folding. Cysteine 132 is known act as disulfide-bridge linker and thus, when mutated inhibit dimer-formation by disrupting the disulfide bridge.

3.1.6 Immunoglobulin E (IgE) variants and human FCERIα$_{Val26\text{-}Gln205}$ can be expressed in the HEK293-6Eexpression system

To obtain a deeper understanding in which way Sm IPSE binds and interacts with IgE, different IgE variants were recombinantly expressed in the HEK293-6E expression system. Besides IgE motavizumab (IgE-mota), two truncated forms of IgE, namely 2-4 IgE (Cε2-4 domains), 3-4 IgE (Cε3+4 domains), as well as IgE's high affinity receptor human FcεRIα$_{Val26\text{-}Gln205}$, corresponding to the extracellular region (minus its signal peptide) of the receptor that is responsible for IgE binding, were acquired. Figure 23 shows diverse SDS-PAGEs and Western Blots of successfully expressed and purified proteins under reducing conditions. Figure 23 A and B underline that only the heavy chain of IgE (ca. 95 kDa) can be detected via Western Blot (B), whereby the light chain expected to run at 34 kDa was only detected using SDS-PAGE (A). As

expected, bands of 2-5 IgE appear run slightly lower as full length IgE (Figure 23 C, D) and, in the case of 3-4 IgE, the protein can be detected at ca. 60 kDa, since two chains are missing (Figure 23 E, F). Here, we also find some degradation of the truncated protein, running at approximately 43kDa in the Western Blot. Furthermore, the Figure also contains a Western Blot and SDS-PAGE showing the successful expression and purification of the high affinity receptor human FcεRIα$_{Val26\text{-}Gln205}$ (Figure 23 G, H), which will be used for further complexing with IgE.

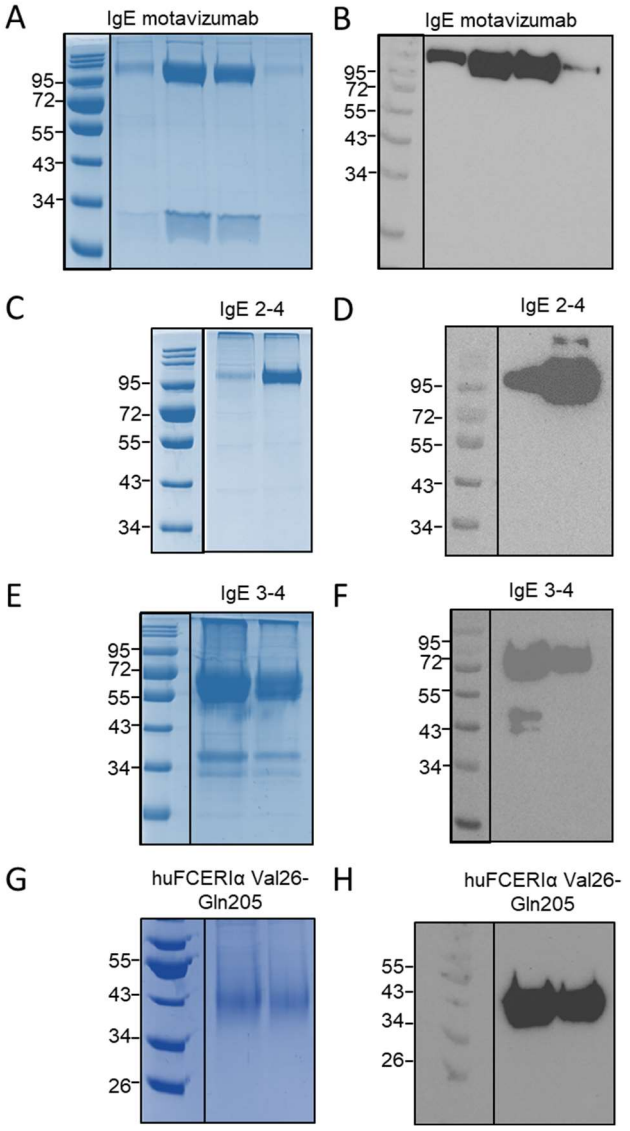

Figure 23 Expression of different IgE variants and the high-affinity receptor (alpha chain) of IgE. (A+B) 12% SDS-PAGE and Western Blot (reducing conditions) showing the expression and purification of IgE motavizumab. (C+D) 12% SDS-PAGE and Western blot under reducing conditions displaying the expression and purification of IgE 2-4. (E+F) Expression of IgE 3-4 shown in a 12 % SDS-PAGE (reducing) and Western Blot. (G+H) SDS-PAGE and Western Blot of expressed and purified huFcεRIα Val26-Gln205. For all blots the following antibodies were used: Monoclonal Anti-6X His tag produced in mouse and 2nd AB goat anti-mouse IgG HRP 1:20000.

3.1.7 Expression of IgE λ is limited to small scale expression and lack of release into the supernatant

Since we aimed to also include IgE λ in all of the following assays, we expressed the protein as described for the other IgE forms. For subsequent experiments, we attempted to insert a His-tag into the obtained pVITRO1-102.1F10-IgE/λ expression plasmid (Addgene #50365) to purify the expressed protein via IMAC.

To this end, site-directed mutagenesis was conducted using a 8xHis-Tag primer pair, which was unsuccessful. Thereafter, an attempt was made to insert the His-tag with the help of a Gibson-Assembly Reaction. Here, Figure 24 B displays a 0.8% Agarose-gel where most of the generated plasmid DNA was stuck in the pockets. Therefore, it was decided that the PCR-product of the reaction was to be initially cleaned up before subsequent usage. This improved the separation on the gel immensely (Figure 24 C). As a result, the band was cut and used for subsequent bacterial transformation, which turned out unsuccessful. Therefore, a new set of primers for insertion of a 6xHis-Tag were created and used for site-directed mutagenesis (Figure 24 D). Here, an unusual band pattern, showing more than the expected three bands became visible. The assumption that something might be wrong the pVITRO1-102.1F10-IgE/λ plasmid was supported by the absence of bacterial growth after bacterial transformation. Thus, it was speculated that the plasmid was somehow contaminated, possibly by another plasmid not bearing the IgE λ λ gene. This was further confirmed by restriction digestion of the plasmid, resulting in two bands instead of one when cut with either *NcoI* or *NdeI* and three when cutting with both *NcoI* and *NdeI*. The bands appear at circa 9 kb and 5.5 kb when cut with one enzyme, which also do not fulfill our expectations (Figure 24 E). Ultimately, full plasmid sequencing (Figure 24 F) revealed that it was indeed the plasmid bearing the gene mixed or linked with the one not containing the IgE λ gene, as instead of circa 9000 bp, 14666 bp were obtained. After deducting the length of the IgE λ gene from the plasmid and probably the loss of other gene cassettes the size of the plasmid would match circa 5500 bp. When consulting Addgene, they declared that they had been sending a wrong, contaminated batch.

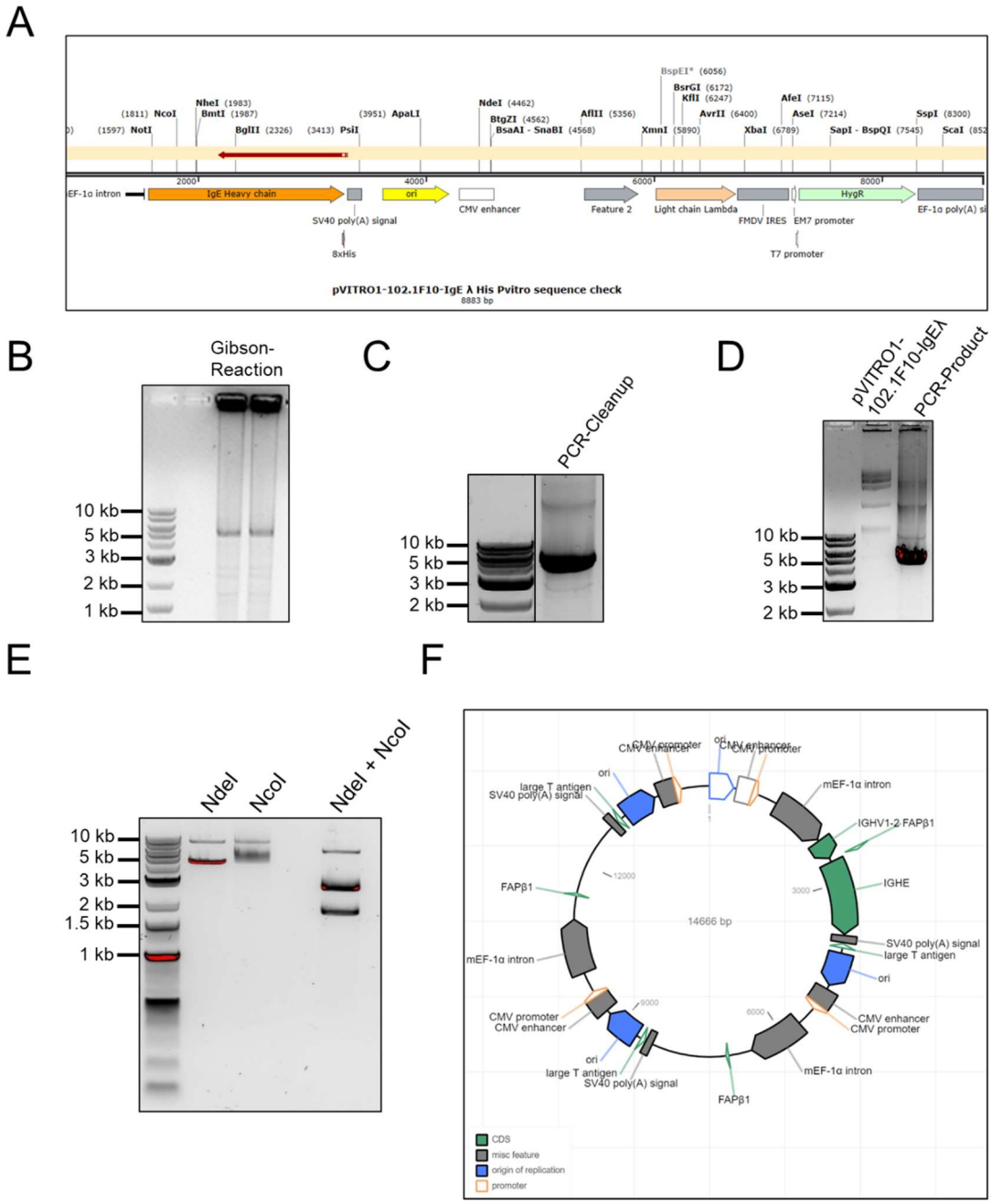

Figure 24 Attempts to insert a 8x-His-tag into pVITRO1-102.1F10-IgE/λ via site-directed mutagenesis and sequence alignment. (A) Sequence of pVITRO1-102.1F10-IgE/λ showing alignment to the template plasmid. (B) Picture of the Gibson-Reaction of pVITRO1-102.1F10-IgE/λ and the 8xHis-Tag. DNA was mostly stuck in the gel pockets. Dominant band around 6 kb was used for further experiments. (C) Repeat of Gibson-Reaction with an additional PCR-cleanup step with a clearer band. (D) Image of 0.8% Agarose-Gel containing the PCR-product of pVITRO1-102.1F10-IgE/λ after site-directed mutagenesis using specific 6xHis-Primer combination and the untreated plasmid. Since the band pattern is showing more than three expected bands for a plasmid, a problem with the original plasmid was suspected. (E) pVITRO1-102.1F10-IgE/λ digested with the restriction enzymes NcoI and NdeI. Implicating that the original plasmid must contain two different plasmids. (F) Full plasmid sequence of pVITRO1-102.1F10-IgE/λ proving that the original plasmid obtained from AddGene was contaminated.

Once a new batch of the pVITRO1-102.1F10-IgE/λ plasmid was received, Sanger sequencing (Figure 25 A) and full plasmid sequencing was performed (Figure 25 B), which confirmed the plasmid's identity.

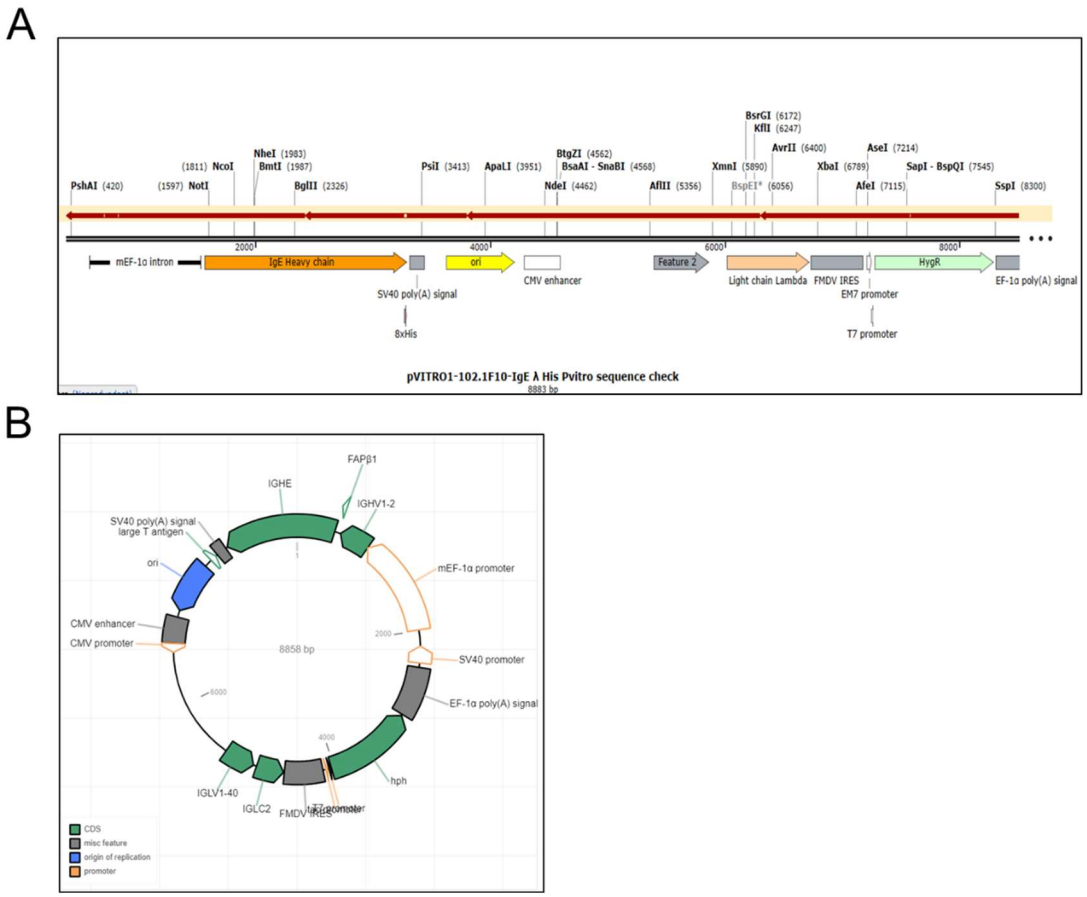

Figure 25 Full plasmid sequencing of the "new" batch of pVITRO1-102-1F10-IgE/λ. (A+B) Plasmid maps aligned with sequences received after full plasmid sequencing (MicroSynth) with „new" batch of pVITRO1-102-1F10-IgE/λ proving that this is the right batch, as the obtained sequence perfectly matches the template map in alignment and size.

Site-directed mutagenesis of the new plasmid batch was anticipated using the 6xHis-tag primer pair. However, this methodology led to the excision of the IgE λ gene, resulting in two strong bands at approx. 9000 bp and 4500 bp, respectively (Figure 26 A). When sequencing the purified plasmid after bacterial transformation, the alignment confirmed the loss of the gene of interest (Figure 26 B). Thereupon, it was decided to repeat the PCR with different elongation temperatures followed by gel extraction and bacterial transformation. Sequencing of the obtained plasmid finally showed the successful insertion of a 6xHis-tag (CAT CAT CAT CAC CAC CAC TAG) into the pVITRO1-102.1F10-IgE/λ plasmid (Figure 26 C, D), which could be used for protein expression.

Before expressing the protein in large scale, a small-scale transfection in HEK293-6E cells was carried out. After TCA-precipitation of the supernatant and the application of the pellet on an SDS-PAGE for Western Blotting, it was found that the protein was only present in the pellet and not as described by Dodev et al., (2014) secreted in the supernatant (Figure 26 E) (IgE gene casseste bears an internal secretion signal). Following attempts to express IgE λ in higher levels with release into the supernatant, including antibiotic selection, failed.

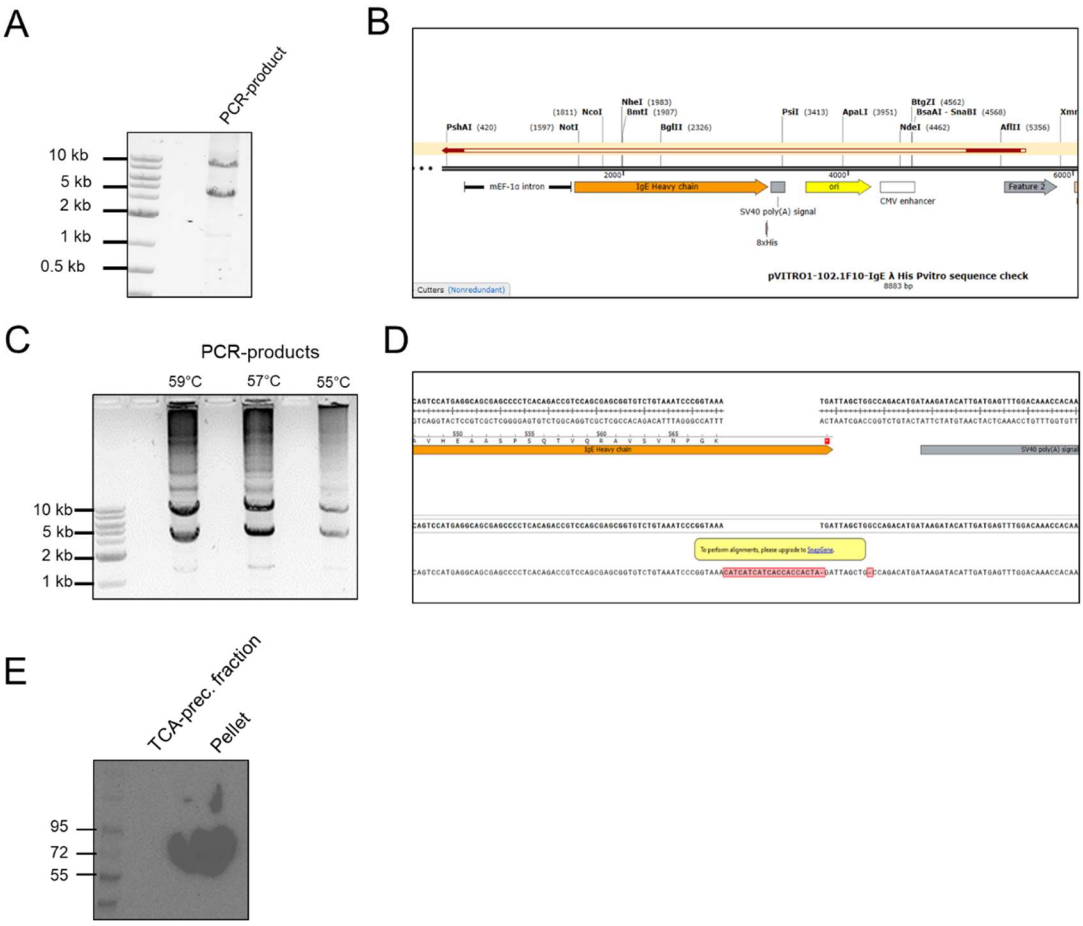

Figure 26 Sequence alignments, PCR-products and small scale protein expression of IgEλ (A) PCR-product after site-directed mutagenesis of plasmid with 6x-Histag primer, resulting in a band with the expected size of circa 9 kb, and one around 4.5 kb implying the loss of the IgEλ-gene. (B) Sanger-Sequence of the plasmid recovered from the PCR-product transformed into *E. coli* alpha5 confirms the loss of the IgE-gene. (C) Repetition of site-directed mutagenesis at different temperatures, resulting in two bands. Bands of 9 kb were cut out and further used for bacterial transformation. (D) Successful insertion of 6xHis-Tag (CAT CAT CAT CAC CAC CAC TAG) into pVITRO1-102-1F10-IgE/λ. (E) Western Blot (anti-6xHis antibody) of IgEλ expressed in HEK293-6E cells at small scale, showing that the immunoglobulin is only abundant in the cell pellet and not TCA-precipitated supernatant fraction.

3.2 IPSE - IgE interaction

3.2.1 IgE mota is able to form a stable complex with huFcεRIα, but not with Sm IPSE in FPLC

Sm IPSE was queried for its capacity to form a stable complex with IgE-mota. Here, in order to collect this complex, both proteins (IgE-mota and Sm IPSE, as well as the IgE high affinity receptor HuFcεRIα were incubated and subsequently pre-run on a Superdex tm 200 10/300 GL (GE Healthcare) column. The reference values of each individual protein were thus maintained as controls for subsequent curves obtained from the size exclusion chromatography runs with the pre-incubated or complexed proteins. Single proteins lead to peaks at approx. 11.35 mL for IgE-mota (Figure 27) approx. 14.95 mL for Sm IPSE (Figure 28) and finally 15.7 mL for huFcεRIα (Figure 29). In case of IgE-mota, additional, later peaks show protein degradation and residual contaminants from previously used Nickel—NTA-column. For huFcεRIα, multiple peaks were detected, which might represent two aggregated proteins, monomeric or degraded proteins.

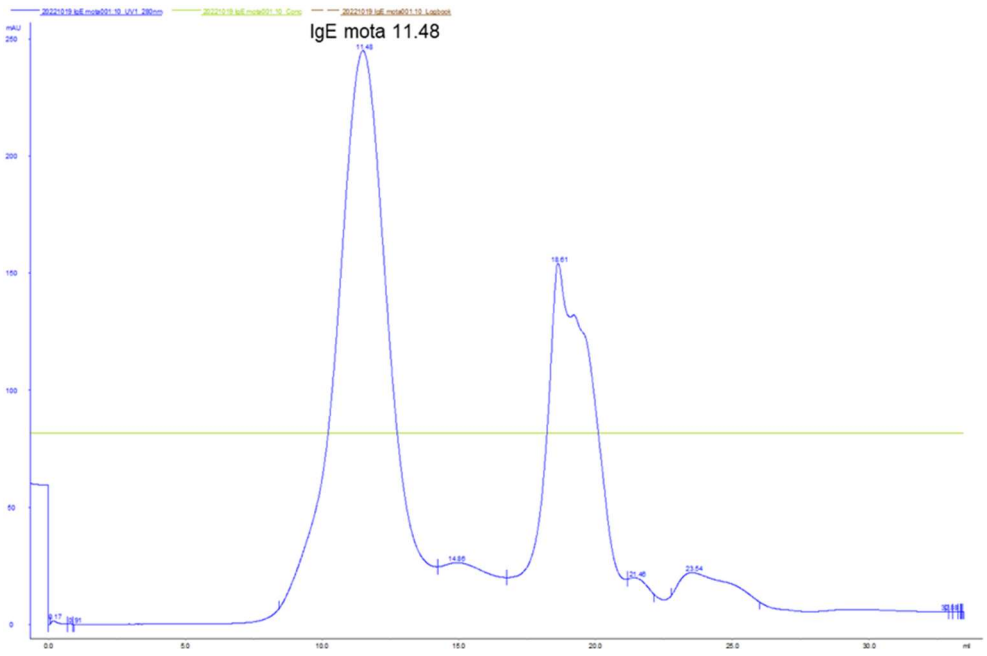

Figure 27 Size exclusion chromatography of recombinantly expressed IgE-motavizumab using a Superdex tm 200 10/300 GL. PBS served as running buffer. IgE-motavizumab (ca. 180 kDa) peak appears at 11.48 mL. Later occurring peaks show possible protein degradation and residuals of Nickel-IMAC.

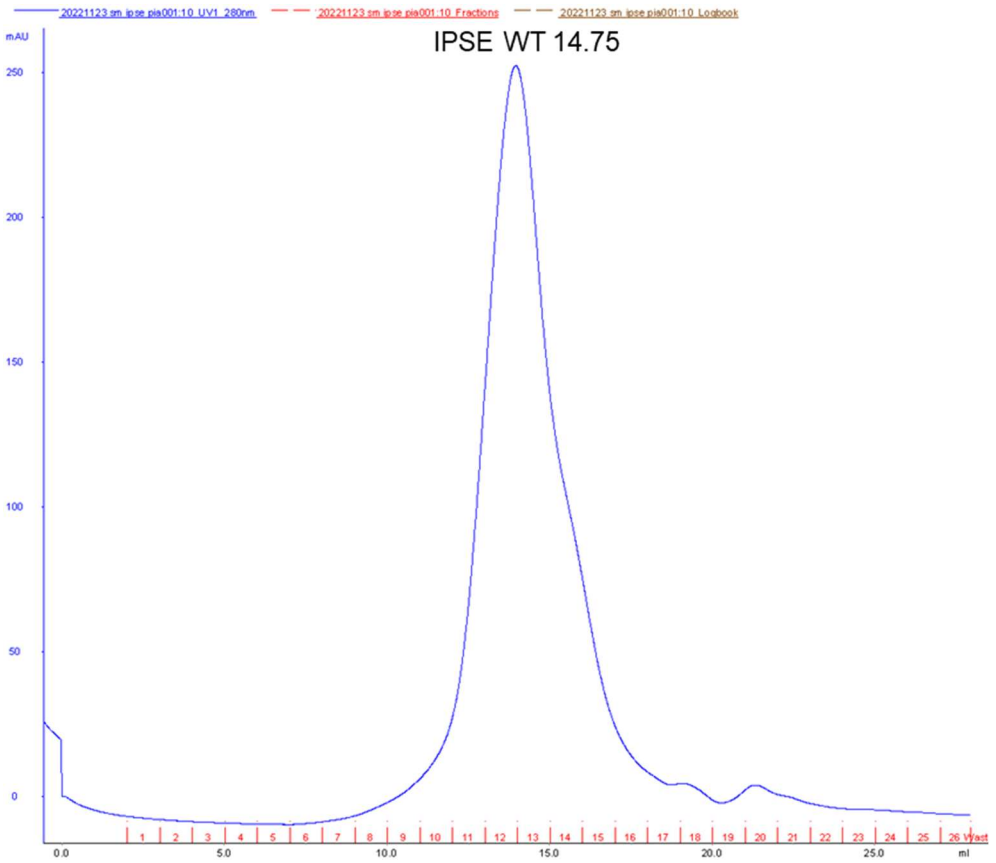

Figure 28 Size exclusion chromatography of recombinantly expressed Sm IPSE using a Superdex tm 200 10/300 GL (GE Healthcare, Lot#10050642). PBS served as running buffer. Sm IPSE (40 kDa) peak appears at 14.75 mL.

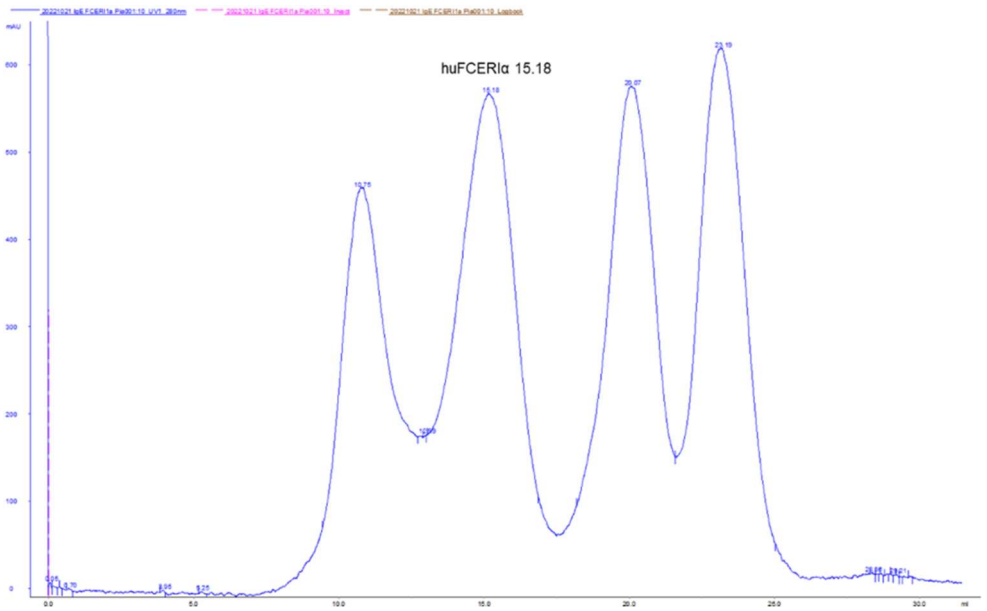

Figure 29 Chromatogram of the recombinantly expressed high affinity receptor huFcεRIα. The expected size of the protein would be around 40 kDa, fitting to the peak at 15.18 mL.

Once the baseline was established, complexed proteins were run via FPLC. First, IgE-mota (approx. 180 kDa) was complexed with its high affinity receptor, the recombinant expressed huFcεRIα (approx. 40 kDa), which would result in a protein complex of a size of approx. 220 kDa, and conclusively an earlier release from the column (i.e. less volume). Indeed, the chromatogram (Figure 30) shows that the peak of the FPLC was shifted towards 10.6 mL, leading to the conclusion that there is a stable complex formed by the two proteins.

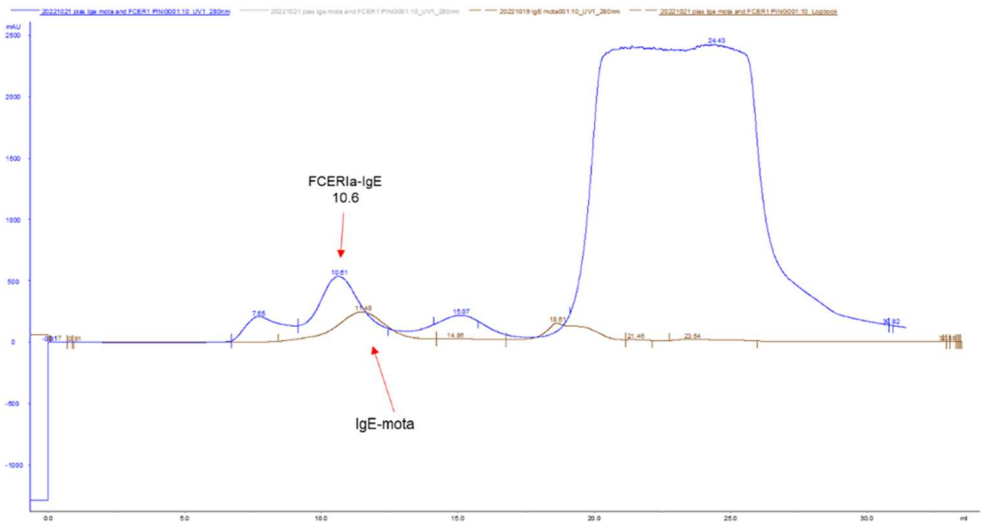

Figure 30 Overlay of FPLC curves of IgE-motativzumab uncomplexed (brown) and the IgE-motavizumab-FcεRIα complex (blue) (molar ratio 1:1) (column: Superdex tm 200 10/300 GL (GE Healthcare, Lot#10050642). A shift of the peak from uncomplexed IgE (11.48 mL) to 10.6 mL indicates that both proteins formed a stable complex.

In case of Sm IPSE and IgE-mota, a similar effect was expected. However, no conclusive result was attained for the complexation of IgE and IPSE with a molar ratio of 1:1 (data not shown). Therefore, subsequent complexation experiments were carried out with ratios of 1:2 of IgE and IPSE. In this case, no shift of the IgE-peak was detectable, indicative of failure of complexion (Figure 31). Nevertheless, the 11.38ml peak fractions were collected and applied to an SDS-PAGE followed by Western blotting to exclude the possibility of having attained a protein complex difficult to detect by a peak shift. Notably, the isolation shows that both proteins can indeed be found in the 11.38ml peak fractions, as bands can be detected in the Western blot at approx. 95 kDa as well as at 25 kDa (Figure 32). This cautiously indicates that IPSE might bind IgE-mota but in an unstable manner.

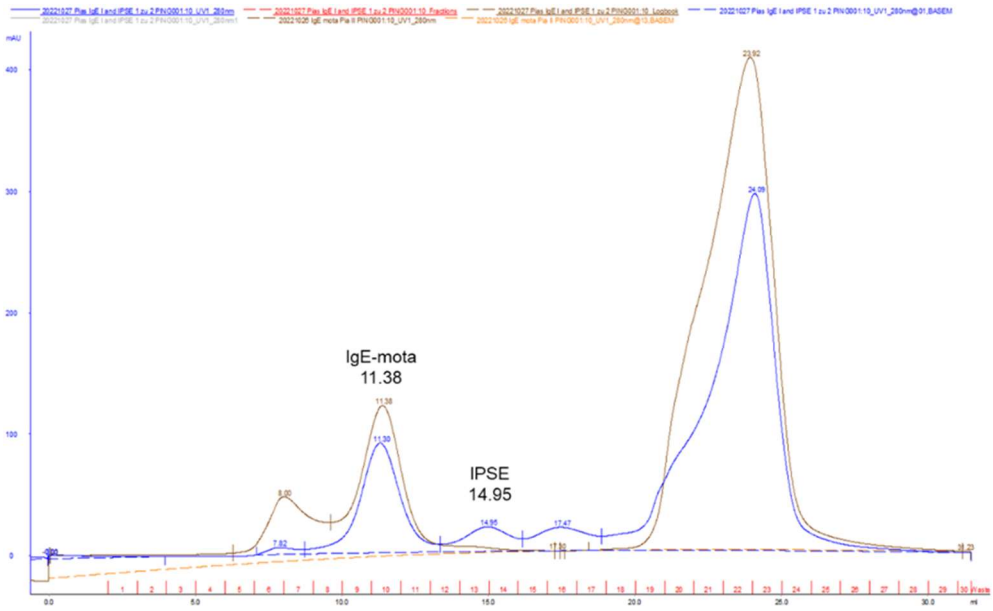

Figure 31 Chromatogram (SEC) of IgE-mota incubated with Sm IPSE (blue curve) in a 1:2 molar ratio. No stable complex of IgE-motavizumab and recombinant Sm IPSE can be detected, since the peak of IgE-motavizumab remains at around 11.3ml. Curve is overlayed with FPLC of IgE-motavizumab (brown). The peak at 14.95ml displays Sm IPSE. Fractions from peak 11.38ml were collected.

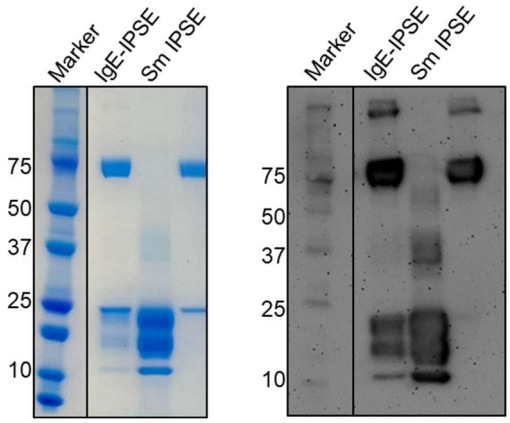

Figure 32 SDS-PAGE and Western Blot of FPLC fractions (IgE: IPSE 1:2) under reducing conditions, detecting both proteins in one fraction with the help of anti-His-tag antibody.

3.2.2 Sm IPSE forms oligomers at designated protein concentrations and does not form a stable complex with IgE-motavizumab (IgE-mota)

To further determine the binding stoichiometry and the binding-site of Sm IPSE to IgE, samples of the single protein and the potential ternary IgE-huFcεRIα-Sm IPSE were visualised with negative staining in electron microscopy. In this method a heavy metal salt is used to enhance the contrast between the background and the protein's image,

making the protein visible under the microscope. To establish an understanding of uncomplexed Sm IPSE in negative staining, the protein was examined in different concentrations under the electron microscope (Figure 31). Interestingly, Images of Figure 33 A,B,D show that at relative low concentrations from 15µg/mL and higher, the protein, displayed as brighter parts, aggregates and forms oligomers, such as tetramers and hexamers. Only at the lowest concentration of 7.5 µg/mL, the naturally occurring dimer was recognized as a strong white signal. In general, it can be concluded, that images of the proteins in TBS/TBE (Figure 33 C, D) are of higher quality than those obtained in PBS (Figure 33 A, B), as the proteins are easier to detect, since less background is obtained.

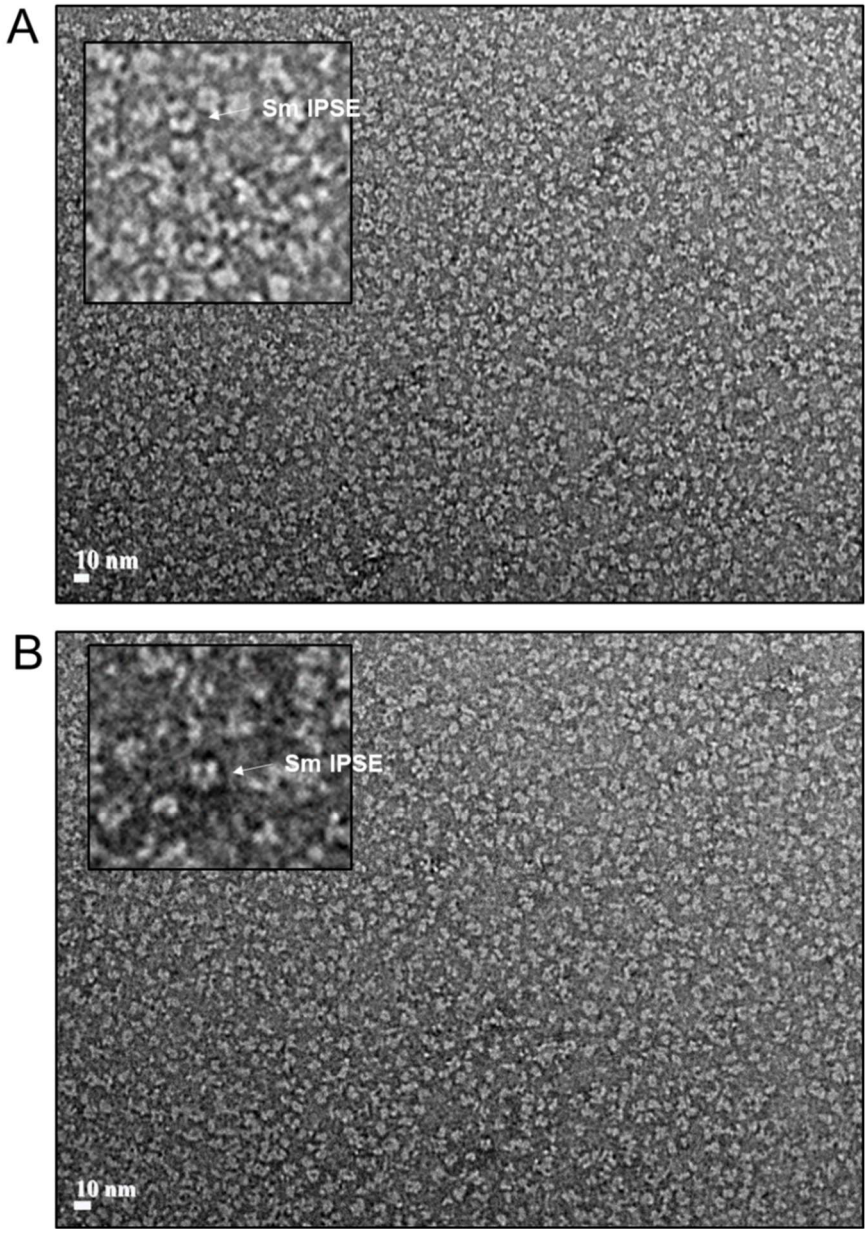

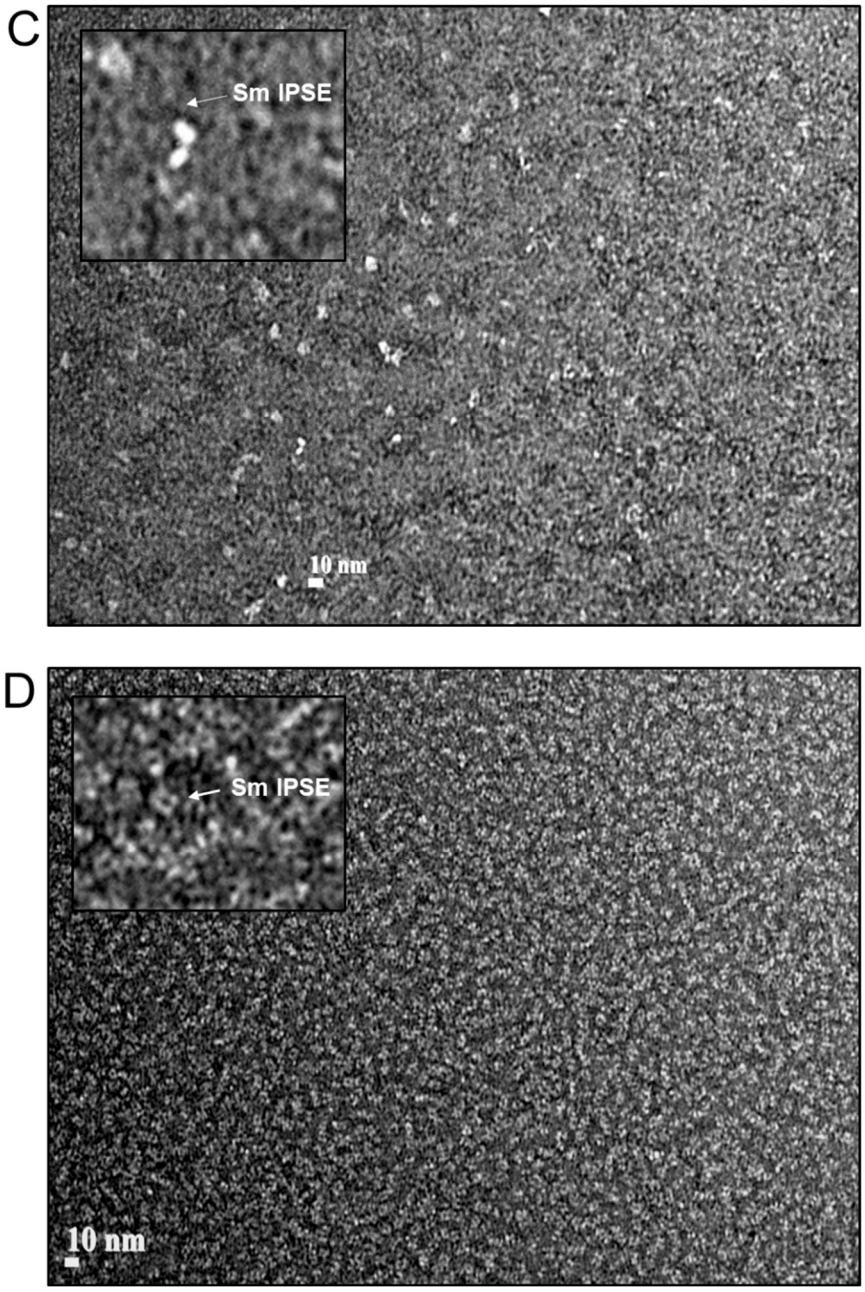

Figure 33 Negative Staining of IPSE in different concentrations and buffers (A+B) images of Sm IPSE (15 µg/mL) in PBS made visible with Negative staining. Photos were taken with an electron microscope. Instead of separated dimeric proteins, multiple proteins assembled to oligomers such as hexamers and tetramers. (C) Negative stained Sm IPSE (7.5 µg/mL) in TBS, showing nice examples of the dimeric protein. (D) Pictures of Sm IPSE (20 µg/mL) in TBE. Sm IPSE forms oligomers.

Next, samples of the pre-incubated immunoglobulin-receptor complex (IgE-mota and the high affinity receptor huFcεRIα) or sole IgE were assembled with Sm IPSE in a 1:1:1 molar ratio, shown in Figure 34. As IgE-mota is easily recognizable, it becomes obvious that a stable complex of IgE-mota and Sm IPSE is not detectable, considering Sm IPSE and IgE are not to be found attached to each other. Single proteins can be

observed in Figure 34 A. Nevertheless, only in Figure 34 C one IgE-mota possibly bound to Sm IPSE. However, this might as well be the receptor-IgE-complex, as is it also recognized in Figure 34 C+D.

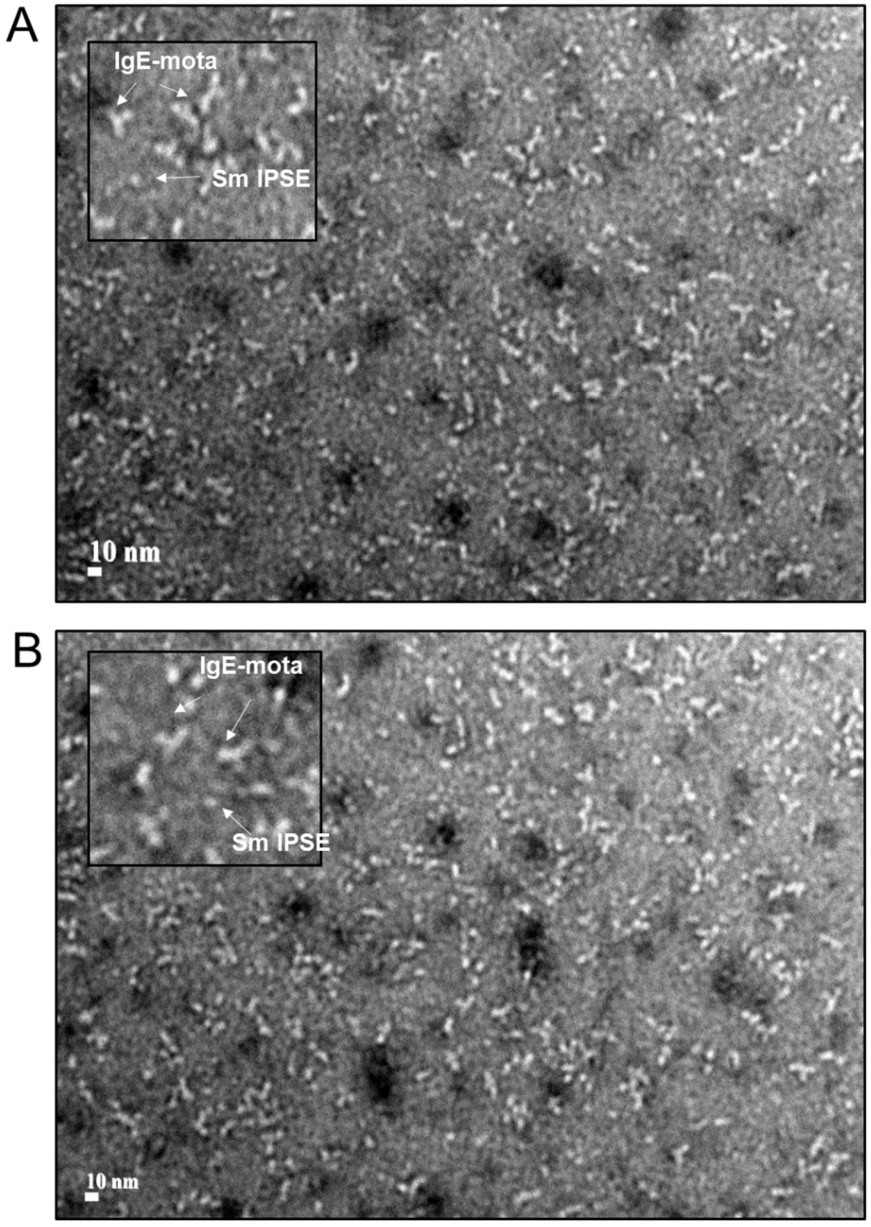

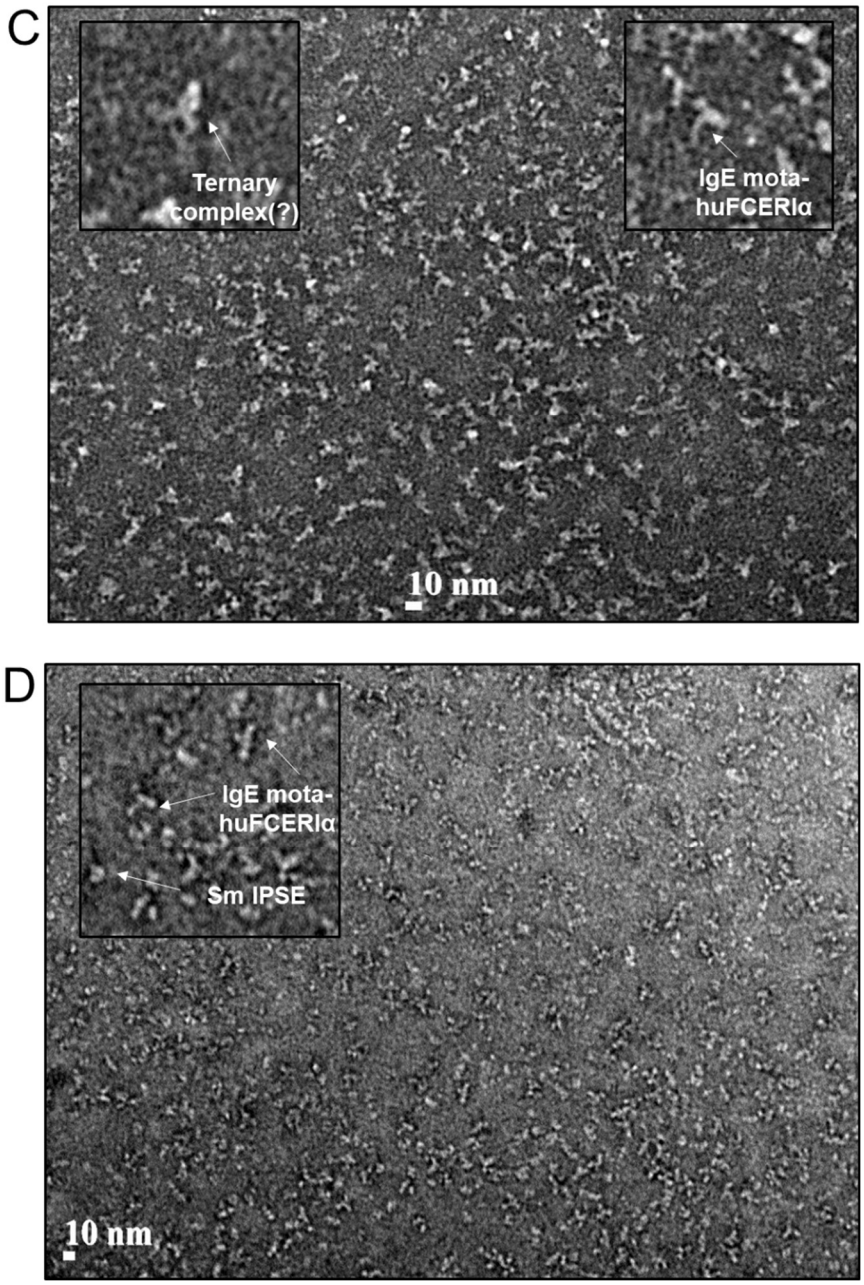

Figure 34 Negative staining of IPSE pre-incubated with IgE-mota or IgE-mota/huFCεRIα (A+B) EM-Image of pre-incubated Sm IPSE with IgE-mota (10 µg/mL) PBE in a molar ratio of 1:1. The Y-shaped IgE-mota is visible, as well as the small molecule Sm IPSE. But no binding-interaction between those two proteins can be detected. (C) Picture of the Negative stain of the pre-incubated IgE-mota-huFcεRIα-complex (15 µg/mL) with Sm IPSE (molar ratio 1:1:1). The binary receptor-Immunoglobulin complex can be easily detected. A possible ternary complex might be detected as well. (D) Negative stain image of the same complex at a lower concentration (10 µg/mL). Only the binary complex, but not the ternary complex can be found.

3.2.3 Determination of the IPSE-IgE binding affinity using ELISA

It is known that IPSE binds to IgE and IgG (Schramm et al. 2003; Meyer et al. 2015), but not with which affinity. To determine the IgE-IPSE binding affinity, diverse ELISAs were performed investigating at which concentrations synthetic IgE-mota consisting of the constant domains of IgE and the variable chain of motavizumab (an IgG derivate). This assay was further repeated with the binary complex of IgE-mota-huFcεRIα with Sm IPSE. On the basis of the assay, the calculations lead us to a K_D of 11.04 nM regarding the interaction of Sm IPSE with IgE-mota (Figure 35 A) and a K_D of 10.07 nM in case of IPSE binding to the binary IgE-mota-huFcεRIα-complex (Figure 35 B). Additionally, to elucidate whether IPSE has a differential binding affinity between the light chains of IgE, an ELISA was conducted using IgEλ (Bio Rad). Here, as depicted in Figure 35 C, IPSE binds to IgEλ with a high affinity, causing a saturation at the low concentration of 1 nM IgEλ, which led to the inability to determine an exact K_D.

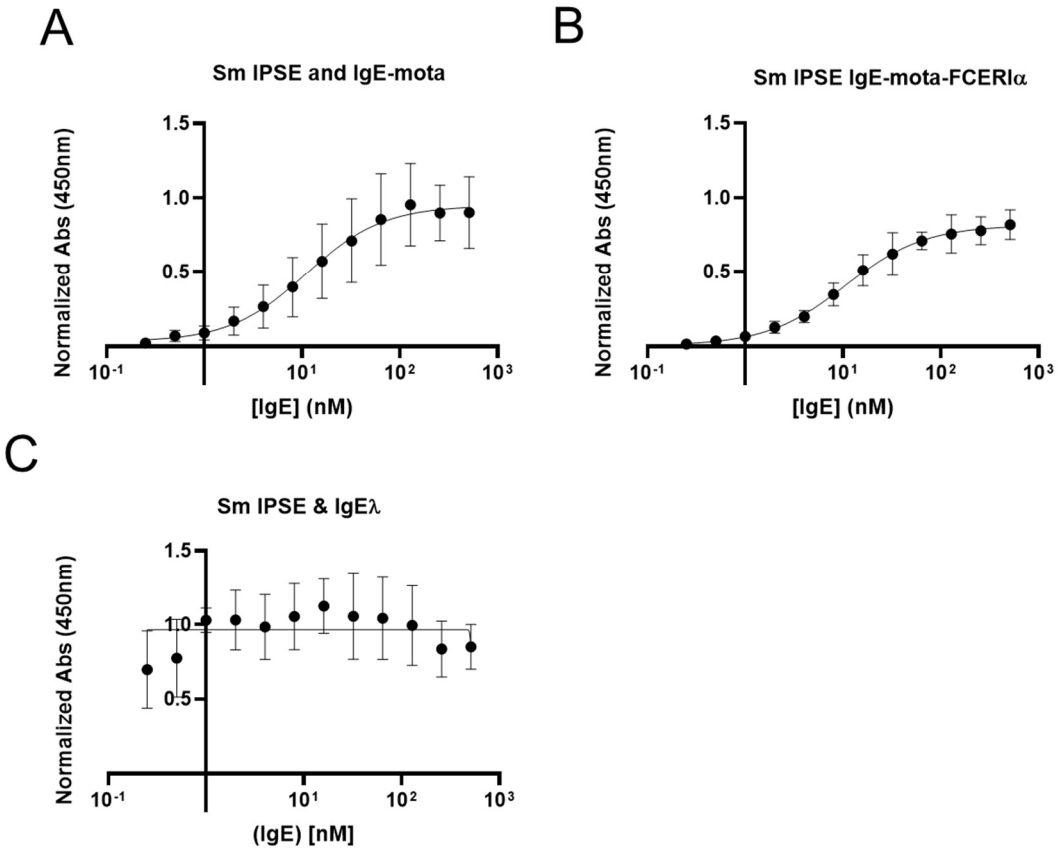

Figure 35 Determination of the binding affininty of IPSE to IgE-mota (huFCεRIα) and IgEλ in ELISA (A) ELISA of recombinantly expressed IPSE immobilized on plates and blocked with different concentrations of IgE-motavizumab. Mouse mAB to Human IgE [B3102E8] HRP functioned as secondary antibody. IPSE binds to IgE-mota with a K_D 11.4 nM. (B) Graph displays the binding interaction with Sm IPSE wild

type and the binary IgE-mota-huFcεRIα complex with a K_D = 10.07 nM. (C) ELISA of IgEλ binding to Sm IPSE with high affinity leading to an immediate saturation even at the low concentration of 1 nM, resulting no determination of the K_D.

Further ELISAs were performed to determine whether there is a difference in affinity for selected Sm IPSE mutants shown to display incapability to enable basophil activation via IgE-binding (C132A, T92Y/R127L = SmCKBP) and between the *Schistosoma* species. However, in all cases the K_D-values could not be determined due to the lack of a saturation of the binding curve, suggesting a much lower affinity of both investigated Sm IPSE mutants (C132A, T92Y/R127L) and both orthologues Sh03 (Figure 36 A) and Sh06 (Figure 36 B) of Sm IPSE. In case of the monomeric mutant C132A (C), the CKBP (D) and Sh03 (A) IPSE binding affinity starts to rise with the three highest molarities of IgE mota (512, 256 and 128 nm). In case of Sh06 (B), it seems as if the protein itself binds to the secondary antibody with a high affinity, leading to an unclean result.

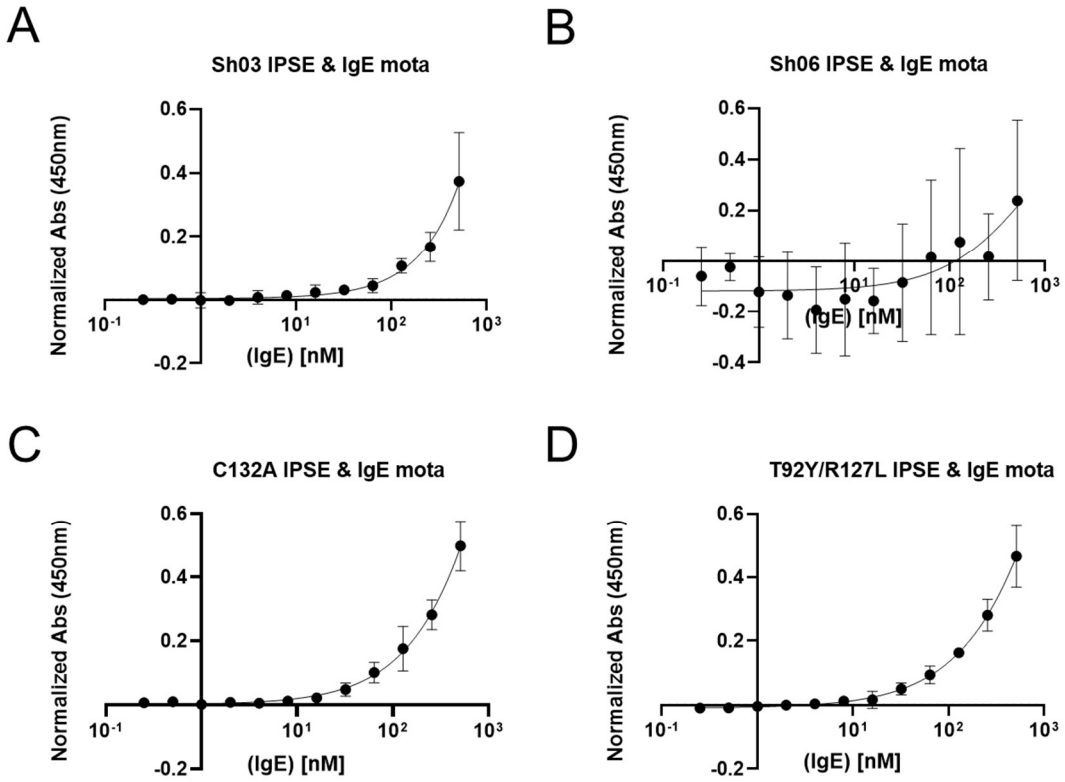

Figure 34 ELISA with different IPSE variants and mutants using IgE-mota as binding-partner. Plates were coated with IPSE and IgE-motavizumab was used as binding partner. Mouse mAB to Human IgE [B3102E8] HRP served as secondary antibody. Absorbance was measured at 450 nm. (A) ELISA of IgE-mota binding to Sh03 IPSE coated on plate. Even at the highest molarity of IgE mota 512 nm, the binding

curve does not reach a plateau. Leading to an inability to determine the KD. (B) Graph shows that a proper binding curve between IgE mota and Sh06 IPSE could not been created, since Sh06 seems to bind with a high affinity to the secondary antibody. (C) Shows the Graph of the ELISA including IgE-mota binding to the monomeric IPSE form (C132A), also not leading to a saturated curve resulting in the inability to obtain a KD-value. (D) Showing a similar result as of the binding affinity of IgE-mota to the chemokine binding protein form T92Y/R127L Sm IPSE, also not conducive to the determination of a KD-value.

The ELISAs carried out using different truncated forms of IgE to investigate the interaction domain of IgE with IPSE did not yield any absorbent signal, leading us to the conclusion that IPSE binds neither to IgE 2-4, nor to IgE 3-4 (Figure 37).

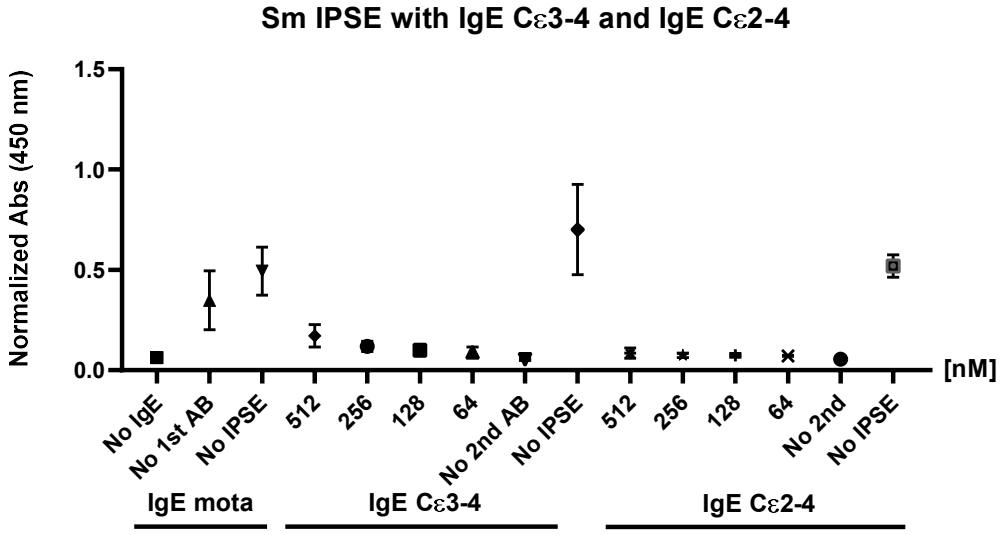

Figure 37 ELISA of recombinantly expressed IPSE immobilized on plates and incubated with different concentrations of the two truncated IgE forms. Mouse mAB to Human IgE [B3102E8] HRP (lot# GR3457438-1) functioned as secondary antibody. IgE 2-4 and IgE 3-4 (3-4 IgE = Cε3+4 domains and 2-4 IgE = Cε2+3+4 domains) showing no binding activity with Sm IPSE. IgE-motavizumab served as positive control.

3.2.4 No detectable interaction of Sm IPSE with IgE-motavizumab with Biolayer Interferometry

To further investigate the protein-binding properties of Sm IPSE to IgE-motavizumab, Biolayer Interferometry was performed. To detect a probable change in binding affinities, the chemokine binding mutant (T92Y/R127L) was included in the assay.

In the first experiment, streptavidin tips and multi-biotinylated IgE-mota were used in various concentrations. As it can be seen in Figure 38, no binding signal between Sm IPSE and IgE-mota was detectable. PBE was employed as negative control.

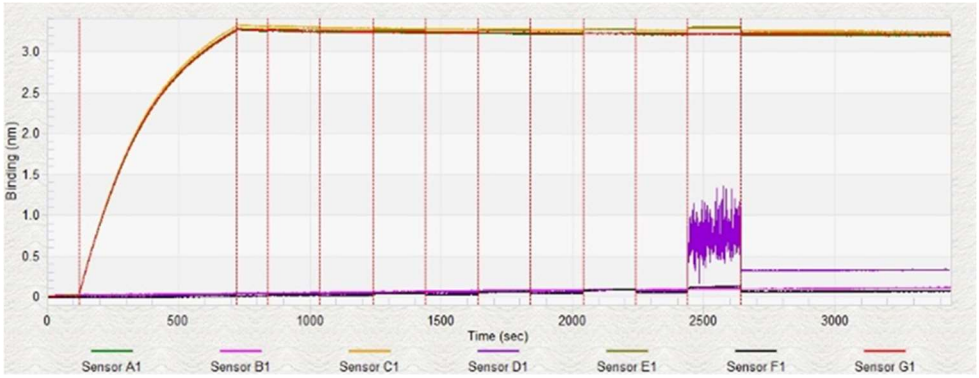

Figure 38 Diagram of BLI using Streptavidin-Tips pre-incubated in multi-biotinylated IgE-mota. During the assay the following Sm IPSE molarities were used: 256, 512, 1024, 2048, 4096 nM. Sensor A1+B1 Sm IPSE WT, Sensor C1+D1 Sm IPSE T92Y/R127L, Sensor E1+F1 Sm IPSE, Sensor G1 PBE. No binding signal could be detected.

The second attempt (Figure 39) included Ni-NTA Tips which were pre-incubated with the recombinant expressed His-tagged Sm IPSE. The set-up included different molarities of previously TEV-cleaved IgE-motavizumab. In this case, too, no binding signal between Sm IPSE and IgE-mota could be detected. This overall leads to the conclusion that Sm IPSE does not form a stable complex to IgE-mota.

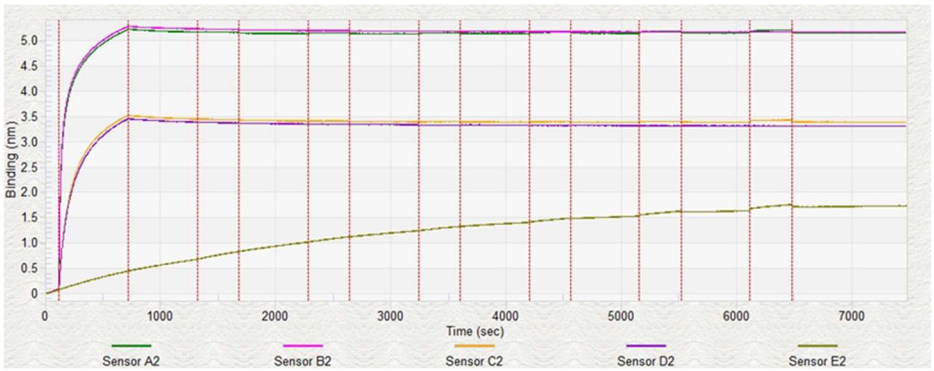

Figure 39 Diagram of BLI conducted with Ni-NTA Tips treated with recombinantly expressed His-tagged Sm IPSE. Sensor A2+B2 Sm IPSE WT, Sensor C2+D2 Sm IPSE T92Y/R127L, Sensor E2 PBE. For the assay IgE-mota was used with the following molarities 32, 64, 120, 256, 512 nM. No binding signal visible.

3.2.5 Basophil degranulation reporter assay of Sm IPSE, Sh06 IPSE und Sh03 IPSE reveals strong stimulation capacity of all orthologues

To determine whether the IPSE orthologues used in this study can stimulate basophil degranulation, a luciferase-based reporter assay (Wan et al., 2020) was performed. Here, both *S. haematobium* IPSE orthologues and the Sm IPSE variant significantly

stimulated basophil activation (reflecting the cytokine and chemokine release) measured as luciferase expression (Figure 40, Table 4). Only at the lowest tested concentration, Sh03 IPSE didn't show any significant reporter activity in RS-ATL8 cells (one-way ANOVA, Table 4). Indeed, in comparison to Sm IPSE, Sh03 IPSE triggered the basophils less (T-test, Table 5), especially in the range of 0.01 and 1 µg/mL IPSE protein, whereas Sh06 IPSE harbors similar activation properties as Sm IPSE (Table 5). Taken together, it can be said that all IPSE orthologues exhibit the ability to activate basophils, but Sh03 IPSE, slightly triggers the basophils less to express luciferase.

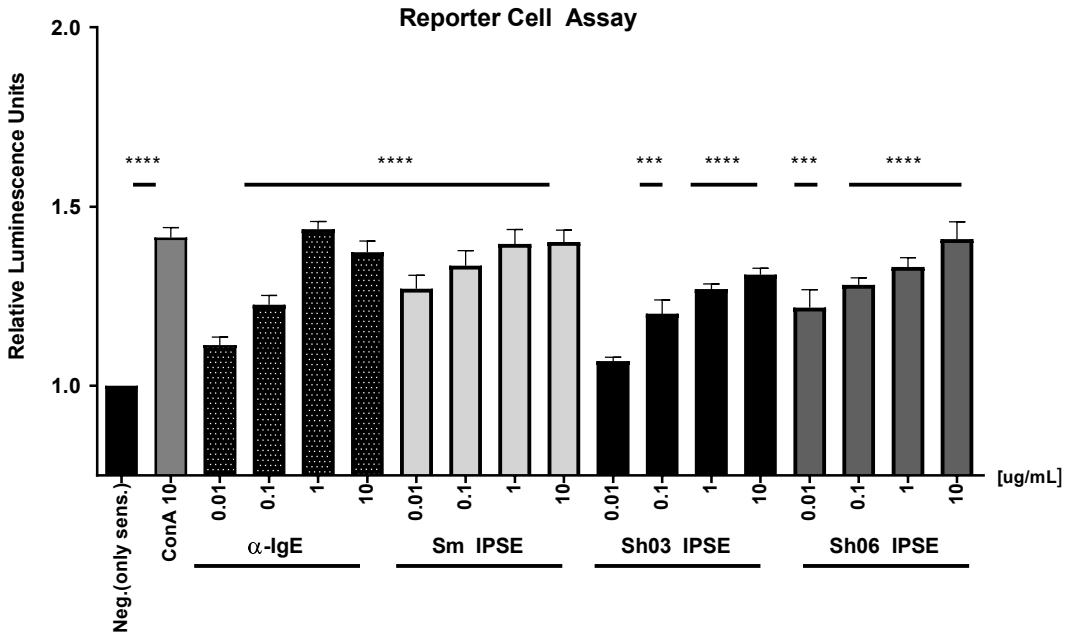

Figure 40 Evaluation of reporter assay using sensitized (human sera) RS-ATL8 cells that have been stimulated with IPSE and its orthologues. IPSE and its orthologues (Sh03 and Sh06) manifest significantly higher basophil-stimulation activity (corresponding to IgE-binding capacity) compared to the negative control, whereas only the Sh03 ablated activation completely at the lowest concentration. The binding-activity was assessed by measuring the relative luminescence of activated RS-ATL8 reporter cells, treated with human serum and different stimuli. Significance was established using the one-way ANOVA.

Table 4 Evaluation of Reporter Cell Assay including different IPSE orthologues. Statistical analysis with ordinary one-way ANOVA (Dunnett's multiple comparisons test); significance was tested against negative control (non-stimulated cells).

Dunnett's multiple comparisons test	95,00% CI of diff.	Significance	Adjusted P Value
Neg.(only sens.) vs. ConA I 10 µg/mL	-0,5550 to -0,2728	Yes	<0,0001
Neg.(only sens.) vs. a-IgE 0.01 µg/mL	-0,2445 to 0,01682	No	0,1224
Neg.(only sens.) vs. a-IgE 0.1 µg/mL	-0,3570 to -0,09575	Yes	<0,0001
Neg.(only sens.) vs. a-IgE 1 µg/mL	-0,5674 to -0,3061	Yes	<0,0001
Neg.(only sens.) vs. a-IgE 10 µg/mL	-0,5030 to -0,2417	Yes	<0,0001
Neg.(only sens.) vs. Sm IPSE 0.01 µg/mL	-0,4015 to -0,1402	Yes	<0,0001
Neg.(only sens.) vs. Sm IPSE 0.1 µg/mL	-0,4657 to -0,2044	Yes	<0,0001
Neg.(only sens.) vs. Sm IPSE 1 µg/mL	-0,5263 to -0,2650	Yes	<0,0001
Neg.(only sens.) vs. Sm IPSE 10 µg/mL	-0,5319 to -0,2706	Yes	<0,0001
Neg.(only sens.) vs. Sh06 IPSE 0.01 µg/mL	-0,3487 to -0,08736	Yes	0,0001
Neg.(only sens.) vs. Sh06 IPSE 0.1 µg/mL	-0,4122 to -0,1509	Yes	<0,0001
Neg.(only sens.) vs. Sh06 IPSE 1 µg/mL	-0,4620 to -0,2007	Yes	<0,0001
Neg.(only sens.) vs. Sh06 IPSE 10 µg/mL	-0,5397 to -0,2784	Yes	<0,0001
Neg.(only sens.) vs. Sh03 0.01 µg/mL	-0,1999 to 0,06142	Yes	0,6833
Neg.(only sens.) vs. Sh03 0.1 µg/mL	-0,3313 to -0,06996	No	0,0005
Neg.(only sens.) vs. Sh03 1 µg/mL	-0,4012 to -0,1399	Yes	<0,0001
Neg.(only sens.) vs. Sh03 10 µg/mL	-0,4406 to -0,1793	Yes	<0,0001

Table 5 Unpaired T-test of Sm IPSE tested against Sh03 and Sh06 IPSE tested in a reporter cell system. Restults show that only Sh03 IPSE has slightly impaired basophil activation properties compared to Sm IPSE

Unpaired t test	95% confidence interval	Significance	Adjusted P Value
Sm IPSE 0,01 µg/mL vs. Sh06 IPSE 0,01 µg/mL	0,2053 to 0,09957	No	0,4288
Sm IPSE 0,1 µg/mL vs. Sh06 IPSE 0,1 µg/mL	-0,1670 to 0,06011	No	0,2932
Sm IPSE 1 µg/mL vs. Sh06 IPSE 1 µg/mL	-0,1822 to 0,05375	No	0,2311
Sm IPSE 10 µg/mL vs. Sh06 IPSE 10 µg/mL	-0,1372 to 0,1528	No	0,9001
Sm IPSE 0,01 µg/mL vs. Sh03 0,01 µg/mL	-0,2970 to -0,1062	Yes	0,0021
Sm IPSE 0,1 µg/mL vs. Sh03 0,1 µg/mL	-0,2745 to 0,005717	No	0,0573
Sm IPSE 1 µg/mL vs. Sh03 1 µg/mL	-0,2296 to -0,02055	Yes	0,0264
Sm IPSE 10 µg/mL vs. Sh03 10 µg/mL	-0,1854 to 0,002788	No	0,0552

3.2.6 Basophil degranulation reporter cell assay with Sm IPSE mutants reveals differential loss of basophil stimulation capacity

To determine the ability of the Sm IPSE mutants to stimulate basophils, the luciferase-based reporter assays was conducted as previously described, using anti IgE as a positive control for binding and subsequent basophil stimulation. Here, Sm IPSE wild type displayed the highest activation activity throughout all concentrations (ONE-WAY ANOVA against negative control) (Figure 41, Table 6). Meanwhile, Sm CKBP-stimulation did not lead to a significant activation of the basophils as measured luciferase release throughout all concentrations ($p<0.9$). Surprisingly, monomeric IPSE (C132A) was able to activate basophils, starting at a protein concentration of 0.1 µg/mL, although with less capacity than the wild type. This might be explained by possible aggregation of the protein, which resembles the natural dimeric protein and leads to regaining of its original function. Alternatively, two monomeric IPSE molecules might bind independently to IgE. Meanwhile, both single arginine mutations (R127A and R127L) only lead to an impaired basophil degranulation at the lowest concentration ($p = 0.1418$ and $p = 0.0141$, respectively). Higher concentrations displayed a significant reporter release as observed for the Sm IPSE wild type form

(p < 0.0001). In contrast, the change from threonine to tyrosine (T92Y) had a much higher influence on the stimulation capacity, since protein concentrations of 0.01 and 0.1 µg/ml did not lead to activation, whereby 1 µg/mL and 10 µg/mL only achieved reduced luciferase induction (p=0.0215). In line with that, the double mutant T92Y/R127A also displayed impaired activation of the reporter cells at the lowest concentrations (0.01 µg/mL p = 0.9853 and, 0.1 µg/mL).

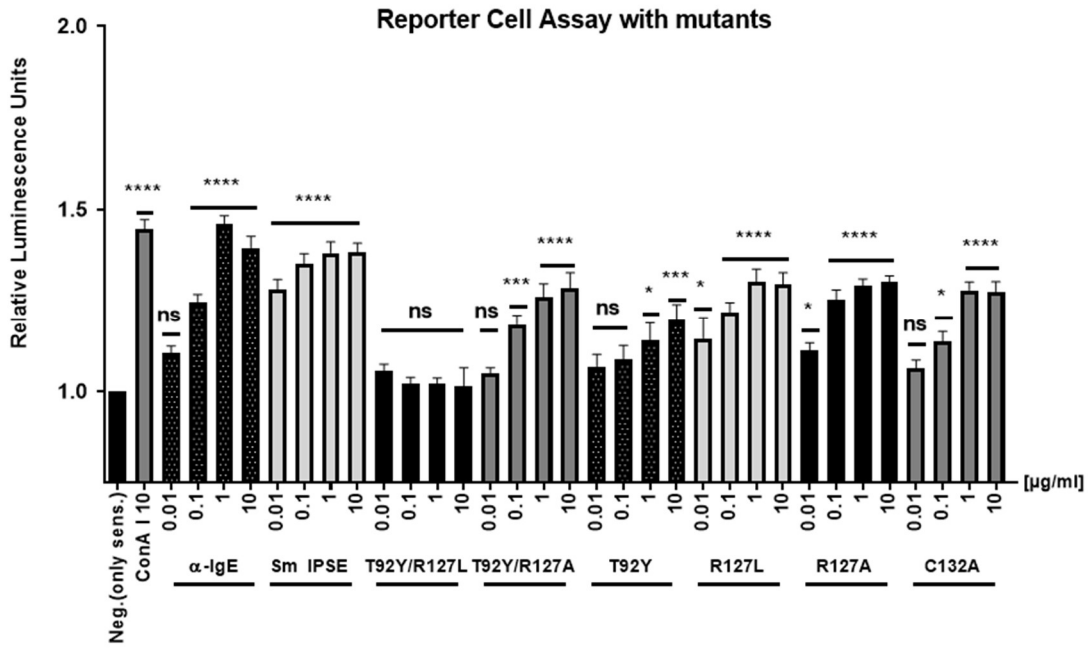

Figure 41 Evaluation of reporter assay conductes with Sm IPSE and its mutants with (human serum) sensitized RS-ATL8 cells. Sm IPSE and the mutants display significantly higher capacity to activate basophils (IgE-binding) and stimulation activity compared to the negative control, whereas only the CKBP mutant ablated activation completely, while the monomeric mutant binds at higher concentrations.The binding-activity was evaluated by measuring the relative luminescence of activated RS-ATL8 reporter cells, treated with human serum and different stimuli. Significance was calculated using one-way ANOVA.

Table 6 IPSE Wild type and IPSE mutants evaluated after conduction of the reporter cell assay. Statistics data analyses was performed using Ordinary one-way ANOVA (Dunnett's multiple comparisons test); significance was tested against negative control (non-stimulated cells).

Dunnett's multiple comparisons test	95,00% CI of diff.	Significance	Adjusted P Value
Neg.(only sens.) vs. ConA I 10 µg/mL	-0,5754 to -0,3182	Yes	<0,0001
Neg.(only sens.) vs. a-IgE 0.01 µg/mL	-0,2263 to 0,01886	No	0,1647
Neg.(only sens.) vs. a-IgE 0.1 µg/mL	-0,3692 to -0,1240	Yes	<0,0001
Neg.(only sens.) vs. a-IgE 1 µg/mL	-0,5832 to -0,3380	Yes	<0,0001
Neg.(only sens.) vs. a-IgE 10 µg/mL	-0,5180 to -0,2729	Yes	<0,0001
Neg.(only sens.) vs. Sm IPSE 0.01 µg/mL	-0,4042 to -0,1591	Yes	<0,0001
Neg.(only sens.) vs. Sm IPSE 0.1 µg/mL	-0,4735 to -0,2283	Yes	<0,0001
Neg.(only sens.) vs. Sm IPSE 1 µg/mL	-0,5039 to -0,2588	Yes	<0,0001
Neg.(only sens.) vs. Sm IPSE 10 µg/mL	-0,5060 to -0,2608	Yes	<0,0001
Neg.(only sens.) vs. C132A 0.01 µg/mL	-0,1868 to 0,05835	No	0,8224
Neg.(only sens.) vs. C132A 0.1 µg/mL	-0,2595 to -0,01434	Yes	0,0172
Neg.(only sens.) vs. C132A 1 µg/mL	-0,4019 to -0,1568	Yes	<0,0001
Neg.(only sens.) vs. C132A 10 µg/mL	-0,3954 to -0,1502	Yes	<0,0001
Neg.(only sens.) vs. T92Y 0.01 µg/mL	-0,1969 to 0,06025	No	0,8066
Neg.(only sens.) vs. T92Y 0.1 µg/mL	-0,2179 to 0,03917	No	0,4138
Neg.(only sens.) vs. T92Y 1 µg/mL	-0,2692 to -0,01204	Yes	0,0215
Neg.(only sens.) vs. T92Y 10 µg/mL	-0,3243 to -0,06722	Yes	0,0002
Neg.(only sens.) vs. T92Y/R127A 0.01 µg/mL	-0,1776 to 0,07951	No	0,9853
Neg.(only sens.) vs. T92Y/R127A 0.1 µg/mL	-0,3129 to -0,05581	Yes	0,9853
Neg.(only sens.) vs. T92Y/R127A 1 µg/mL	-0,3889 to -0,1318	Yes	<0,0001

Neg.(only sens.) vs. T92Y/R127A 10 µg/mL	-0,4126 to -0,1555	Yes	<0,0001
Neg.(only sens.) vs. T92Y/R127L 0.01 µg/mL	-0,1864 to 0,07074	No	0,9448
Neg.(only sens.) vs. T92Y/R127L 0.1 µg/mL	-0,1505 to 0,1066	No	0,9993
Neg.(only sens.) vs. T92Y/R127L 1 µg/mL	-0,1491 to 0,1080	No	0,9994
Neg.(only sens.) vs. T92Y/R127L 10 µg/mL	-0,1439 to 0,1133	No	0,9996
Neg.(only sens.) vs. R127A 0.01 µg/mL	-0,2401 to 0,01704	No	0,1418
Neg.(only sens.) vs. R127A 0.1 µg/mL	-0,3813 to -0,1242	Yes	<0,0001
Neg.(only sens.) vs. R127A 1 µg/mL	-0,4194 to -0,1623	Yes	<0,0001
Neg.(only sens.) vs. R127A 10 µg/mL	-0,4317 to -0,1746	Yes	<0,0001
Neg.(only sens.) vs. R127L 0.01 µg/mL	-0,2748 to -0,01770	Yes	0,0141
Neg.(only sens.) vs. R127L 0.1 µg/mL	-0,3461 to -0,08894	Yes	<0,0001
Neg.(only sens.) vs. R127L 1 µg/mL	-0,4304 to -0,1733	Yes	<0,0001
Neg.(only sens.) vs. R127L 10 µg/mL	-0,4241 to -0,1670	Yes	<0,0001

Comparing the release of the mutants to the wild type (unpaired T-Test (Table 7), it confirms that all mutants – at least at lower concentrations – show a significant reduction in basophil stimulation. The R127L mutant seems to be the least affected, due to the fact that at higher concentrations no difference between it and the wild type was detectable. For a deeper understanding, the data-set was additionally analyzed with an ordinary T-Test (Table 7). The obtained data show that all the mutations, in direct comparison to the different wild type concentrations, are affecting the basophil activation. In contrast, the activating capability of Sm CKBP differs most drastically in each tested concentration. As already mentioned above, the T92Y mutant shows impaired activation activity, which was again clearly visible when the measured luminescence values were compared using the t-test, with all of the different protein concentrations differing from the wild type ($p < 0.001$ for 0.01 and 0.1 µg/mL and < 0.0035 for 1 and 10 µg/mL). Like T92Y, R127L was significantly less effective in activating the cells, although not so strongly as T92Y. Only in the case of the mutant

R127L at higher concentrations and T92Y/R127A (10 µg/mL), no difference to the wild type could be found.

Table 7 Unpaired T-test of basophil activation evaluated in the reporter cell system after stimulation with IPSE mutants. Analysis shows that especially at high concentrations all mutations, have an impact on basophil activation. Results also show that the Threonine 92 mutants, compared to the WT are affected at most, with the SmCKBP not activating at all.

Unpaired t test	**95% confidence interval**	**Significance**	**Adjusted P Value**
Sm IPSE 0,01 µg/mL vs. C132A 0,01 µg/mL	-0,2957 to -0,1391	Yes	0,0001
Sm IPSE 0,1 µg/mL vs. C132A 0,1 µg/mL	-0,3032 to -0,1248	Yes	0,0003
Sm IPSE 1 µg/mL vs. C132A 1 µg/mL	-0,1856 to -0,01845	Yes	0,0216
Sm IPSE 10 µg/mL vs. C132A 10 µg/mL	-0,1962 to -0,02501	Yes	0,0164
Sm IPSE 0,01 µg/mL vs. T92Y 0,01 µg/mL	-0,3096 to -0,1171	Yes	0,0007
Sm IPSE 0,1 µg/mL vs. T92Y 0,1 µg/mL	-0,3654 to -0,1576	Yes	0,0003
Sm IPSE 1 µg/mL vs. T92Y 1 µg/mL	-0,3645 to -0,1171	Yes	0,0017
Sm IPSE 10 µg/mL vs. T92Y 10 µg/mL	-0,2953 to -0,07996	Yes	0,0034
Sm IPSE 0,01 µg/mL vs. T92Y/R127L 0,01 µg/mL	-0,3003 to -0,1473	Yes	<0,0001
Sm IPSE 0,1 µg/mL vs. T92Y/R127L 0,1 µg/mL	-0,4086 to -0,2493	Yes	<0,0001
Sm IPSE 1 µg/mL vs. T92Y/R127L 1 µg/mL	-0,4427 to -0,2789	Yes	<0,0001
Sm IPSE 10 µg/mL vs. T92Y/R127L 10 µg/mL	-0,4857 to -0,2505	Yes	<0,0001
Sm IPSE 0,01 µg/mL vs. T92Y/R127A 0,01 µg/mL	-0,3078 to -0,1574	Yes	<0,0001
Sm IPSE 0,1 µg/mL vs. T92Y/R127A 0,1 µg/mL	-0,2552 to -0,07784	Yes	0,0021
Sm IPSE 1 µg/mL vs. T92Y/R127A 1 µg/mL	-0,2268 to -0,01525	Yes	0,0293
Sm IPSE 10 µg/mL vs. T92Y/R127A 10 µg/mL	-0,2067 to 0,007979	No	0,0658

Sm IPSE 0,01 µg/mL vs. R127L 0,01 µg/mL	-0,2705 to -0,0002780	Yes	0,0496
Sm IPSE 0,1 µg/mL vs. R127L 0,1 µg/mL	-0,2245 to -0,04231	Yes	0,009
Sm IPSE 1 µg/mL vs. R127L 1 µg/mL	-0,1837 to 0,02467	No	0,1183
Sm IPSE 10 µg/mL vs. R127L 10 µg/mL	-0,1765 to 0,0008472	No	0,0518
Sm IPSE 0,01 µg/mL vs. R127A 0,01 µg/mL	-0,2518 to -0,08844	Yes	0,0011
Sm IPSE 0,1 µg/mL vs. R127A 0,1 µg/mL	-0,1885 to -0,007865	Yes	0,0362
Sm IPSE 1 µg/mL vs. R127A 1 µg/mL	-0,1753 to -0,005802	Yes	0,0388
Sm IPSE 10 µg/mL vs. R127A 10 µg/mL	-0,1490 to -0,01156	Yes	0,0268

To facilitate the understanding how the different mutations can interfere with IPSE-IgE binding, prediction models of the IPSE WT and the Threonine mutation T92Y (Figure 42) and Arginine mutations R127A and R127L (Figure 43) were created using AlphaFold2 and ChimeraX. It can be observed that T92 is located in the centre of a flat surface of the IPSE monomer, which might be involved in IgE binding. Noteworthy, this mutation replaces a rather smaller and hydrophilic Threonine with a more hydrophobic and bulkier Tyrosine. This might affect the IgE-IPSE interaction. The second mutation R127L introduces a large and hydrophobic residue in close proximity of a strongly positively charged pack, which might also lead to disrupting the interaction, whereas the introduced Alanine (127A) with shorter chains, is smaller potentially leading to a less steric hindrance.

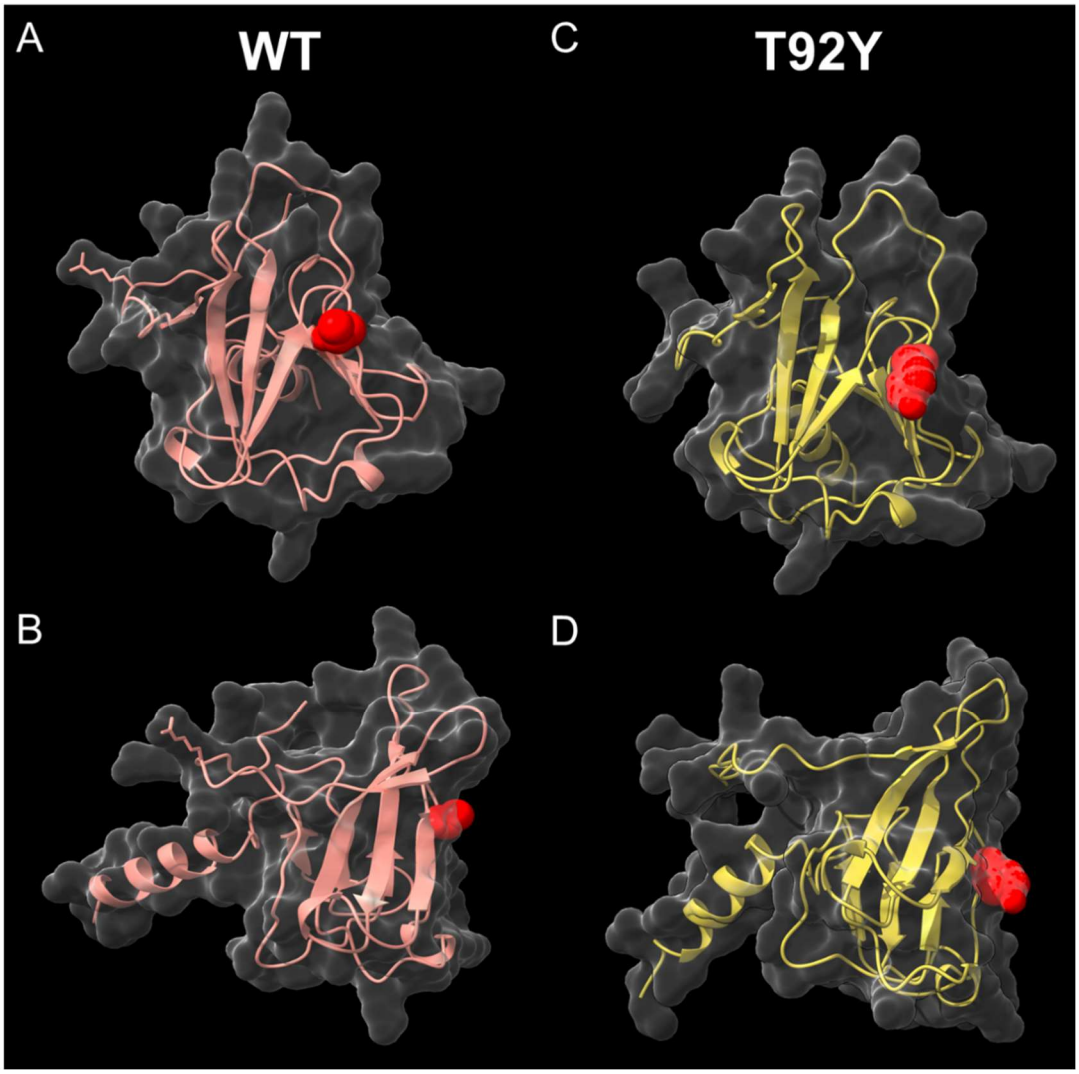

Figure 42 Prediction model of IPSE (T92) and its mutant form T92Y. T92 is located in a rather flat surface (B) in the very centre of the monomer (A). This surface may be needed for IgE binding. The mutant (T92Y) replaces the smaller and hydrophilic Threonine with a more hydrophobic and bulkier Tyrosine (C,D) that might lead to disruption of IgE-IPSE interaction. Protein models were created with AlphaFold2 and ChimeraX.

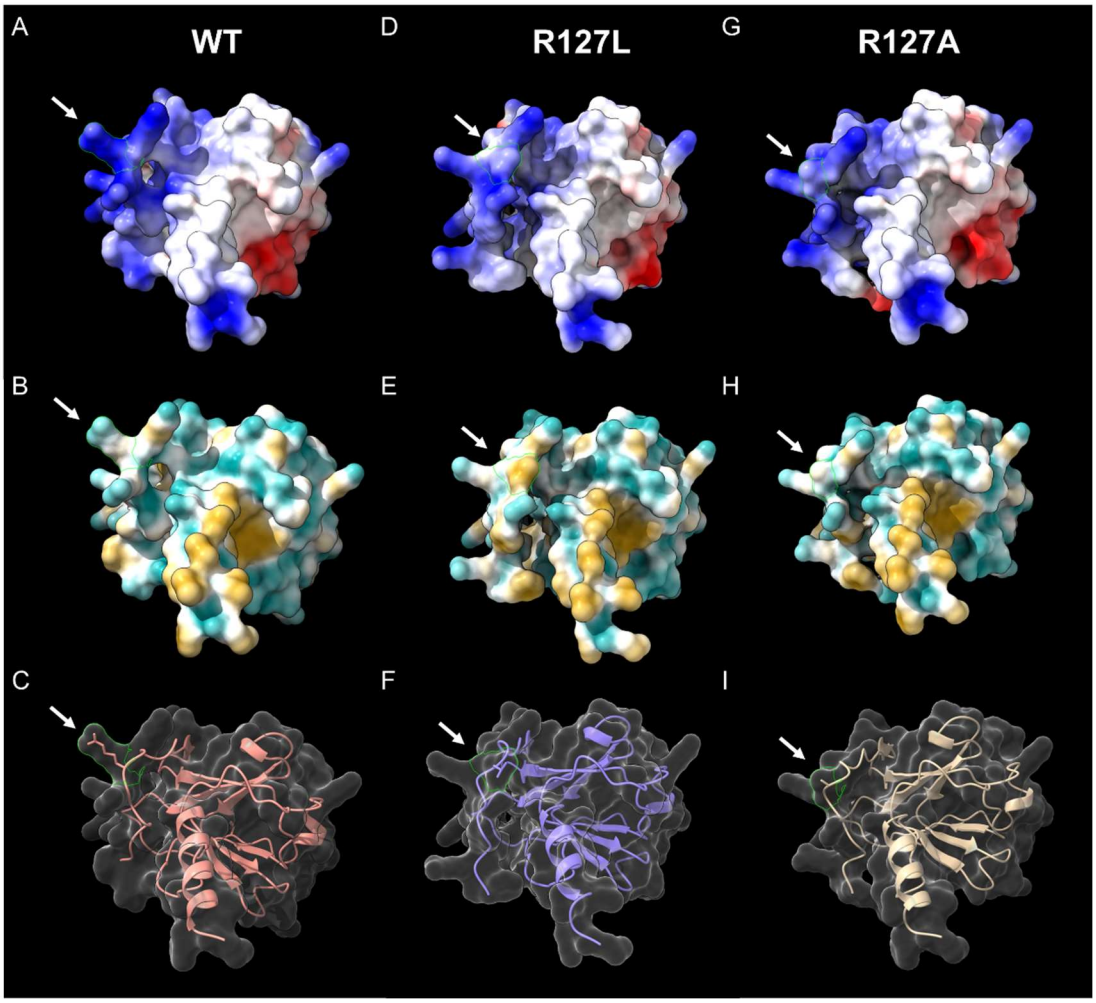

Figure 43 Prediction model of IPSE (R127) and the two mutations: R127L and R127A. The R127L (Leucine) introduces a large and hydrophobic residue (D, E, F) in close proximity of a highly positively charged patch. Whereas the R217A (Alanine) mutant introduces a smaller residue. Hydrophobicity map: Cyan – hydrophilic, amber – hydrophobic. Electrostatic potential map: Blue – positive, Red – negative

Importantly, considering the CKBP mutant (T92Y/R127L) is seemingly more robustly impaired in its stimulatory activity in comparison to the T92Y/R127A mutant and the respective single mutants, which points to the possibility that not only are both amino acids contributing to the basophil activation, but also that the substitution of an arginine with a leucine rather than an alanine is more detrimental to its function only in a double-mutant context.

3.2.7 Sm IPSE requires IgE λ sensitization to activate basophiles

To get a better understanding to which part of IgE the recombinant expressed Sm IPSE binds for subsequent basophil activation, the reporter cell assay was repeated using different IgE forms for sensitizing the RS-ATL8 cells (Figure 44). Here, all herein queried IgE forms possess the ability to successfully sensitize basophils for

subsequent stimulation with positive control anti-IgE (compared to unstimulated cells, Table 8, 9, 10 and 11). Notably, recombinantly expressed Sm IPSE only stimulates significant luciferase-induction of the reporter cells when cells were sensitized with IgEλ (Figure 44 B). All the other forms, IgE-motavizumab (A), IgE Cε2-4 (C) and IgE Cε3-4 (D), did not display any statistically significant activation after the stimulation with Sm IPSE when comparing with one-way ANOVA. In case of IgEλ, degranulation of cells occurred in all four concentrations in a highly significant way, since all of the p-Values are <0.0001.

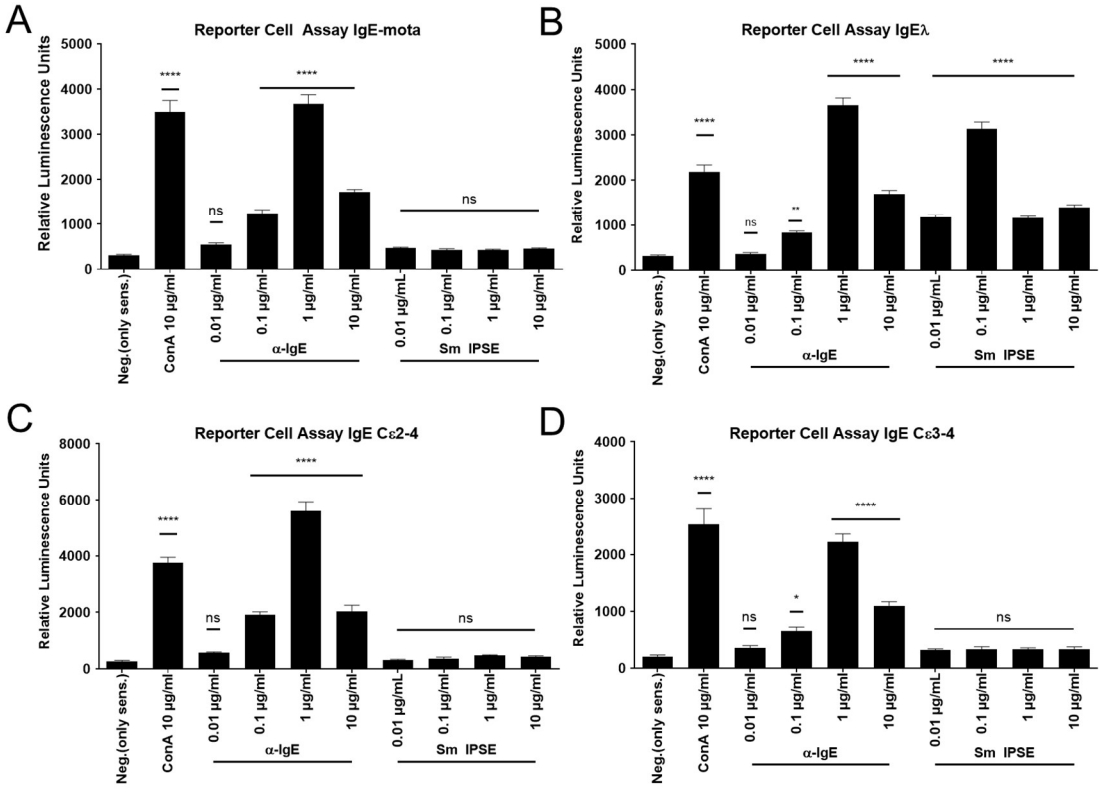

Figure 44 Reporter assay with RS-ATL8 cells sensitized with different IgE forms over night and stimulated with IPSE. (A) IgE-moavizumab (B) IgEλ (C) IgE Cε2-4 and (D) IgE Cε3-4. Cells were stimulated with Sm IPSE. IPSE only manifest significantly high Luciferase-induction activity compared to the negative control, with cells sensitized with IgEλ. The binding-activity was assessed by measuring the relative luminescence of activated RS-ATL8 reporter cells. Significance was established using the one-way ANOVA.

IgE-motavizumab

Table 8 Reporter Assay evaluation after IPSE-stimulation of IgE-motavizumab (κ)-sensitized RS-ATL8 cells. Statistics data analyses was performed using Ordinary one-way ANOVA (Dunnett's multiple comparisons test); significance was tested against negative control (non-stimulated cells).

Dunnett's multiple comparisons test	95,00% CI of diff.	Significance	Adjusted P Value
Neg.(only sens.) vs. ConA I 10 µg/mL	-3608 to -2776	Yes	<0,0001
Neg.(only sens.) vs. a-IgE 0.01 µg/mL	-622,5 to 148,5	No	0,4116
Neg.(only sens.) vs. a-IgE 0.1 µg/mL	-1325 to -554,0	Yes	<0,0001
Neg.(only sens.) vs. a-IgE 1 µg/mL	-3749 to -2978	Yes	<0,0001
Neg.(only sens.) vs. a-IgE 10 µg/mL	-1807 to -1036	Yes	<0,0001
Neg.(only sens.) vs. Sm IPSE 0.01 µg/mL	-555,2 to 215,7	No	0,7539
Neg.(only sens.) vs. Sm IPSE 0.1 µg/mL	-500,2 to 270,7	No	0,9574
Neg.(only sens.) vs. Sm IPSE 1 µg/mL	-498,7 to 272,2	No	0,9604
Neg.(only sens.) vs. Sm IPSE 10 µg/mL	-530,0 to 241,0	No	0,8682

IgEλ

Table 9 Reporter Assay evaluation after IPSE-stimulation of IgEλ (Bio-Rad)-sensitized RS-ATL8 cells. Statistics data analyses was performed using Ordinary one-way ANOVA (Dunnett's multiple comparisons test); significance was tested against negative control (non-stimulated cells).

Dunnett's multiple comparisons test	95,00% CI of diff.	Significance	Adjusted P Value
Neg.(only sens.) vs. ConA I 10 µg/mL	-2258 to -1486	Yes	<0,0001
Neg.(only sens.) vs. a-IgE 0.01 µg/mL	-427,8 to 344,3	No	0,9996
Neg.(only sens.) vs. a-IgE 0.1 µg/mL	-911,5 to -139,5	Yes	0,0039
Neg.(only sens.) vs. a-IgE 1 µg/mL	-3732 to -2960	Yes	<0,0001

Neg.(only sens.) vs. a-IgE 10 µg/mL	-1768 to -996,0	Yes	<0,0001
Neg.(only sens.) vs. Sm IPSE 0.01 µg/mL	-1250 to -477,7	Yes	<0,0001
Neg.(only sens.) vs. Sm IPSE 0.1 µg/mL	-3206 to -2434	Yes	<0,0001
Neg.(only sens.) vs. Sm IPSE 1 µg/mL	-1232 to -460,2	Yes	<0,0001
Neg.(only sens.) vs. Sm IPSE 10 µg/mL	-1462 to -690,2	Yes	<0,0001

IgE Cε2-4

Table 10 Reporter Assay evaluation after IPSE-stimulation of IgE Cε2-4 -sensitized RS-ATL8 cells. Statistics data analyses was performed using Ordinary one-way ANOVA (Dunnett's multiple comparisons test); significance was tested against negative control (non-stimulated cells).

Dunnett's multiple comparisons test	**95,00% CI of diff.**	**Significance**	**Adjusted P Value**
Neg.(only sens.) vs. ConA I 10 µg/mL	-4085 to -2897	Yes	<0,0001
Neg.(only sens.) vs. a-IgE 0.01 µg/mL	-884,0 to 303,5	No	0,6562
Neg.(only sens.) vs. a-IgE 0.1 µg/mL	-2222 to -1034	Yes	<0,0001
Neg.(only sens.) vs. a-IgE 1 µg/mL	-5912 to -4724	Yes	<0,0001
Neg.(only sens.) vs. a-IgE 10 µg/mL	-2362 to -1174	Yes	<0,0001
Neg.(only sens.) vs. Sm IPSE 0.01 µg/mL	-627,8 to 559,8	No	0,9998
Neg.(only sens.) vs. Sm IPSE 0.1 µg/mL	-677,8 to 509,8	No	0,9994
Neg.(only sens.) vs. Sm IPSE 1 µg/mL	-791,3 to 396,3	No	0,9236
Neg.(only sens.) vs. Sm IPSE 10 µg/mL	-760,0 to 427,5	No	0,9696

IgE Cε3-4

Table 11 Reporter Assay evaluation after IPSE-stimulation of IgE Cε3-4 -sensitized RS-ATL8 cells. Statistics data analyses was performed using Ordinary one-way ANOVA (Dunnett's multiple comparisons test); significance was tested against negative control (non-stimulated cells).

Dunnett's multiple comparisons test	95,00% CI of diff.	Significance	Adjusted P Value
Neg.(only sens.) vs. ConA I 10 µg/mL	-2764 to -1890	Yes	<0,0001
Neg.(only sens.) vs. a-IgE 0.01 µg/mL	-592,7 to 281,7	No	0,8951
Neg.(only sens.) vs. a-IgE 0.1 µg/mL	-884,2 to -9,809	Yes	0,0432
Neg.(only sens.) vs. a-IgE 1 µg/mL	-2455 to -1581	Yes	<0,0001
Neg.(only sens.) vs. a-IgE 10 µg/mL	-1336 to -461,3	Yes	<0,0001
Neg.(only sens.) vs. Sm IPSE 0.01 µg/mL	-554,9 to 319,4	No	0,9758
Neg.(only sens.) vs. Sm IPSE 0.1 µg/mL	-568,2 to 306,2	No	0,9555
Neg.(only sens.) vs. Sm IPSE 1 µg/mL	-573,9 to 300,4	No	0,9441
Neg.(only sens.) vs. Sm IPSE 10 µg/mL	-573,2 to 301,2	No	0,9457

3.3 IPSE - host cell interaction

3.3.1 Recombinantly expressed Sm IPSE differentially enters host cells, but not the nucleus

To study the cellular uptake of Sm IPSE into different host cells, three cell lines (CHO-Trvb, HCT-116 and HepG2) were incubated with exogenously added His-tagged Sm IPSE expressed in HEK293-6E cells. Immunofluorescence microscopy was initially carried out with a primary anti-6xHis antibody staining against the his-tagged Sm IPSE. However, the antibody bound non-specifically to cytoskeletal filaments (Figure 45).

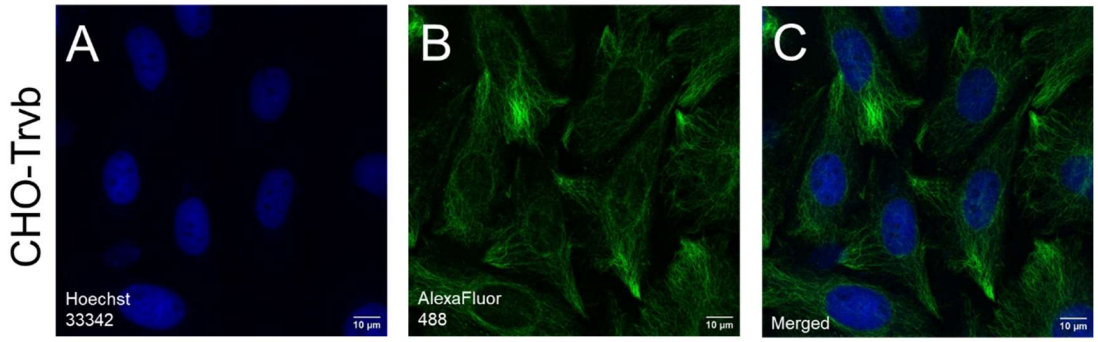

Figure 45 Non-specific binding of anti-His antibody visualized by confocal microscopy in CHO-Trvb cells, showing fluorescent signal in a filamentous pattern.

For this reason, the following experiments were performed using a specific anti-IPSE antibody for staining. This way, a differential pattern of Sm IPSE distribution in different cell lines was revealed. As shown in Figure 46, all three different cell lines internalize the protein differently. The protein is highly abundant in a punctate appereance in the cytoplasm, especially in the case of HepG2 and CHO cells, whereas HCT-116 cells show a lower fluorescent signal. Interestingly, the distribution pattern of Sm IPSE differs between the cell lines, as for HepG2 cells Figure 46 C, fluorescent signal of the antibody binding to the protein is detected in vesicles or granules distributed in the entire cell but with the highest density perinuclearly. In contrast to that, most of the protein in the HCT-116 (Figure 46 F) appears to be located around the cell membrane in a rather smooth distribution, which might indicate a different or even unfinished or rather a completely lacking internalization process. In CHO cells (Figure 46 I), Sm IPSE is distributed around the cytoplasm in a highly punctated pattern, displaying a strong fluorescent signal overall. Generally, the

differential distribution might indicate diverse endocytotic pathways exploited in the cellular entry of Sm IPSE into different host cells. Unexpectedly, in all cell lines, Sm IPSE appears to be entirely excluded from the host cell nucleus.

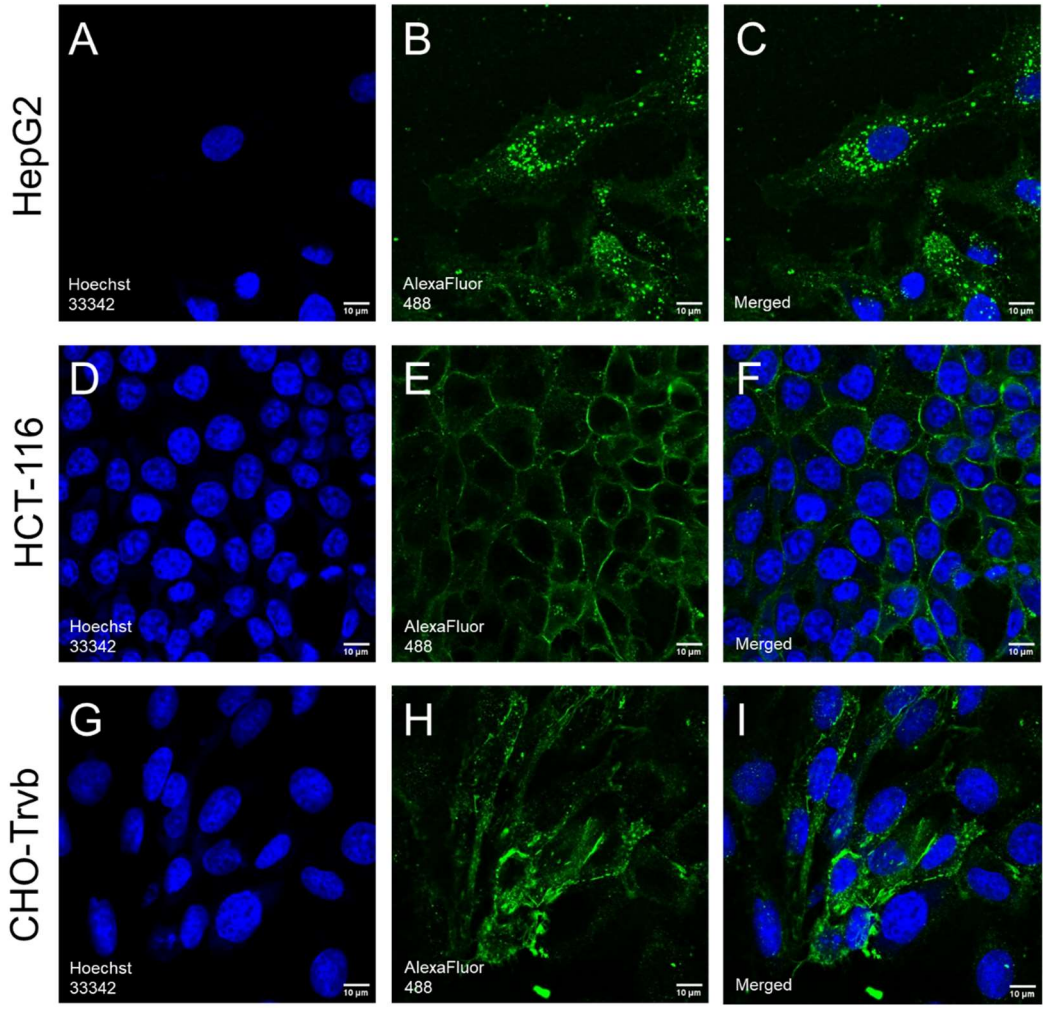

Figure 46 Subcellular localization of recombinantly expressed Sm IPSE in different cell lines. Immunofluorescence microscopy photographs were taken with a CLSM. Cells were treated with the protein for 3h at 37°C and stained with a monoclonal anti-IPSE antibody that was detected by a secondary anti-mouse Alexa Fluor488 conjugated antibody. (A) (B) (C) demonstrate the subcellular uptake in HepG2 cells. (D) (E) (F) show fluorescent signal restricted to the membrane of HCT-116 cells and (G) (H) (I) in CHO-Trvb cells. Scale bar indicative of 10µm.

3.3.2 Flash-TC IPSE

Recombinant expressed Sm IPSE bearing a Tetracysteine-Tag was supposed to be used for live cell imaging in combination with the biarsenical dye FlAsH-ETD_2. As the pictures (Figure 47 A-C) taken with CLSM show, in HCT-116 cells not pre-incubated with recombinant TC-IPSE, the FlAsH-dye itself already leads to a major fluorescent signal even at low laser-intensities. This makes it nearly impossible to distinguish the signal of the protein itself from the strong background (Figure 47 D-F), even though the fluorescent signal in general looks more intense in the IPSE-treated sample, than in non-treated cells.

When completely subtracting the background/ adapting the laser to almost no fluorescent signal of non-IPSE treated cells (Figure 47 G-I), a slight fluorescent signal in TC-IPSE treated cells can be observed all over the cell (Figure J-L). Nevertheless, it is hard to determine whether it is not residual background noise after all.

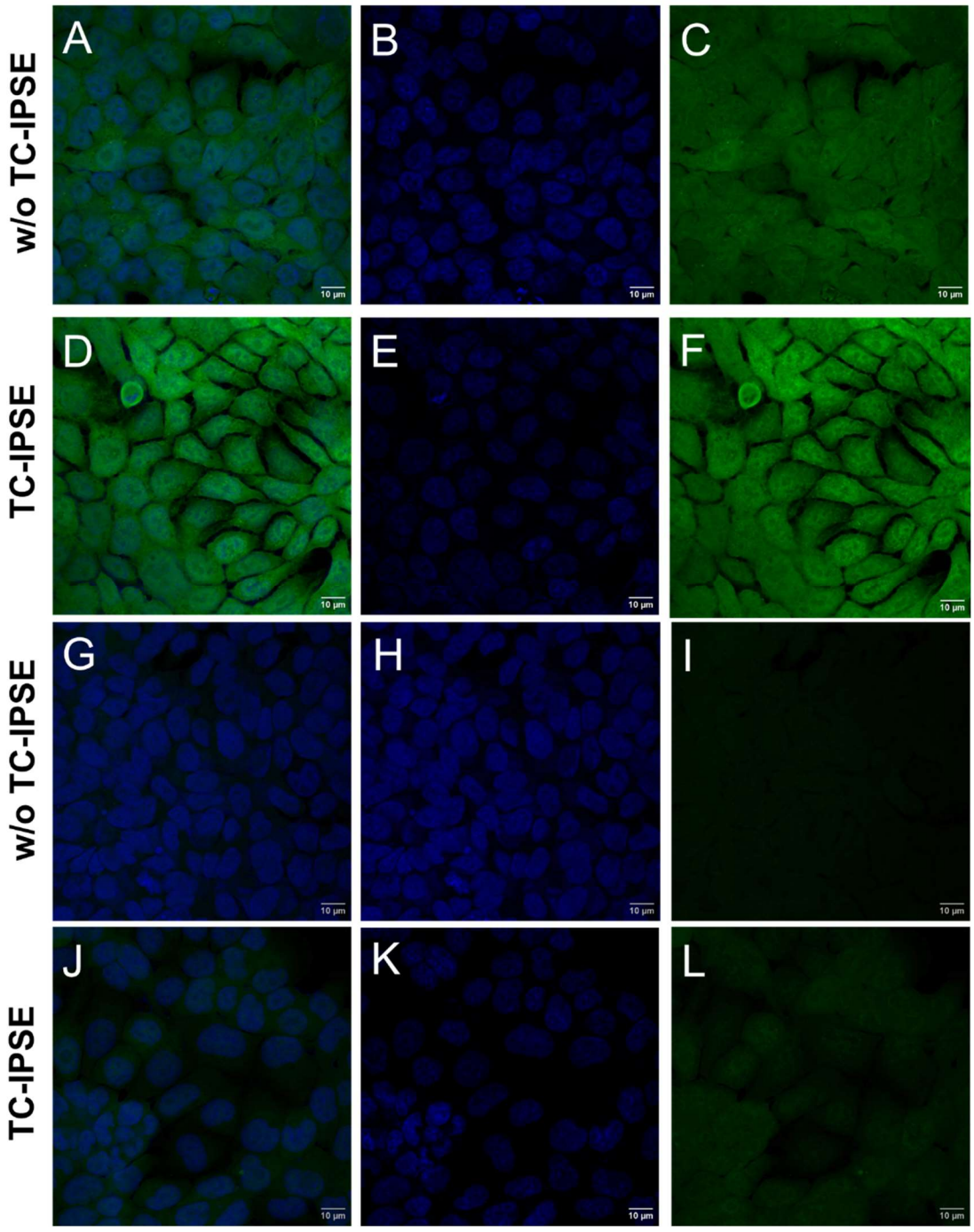

Figure 47 Confocal Images of HCT-116 cells preincubated 3h with 1.5 µg/mL Sm C-TC IPSE and subsequently treated with FlAsH-EDT_2 (D-F & J-L) including the negative control only treated with FlAsH-ETD_2 (A-C & G-I). Images of the negative control display a strong fluorescent signal, in spite of excessive washing steps. The high autofluorescence of the biarsenical dye makes it impossible to distinguish the protein from the background. (A-F) “unadapted” channel at low laser-intensity. (D-L) Images taking with an strongly reduced laser signal, showing a slightly higher fluorescent signal in IPSE-incubated cells all over the cell.

3.3.3 Different cell types temperature-dependently take up DyLight488 labelled Sm IPSE at different extents

To further investigate the difference of cellular uptake of Sm IPSE in different cell lines, HCT-116, CHO-Trvb and HepG2 cells were incubated with DyLight488 conjugated Sm IPSE and fluorescent signal was detected with flow cytometry. Another aspect of this study was to determine whether IPSE is taken up by cells in a temperature-dependent manner, helping to elucidate the underlying uptake-mechanism. FITC-conjugated Human Transferrin served as uptake control, as it is taken up by cells in a temperature-dependent manner (no uptake at 4°C).

The experimental setup included the treatment with Sm IPSE DyLight488 or FITC-conjugated human Transferrin (hTrf) at 37°C and in case of HCT-116 cells an additional incubation temperature of 4°C. FACS was conducted with a BB515-A laser-channel (blue laser designed for exciting with blue laser at 488 nm) (DyLight excitation: 493 nm and emission: 518 nm; FITC excitation 491 nm and emission: 516 nm). For each cell line, the gating strategy was adapted and kept constant within each experiment (example Figure 48). For that purpose, living cells were gated with the help of the FSC-A (size) vs SSC-A (granularity) plot. Afterwards the mean fluorescence intesity was calculated and displayed in an overlay histogram. For further analysis, the geometric mean of the gated cells was calculated, and subsequently used for more detailed comparisons by developing the ratio between unquenched (PBS) and quenched (TB=Trypanblue) groups (Unpaired T-Test, Table 12). Quenching with TB should block the fluorescent signal on the cell surface, i.e. labelled-protein that is attached (not internalized) to the (outer) cell membrane, without interferring with the fluorescent signal derived from internalized labelled protein. Comparison of quenched (TB) vs. unquenched (PBS) signals, reveals differences in protein uptake levels.

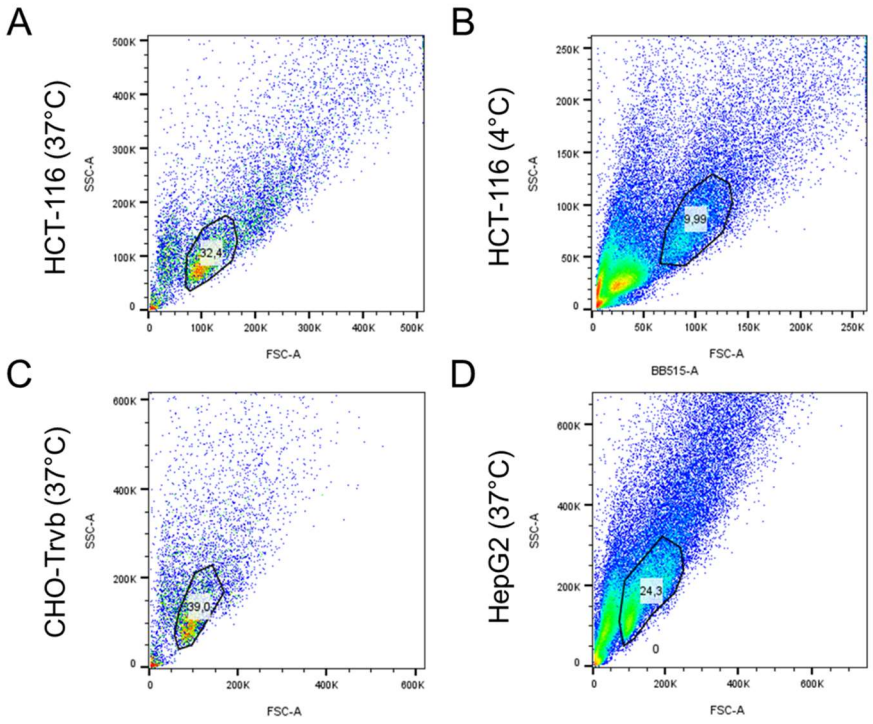

Figure 48 Examples for gating strategy adapted to every cell line and FACS experiment. Cells analysed by the use of forward scatter (FSC-A) and sideward scatter (SSC-A). Afterwards, the mean fluorescence intensity was calculated. (A) Dot plot of HCT-116 cells treated with Sm IPSE DyLight488. (B) Gated cell population of HCT-116 cells incubated with Sm IPSE DyLight488 at 4°C. (C) Histogram of CHO-TrvB cells treated with Sm IPSE DyLight488. (D) Histogram of gated HepG2 cell incubated with Sm IPSE DyLight488. FACS was conducted with a BB515-A laser-channel (blue laser designed for exciting with blue laser at 488 nm) (DyLight excitation: 493 nm and emission: 518 nm; FITC excitation 491 nm and emission: 516 nm).

Table 12 Ratios of quenched and unquenched geometric means (fluorescent signal chanel: BB515) of tested cell lines for IPSE-internalization, whereby the quenched means were divided by the unquenched means.

Cell Line	**Ratio: Untreated TB vs. Untreated PBS**	**Ratio: Sm IPSE TB vs. Sm IPSE PBS**	**Ratio: hTrf TB vs. hTrf PBS**
HCT-116 (37°C)	1:0.75	1:5.88	1:0.94
HCT-116 (4°C)	1:0.84	1:13.03	1:1.1
CHO-Trvb (37°C)	1:0.78	1:1.4	1:0.78
HepG2 (37°C)	1:0.59	1:3.24	1:1.35

Considering the ratio of quenched vs unquenched signal (Table 12 and 13), differences in the fluorescent signal after the incubation with Sm IPSE DyLight488 appear, as expected. Accordingly, in case of HCT-116 cells (37°C) the IPSE with a 1:5.88 the fluorescent signal is almost six times higher in unquenched (PBS) cells compared to the quenched (TB) cells, whereas the fluorescent signal of hTrf-FITC does not show a great difference, as the ratio amounts to 1:0.94. These findings are supported by the T-Test results showing a significant difference (p=0.038) between unquenched and quenched in case of Sm IPSE DyLight488 treatment and none between the hTrf-FITC treated cells (p=0,8982). As expected, both treatments lead to a significant higher fluorescent signal compared to the untreated cells even after quenching the membranous signal with Trypan Blue (p=0.001 and p=0.0118, respectively). Based on Figure 49 it also can be noted that in general HCT-116 cells incubated with Sm IPSE DyLight488 display a higher fluorescent signal, which only approximates the signal of hTrf-FITC after quenching. This is indicative of a higher uptake of Sm IPSE in these cells.

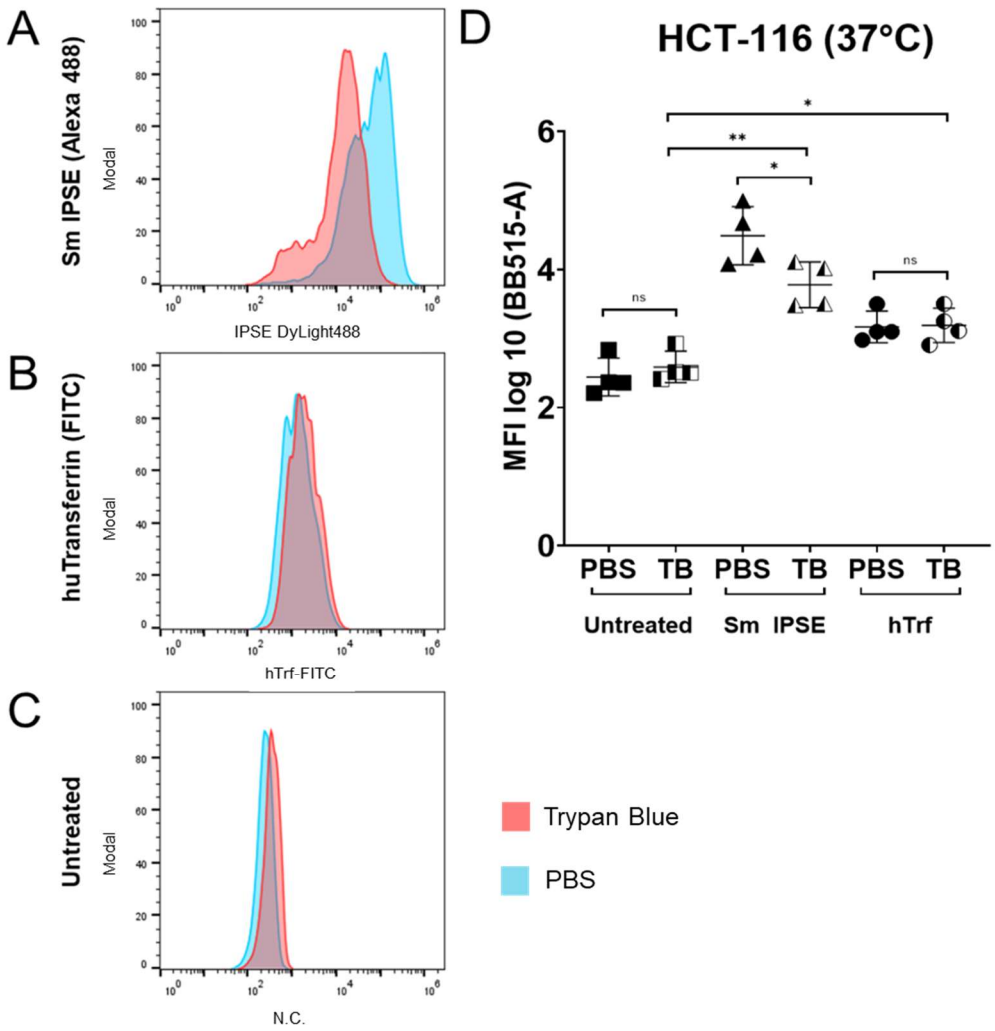

Figure 49 Analyses of HCT-116 pre-incubated with either Sm IPSE DyLight488 or human Transferrin-FITC at 37°C with FACS measuring BB515-A (channel designed for exciting with blue laser at 488 nm). Here, the geometric mean of in total three independent experiments (i.e., performed on different days) was used for statistical analysis. (A) Example for fluorescent signal of HCT-116 cells treated with Sm IPSE DyLight488. Showing a peak shift from unquenched cells (blue, PBS) to a lower signal in quenched (red, Trypanblue) cells. (B) Histogram of HCT-116 cells incubated with hTrf-FITC showing no remarkable shift between unquenched (blue, PBS) and quenched (red, TB). (C) Another example for a Histogram of quenched (red, TB) and unquenched (blue, PBS) HCT-116 with a marginal shift of the peak standing for the fluorescent intensity. (D) Graph containing the Log of geometric means of all three replicates, whereby the T-Test results are included. ($p < 0.05$ *, $p < 0.001$ **, $p < 0.0001$ ***)

Table 23 T-Test analyses of HCT-116 cells treated with either Sm IPSE DyLight488 or human transferrin-FITC at 37°C in comparison with untreated cells and with respect to unquenched (PBS) and quenched (TB) signals. Geometric means derived from FACS-analysis (BB515-A) were used for statistical analysis. Significant: p=<0.05

Unpaired T-Test HCT-116 (37°C)	**95,00% CI of diff.**	**Significance**	**Adjusted P Value**
Untreated PBS vs. Untreated TB	-0,2901 to 0,5817	No	0,4444
hTrf PBS vs. hTrf TB	-0,3917 to 0,4369	No	0,8982
Sm IPSE PBS vs. Sm IPSE TB	-1,365 to -0,05432	Yes	0,038
Sm IPSE TB vs. Untreated TB	0,6993 to 1,683	Yes	0,001
hTRF TB vs. Untreated TB	0,6033 ± 0,1692	Yes	0,0118

Intriguingly, the uptake properties of the HCT-116 cells (Figure 50, Table 14) completely change after the incubation at 4°C with the two proteins. As expected, the uptake ratio between hTrf-FITC unquenched and unquenched the ratio amounts to 1:1.1 (Table 12), resulting in no significant difference (p=0.2764). Unexpectedly, hTrf-treated cells have led to a significant higher fluorescent signal when quenched, than untreated cells (p=0.0364). However, cells treated with Sm IPSE DyLight488, display a completely different pattern, as the fluorescent signal is thirteen times higher in unquenched cells (ratio 1:13.03). In line with that, a significant difference between untreated and treated cells after quenching cannot be detected, as p=0.1979. Whereby, it was previously highly significant in unquenched untreated and IPSE-treated cells (p=0.0007).

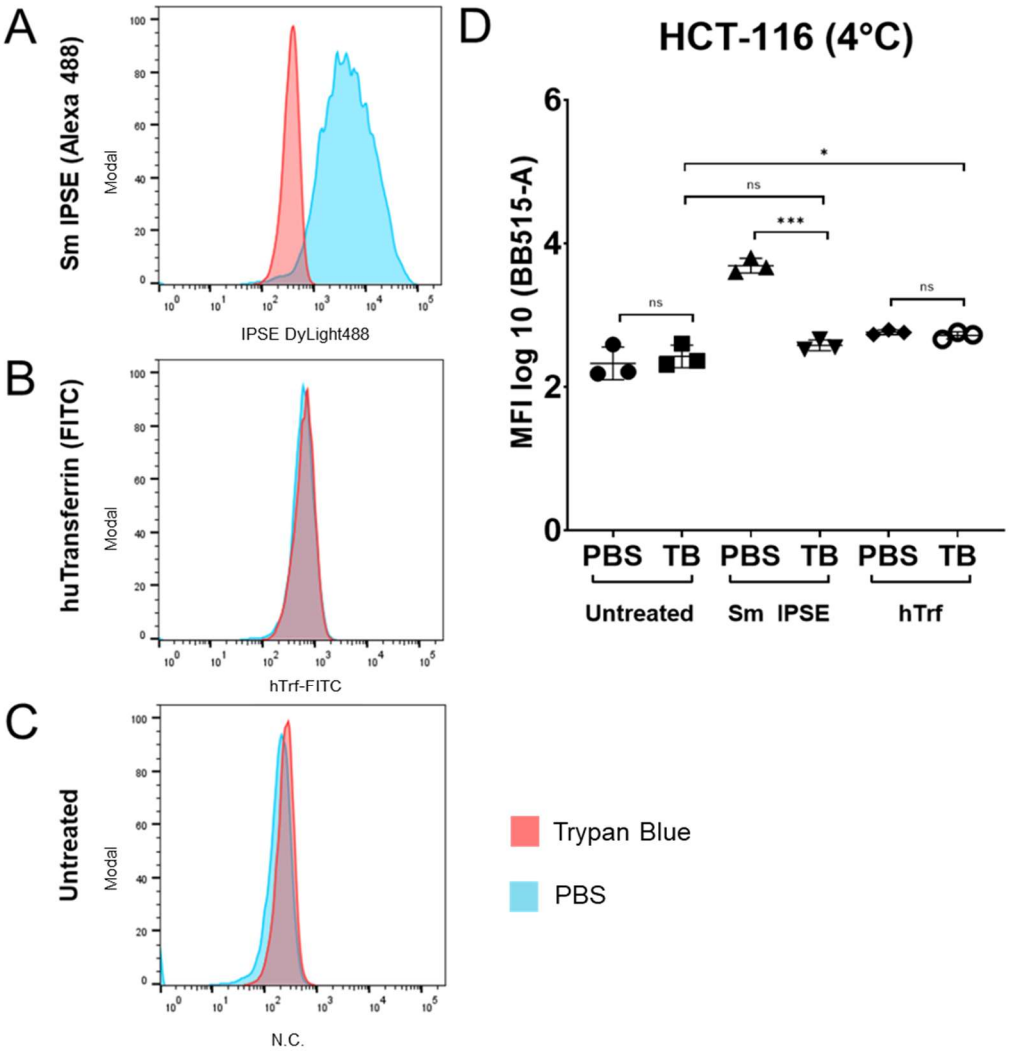

Figure 50 Analyses of HCT-116 cells pre-incubated with either Sm IPSE DyLight488 or human Transferrin-FITC at 4°C with FACS measuring BB515-A. Here, the geometric mean of in total three experiments was used for statsitical analysis. (A) Example for fluorescent signal of HCT-116 cells treated with Sm IPSE DyLight488. Showing a peak shift from unquenched cells (blue, PBS) to a lower signal in quenched (red, Trypanblue) cells. (B) Histogramm of HCT-116 cells incubated with hTrf-FITC showing no remarkable shift between unquenched (blue, PBS) and quenched (red, TB). (C) Another example for a Histogram of quenched (red, TB) and unquenched (blue, PBS) HCT-116 with a marginal shift of the peak standing for the fluorescent intensity. (D) Graph containing the Log of geometric means of all three replicates, whereby the T-Test results are included. ($p < 0.05$ *, $p < 0.001$ **, $p < 0.0001$ ***)

Table 14 T-Test analyses of HCT-116 cells treated with either Sm IPSE DyLight488 or human transferrin-FITC at 4°C in comparison with untreated cells and with respect to unquenched (PBS) and quenched (TB) signals. Geometric means derived from FACS-analysis (BB515-A) were used for statistical analysis. Significant: p=<0.05

Unpaired T-Test HCT-116 (4°C)	**95,00% CI of diff.**	**Significance**	**Adjusted P Value**
Untreated PBS vs. Untreated TB	-0,3449 to 0,5406	No	0,5727
hTrf PBS vs. hTrf TB	-0,1395 to 0,05247	No	0,2764
Sm IPSE PBS vs. Sm IPSE TB	-1,314 to -0,9079	Yes	0,0001
Sm IPSE TB vs. Untreated TB	-0,1231 to 0,4306	No	0,1979
Sm IPSE PBS vs. Untreated PBS	0,9618 to 1,764	Yes	0,0007
hTRF TB vs. Untreated TB	0,03007 to 0,5546	Yes	0,0364

Since CHO-Trvb cells (Figure 51, Table 15) are lacking a transferrin-receptor, it is no surprise that in both cases, quenched and unquenched hTrf-FITC-treated cells, no significant difference of fluorescent signal can be detected. Accordingly, the ratio reveals (1:0.78) (Table 12), supported by the conducted T-Test analysis (p=0.3455), does not show a remarkable difference between treatments. These findings are supported by the fact that there is no significant difference (p=0.9929) between untreated and hTRf-treated CHO-Trvb cells. Nevertheless, the Sm IPSE DyLight488 uptake properties in CHO-Trvb cells differ to the one of HCT-116 cells. Here, the ratio between quenched and unquenched is not significantly different (1:1.4, p=0.8387). Correspondingly, the fluorescent signal between untreated and Sm IPSE treated quenched cells is significantly different (p=0.027).

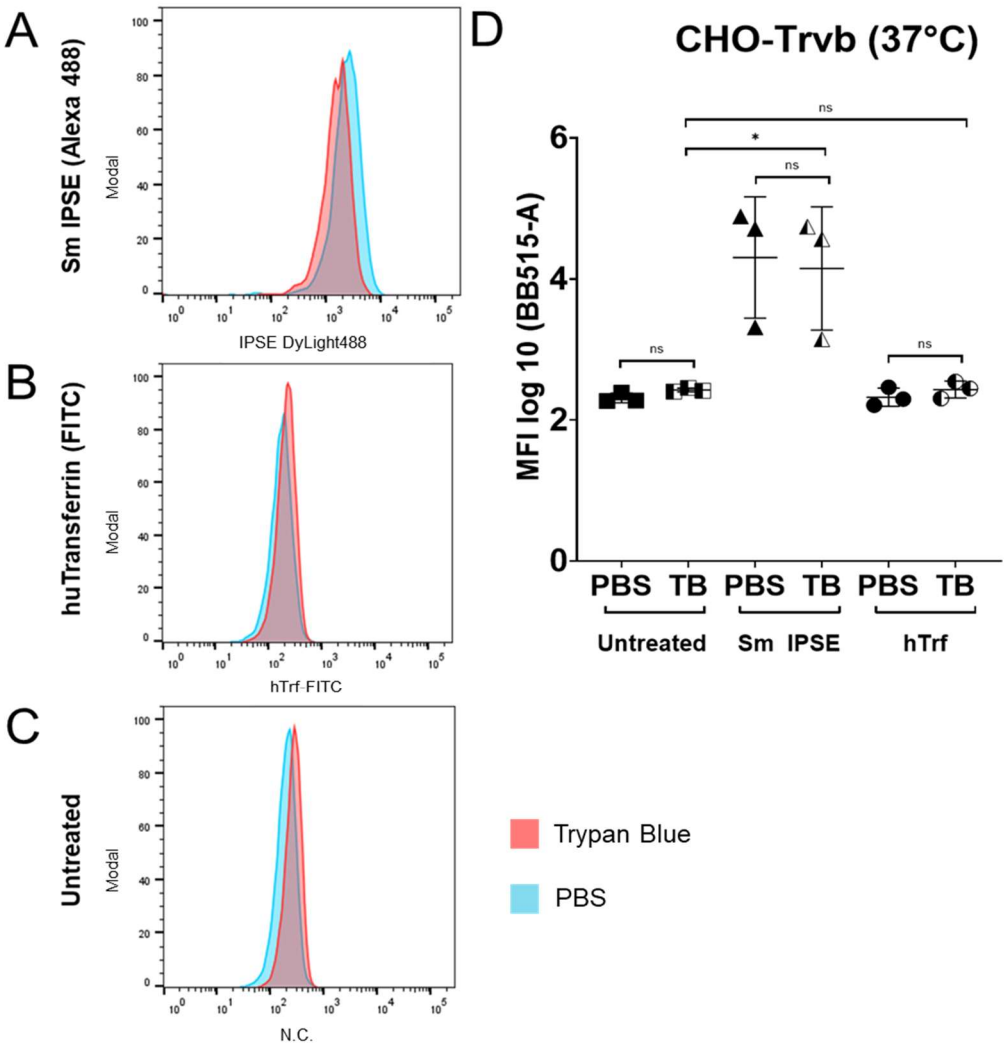

Figure 51 Analyses of CHO-Trvb cells pre-incubated with either Sm IPSE DyLight488 or human Transferrin-FITC at 37°C with FACS measuring BB515-A. Here, the geometric mean of in total three experiments was used for statsitical analysis. (A) Example for fluorescent signal of HepG2 cells treated with Sm IPSE DyLight488. Showing a peak shift from unquenched cells (blue, PBS) to a lower signal in quenched (red, Trypanblue) cells. (B) Histogramm of CHO-Trvb cells incubated with hTrf-FITC showing no remarkable shift between unquenched (blue, PBS) and quenched (red, TB). (C) Another example for a Histogram of quenched (red, TB) and unquenched (blue, PBS) HCT-116 with a marginal shift of the peak standing for the fluorescent intensity. (D) Graph containing the Log of geometric means of all three replicates, whereby the T-Test results are included. ($p < 0.05$ *, $p < 0.001$ **, $p < 0.0001$ ***)

Table 15 T-Test analyses of CHO-Trvb cells treated with either Sm IPSE DyLight488 or human transferrin-FITC at 37°C in comparison with untreated cells and with respect to unquenched (PBS) and quenched (TB) signals. Geometric means derived from FACS-analysis (BB515-A) were used for statistical analysis. Significant: p≤0.05

Unpaired T-Test CHO-Trvb (37°C)	95,00% CI of diff.	Significance	Adjusted P Value
Untreated PBS vs. Untreated TB	-0,002535 to 0,2289	No	0,0532
hTrf PBS vs. hTrf TB	-0,1740 to 0,3916	No	0,3455
Sm IPSE PBS vs. Sm IPSE TB	-2,122 to 1,814	No	0,8387
Sm IPSE TB vs. Untreated TB	0,3218 to 3,129	Yes	0,027
hTRF TB vs. Untreated TB	-0,1898 to 0,2044	No	0,9229

For HepG2 (Figure 52, Table 16) cells, the distribution of significant differences in fluorescent signal of the cells slightly differs from the other two cell lines. Here, in each group, unquenched and unquenched cells display a significantly different signal, as for untreated cells a p-Value of 0.0084, 0.031 for hTrf-FITC treated cells and 0.0235 for Sm IPSE DyLight488 incubated cells was obtained. Nevertheless, the ratio of quenched and unquenched in case of Sm IPSE DyLight488-cells reveals a three -fold higher signal in quenched HepG2 cells (ratio 1:3.24) (Table 12). Moreover, hTrf-FITC treated cells only show a minimal shift in fluorescent signal as the ratio is 1:1.35. Above these findings, compared to the quenched untreated cells, both protein-treatments (quenched) lead to a significant change of signal (T-test $p<0.0001$ and $p=0.0004$, respectively), which implies a significant cellular uptake of both proteins by the cell.

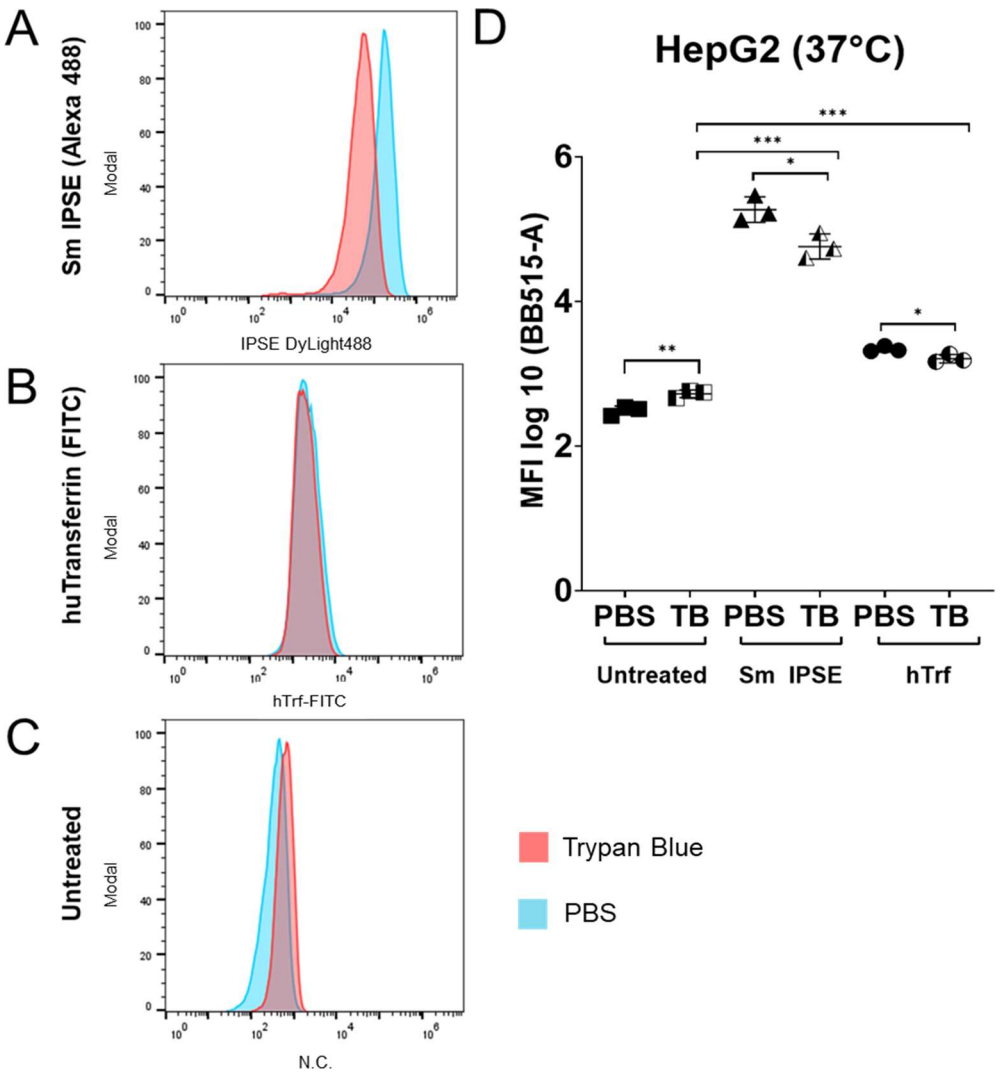

Figure 52 Analyses of HepG2 cells pre-incubated with either Sm IPSE DyLight488 or human Transferrin-FITC at 37°C with FACS measuring BB515-A. Here, the geometric mean of in total three experiments was used for statsitical analysis. (A) Example for fluorescent signal of HepG2 cells treated with Sm IPSE DyLight488. Showing a peak shift from unquenched cells (blue, PBS) to a lower signal in quenched (red, Trypanblue) cells. (B) Histogramm of HepG2 cells incubated with hTrf-FITC showing no remarkable shift between unquenched (blue, PBS) and quenched (red, TB). (C) Another example for a Histogram of quenched (red, TB) and unquenched (blue, PBS) HCT-116 with a marginal shift of the peak standing for the fluorescent intensity. (D) Graph containing the Log of geometric means of all three replicates, whereby the T-Test results are included. ($p < 0.05$ *, $p < 0.001$ **, $p < 0.0001$ ***)

Table 16 T-Test analyses of HepG2 cells treated with either Sm IPSE DyLight488 or human transferrin-FITC at 37°C in comparison with untreated cells and with respect to unquenched (PBS) and quenched (TB) signals. Geometric means derived from FACS-analysis (BB515-A) were used for statistical analysis. Significant: p=<0.05

Unpaired T-Test HepG2 (37°C)	95,00% CI of diff.	Significance	Adjusted P Value
Untreated PBS vs. Untreated TB	0,09854 to 0,3630	Yes	0,0084
hTrf PBS vs. hTrf TB	-0,2437 to -0,01957	Yes	0,031
Sm IPSE PBS vs. Sm IPSE TB	-0,9060 to -0,1127	Yes	0,0235
Sm IPSE TB vs. Untreated TB	1,746 to 2,330	Yes	<0,0001
hTRF TB vs. Untreated TB	0,3611 to 0,6127	Yes	0,0004

Taken together, in all the three cell lines the fluorescent signal appears to be a little higher in untreated quenched cells than in unquenched cells, whereas in the case of HepG2 cells protein treatment leads to a significant difference between the quenched and unquenched groups (0.0084). This might be due to the fact, that Trypanblue might be cytotoxic after a certain amount of time, leading to a different laser-refraction of the single cell (S. I. Kim et al., 2016).

In summary, in terms of cellular uptake of Sm IPSE DyLight488, differences between each cell line in regard of the quenched-unquenched ratio can be found. Hence, it can be stated that CHO-Trvb seem to intake most of Sm IPSE since the ratio amounts to circa 1:1. This is followed by HepG2 cells displaying an uptake ratio of 1:3 and last, HCT-116 cells where the fluorescent signal of unquenched cells is over 13 times higher (1:13) compared to quenched ones.

3.3.4 Analysis of transcriptome of HepG2 cells with RNA-seq

Aiming to understand the transcriptional changes elicited by Sm IPSE treatment of liver cells, HepG2 cells were incubated with 1.5 µg/mL recombinantly expressed Sm IPSE.

Gene expression shifts were examined through RNAseq, for which isolated RNA of HepG2 cells after 4h of IPSE-treatment, was used. Untreated cells were used as negative control. In order to validate the quality of the isolated RNA, samples were run on a 1% Agarose gel, showing the usual pattern expected for eukaryotic RNA with the two strongest bands representing 28S and 18S rRNA at approx. 2 and 1 kb, respectively (Figure 53). RNA-seq was carried out to a considerable depth ~20x10^6 reads per sample), with generally more than 95% of the sequenced reads aligning successfully to the human reference genome (see Table 17). Subsequently, gene expression profiles were directly compared between IPSE-treated and untreated cells.

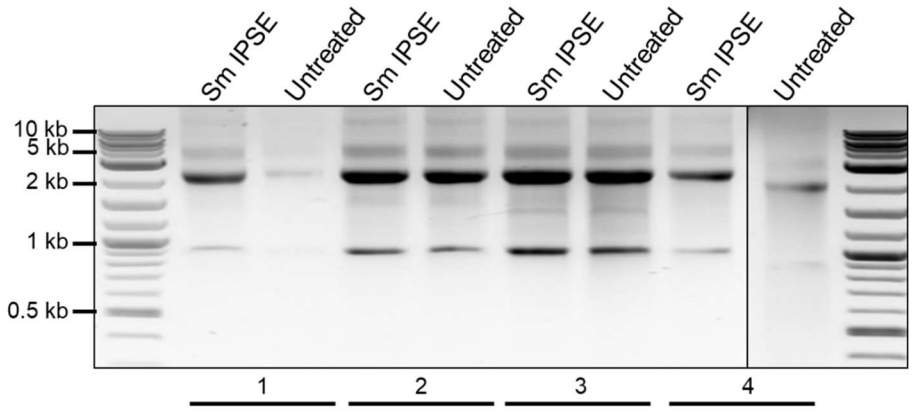

Figure 53 Isolated RNA of HepG2 samples either treated with Sm IPSE for 4h or with no added stimulus. 1-4 represent the biological replicates. All samples show the same band pattern, whereby the strongest bands can be detected around 2kb and 1kb, which represent 28S and 18S rRNA, respectively. Faint bands/smear between 1-10 kb display residual mRNA.

Table 17 Sequencing and alignment statistics of analyses of the transcriptome of cell treated with IPSE. Nreads2x = number of reads sequenced, Nalign = number of Nreads2x which have been successfully aligned to the reference genome; Percent Aligned = percentage of aligned over total sequenced reads.

Sample	Nreads2x	Nalign	Percent Aligned
IPSE_1	67660100	64883116	95.90
IPSE_2	56991684	54620549	95.84
IPSE_3	55660318	53230702	95.63
IPSE_4	54703248	52328240	95.66
Ctr_1	63734736	61043636	95.78
Ctr_2	51276148	49123359	95.80
Ctr_3	62236914	59292724	95.27
Ctr_4	51855044	49770486	95.98

Results reveal, that in comparison to untreated cells, 2 genes were downregulated and 15 upregulated, when applying a cut-off for the adjusted p-value of < 0.05 and for the log2fc of > 0.8 or < -0.8. Since only 17 (Table 18) genes were significantly deregulated according to these thresholds, it was decided to focus on the top 100 differentially expressed genes (DEGs) for further analysis (sorted for p-value).

Table 11 List of statistically significantly deregulated genes (applied criteria: adjusted p-value of < 0.05 and for the log2fc of > 0.8 and < -0.8). baseMean = the average of the normalized count values, dividing by size factors, taken over all samples; log2FoldChange = The effect size estimate. This value indicates how much the gene or transcript's expression has changed between the comparison and control groups. This value is reported on a logarithmic scale to base 2; stat = the value of the test statistic for the gene or transcript; p-value = P-value of the test for the transcript; P-adj. = Adjusted P-value for multiple testing for the gene or transcript.

Gene	baseMean	log2FoldChange	stat	p-value	P –adj.
CYP1A1	1279,17	2,75	6,33	2,3996E-10	3,8014E-06
SKIL	1015,12	1,06	5,5	3,7589E-08	0,00014887
SLC30A1	2992,86	0,92	5,51	3,5199E-08	0,00014887
ATOH8	341,02	1,05	5,1	3,4249E-07	0,00045214
SH2B3	926,74	0,83	4,66	3,224E-06	0,00255373
BMF	319,9	1,18	4,63	3,7119E-06	0,00280022
BMP6	31,3	1,63	4,45	8,7061E-06	0,00539702
IHH	88,17	0,94	4,05	5,2214E-05	0,01923653
SYNPO	206,91	0,88	4,0	6,4411E-05	0,02218274

SLC7A11	2419,26	1,51	4,0	6,373E-05	0,02218274
MT1XP1	17,12	2,61	3,9	9,5418E-05	0,02748386
LOC124904949	99,4394763	3,54777099	3,89241836	9,925E-05	0,02807709
WNT11	69,8676038	1,15063113	3,82531554	0,0001306	0,0356731
MT1X	1526,76538	2,69705885	3,75795038	0,00017131	0,04307788
LFNG	87,1184888	1,0491763	3,74242729	0,00018225	0,04511289
PGF	416,825319	-0,9058102	-4,9166649	8,8031E-07	0,00099613
SLC39A10	775,896472	-0,8156845	-4,2930842	1,7621E-05	0,00901363

The top 100 DEGs were subjected to an over representation analysis (ORA) using the Gene Ontology Resource database (Ashburner et al., 2000). Results of ORA are displayed in the heat map (Figure 54) and tree plot (Figure 55), where the major deregulated GO terms were assigned by similarity of the contributing genes displayed as supersets 1-5. A binary indicator was added to the heat map (fig##), which visualizes the membership of the DEGs to the corresponding terms.

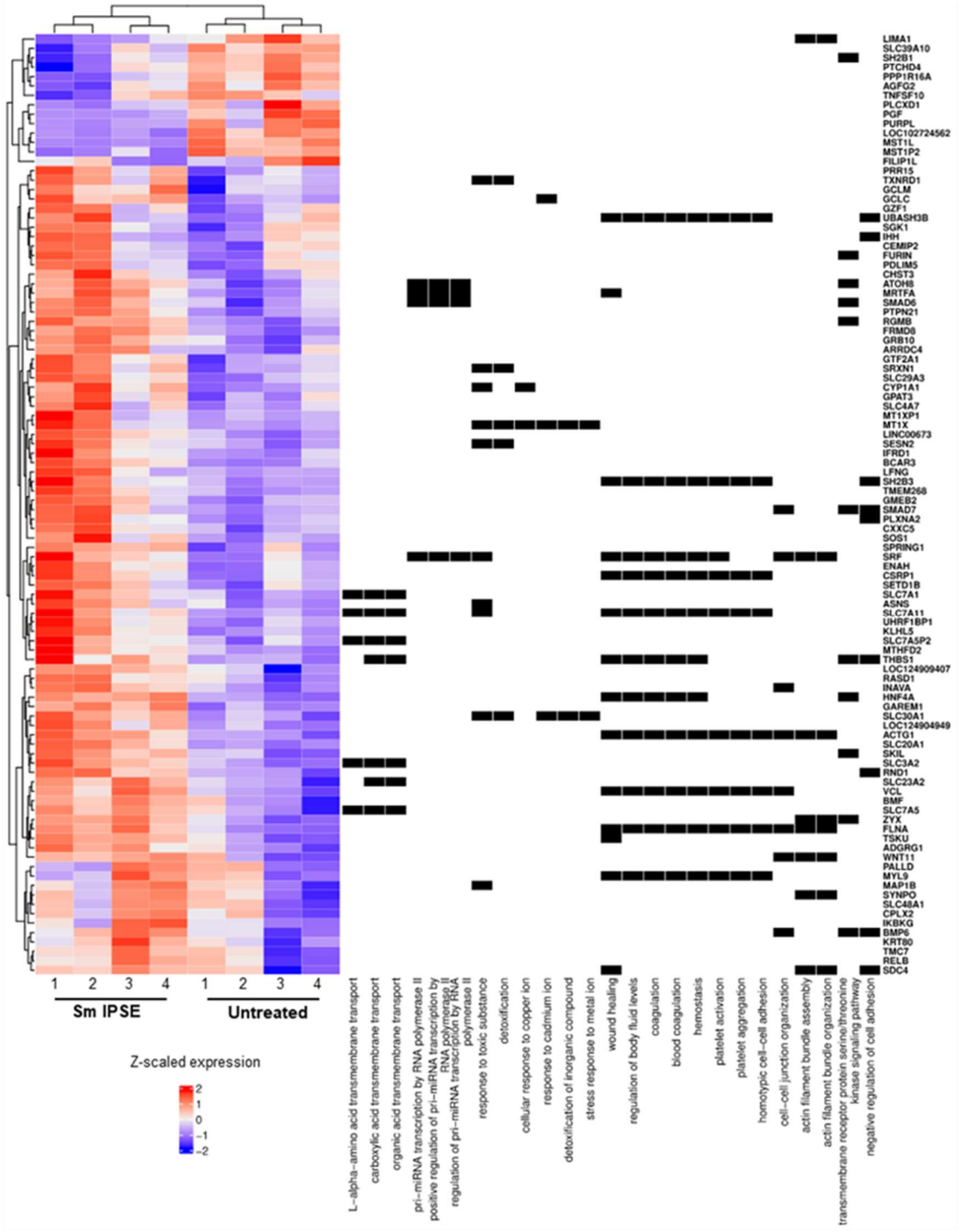

Figure 54 Effects of Sm IPSE on transcription of top 100 differentially expressed genes, displayed in a heat map showing levels of expression of these genes. Blue designates the degree of gene downregulation while red denotes upregulation expressed as z-scaled expression values. Membership of genes to GO-terms identified in an over-representation analysis are in the binary heatmap to the right. Notably, gene ontologies are attempts to find sets of controlled vocabulary to describe gene functions.

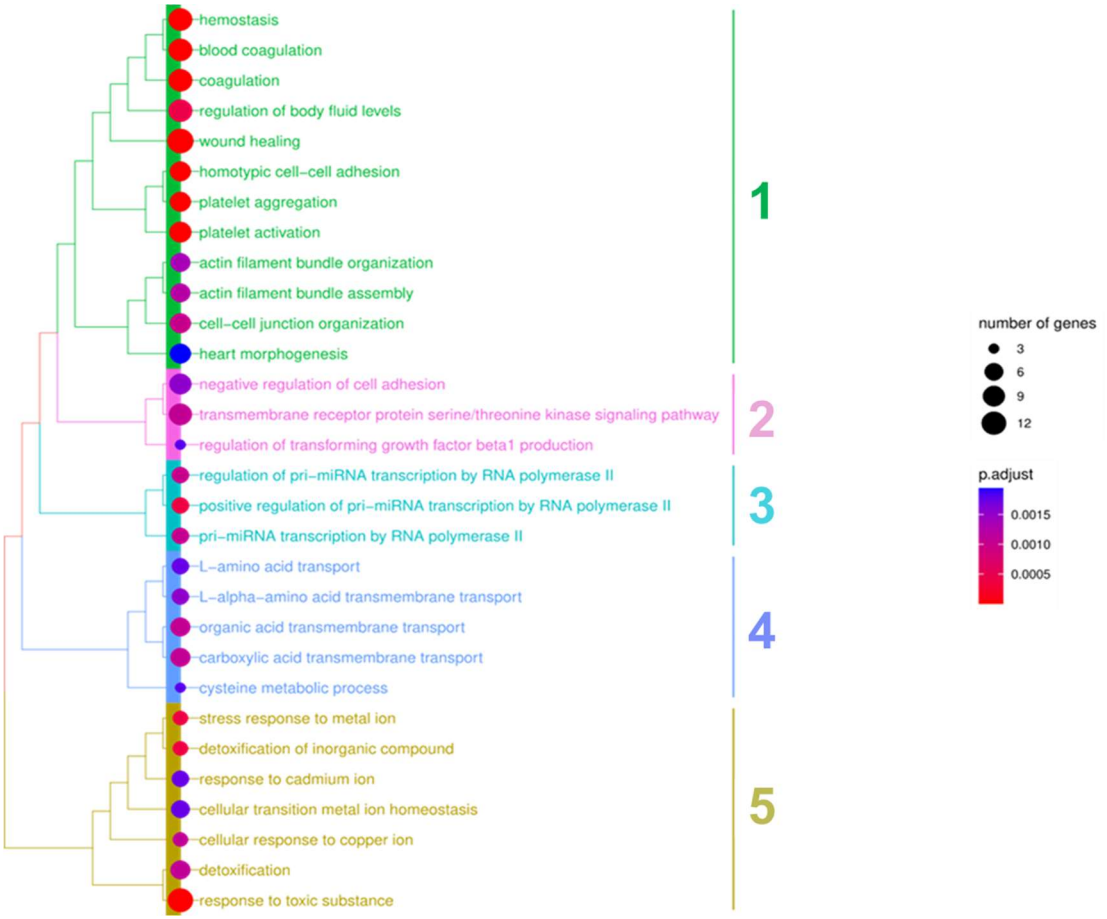

Figure 55 Dendrogram of the top 40 deregulated pathways after 4h Sm IPSE treatment of HepG2 cells according to Gene Ontology. Colours indicate clustering, with clusters representing pathways associated with similar biological functions and genes. The size of the circles represent the numbers of deregulated genes associated with the respective pathway.

Intriguingly, the identified GO terms for the first superset seem to be mostly associated with wound healing, as well as cell-cell junction and actin filament organization (Figure 55, cluster 1). Furthermore, terms of this superset include the most deregulated genes and are consequently characterized with the lowest p-values. Deregulated genes such as CSRP1, SLC7a1 ACTG1, VLC, FLNA, WNT11, BMP6 and SDC41 belong to the “cell-cell junction” GO term and partly to the “actin filament bundle organization” term, as well. Noteworthy, the term “negative regulation of cell adhesion” from superset 2 contains several deregulated genes, which are also associated with terms of superset 1, namely THBS1, SH2B3, SDC4, BMP6, SMAD7 and UBASH3B1. This trend is not as strong in the two other terms from superset 2, the receptor mediated kinase signalling pathway and regulation of transforming growth factor beta1 production. But also with the regulation of transforming growth factor beta1. The third superset embodies the group containing terms describing the regulation of pri-miRNA

transcription by RNA polymerase II. Here,all deregulated genes, such as SRF, ATOH8, MRTFA and SMAD6, appear to be involved in all three deregulated GO terms. Besides that, the fourth group contains deregulated terms dealing with amino acid transports and in general transmembrane transports of acidic components belonging to the solute-carrier-gene superfamily. The last group includes a set of GO terms being associated with cellular responses to metal ionic stress and toxic substances. Genes associated with these biological processes are SLC30A1, MT1XP1, MT1X1, SRXN1, CYP1A1, MAP1b, ASNS, SESN2 and SLC7A11.

An alternative way for studying the concordant changes of gene expression of gene sets, is available through the Gene Set Enrichment Analysis (GSEA) method. For the GSEA two different databases, GO and Reactome, were used. In contrast to the ORA, GSEA uses all genes, ordered for their DESeq2 test statistic instead of using a determined set of genes determined as being up- or down-regulated by applying arbitrary thresholds. This analysis serves as a complement for the above-described ORA. GSEA can recapitulate findings made by ORA but may identify additional more subtle trends not affected by the most highly differentially expressed genes. Comparing both results represented by Figure 56 and 57, it becomes evident that the Reactome analysis differs in several points from the GO analysis, but generally supports previous findings. This is exemplified by the identification of many upregulated biological processes such as the ones belonging to the regulation of transforming growth factor beta production, pri-mRNA transcription and blood vessel development-associated pathways when applying the GO database either to the ORA orGSEA. These terms however, are not included in the highest deregulated Reactome pathways. Notably, top deregulated GO terms and Reactome pathways generally differ between both databases, with the exception of some interesting terms. Both sets of annotation detect an upregulation in cell junction associated pathways, as well as L-amino acid transport and the response to metal ions. In addition to that, it can be stated that both GO's and Reactome's dowonregulated terms are only associated with very general cellular functions, such as mitosis and protein folding (chaperones). Also, in both GSEAs pathways and terms in context with the respiratory electron transport chain appear to be downregulated. Moreover, both GSEAs also point at pathways standing in line with NGF (Nerve Grwoth Factor)-stimulated transcription and nuclear events containing kinase and transcription factor activation for a wide array of transcriptional targets. Finally, unsing the Reactome data base some unique deregulated pathways were identified that are not found within the GO data base. For example, pathways standing in context with semaphorin signalling, ECM (Extracellular matrix) interactions or tRNA Aminoacylation can be found only in

the highest ranked hits of the Reactome analysis. Moreover, GO reveals downregulation of biological processes designated to protein transport.

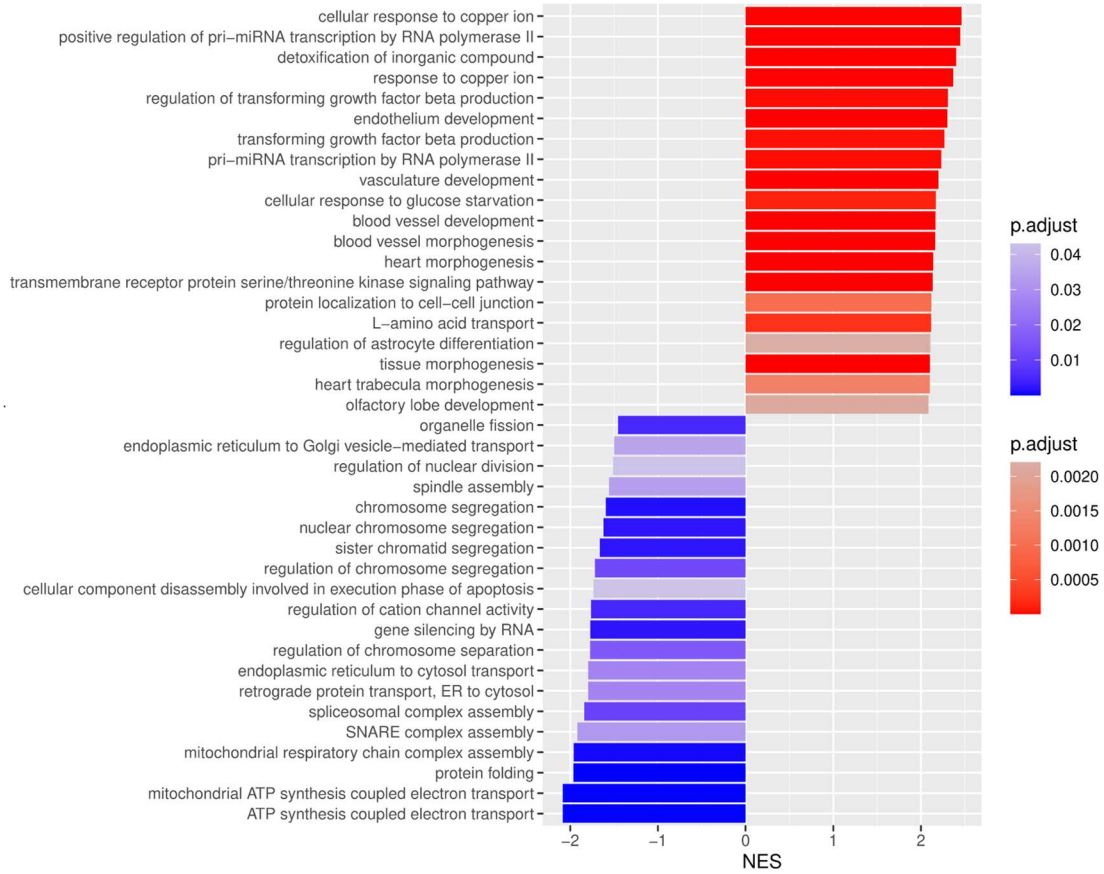

Figure 56 Top 40 deregulated GO biological processes identified with GSEA. Notably, here the strongest deregulated terms are linked to iron insult regulation of pri-miRNA, as well as processes associated with ATP synthesis coupled electron transport. Upregulated terms are designated in red and downregulated in blue.

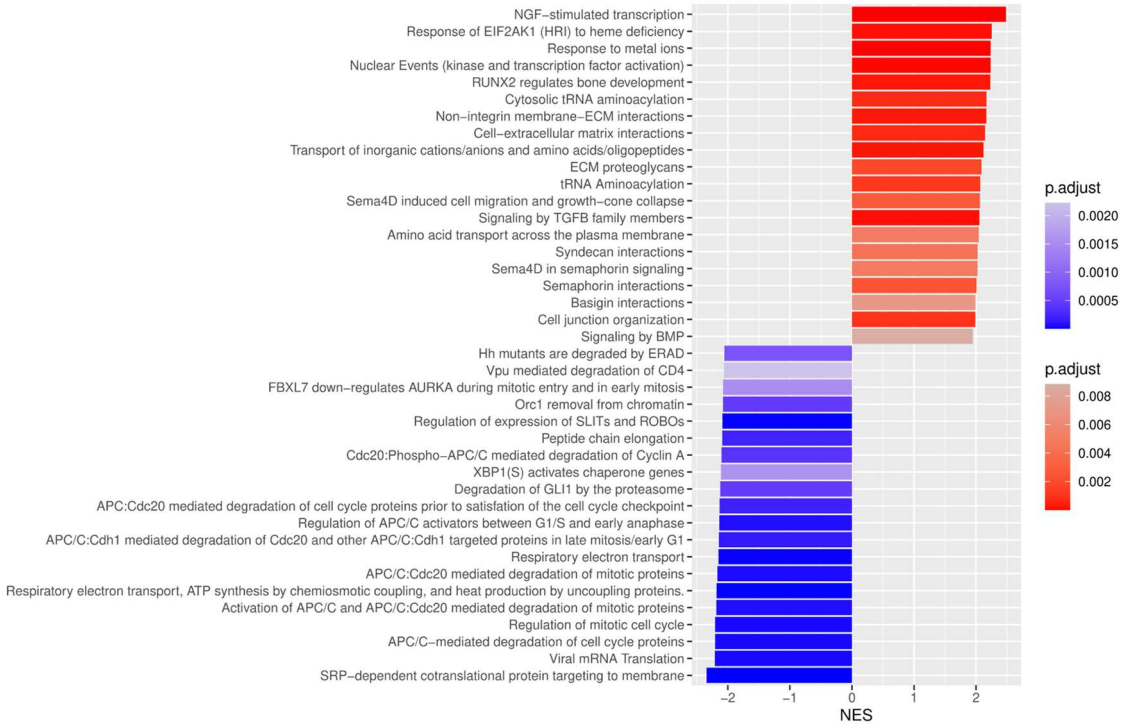

Figure 57 Top 40 deregulated Reactome pathways identified with GSEA. Notably, here the strongest deregulated pathways to iron insult and NGF-stimulated transcription, as well as pathways associated with regulation of mitotic cell cycle. Upregulated pathways are designated in red and downregulated in blue.

Furthermore, Figure 58 shows an example of a GSEA enrichment plot displaying the deregulation of genes associated with the cell-substrate junction organization GO term after Sm IPSE treatment of the HepG2 cells, indicating a coordinated up-regulation of genes associated with this biological function.

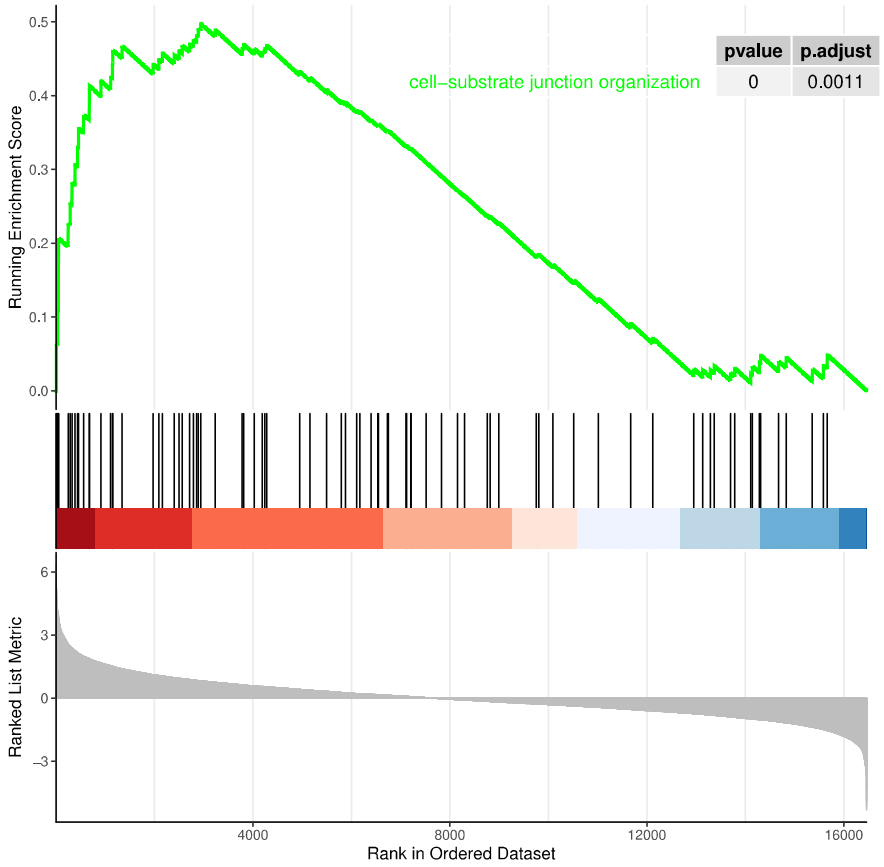

Figure 59 GSEA enrichment plot representing the GO biological process term cell-substrate junction organization. Most genes which are connected to this pathway, seemingly were upregulated after Sm IPSE treatment of the cells.

3.3.5 Sm IPSE WT has the fundamental ability to bind to DNA

Since it is assumed that Sh IPSE orthologues can bind to DNA similarly to what has been shown for Sm IPSE (Ishwinder Kaur, PhD Thesis Nottingham, 2011), a classical EMSA was used to detect such interactions of Sm IPSE. Before starting the experiment, the oligonucleotides were first successfully hybridized (Figure 59 A), as the amount of base pairs doubles compared to the non-hybridized oligomers.

Next, a pilot assay was performed in which Sm IPSE and its NLS triple mutant (NLS-AAA) (Figure 59 B) were incubated in advance with a 100 bp DNA ladder. Indeed, compared to negative control (BSA), the marker could not continue to run undisturbed, indicating DNA binding. Rather, in the case of Sm IPSE, the marker remained at the beginning of the gel, which could be attributed to a strong binding of the protein to the DNA, building large protein DNA aggregates. A similar event can also be recognized in the NLS-AAA mutant, although here the marker was able to continue, but in a

significantly weakened form. This suggests that the NLS-AAA mutant also exhibits binding activity, but to a much lesser extent than the wild type. The assay was repeated including Sh06 IPSE, which was previously shown to exhibit DNA-binding capacity (Figure 59 C). Notably, binding was confirmed as for Sm IPSE, but a few separated bands could nevertheless be detected in the lane of Sh06, indicating lower binding affinity of Sh06 IPSE to DNA than Sm IPSE.

To see if IPSE binds to DNA indiscriminately, e.g. by interaction of its highly positively charged NLS with the phosphates in the DNA double helix, the EMSA which included Sh06 pre-incubated with the hybridized oligonucleotides was performed using additionally a 10 bp marker to illustrate the binding of Sm and Sh06 IPSE (Figure 49D). Importantly, in this case no inhibition of marker progression was seen in either case, indicating that both IPSE forms cannot bind to the specific DNA sequences of the 10bp marker. Furthermore, no binding of Sh06 IPSE to the oligonucleotides was detected, as the band pattern resembles the ones of the negative controls. The EMSA was then repeated using different molarities of the DNA, aiming for different results. Nonetheless, no change in marker progression was detected, indicating that neither Sm nor Sh06 IPSE bind to the designated oligonucleotides (Figure 49E).

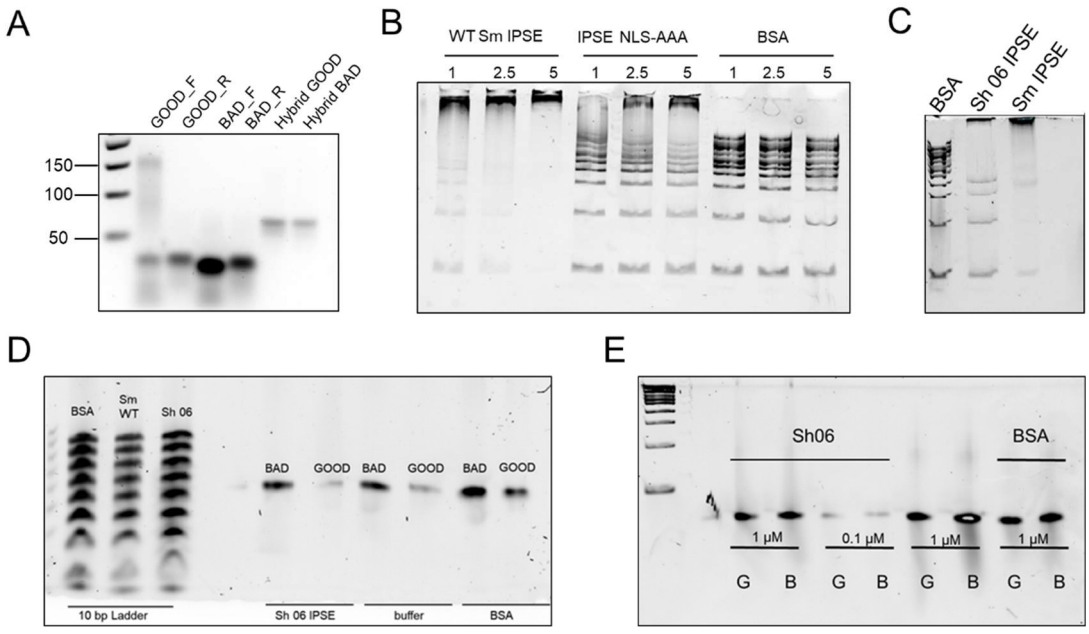

Figure 59 Hybridization of oligonucleotides and Native PAGEs after EMSA conducted with IPSE forms (A) Successful hybridisation of the forward and reverse „Good“ and „Bad“ oligonucleotides (B) 7 % Native PAGE of 100 bp ladder (NEB# N3271S). Band pattern implicates a high binding affinity from Sm IPSE WT to ladder and a lower one in case of the NLS mutant. The control protein BSA is not binding to the DNA ladder. The Experiment was repeated including Sh06 IPSE (C) showing binding properties, but not as much as Sm IPSE. (D) Native PAGE showing that none of the IPSEs bind to 10bp DNA Step Ladder

Promega ladder. Also shows that Neither Sh06 IPSE, nor BSA bind to hybridized oligonucleotides. Samples were prepared with Hybridisation buffer. (E) Repeated Native PAGE with different protein molarities, also not displaying any binding activity between Sh06 IPSE and the oligonucleotides.

3.3.6 Sm IPSE does not lead to an obvious change of subcellular distribution of importinα

Previous studies suggested that Sm IPSE might inhabit the capability of entering the cell nucleus via NLS-importin-alpha interaction (Ishida et al., 2020; Kaur et al., 2011). Therefore, DsRed-importinα expressing cells (later identified as Rs-ATL8 cells) were treated with Sm IPSE for a defined period of time (15, 30, 45, 60min). The shift of fluoro-labelled importinα was to be tracked in time with fluorescence-microscopy.

Figure 60 shows fluorescence images of untreated cells and cells exogenously treated with Sm IPSE in direct comparison. Here, none of the different time points exhibited a difference between untreated and treated cells concerning the overall distribution of DsRed-importinα in the cytoplasm. Meaning, even after 60 min of incubation no shift of importinα towards the nucleus was observed in IPSE-treated cells. The photographs demonstrate that the fluorescent pattern between both cells, looks similar, regardless of the treatment of the cell. To achieve an accurate result, the experiment was repeated including a nuclear stain with Hoechst 33342 (Figure 61). Here, too, no shift in the cytoplasm towards the stained nucleus was recognized comparing the Sm IPSE incubated and the untreated cells. Conclusively, Sm IPSE does not cause a shift of importin alpha towards the host cell nucleus.

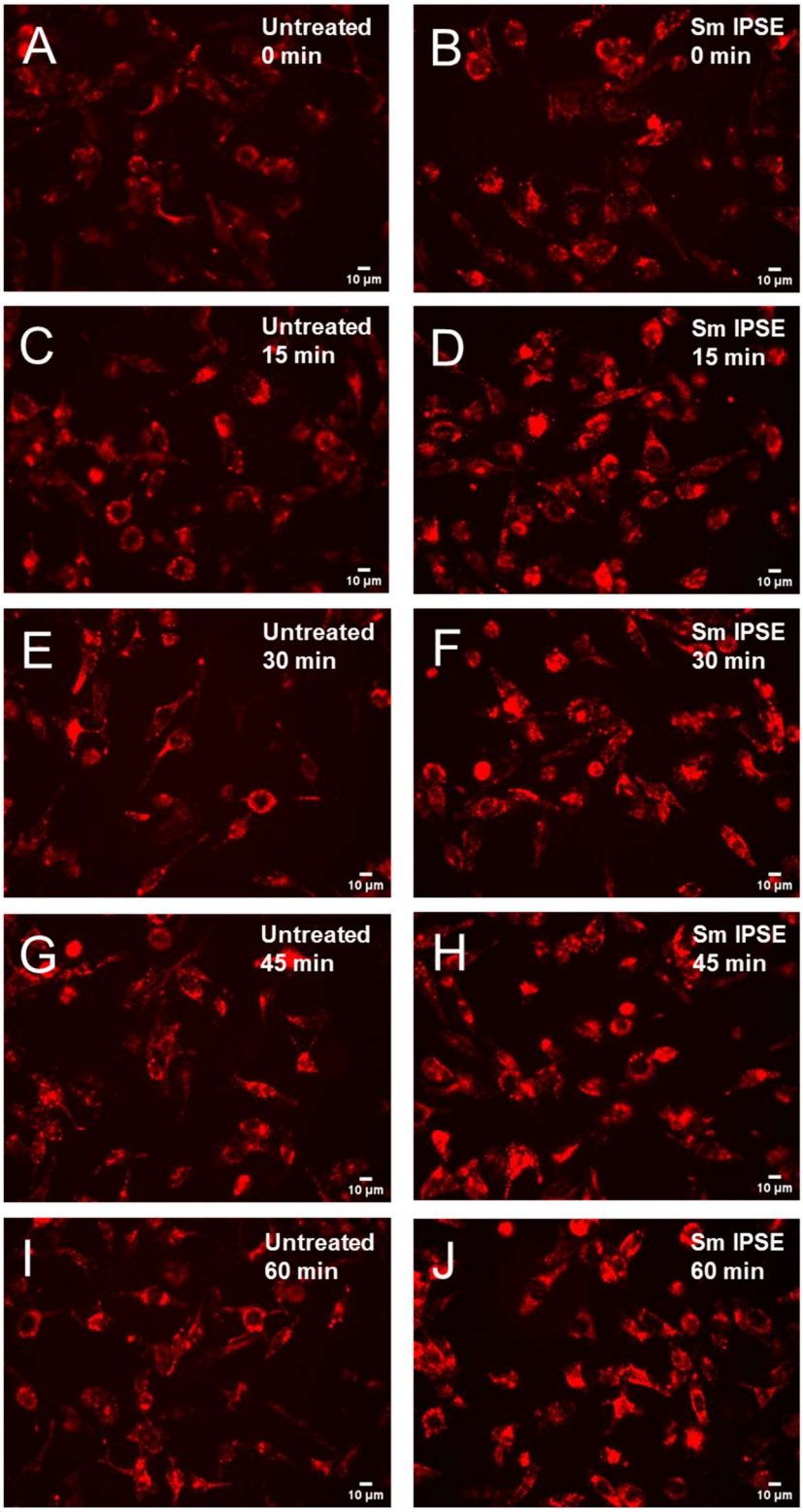

Figure 50 Subcellular localization of DsRed-importinα expressed in RS-ATL8 cells after exogenous incubation of cells with IPSE. A,C,E,G and I represent untreated cells and images B,D,F,H and J show the fluorescent importinα expressing cells treated with recombinant expressed Sm IPSE. Pictures were taken at different time points after IPSE-treatment (0, 15, 30, 45 and 60 min). The overall distribution pattern of importinα appears to be similar between the treated and untreated cells, as well as between the different time points.

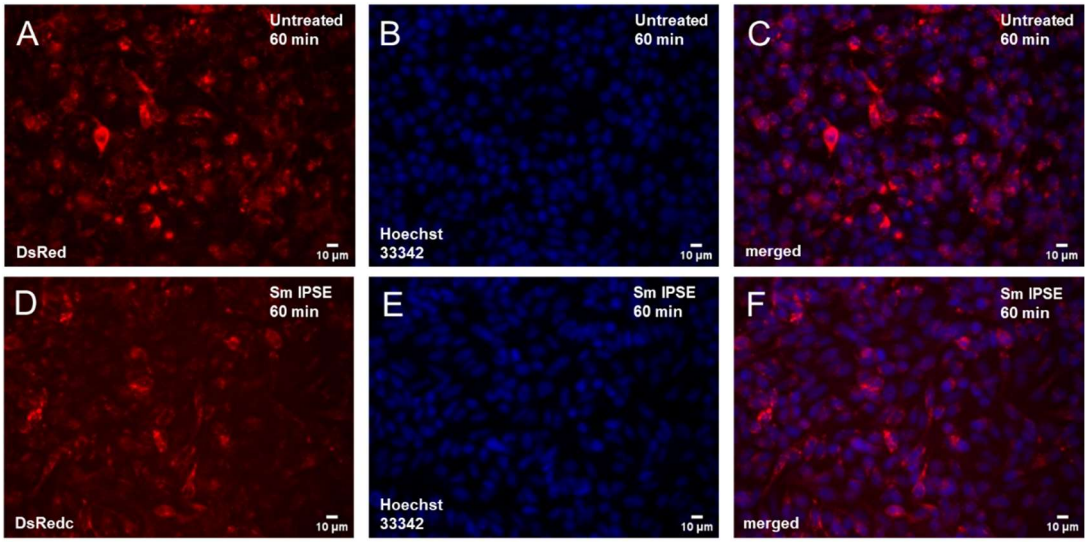

Figure 61 Localization of DsRed-importinα in the cytoplasm with and without exogenous treatment of the Rs-ATL8 cells with recombinant IPSE, including a nuclear stain with Hoechst 33342. No obvious difference in the fluorescence distribution pattern between the untreated cells (A,B and C) and Sm IPSE treated cells (D, E and F) can be detected after 60 min of incubation.

3.3.7 Species Identification via PCR reveals that pDsRed-Importinα cells originate from rat – not from human

Based on the assumption that batches of cells might have been accidentally swapped U2-OS-cells with RS-ATL8 cells, a verification was conducted by identifying the species with PCR. For that purpose, the potentially swapped pDsred-importinα transfected cell line (batch 4) and three different U2-OS batches (batch 1-3) were included in this study. The gel (Figure 62) perfectly shows, that batches 1-3 are indeed from human origin, showing a single strong bands expected at approx. 350 bp when PCR was performed using the human primer pairs. Above that, as assumed, the transfected cells are rat cells, as we receive a clear single band in case for rat-primers.

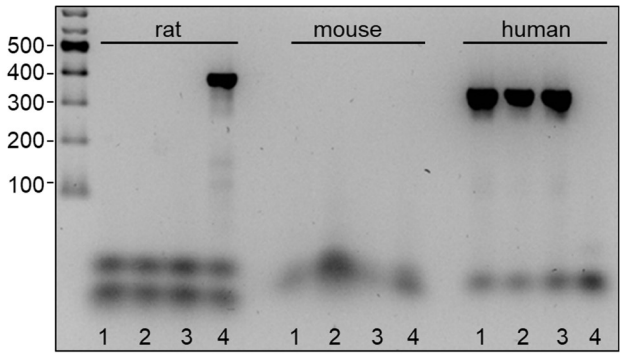

Figure 62 Results of species identification by PCR. 1 = U2-OS batch 1, 2 = U2-OS batch 2, 3 = U2-OS batch 3 and 4 = dsRedimportin-α U2-OS. Ladder: TriDye™ 100 bp DNA ladder Species identification reveals that batch 1-3 indeed are human origin and that, as expected number 4, the transfected cell line must originally be a rat cell line.

4. Discussion

The general aim of this work was to gain deeper understanding in terms of structural biology of the unique binding mechanism of Sm IPSE to IgE. We further aimed to gain more knowledge about IPSE's mode of action inside the host cell.

4.1 Establishment of basic experimental conditions

4.1.1 Expression of Sm IPSE and mutants in HEK293-6Ecells is successful

Since Falcone et al., (1996) implied binding between IgE and Sm IPSE, and further studies conducted by Meyer et al., (2015) suggested a cross-linking independent interaction; we aimed to understand the underlying mechanism. Therefore, different IPSE mutants were created bearing specific mutations based on the knowledge that neither monomeric nor the chemokine binding protein (CKBP) IPSE forms enable basophil activation mediated by IgE-binding (Kaur et al., 2011; N. H. Meyer et al., 2015; Smith et al., 2005). To generate the mutants, site-directed mutagenesis was carried out, leading to a successful creation of Sm IPSE T92Y, C132A (monomeric IPSE), T92Y/R127L (CKBP), T92Y/R127A, R127L and R127A pTT5 plasmids, most of them being variants from the above-mentioned non-basophil-activating IPSE types. In addition to that, a NLS-mutant was generated in order to perform DNA-interaction studies.

Overall, it can be said that site-directed mutagenesis was an effective and easy tool, to change up to three different triplets encoding for three amino acids in one plasmid.

Due to the fact that these pTT plasmids were especially designed for transient or stable expression in the HEK293 model (National Research Council Canada, file 11565 HEK293SF-3F6 and HEK293-6E expression platforms (L-10894 / 11266 / 11565) - National Research Council Canada), the successful insertion of mutations was followed by protein expression in HEK293-6Ecells. Three advantages come with the expression in mammalian cells. Firstly, the used HEK293-6E cells are adapted to serum-free chemically defined medium, which enables one-step purification due to the absence of large amounts of contaminating protein derived from the use of serum. Secondly, in contrast to *E. coli* expression, HEK cells allow posttranslational modifications such as glycosylation of the proteins, which helps to reach a more natural state for a glycoprotein. This is of importance, since it is believed that aspects

of egg-induced immune processes are partially driven by protein glycosylation of SmEAs (Hokke & Yazdanbakhsh, 2005). In case of IPSE, it was shown that its glycosylation (antennae fucoses) plays a crucial role in binding to DC-SIGN (DC-specific ICAM3-grabbing non-integrin) and MRs (Mannose receptors) in a cellular context with dendritic cells and single CLR (C-type lectin-receptors)-cell lines (Meevissen et al., 2012). Finally, compared to attached cells, suspension cells can be cultivated at higher densities, resulting in higher protein yields (National Research Council Canada, file 11565). As suggested, a range of plasmid concentrations and DNA-PEI ratios were proposed in the general protocol for PEI-transfection in HEK293-6Ecells (National Research Council Canada), a determination for the best DNA-PEI-ratio was carried out in smaller scales. The results of the transfection und subsequent TCA-precipitation show that both DNA-PEI Max ratios 1:2 and 1:3, as well as a plasmid concentration of 2.5 µg/mL seem to be the most suitable for IPSE pTT5 transfections, leading to high yield expression of the wanted IPSE variants and its mutants. Subsequent purification with the aid of IMAC using Ni^{2+}-NTA-columns was successful as all IPSE variants were recovered without any residuals from the expression.

4.1.2 HEK cell expression of IgE forms was successful, except for IgEλ

For further insights into the binding mechanism of Sm IPSE to IgE, we aimed to understand to which domain of the immunoglobulin the parasitic glycoprotein binds. Previous in silico predictions carried out by Meyer et al 2015, suggested a binding of IPSE to the negatively charged Cε2 domain of IgE. Therefore, different forms of IgE, namely the truncated forms Cε 3-4 IgE and Cε 2-4 IgE, as well as IgE-motavizumab a synthetic full length IgE consisting of IgE Cε1-4, motavizumab VH and Ig-κ, were recombinantly expressed in HEK-2936E cells. In addition to that, the high affinity receptor huFcεRIα was expressed and purified, as well. Expression of IgE λ remained unsuccessful. Furthermore, IgE λ (plasmid pVITRO1-102.1F10-IgEλ Addgene# 50365) was supposed to be expressed and purified, too. It was therefore aimed, to facilitate the purification by inserting a His-Tag into pVITRO1-102.1F10-IgEλ for subsequent IMAC. After many fails, the tag was finally inserted, but I was only able to express the immunoglobulin once in small scale. In addition to that, it was claimed by the providers that the protein would be secreted into the supernatant (Dodev et al., 2014) but in this case it could only be detected in the pellet. This might be led back to a problem with the secretion signal. Even after, following the exact description of

Dodev et al., (2014) by additionally selecting under antibiotic pressure with Hygromycin B, no success was achieved. This raises the question whether the plasmid is suitable for HEK293-6E expression at all or if the plasmid is defective. In the original publication FreeStyle™HEK293-F cell-line with FreeStyle™MAX transfection reagent (Life Technologies) were used for expression. Another approach to finally express the protein could be linearization of the plasmid and subsequent nucleofection into HEK cells. Due to the incapability to express IgE λ, it was decided to use Bio-Rad IgEλ (HCA-171). Unfortunately, because of its high price, the experimental setups including IgEλ were limited.

4.1.3 Thermal Shift Assay and Missense 3D

To exclude any possibility of the inability of certain mutants being able or unable to activate basophils by binding to IgE being caused by protein misfolding, a Thermal Shift Assay was carried out as described by (Huynh & Partch, 2015). The assay relies on SYPRO Orange binding to the hydrophobic amino acids usually situated in the protein's core. Here, rising temperatures cause unfolding, exposing its hydrophobic side chains. This allows SYPRO Orange to bind to the protein, resulting in a peak of fluorescence corresponding to the melting temperature of the protein. The melting temperature (Tm) is defined as the temperature at which 50% of the protein is unfolded. Destabilising effects of amino acid substitutions would appear as lower Tm value, whereas stabilising substitutions would appear as increased Tm. Herein, the assay was initially performed with lysozyme to determine experimental conditions. However, upon performing the Thermal Shift Assay with the IPSE mutants, several peaks were detected for each, making it impossible to determine any melting temperature for the proteins. To exclude the possibility that any contamination of the protein sample caused the problem, all Sm IPSE variants were purified in another step with Size Exclusion Chromatography. However, this did not lead to any success either. It was therefore speculated that IPSE's glycosylation might be the interference factor. Notably, each IPSE dimer bears four N-glycan sites (Wuhrer et al., 2006). Not all molecules are fully glycosylated, leading to hetereogeneous glycosylation variants with different Tms. Thus, to prevent glycan interference the assay was repeated with non-glycosylated IPSE expressed in *E. coli*. In this case, only one peak could be observed, supporting the assumption that the glycosylation of IPSE led to previously inconclusive results. However, for downstream applications HEK expression was preferable. As thermal shift assay with these glycosylated mutants was not

successful, it was decided to analyse each mutant sequence in silico using the Missense3D tool (Ittisoponpisan et al., 2019). The analysis suggested that none of the inserted mutations should lead to a conformational change of the protein, cautiously excluding the possibility of the mutants being misfolded and therefore incapable to bind to IgE. In contrast, in case of the cysteine mutation which leads to the inability of the protein to form dimers. It was therefore assumed that all IPSE mutants were properly folded a and thus theoretically able to bind to IgE.

4.2 IPSE - IgE interaction

4.2.1 IgE Reporter Cell Assay (Rs-ATL8) with IPSE mutants

In order to gain more insights in the unique binding mechanism, the generated mutants were used for a basophil-based reporter cell system (Nakamura et al., 2012). In this method, binding of an antigen to receptor-bound IgE of the basophil reporter cells, results in their activation, measured by NFAT-translocation. NFAT-translocation from the cytosol to the nucleus leads to the production of Luciferase in the cytosol. For a downstream chemiluminescent signal read-out, a specific luciferase-substrate is added; whose chemical reaction subsequently allows the measurement of the relative luminescence of activated RS-ATL8 reporter cells. In this experimental setup, human serum from an immunologically naïve but allergic donor with high levels of IgE was used to sensitize the chimeric basophils expressing the human high affinity receptor (FcεRI) which binds to IgE. The binding-activity of IPSE to IgE was eventually evaluated by measuring the relative luminescence of activated RS-ATL8 reporter cells.

As shown in the results, all IPSE mutants displayed significantly higher binding activity and subsequent basophil release compared to the negative control, whereas only the T92Y/R127L mutant impeded the activation completely. This is in line with our expectations as this specific mutant was previously described as Chemokine Binding Protein, capable of binding to chemokines but not IgE, thus resulting in the incapability to stimulate basophils to degranulate (N. H. Meyer et al., 2015; Smith et al., 2005). However, contrary to our expectations, the monomeric mutant form (C132A) was still able to cause degranulation, although higher concentrations were necessary. Concluding, it was hypothesized that, at higher concentrations, two monomers independently bind to distinct areas of the IgE molecule, imitating the binding of intact IPSE dimers and thus resulting in a productive IgE-interaction. These findings were

subsequently supported by the findings in Negative Staining, showing that IPSE in general tends to form oligomers at concentrations starting at 15 µg/mL.

Notably, although all mutants led to basophil degranulation, they displayed a lower relative signal. Therefore, all mutations seem to have an impact on binding and the subsequent basophil activation, when compared to the wild type of Sm IPSE. In fact, it can be stated that mutants bearing a switch from Threonine 92 to Tyrosine, are affected the most. T92 is located in the very centre of a flat surface of the protein, which may be involved in the binding to IgE (see Figure 42, Results). Indeed, this mutation replaces a smaller and hydrophilic Threonine, with a more hydrophobic and bulkier Tyrosine, which finally may disrupt the interaction between IPSE and IgE. Since these mutants maintain lower capacity to stimulate basophils, it can be stated that the mutation of R127L (see Figure 43) in the context of the double-mutant, provides the “coup de grace” in binding disruption to IgE. This second mutation introduces a large, hydrophobic residue in close proximity of a strongly positively charged patch. This stands in line with the statement of Meyer et al., 2015 suggesting that IPSE interacts with IgE via this large surface and a flexible loop (crystalline fold) that consists of positively charged and aromatic amino acid, thus electrostatic and charged interactions.

In addition to these findings, the results reveal that among all IPSE orthologues, Sm IPSE has the strongest effect on basophil activation. Both Sh03 and Sh06, show comparably lower detectable luminescence, directly correlated to basophil activation. This is in line with the fact that both S. *haematobium* forms were shown to bind to IgG rather than to IgE (Personal communication, Luke Pennington, Stanford University).

Finally, it can be concluded that the binding ability of Sm IPSE relies on interactions between T92 and R127 with IgE, indicating the binding is dependent on amino-acid interaction provided by positive charges (electrostatical potential), hydrophobicity and surface properties. This is based on the finding that the only mutant incapable of binding is SmCKBP (T92Y/R127L). Moreover, a direct comparison of the IPSE orthologues pointed out the different binding affinities to IgE. Notably, both *S. haematobium* forms bear a change of amino acids for Threonine 92 which is replaced by an Alanine (see Figure 7, Introduction). This might be an explanation for their lower binding capability to IgE compared to Sm IPSE (Pennington et al., 2017). This once again supports the assumption that Threonine 92 must be predominantly involved in stable IgE binding.

4.2.2 ELISA

Initially, ELISAs were carried out to measure the binding affinity of Sm IPSE to the IgE forms. This way it was demonstrated that Sm IPSE binds to IgE-motavizumab with a K_D of 11.4 nM. Next, pre-incubated IgE-mota to huFcεRIα (K_D = 10.07 nM) was included, but no significant difference could be detected, leading to the assumption that the IgE-receptor complex is not necessarily needed for IPSE-IgE binding. It was also found that IPSE does not show any binding at all to both truncated forms (Cε2-4 and Cε3-4). Since it was proposed by Meyer et al., (2015) that one of the IPSE monomers binds to the Cε2 domain of IgE, facilitating the binding of the second monomer to the Fab region, I would have expected at least some binding of IPSE to the Cε2-4 form. Do these findings suggest that Sm IPSE, instead of binding to the assumed second constant domain, rather binds either to the first constant domain or even both? Or is the binding mostly mediated by the Fab region of IgE, in particular the light chain or - contrary to our expectations - to the variable chain? However, a binding of IPSE to the IgE variable chain can be excluded, since it was found that IPSE as general immunoglobulin binding factor, irrespective of IgE's antigen specifity, as well as IPSE bearing the capability to bind to both Fab and Fc region of IgG (N. H. Meyer et al., 2015; Schramm et al., 2003). These findings were supported by the RS-ATL8 reporter assay conducted with the different IgE forms used for sensitisation of the cells. Here, Sm IPSE was not able to activate basophils, which were previously treated with both truncated IgE forms. It can be excluded that these IgE forms are not intact and thus not suitable for this assay, due to the fact the activation occurred by anti-IgE antibody binding serving as positive control.

We were also interested, if a difference between the Sm and Sh IPSE, as well as the monomeric IPSE form and the CKBP mutant, can be observed. Indeed, in all cases, the binding affinity was too low, which meant that no K_D value could be determined. These results meet our expectations, as similar results have already been found in the reporter assay. Nevertheless, it should be noted that in case of Sh06 IPSE, the ELISA was completely disrupted by Sh06 IPSE being an IgG-binding protein, resulting in unspecific binding to the secondary HRP-conjugated antibody. After the performance of other experiments with IgE-mota and Sm IPSE, which did not lead to any satisfying result, an ELISA was conducted using IgEλ with the same molarities as used before. Here, we found that IPSEs binding affinity is much higher to IgEλ than to IgE-mota, which contains a κ light chain. Saturation was reached even at low molarities (1 nM), which meant that no K_D could be calculated. Correspondingly, IgEλ and IgE-mota were also tested with Sm IPSE in the Reporter Cell Assay and revealed

a surprising result. In the Reporter Assay, in case of IgE-mota (κ), no significantly different luminescence to unsensitised cells could be detected. In contrast to that, cells sensitized with IgEλ displayed high luminescence after stimulation with lower IPSE concentrations. These findings point to the conclusion that the unique binding mechanism might be mediated by the different light chain of IgE, in this case the λ-light chain. Interestingly, it was stated that in general the human peripheral blood contains more antibodies with κ-light chain than λ. However, it was also reported that in antigen-selected populations, the ratio can differ depending on the antibody-(Chui et al., 1990; Molé et al., 1994; Montaño & Morrison, 2002b). An explanation why IPSE binding to IgE λ appears to be more stable/effective, might be due to several differences between the two antibody types such as half-life in vivo (Montaño & Morrison, 2002b) or conformational flexibility led back to its larger elbow angle (Stanfield et al., 2006). (Townsend et al., 2016) established that the complementary-determining regions CDR-L3 show dissimilarities in the physiochemical and structural properties. In case of IgE-λ, these regions were described as longer and more hydrophobic than in IgE-κ (DeKosky et al., 2016), as well as having a higher aliphatic index. CDR-L3 are also displaying a variety of canonical structures, whereas κ canonical structures mostly remain similar. IgE λ was attributed to be preferentially involved in the ability to rescue polyspecific antibodies (Townsend et al., 2016). Nonetheless, it was stated that these different types of light chains have evolved to respond in different ways to a specific antigen (Townsend et al., 2016) and thus lead to different roles in the humoral immune response. Moreover, it was shown that these CDRs are involved in antigen binding, usually referring to CDR-H3, but also CDR-L3, which could possibly be the key for IPSE-IgE interaction (Kabat, 1978; Tsuchiya & Mizuguchi, 2016). One might cautiously speculate that the longer and more hydrobhobic CDR-L3 structures present a larger binding surface for IPSE's interaction site that includes the hydrophilic Threonine, resulting in a more stable binding complex with IgEλ, compared to IgEκ.

Since primary ELISAs showed binding of Sm IPSE to IgE-mota, further experiments to determine the binding stoichiometry of IPSE to IgE, such as size exclusion chromatography (SEC) and BLI were carried out. To have a direct comparison, SEC was initially performed with IgE-mota pre-incubated with huFcεRIα, showing a clear peak shift. A similar shift was expected in the case of Sm IPSE incubated with IgE-mota, but this failed to happen. After the incubation of IgE with IPSE with molar ratios of at least 2:1, both proteins could be detected in one peak with no remarkable shift. This could be attributable to either a peak overlay, as IPSE tends to stick together at higher concentrations, or that the IPSE-IgE complex is rather unstable. Meyer et al.,

2015, were performing size exclusion chromatography with Sm IPSE and IgE, too. Here, they stated to have detected a shift between the peaks, but similar to our results, there is no clear shift detectable, which might be due to the above-mentioned reasons. Thereupon, collected fractions were subsequently used for negative staining, including samples of the possible ternary complex between Sm IPSE, IgE-mota and huFcεRIα. Here, again, only the binary immunoglobulin-receptor complex could be visualized. In one case, a complex between Sm IPSE and IgE could be suspected. Interestingly, when determining the most convenient concentration of IPSE in negative staining, we found that even at relatively high concentrations, Sm IPSE molecules aggregated resulting in oligomer formation. This is well-known to labs working on IPSE, as it is not possible to concentrate the protein beyond a certain level, after which it starts precipitating. This might be an explanation why the monomeric IPSE C132A enables basophil activation by binding IgE in the reporter system at higher concentrations. Moreover, the finding that IPSE does not seem to form a stable complex with IgE-mota and the failure of all different BLI setups, underline IPSE's preference to only bind effectively to IgEλ, but not IgE-mota, which has a κ light chain. Nevertheless, at least the ELISA results displayed an interaction between these two proteins.

Summarizing this study, it can be excluded that Sm IPSE binds to the IgE's constant domains Cε2-4. Rather, it may be assumed that mainly the light chain is responsible for forming a stable IgE/IPSE-complex, preferentially the λ-chain. Nevertheless, it should be considered that probably either the Cε2 and/or Cε1 are involved in binding, as well, which would explain IPSE's ability to bind to IgE mota (κ) in ELISA experiments.

Noteworthy, it should be acknowledged that IgE mota not only consists of the Cε1-4 derived from the human IgE, but also of humanized motavizumab variable region of the heavy and light chain (κ). Even though humanization of the variable region is believed to exhibit same properties as a "natural" human variable region, it should be also considered that this might interfere with proper binding of IgE to IgE mota. However, this in turn would also indicate that stable binding is highly dependent from either the light chain and/or the variable region. It should therefore be considered to include full human IgE κ into further studies.

In conclusion it can be stated, that we were able reveal the key insight that there is a selectivity for IPSE to bind to the λ light chain. Here we show that light chains might also play a crucial role in antigen-IgE interaction. Additionally, we were demonstrating

that both mutations of SmCKBP are needed for complete basophil-activation capacity-loss and that most likely T92 plays the most important role in IgE-binding.

To gain more insights in the binding mechanism of IPSE to IgE, especially in terms of mapping the exact binding part of IgE, conduction of imaging techniques, such as Negative Staining or Cryo-EM with IPSE and IgE λ, should be considered.

4.3 IPSE - host cell interaction

4.3.1 Analysis of the transcriptome (Bulk RNAseq)

Most of the literature about transcriptomic approaches to the biology of parasites deals with the parasitic transcriptome itself rather than the transcriptional effect on the host (Lu et al., 2017; Morales-Vicente et al., 2022; Wendt et al., 2020). In contrast, this study focussed on the modulation of the host transcriptome by a parasite protein (IPSE) trying to infer the regulatory outcomes mediated by IPSE-host cell infiltration. Therefore, this study and experimental setup served as novel approach for further analysis towards this interaction. Only Ishida et al. 2020 (Ishida et al., 2020) and Mbanefo et al. 2018 (Mbanefo et al., 2020) carried out a similar approach by injecting a single dose of *Schistosoma haematobium* IPSE into a living mouse as pre-treatment to chemical (resiniferatoxin and ifosfamide, respectively) insult. In contrast to these studies, our work solely focussed on the IPSE-mediated effects in a cell culture model using human liver (HepG2) cells.

When designing the experiment, it was taken into consideration that Sm IPSE has immunomodulatory effects. Following from this, the incubation time of Sm IPSE was determined leaning on studies working with immunomodulatory proteins such as chemokines, which was usually short-term (Riedlinger et al., 2019). Referring to both *Schistosoma haematobium* IPSE studies (Ishida et al., 2020; Mbanefo et al., 2020), which were conducted in a mouse model, it should be considered to prolong the incubation time, as here the researchers were treating the mouse 24 h with IPSE before extracting the RNA. This might result in overall more visible effects, but some might be rather indirect effects. Another factor that plays an important role and should therefore not be ignored is the dose of the applied protein, which raises the question whether it is likely to occur locally at this concentration in the infected tissues, or if the application was much higher or lower than it would occur in a natural infection. Here, HepG2 cells were incubated with 1.5 µg/mL recombinant expressed Sm IPSE, from which it is unclear to represent a naturally occurring protein concentration in

penetrated host cells. So far, it is not known how much Sm IPSE is secreted by a single egg, but it was shown to be the most abundant egg antigen (Mathieson & Wilson, 2010). Even knowing this, it is difficult to estimate how high the dose should be, as the egg load in the tissue varies greatly but was measured up to 300 eggs per female per day (Moore & Sandground, 1956). In summary, as IPSE might elicit different cellular reactions due to the concentration and time of exposure and it is therefore advisable to test a broader range of IPSE concentrations and different exposure times. Furthermore, the choice of the negative control should be reconsidered.

In this study, untreated cells were used as control, but after analysing the data, one of the major GO-terms associated with the top de-regulated genes was response to metal ion. This could be interpreted as cellular stress response to metal ion, resulting in the upregulation of detoxification-pathways. These findings might be led back to the protein purification with IMAC in a Nickel-containing column and thus residual Nickel being bound to IPSE's His-Tag or other parts of the protein. I would therefore recommend, to either add EDTA to the samples before the dialysis or, instead of no treatment, as negative control, rather use the same protein sample (same purification) being inactivated by heat or other denaturing strategies in order to rule out the possibility of this effect originating from residual Nickel.

Nevertheless, it also provides a different interpretation, where upregulated detoxification pathways might be simply a physiological effect triggered by IPSE. Noteworthy, the most recent study about the Schistosome egg's transcriptome in different tissues reveals that (only) mature liver eggs display an upregulation of metal ion transport, which could be connected to the cellular response to metal ion found in this study (Peterková et al., 2024). This could point to IPSE being a key-player in a liver-protective mechanism, although that would stand in contrast to findings of IPSE excerting hepatotoxicity in a dose-dependent manner in vitro. Notably, in this study, toxicity was only determined by measuring one parameter, namley alanine transaminase (marker for hepatocyte injury) release by cultured mouse primary hepatocytes, and no further morphological analysis (Abdulla et al., 2011). Taking a closer look into the data-set (appendix) of Ishida et al., (2020), an upregulation of the response to metal ion was detected, too.

Standing in line with IPSE possibly, bearing host protective capacities, the set of deregulated genes involved in the cellular response to iron and stress, mainly appear to belong to the metallothionine family (eg. MT1X). Even though genes of this family

are associated with antioxidant activity and protective effects of molecules against toxic metal, especially one gene, MT1X, has been identified as a tumour repressor involved in the inhibition of the progression of hepatocellular carcinoma (Z. Liu et al., 2018; Sutherland et al., 2010). The finding that MT1X was also significantly upregulated in the here obtained transcriptome, it further rises the question whether IPSE might induce other liver-tissue protecting mechanisms, too.

When comparing the over representation analysis results of this study to the findings of studies performed by Ishida et al., (2020) and Mbanefo et al., (2018), it becomes evident that the results differ immensely. This might be due to the different experimental setups such as injection of a single dose of Sh06 IPSE into a murine model that was pre-treated with either ifosfamide or resiniferatoxin, respectively and RNA-isolation of bladder tissue after 24h incubation time. Exemplarily, Ishida et al. (2020) found a relative increase in metabolic gene expression relevant for oxidative phosphorylation, which stands in contrast to the here presented results implying a downregulation of genes coded for mitochondrial respiratory chain complex assembly and ATP synthesis coupled to electron transport. Nonetheless, a further common up-regulation could be detected in terms of pathways involved in tissue morphogenesis (Ishida et al., 2020). As it is known for egg migration in Schistosomiasis, eggs need to migrate through several tissues layer, to finally being excreted from the intestine or even for escaping the liver, if swept back through the mesenterial vessels (Moore & Sandground, 1956). It can be assumed that these egg migrations force the host cells to reorganize or rebuild cell networks or tissues, to either facilitate the migration step or to repair tissue damage.

When investigating Sm IPSE's involvement in immunomodulation and tissue reorganization, the conducted analyses also suggest that after IPSE-treatment several pathways related to transforming growth factor beta 1 (TGF-β1) are de-regulated. TGF-beta1 (Transforming Growth Factor-beta 1) is known as a cytokine involved in many cellular signalling pathways, such as cell differentiation, cell growth, apoptosis, advanced expression to extracellular matrix-proteins, immunosuppression, liver cell proliferation and cell homeostasis (Yang et al., 2014). Interestingly, Johnston et al., (2017) found a structurally distinct TGF-beta mimic derived from the helminth *H. polygyrus*, an intestinal parasite, which actually mimics TGF-beta by inducing regulatory B-cells, underlining the possibility of a helminthic protein serving as immunomodulatory mimic. Here, the results point to two different directions namely to "transmembrane receptor protein serine/threonine kinase signalling" pathway and to negative regulation of cell adhesion connected to TGF-beta1. The former could

indicate a potential interaction between IPSE and a transmembrane receptor, just like TGF-beta1 does (Heldin & Moustakas, 2016). Whereas the second also supports the findings that numerous pathways associated with cell-cell junction organization and actin filament organization are affected by internalized IPSE. This is also supported by the fact that some of the modulated genes (e.g. THBS1 encoding for Thrombospondin 1, which plays a role in focal adhesion but also in platelet aggregation, angiogenesis and microtubule formation as downstream mediator of TGF-beta) that are found in the TGF-beta1 superset is also associated with the superset 1 identified in the over-representation analysis (Joseph et al., 2022; Miller et al., 2015; Shen et al., 2018). The first superset also includes pathways connected to wound healing and coagulation, which is hard to interpret since the work was carried out with HepG2 (Hepatoma cells with an epithelial cell-like morphology) cells and not platelets. Taking a closer look at genes related to these pathways, it becomes evident that these are mostly related to cytoskeletal proteins. One example is the VCL gene that encodes for the protein Vinculin involved in cell-cell and cell-matrix junctions, since it is considered to be part of anchoring the F-actin to the cell membrane (Bakolitsa et al., 2004; Geiger, 1979). These findings point to the idea of Sm IPSE being involved in the remodelling of the cell-tissue, especially the cell-cell junctions, which might be useful for the egg to flee the “liver-trap” or to keep the host damage low in order to preserve a stable reservoir (the human body) for the Schistosomes.

As cell-cell junction and actin skeleton remodelling pathways were shown to be deregulated in our results, as well as in Ishida’s work, these findings support the idea of IPSE’s involvement in these biological processes (Ishida et al., 2020). Both publications on *Schistosoma haematobium*-IPSE’s effect on the mouse transcriptome, point out IPSE’s involvement in the downregulation of inflammatory signals, whereby their focus is set on the deregulation TNF-α signalling via NF-KB and the downregulation of interferon signalling and oxidative stress (Ishida et al., 2020 & Mbanefo et al., 2018). None of these are found to be deregulated in our study, which might be due to the prior treatment with resiniferatoxin that is known to lead to bladder-pain-related freezing and ifosfamide which induces hemorrhagic cystitis (inflammation symptoms), leading to high inflammation and pain-related licking behaviour in mice and a subsequent reaction of IPSE to these circumstances (Ishida et al., 2020; Mbanefo et al., 2020). Due to these pre-treatment of mice and the injection of IPSE that was intended to function as treatment to show amelioration of the symptoms, comparisons of the results with ours should be taken cautiously. These studies focused rather on IPSE’s immunomodulatory capacities in terms of its involvement in

inflammation-related and pain-related pathways and not on the overall-function or activity of IPSE.

Nevertheless, the fact that TGF-β is also involved in immunomodulation should not be neglected. In particular, the involvement of TGF-beta 1 in granulocyte recruitment seems to be of interest in context of Sm IPSE being found in high abundance in liver granulomas, but rather in low abundaces in intestinal granulomas (Peterková et al., 2024; Sporn et al., 1986; Wahl et al., 1987).

A further up-regulated set of pathways can be linked to amino acid transport, whereby these biological processes are mainly found to be linked to transmembrane transport of amino acids. Genes associated with these pathways belong for instance to the human solute carrier gene superfamily (SLC) that play a role in transport of amino acids, glucose , inorganic cations and many more molecules as reviewed by He et al., (2009) (He et al., 2009). Interestingly, a recent work reported an association of the cellular interaction of the hosts SLC3A2 encoded transporter in immature blood cells with the *Plasmodium vivax* secreted PvRBP2a (merozoite) parasite ligand (Malleret et al., 2021), resulting in the entering of the parasite into this cell type. This may give a hint of the involvement of this particular gene-family into parasitic activities, such as cell invasion.

Another cluster of deregulated terms (superset 3) deals with up-regulated biological processes belonging to the pri-miRNA transcription by RNA polymerase II. Pri-miRNAs are precursors of miRNA, which are involved in regulation of translation, thus gene expression by silencing genes or even by triggering the binding of certain proteins to specific parts of the DNA (Bartel, 2004; V. N. Kim, 2005; Lee et al., 2004). As stated by previous studies, IPSE might be involved in the regulation of transcription or translation. This was attributed to the finding that Sm IPSE enters the host nucleus and was found to bind to DNA (Pennington et al., 2017; Kaur PhD thesis, 2011). In addition to that, miRNAs have also been associated with several *Schistosoma* species, as they themselves also secrete miRNAs to interact with host cells (J. Liu et al., 2019; Meningher et al., 2020).

Taken together, this approach suggests several interesting insights into the functions exerted by IPSE when internalised into host cells. Despite the overall number of de-regulated genes was relatively low, associated biological functions and pathways point at the involvement of IPSE protein into several processes related to cell-cell junction organization and regulation of TGFbeta1. The transcriptomic approach

thereby provides interesting targets for future studies focussing on the role of IPSE's involvement in inducing protective mechanisms for the host tissue/restrict host tissue damage or might even indicate a last attempt to be freed from the "liver trap".

4.3.2 Uptake and nuclear localization of Sm IPSE in different host cells

Schistosoma eggs are not only abundant in the intestine, where they are laid by the mature females, but also in the liver tissue when being swept back after a failed transition (Moore & Sandground, 1956). Hence, one objective of this thesis was to explore possible differences in the cellular Sm IPSE/alpha-1 uptake in different tissues. Therefore, in this study two experimental setups using immunofluorescence microscopy and flow cytometry (FACS) were employed in three different cell types representing the following tissues: HCT-116 (colon), HepG2 (liver) and CHO-Trvb (hamster ovary). CHO-Trvb cells were chosen, due to the fact that previous studies were showing internalization of recombinant (*E. coli*) IPSE in this cell line and therefore served as "uptake control".

Accordingly, it was initially sought out to elucidate the basic mechanism and pathways of cellular Sm IPSE uptake. For that purpose, a fluorescence-based IPSE and hTrf uptake assay was performed at 37°C or low temperatures (4°C). Human Transferrin (hTrf) is an iron-binding carrier protein which is known to be rapidly taken up by receptor-mediated endocytosis via the Transferrin receptor, and served here as an uptake control (Richardson & Ponka, 1997; Schade et al., 1949; Schade & Caroline, 1946). Moreover, low temperatures were chosen to determine whether the IPSE uptake was temperature-sensitive, which would point towards host-mediated endocytosis rather than a cell-penetrating peptide-like mechanism (Jiao et al., 2009). In this assay, cells were constantly kept at low temperatures. Here, a high fluorescent signal for Sm IPSE was detected in unquenched cells, whereby cells incubated with Sm IPSE and treated with Trypan Blue show almost no signal at all. This indicates that the low temperature prevented the uptake of Sm IPSE as well as the control hTRF in HCT-116 cells. Such temperature-sensitivity indicates that uptake of IPSE takes place via endocytosis, which is known to be impaired in direct relation to lowering the incubation temperature (Delvendahl et al., 2016). This is in line with other reports of an increasing cellular hTrf-uptake with rising incubation temperature from 0 - 37°C (Klausner et al., 1983). Due to these findings, the possibility of IPSE belonging to the group of cell-penetrating peptides can be excluded, as it was shown that cell-

penetrating peptides easily enter cells even at incubation temperatures below 12°C and even 4°C (Fretz et al., 2007; Jiao et al., 2009).

Notably, the assay further revealed immense differences in fluorescence intensity between IPSE and hTrf, where the intensity caused by IPSE was substantially higher. Consequently, it was initially assumed that the exogenously applied fluorescently labelled hTrf competed with unlabelled bovine Trf from the serum-containing cell culture medium for its uptake. However, even upon using serum-depleted media, the outcome was similar (data not shown), therefore this hypothesis was discarded. Alternatively, it may be hypothesized that the intensities differ substantially due to the self-labelled Sm IPSE bearing more fluorescent tags (calculated circa. 18 per molecule), whereas hTrf might have fewer FITC attached (no details from the manufacturer). More likely, these differences might also be caused different properties described by the provider, such as less brightness compared to other green-fluorescing dyes or rapid photobleaching. Thereby, it cannot be excluded that the different intensity between IPSE and the control hTrf might have been caused by the different properties of the two green-fluorescent dyes rather than differences in uptake quantity. However, this requires further investigation and prevents further conclusions regarding uptake quantity of either.

Another notable aspect in the uptake assays were differences observed in the variable intensity of autofluorescent signal between the different untreated controls. Unexpectedly, untreated cells resuspended in Trypan Blue displayed a higher autofluorescence than cells maintained in PBS. Trypan Blue is a cell stain which is not taken up unless the cells' integrity is compromised (e.g. death), upon which the agent will stain the cell. Notably, Trypan Blue (0.4 %) is cytotoxic by itself, and was shown to cause cell death after a certain period of incubation (S. I. Kim et al., 2016). Dead cells have an unsmooth shape, which refracts the flow cytometer's laser in another pattern, causing elevated auto fluorescence (S. I. Kim et al., 2016). When measuring the viability during the assay, it became obvious that cells, regardless of the cell line, resuspended in TB, lead to a lower cell viability. Unfortunately, we were not able to rule this effect out with our gating strategy, as for that a specific laser (660 nm, red light) that helps excluding dead cells stained with TB, is required. It should be considered that the experimental setup could be improved by adding the trypan-blue solution just before conducting flow cytrometry in order to prevent cells from dying.

Nevertheless, comparing the different cell types at permissive uptake temperature (at 37°C), it can be said that CHO-Trvb cells seem to easily take up Sm IPSE. This is supported by both performed experiments, where a strong fluorescent signal was

detected in all over the cytoplasm (no nuclear translocation) in immunofluorescence microscopy and the fact that in the flow cytometry-based endocytosis-assay differences between unquenchend and quenched groups were quite low (1:1.4), leading to the assumption that most of the protein was taken up.

Images taken with the CLSM further revealed that in case of HepG2 cells, the fluorescent signal of Sm IPSE within the cell seems to be high, but the protein distribution occurs in a vesicle-like pattern, exclusively found in the cytosol. A similar pattern was detected in CHO-Trvb cells. This pattern might indicate a cellular uptake in endosomes without subsequent endosomal escape (a prerequisite for nuclear transloaction). This is in line Kaur et al., (2011), where a similar pattern can be spotted in live cell images in monocyte-derived dendritic cells. However, the aforementioned study used PF-647-and FITC-labeled IPSE, obtained with a chemical conjugation procedure, which will alter the properties of the NLS, inactivating its nuclear translocation inducing capability. Hence, it is important to take into consideration any modifications due to fluorophore conjugation and its effects on subcellular targeting when interpreting results. From this point of view, the use of a fluorescently labelled antibody is preferable.

In spite of the similar vesicle-like pattern, Kaur et al. (2011) have excluded the possibility of Sm IPSE being situated in lysosomes after cellular uptake by co-staining the respective marker (LysoTracker) but do not further explore other vesicular species associated to endocytotic uptake. Therefore, the precise subcellular location of Sm IPSE in HepG2 cells upon uptake remains elusive. Nevertheless, the uptake differences visualized by ratios indicates there being a three-fold higher signal obtained in unquenched cells than in quenched ones, implying an overall less efficient uptake in Hep2G compared with CHO-Trvb cells.

Interestingly, compared to the two other cell lines, HCT-116 (37°C) cells seemed to be the least efficient in taking up Sm IPSE. Here, immunofluorescence images showed that not only a robustly lower fluorescent signal in HCT-116 cells which is mostly restricted to the membrane. Moreover, the endocytosis assay revealed that a major amount of the exogenously added IPSE seems to stay at the outside of the cell at the cell membrane, whereby a ratio between quenched and unquenched IPSE signals of 1:6 supports this finding. On the one hand, this might indicate that IPSE is not completely taken up in HCT-116 cells. Alternatively, it may also be an indicator that the endocytosis-uptake is slower and still in progression in this cell type. Perhaps a comparison of the two cell types (colorectal carcinoma HCT-116 vs hepatocellular carcinoma HepG2) is the key to the uptake pathway. It would be interesting to

compare which receptors are expressed on the surface of the two cell types, as this may directly point to receptors mediating IPSE uptake. From an evolutionary point of view, it is intriguing to note that the colorectal cell line does not take up IPSE, while the hepatoma cell line does, as the evolutionary pressure on the eggs is to exit the gut, not the liver, which is a dead end in terms of supporting the parasite's life cycle.

Finally, different distribution patterns of IPSE in each cell line might also indicate that IPSE enters each cell line via a different endocytosis mechanism, such as Caveolin- or Clathrin-mediated endocytosis. This however remains to be shown in future research.

Isihida et al., (2020) have previously performed a FACS-based screen of Sh06 IPSE uptake in HCV-29 urothelial cells versus Cath.a mouse cells, where IPSE was taken up with similar efficiency in both cell types. Notably, the cells employed in this study are not only differing in size, but also derived from different species (human and hamster). Additionally, it must also be taken in consideration that different cell lines express variable endocytosis-receptors, also on different expression levels, on their surface and might therefore be more efficient in some or favour particular uptake pathways. However, uptake of the control hTrf-FITC occurred in a similar way in HepG2 and HCT-116 cell lines (at 37 °C), where no difference between quenched and unquenched signals was detected. Therefore, general capacity of uptake was seemingly uniform. Nevertheless, Sm IPSE specific receptor-engagement might have influenced uptake efficiency in different cell types, an effect that may not be captured by the positive control. Notably, Sm IPSE, abundance was immunohistologically reported in liver tissue, but was absent in intestinal tissue (Peterková et al., 2024; Schramm et al., 2003). Peterková et al., (2024) thereby detected IPSE in high abundance in the subshell area of liver-eggs, but only in low concentrations in intestinal eggs. This might indicate that Sm IPSE is rather destined to infiltrate liver cells, than intestinal cells, resulting from thousands of years of adaption from the parasite to the host. This further raises the question of how the egg 'knows' in which tissue it is localized, and if the expression of IPSE is driven by specific signalling from host or egg. Alternatively, if IPSE plays a key role in supporting translocation across the gut wall, eggs will transit through the gut rapidly, and will not stay in the tissues long enough to accumulate large amounts of IPSE and other secretory components around them; while in the liver, the eggs are trapped, hence keep producing large amounts of IPSE which accumulates around the eggs, without ever being able to leave the tissue.

Previous studies showed that IPSE inhabits the ability to translocate to the nucleus where it might interact with DNA (Kaur et al., 2011; Pennington et al., 2017).Therefore, nuclear translocation was investigated in the scope of this study. Yet, in each cell line tested herein, HEK293-6E expressed Sm IPSE did not seem to be able to enter the host cell nucleus. Noteworthy, it should be mentioned that in compared to this study, previous work provided by Kaur et al., (2011), nuclear localization was seen by either directly transfecting the host cell itself with an IPSE coding plasmid (Huh7 and U-2 Os cells) or treating cells (CHO-Trvb1) with *E. coli* derived Sm IPSE. However, *haematobium*-IPSE used in the study by Pennington et al., (2017) was produced in HEK293 cells, and added as exogenous protein to HTB-9 cells for 24 hours, resulting in full nuclear localisation, as shown by confocal microscopy using DRAQ5 for staining of nuclei and a a mouse anti-His antibody and Alexa Fluor 555-conjugated goat anti-mouse IgG(H+L) as a secondary antibody. An H03 triple NLS mutant (SKAAAKY instead of SKRRRKY) failed to enter the nucleus and remained confined to the cytoplasmic compartment. Similarly, in the scope of his PhD thesis, Alouffi (2017) was able to show that Sm IPSE recombinantly expressed in HEK293-6E cells exhibited nuclear localization in Huh7 (hepatocyte-derived cell line) cells. Since our results differ completely from the aforementioned studies, it should be considered that nuclear localization of IPSE might be cell-dependent and might be mediated by the different cellular uptake.

Might the lack of adequate post-translational modification be a possible reason for an impaired nuclear uptake? When expressing proteins of interest in HEK293-6Ecells, glycosylation is only achieved by modifying the protein posttranslationally with agalacto-type biantennary core-fucosylated N-glycan structures to proteins (Böhm et al., 2015). Meanwhile, schistosome-expressed IPSE contains difucosylated diantennary glycans (Wuhrer et al., 2006), which might also impact its translocation to the nucleus. Indeed, it was shown that some proteins need specific O-glycosylations to be able to enter the nucleus (Snow & Hart, 1998), which does not exclude the possibility that for Sm IPSE nuclear translocation specific glycans are needed. However, IPSE only contains N-glycans and no O-glycans, hence this is unlikely to be an explanation for the discrepancy between the results obtained by me and previous work.

Therefore, it cannot be excluded that either fluorescence labelling or HEK-derived posttranslational modifications might interfere with the translocation. Of note, nuclear localization potential of Sm IPSE has not yet been tested in native egg-derived Sm IPSE, therefore it cannot be said that native IPSE translocates to the host cell nucleus.

Nevertheless, taking a closer look at the previous published work of Peterková et al., (2024), who detected IPSE via immunolocalization in an confocal microscope (Figure 63), IPSE does also not seem to translocate to the stained nucleus, as they obtained a similar distribution pattern to my results (Figure 46, Results).

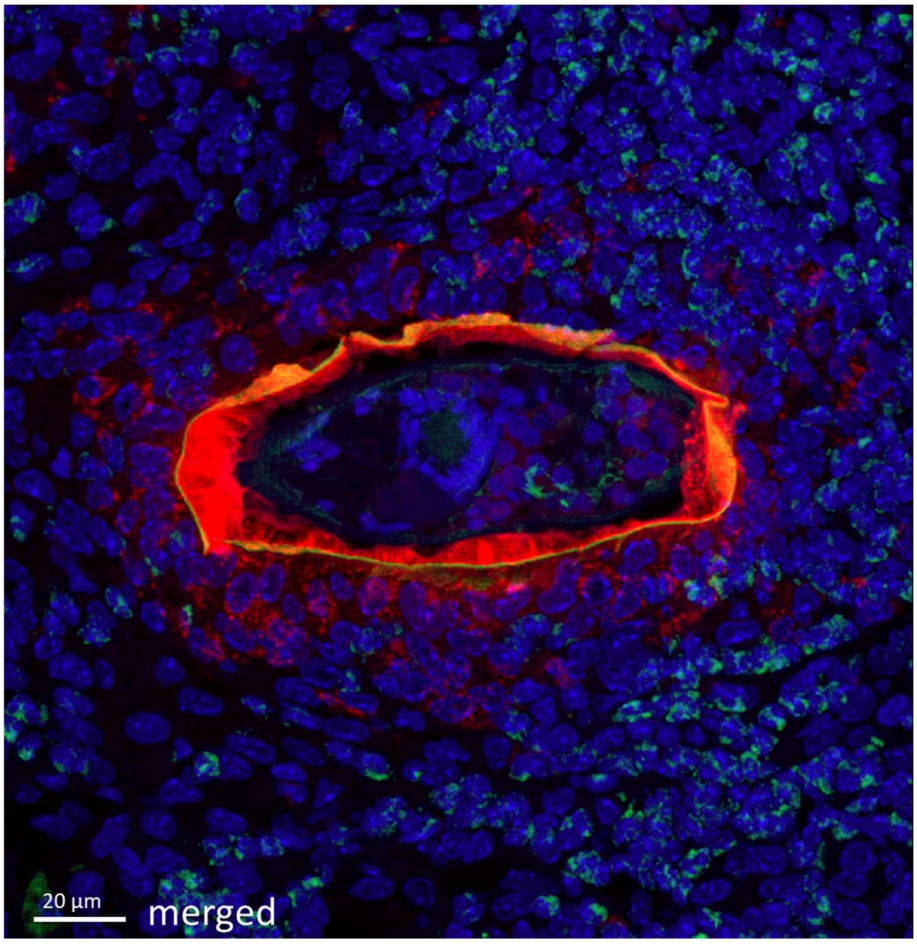

Figure 63 Immunolocalization of IPSE in mouse liver infected with *S. mansoni*. Extracted from Figure 12 C in a higher resultion provided by the authors (Peterková et al., 2024). Red = anti-IPSE antibody-specific sites, green = eggshell autofluorescence and blue for DAPI-labeled cell nuclei.

Another possible reason for different IPSE-destinations within the cell, might be the cellular uptake pathway employed, which may be influenced by the presence or absence of glycans and might therefore lead to misdirection of the protein if it was not in its native state. It was previously shown, that glycan-carrying *Schistosoma* egg antigens can interact with C-type Lectin receptors (CLRs). These mediate an endocytosis-dependent uptake via L-SIGN, for the internalization of the proteins (S. Meyer et al., 2007) implicating an indispensable glycosylation of the protein for successful cellular internalization via these receptors. In case of Sm IPSE it was

shown that the uptake mechanism involves the carbohydrate residues of the protein and C-type lectin receptors, such as the DC-SIGN (dendritic cell-specific ICAM3-grabbing non integrin), mannose receptor and a macrophage galactose-type lectins of the cell (Meevissen et al., 2012). These findings, and the fact that unglycosylated IPSE also enters the host cells; indicate that several uptake mechanism might be involved.

A possible operational mistake such as insufficient treatment with Triton-X to permeabilize the cells, cannot be excluded and therefore might be the reason for not observing any nuclear IPSE signal. However, this seems rather unlikely, since the cell membrane was permeablized and allowed antibody staining. Due to that and, even more importantly, the above-mentioned cytosolic distribution pattern of natural IPSE secreted by liver-eggs (Figure 63), it can cautiously be concluded that glycosylated Sm IPSE does not enter the host cell nucleus in every cell line.

In addition to that, we aimed to perform the conjugation of the biarsenical dye FlAsH-EDT_2 to the TC-tagged IPSE in order to be able to perform cell imaging. As described in the result-section, unclear results were obtained. Due to massive background noise, it was difficult to determine cellular IPSE uptake in HCT-116 cells, even though a very weak signal could be detected when completely adapting the laser intensity. In the obtained data, it is almost impossible to determine whether the fluorescent signal is originating from the cytosol or the cell membrane. This might be lead back to the previous described findings that IPSE-internalization by HCT-116 cells was very low. Noteworthy, this experiment was conducted with other cell lines such as CaCo-2 (colon epithelial) cells and lead to the same result (data not shown). This could further indicate that the intestinal cell lines do not take up IPSE, as also suggested by the discrepancy between permissive hepatocarcinoma HepG2 cells and non-permissive (in terms of IPSE uptake) colorectal HCT-116 cells.

It is important to note that the conjugation reaction may affect the properties of IPSE. Like most labelling technologies, the fluorescent dye is conjugated using the N-Hydroxysuccinimide (NHS)-Ester technology, which leads to stable amide bonds with exposed N-terminal α-Amino groups or the ε-Amino groups in the Lysine side chains. This might negatively affect important Lysine residues, in particular the key Lysine in the PKRRRTY Nuclear Localisation Signal (as shown by Kaur et al.) and therefore possibly affect the ability of IPSE to translocate across the nuclear membrane. Therefore, due to these results, I decided that this kind of visualization of IPSE, at least for the tested intestinal cells, does not seem suitable for my analysis.

4.3.3 IPSE only selectively binds to DNA

As we gathered contradictory results regarding the nuclear translocation of Sm IPSE it was anticipated whether IPSE might interact with importin-α, a carrier protein facilitating nuclear translocation (Kaur et al., 2011; Pennington et al., 2017). Importin alpha-mediated import relies on a positively charged nuclear localization signal (e.g. PKRRRTY in IPSE) in the protein of interest which aligns to the grooves of importin-α needed for binding by its large binding pocket, as predicted by Kosugi et al. 2009 (Kosugi et al., 2009). To gain further insights into nuclear translocation, interaction of importin alpha and IPSE was studied. To that end, a simple experimental setup was performed, where cells were transfected with pDsred importin-α, leading to a strong red fluorescent signal of the importer protein in the cytosol, and subsequent incubation with exogenously added IPSE was supposed to give first insights. Here, a visible shift of the fluorescence pattern towards the nucleus was expected, after potential binding of the karyopherin importin-α to Sm IPSE. Notably, no such shift was detected in IPSE-treated cells during the whole experimental period, which is in line with our previous findings that IPSE is not translocating to the nucleus in our hands.

When cargo proteins bound to Importin alpha and importin beta dock to the nuclear pore complex, the cargo protein and the importin alpha are internalised while the importin beta remains outside. After dissociation of the cargo in an energy-dependent step, both karyopherins are exported to the cytosol, the alpha integrin via its nuclear export signal (NES) and via a nuclear export factor (CAS), complexed with RanGTP (Stewart, 2007). As this is a fast process, it is possible that no shift in distribution is detectable without the use of nuclear export inhibitors such as the non-specific leptomycin B or the specific inhibitors of nuclear export (SINE).

Moreover, it should be considered that in general there are seven different importin-α subtypes and IPSE might still interact with the ones not queried (Miyamoto et al., 2016; Pumroy & Cingolani, 2015). The subtypes were known to exhibit cargo-specific affininty in order to carry subtype-specific molecules to the nucleus, i.e STAT1 (signal transducer and activator of transcription 1) is exclusively carried by importin α5 (Pumroy & Cingolani, 2015; Yoneda, 2000). However, considering the findings herein presented align to each other, technical error can cautiously be excluded. More likely, the chosen technique does not seem to be suitable for examining this interaction.

Previous studies further suggest a fundamental ability of IPSE to bind to host DNA (PhD thesis Ishwinder Kaur 2011). Although IPSE did not appear to translocate to the nucleus, we sought to determine whether the herein used IPSE remained capable of

interacting with DNA. Using EMSA it was found that Sm IPSE seemingly interacts with DNA-ladder, impairing the running of the marker during EMSA. Based on this, it can be concluded that IPSE indeed exhibits DNA-binding capacity. Notably, it was assumed that a substantial part in DNA binding would most likely be mediated by the positive stretch of triple Arginine of the NLS which might bind the negatively charged DNA (Kosugi et al., 2009; Pennington et al., 2017). Indeed, we found that the Sm IPSE NLS-AAA mutant generated herein was not able to block the ladder from running as much as the wild type, indicating a lower binding affinity to DNA. Besides this, the EMSA further revealed that Sm as well as Sh06 IPSE are not capable of binding indiscriminately to all DNA. No binding activity at all was observed with another ladder, as well as with the used oligonucleotides. These findings, as well as the all the other results not showing any localization to the host cell nucleus, might point to IPSE not necessarily interacting with the host DNA or at least not ubiquitously with each DNA fragment.

Taken together, these findings suggest that Sm IPSE-uptake seems to be cell type-specific. Moreover, the results also point to an endocytosis-mediated uptake of Sm IPSE. Once in the cell, IPSE seems to stimulate different pathways which might contribute to the egg's escape as well as maintenance of a "healthy" host tissue. Without being able to reproduce IPSE's nuclear localization, for reasons which we have not been able to pinpoint, it can still be stated that Sm IPSE possesses the ability to bind to host DNA.

4.4 Final Conclusion

With this study, I was able to show that IPSE only binds to full length IgE, but not to truncated forms. IPSE shows a higher binding-affinity to IgEλ than to IgEκ, as shown in ELISA and further with not being able to form a stable complex to IgEκ, which was tried to be visualized in Negative Stainig and Size Exclusion Chromatography. Standing in line with that, IPSE was only able to stimulate basophils that were sensitized with IgEλ and not with other IgE forms. To finally determine the exact binding site and stoichiometry of IPSE to IgE, I would suggest the performance of Negative Staining and/or Cryo-EM with IgEλ.

Supporting findings of previous studies on the IgE-IPSE, in these these conducted experiments, the T92Y/R127L mutant of IPSE had a complete impaired basophil-activation capacity, in a reporter assay using human-serum with high IgE levels to

sensitize chimeric rat basophils. Hereby, the T92Y seemingly plays the leading part, whereas the R127L mutation gives the “coup of grace”.

The obtained data furthermore suggest that IPSE orthologues derived from *S. haematobium*, display a lower binding affininty to IgE, as well as lower basophil-activation capacities.

With these findings, we were able to make a further contribution to elucidate the unique IgE-IPSE binding mechanism, as especially the involvement of the IgE light chain plays a crucial role in effective binding, which might open a new chapter for structural biology of Immunoglobulins. Additionally, this study supports previous findings, as it further supports that Threonine 92 might be part of the IgE-interaction surface and thus is crucial for IgE binding and the subsequent basophil activation.

Another aspect of this study was to gain more insights in the IPSE host-cell interaction and in general IPSE’s function within the host cell. RNAseq data revealed that IPSE-internalization by HepG2 cells leads to the deregulation of several pathways, whereby it might induce several processes of the cell, such as cell- cell reorganization and other pathways involved in tissue damage healing. Might IPSE play a role as tissue protector? Flow cytometry and immunofluorescence analysis demonstrated that IPSE differentially internalized by different cell lines, preferably by CHO-Trvb (hamster ovary) and HepG2 (hepatocellular) cells, compared to HCT-116 (colonal) cells. This would further raise the question of how IPSE and the egg itself ‘knows’ in which tissue they are localized. Moreover, we were able to demonstrate that IPSE-uptake is seemingly mediated by endocytosis, as no IPSE-interalization occurred at 4°C. Even though, IPSE bears the fundamental ability to bind to specific DNA fragments, our results suggest, unlike previous in vitro studies, no nuclear translocation of IPSE to the host cell nucleus.

These findings might be a starting point to focus on IPSEs functions in the liver tissue, with special focus on protective mechanism for the host tissue and the survival of the egg, as well as the last attempt to flee of the egg itself.

5. References

Abbas, A. K., Murphy, K. M., & Sher, A. (1996). Functional diversity of helper T lymphocytes. *Nature*, *383*(6603), 787–793. https://doi.org/10.1038/383787a0

Abdulla, M.-H., Lim, K.-C., McKerrow, J. H., & Caffrey, C. R. (2011). Proteomic identification of IPSE/alpha-1 as a major hepatotoxin secreted by Schistosoma mansoni eggs. *PLoS Neglected Tropical Diseases*, *5*(10), e1368. https://doi.org/10.1371/journal.pntd.0001368

Amaral, K. B., Silva, T. P., Dias, F. F., Malta, K. K., Rosa, F. M., Costa-Neto, S. F., Gentile, R., & Melo, R. C. N. (2017). Histological assessment of granulomas in natural and experimental Schistosoma mansoni infections using whole slide imaging. *PloS One*, *12*(9), e0184696. https://doi.org/10.1371/journal.pone.0184696

Amiri, P., Locksley, R. M., Parslow, T. G., Sadick, M., Rector, E., Ritter, D., & McKerrow, J. H. (1992). Tumour necrosis factor alpha restores granulomas and induces parasite egg-laying in schistosome-infected SCID mice. *Nature*, *356*(6370), 604–607. https://doi.org/10.1038/356604a0

Andrews, P. (1985). Praziquantel: Mechanisms of anti-schistosomal activity. *Pharmacology & Therapeutics*, *29*(1), 129–156. https://doi.org/10.1016/0163-7258(85)90020-8

Ashburner, M., Ball, C. A., Blake, J. A., Botstein, D., Butler, H., Cherry, J. M., Davis, A. P., Dolinski, K., Dwight, S. S., Eppig, J. T., Harris, M. A., Hill, D. P., Issel-Tarver, L., Kasarskis, A., Lewis, S., Matese, J. C., Richardson, J. E., Ringwald, M., Rubin, G. M., & Sherlock, G. (2000). Gene Ontology: Tool for the unification of biology. *Nature genetics*, *25*(1), 25–29. https://doi.org/10.1038/75556

Ashton, P. D., Harrop, R., Shah, B., & Wilson, R. A. (2001). The schistosome egg: Development and secretions. *Parasitology*, *122*(03). https://doi.org/10.1017/S0031182001007351

Bakolitsa, C., Cohen, D. M., Bankston, L. A., Bobkov, A. A., Cadwell, G. W., Jennings, L., Critchley, D. R., Craig, S. W., & Liddington, R. C. (2004). Structural basis for vinculin activation at sites of cell adhesion. *Nature*, *430*(6999), 583–586. https://doi.org/10.1038/nature02610

Bartel, D. P. (2004). MicroRNAs: Genomics, biogenesis, mechanism, and function. *Cell*, *116*(2), 281–297. https://doi.org/10.1016/s0092-8674(04)00045-5

Benjamini, Y., & Hochberg, Y. (1995). Controlling the False Discovery Rate: A Practical and Powerful Approach to Multiple Testing. *Journal of the Royal Statistical Society. Series B (Methodological)*, *57*(1), 289–300.

Bergeron, M. J., Simonin, A., Bürzle, M., & Hediger, M. A. (2008). Inherited epithelial transporter disorders—An overview. *Journal of Inherited Metabolic Disease*, *31*(2), 178–187. https://doi.org/10.1007/s10545-008-0861-6

Böhm, E., Seyfried, B. K., Dockal, M., Graninger, M., Hasslacher, M., Neurath, M., Konetschny, C., Matthiessen, P., Mitterer, A., & Scheiflinger, F. (2015). Differences in N-glycosylation of recombinant human coagulation factor VII derived from BHK, CHO, and HEK293 cells. *BMC Biotechnology*, *15*, 87. https://doi.org/10.1186/s12896-015-0205-1

Brunet, L. R., Finkelman, F. D., Cheever, A. W., Kopf, M. A., & Pearce, E. J. (1997). IL-4 protects against TNF-alpha-mediated cachexia and death during acute schistosomiasis. *Journal of Immunology (Baltimore, Md.: 1950)*, *159*(2), 777–785.

Candido, R., Woodward, R., Graeff-Teixeira, C., Jones, M., & St Pierre, T. (2017). *Preliminary observations on the feasibility of using a magnetic probe for isolation of schistosome eggs from urine*.

Cheever, A. W., Poindexter, R. W., & Wynn, T. A. (1999). Egg laying is delayed but worm fecundity is normal in SCID mice infected with Schistosoma japonicum and S. mansoni with or without recombinant tumor necrosis factor alpha treatment. *Infection and Immunity*, *67*(5), 2201–2208. https://doi.org/10.1128/IAI.67.5.2201-2208.1999

Chui, S. H., Lam, C. W., & Lai, K. N. (1990). Light-chain ratios of immunoglobulins G, A, and M determined by enzyme immunoassay. *Clinical Chemistry*, *36*(3), 501–502.

Cingoz, O. (2009). Motavizumab. *mAbs*, *1*(5), 439–442.

Colley, D. G., Bustinduy, A. L., Secor, W. E., & King, C. H. (2014). Human schistosomiasis. *Lancet (London, England)*, *383*(9936), 2253–2264. https://doi.org/10.1016/S0140-6736(13)61949-2

Colombe, S., Lee, M. H., Masikini, P. J., van Lieshout, L., de Dood, C. J., Hoekstra, P. T., Corstjens, P. L. A. M., Mngara, J., van Dam, G. J., & Downs, J. A. (2018). Decreased Sensitivity of Schistosoma sp. Egg Microscopy in Women and HIV-Infected Individuals. *The American Journal of Tropical Medicine and Hygiene*, *98*(4), 1159–1164. https://doi.org/10.4269/ajtmh.17-0790

Costain, A. H., MacDonald, A. S., & Smits, H. H. (2018). Schistosome Egg Migration: Mechanisms, Pathogenesis and Host Immune Responses. *Frontiers in Immunology*, *9*, 3042. https://doi.org/10.3389/fimmu.2018.03042

DeKosky, B. J., Lungu, O. I., Park, D., Johnson, E. L., Charab, W., Chrysostomou, C., Kuroda, D., Ellington, A. D., Ippolito, G. C., Gray, J. J., & Georgiou, G. (2016). Large-scale sequence and structural comparisons of human naive and antigen-experienced antibody repertoires. *Proceedings of the National Academy of Sciences of the United States of America*, *113*(19), E2636-2645. https://doi.org/10.1073/pnas.1525510113

Delvendahl, I., Vyleta, N. P., von Gersdorff, H., & Hallermann, S. (2016). Fast, Temperature-Sensitive and Clathrin-Independent Endocytosis at Central

Synapses. *Neuron*, *90*(3), 492–498. https://doi.org/10.1016/j.neuron.2016.03.013

Dessaint, J. P., Capron, M., Bout, D., & Capron, A. (1975). Quantitative determination of specific IgE antibodies to schistosome antigens and serum IgE levels in patients with schistosomiasis (S. mansoni or S. haematobium). *Clinical and Experimental Immunology*, *20*(3), 427–436.

deWalick, S., Tielens, A. G. M., & van Hellemond, J. J. (2012). *Schistosoma mansoni*: The egg, biosynthesis of the shell and interaction with the host. *Experimental Parasitology*, *132*(1), 7–13. https://doi.org/10.1016/j.exppara.2011.07.018

Dodev, T. S., Karagiannis, P., Gilbert, A. E., Josephs, D. H., Bowen, H., James, L. K., Bax, H. J., Beavil, R., Pang, M. O., Gould, H. J., Karagiannis, S. N., & Beavil, A. J. (2014). A tool kit for rapid cloning and expression of recombinant antibodies. *Scientific Reports*, *4*, 5885. https://doi.org/10.1038/srep05885

Doenhoff, M. J. (1997). A role for granulomatous inflammation in the transmission of infectious disease: Schistosomiasis and tuberculosis. *Parasitology*, *115 Suppl*, S113-125. https://doi.org/10.1017/s0031182097001972

Dunne, D. W., Bain, J., Lillywhite, J., & Doenhoff, M. J. (1984). The stage-, strain- and species-specificity of a Schistosoma mansoni egg antigen fraction (CEF6) with serodiagnostic potential. *Transactions of the Royal Society of Tropical Medicine and Hygiene*, *78*(4), 460–470. https://doi.org/10.1016/0035-9203(84)90061-0

Dunne, D. W., Jones, F. M., & Doenhoff, M. J. (1991). The purification, characterization, serological activity and hepatotoxic properties of two cationic glycoproteins (alpha 1 and omega 1) from Schistosoma mansoni eggs. *Parasitology*, *103 Pt 2*, 225–236. https://doi.org/10.1017/s0031182000059503

Dunne, D. W., Lucas, S., Bickle, Q., Pearson, S., Madgwick, L., Bain, J., & Doenhoff, M. J. (1981). Identification and partial purification of an antigen (omega 1) from Schistosoma mansoni eggs which is putatively hepatotoxic in T-cell deprived mice. *Transactions of the Royal Society of Tropical Medicine and Hygiene*, *75*(1), 54–71. https://doi.org/10.1016/0035-9203(81)90013-4

Dvorak, A. M. (1998). Cell biology of the basophil. *International Review of Cytology*, *180*, 87–236. https://doi.org/10.1016/s0074-7696(08)61771-4

Eglite, S., Plüss, K., & Dahinden, C. A. (2000). Requirements for C5a receptor-mediated IL-4 and IL-13 production and leukotriene C4 generation in human basophils. *Journal of Immunology (Baltimore, Md.: 1950)*, *165*(4), 2183–2189. https://doi.org/10.4049/jimmunol.165.4.2183

Falcone, F. H., Alcocer, M. J. C., Okamoto-Uchida, Y., & Nakamura, R. (2015). Use of Humanized Rat Basophilic Leukemia Reporter Cell Lines as a Diagnostic Tool for Detection of Allergen-Specific IgE in Allergic Patients: Time for a Reappraisal? *Current Allergy and Asthma Reports*, *15*(11), 67. https://doi.org/10.1007/s11882-015-0568-3

Falcone, F. H., Dahinden, C. A., Gibbs, B. F., Noll, T., Amon, U., Hebestreit, H., Abrahamsen, O., Klaucke, J., Schlaak, M., & Haas, H. (1996). Human basophils release interleukin-4 after stimulation with Schistosoma mansoni egg antigen. *European Journal of Immunology*, *26*(5), 1147–1155. https://doi.org/10.1002/eji.1830260528

Fallon, P. G. (2000). Immunopathology of schistosomiasis: A cautionary tale of mice and men. *Immunology Today*, *21*(1), 29–35. https://doi.org/10.1016/s0167-5699(99)01551-0

Fallon, P. G., Richardson, E. J., McKenzie, G. J., & McKenzie, A. N. (2000). Schistosome infection of transgenic mice defines distinct and contrasting pathogenic roles for IL-4 and IL-13: IL-13 is a profibrotic agent. *Journal of*

Immunology (Baltimore, Md.: 1950), *164*(5), 2585–2591. https://doi.org/10.4049/jimmunol.164.5.2585

Fretz, M. M., Penning, N. A., Al-Taei, S., Futaki, S., Takeuchi, T., Nakase, I., Storm, G., & Jones, A. T. (2007). Temperature-, concentration- and cholesterol-dependent translocation of L- and D-octa-arginine across the plasma and nuclear membrane of CD34+ leukaemia cells. *The Biochemical Journal*, *403*(2), 335–342. https://doi.org/10.1042/BJ20061808

Gabrielli, A. F., & Garba Djirmay, A. (2023). Schistosomiasis in Europe. *Current Tropical Medicine Reports*, *10*(3), 79–87. https://doi.org/10.1007/s40475-023-00286-9

Geiger, B. (1979). A 130K protein from chicken gizzard: Its localization at the termini of microfilament bundles in cultured chicken cells. *Cell*, *18*(1), 193–205. https://doi.org/10.1016/0092-8674(79)90368-4

Gibbs, B. F., Haas, H., Falcone, F. H., Albrecht, C., Vollrath, I. B., Noll, T., Wolff, H. H., & Amon, U. (1996). Purified human peripheral blood basophils release interleukin-13 and preformed interleukin-4 following immunological activation. *European Journal of Immunology*, *26*(10), 2493–2498. https://doi.org/10.1002/eji.1830261033

Gobbi, F., Tamarozzi, F., Buonfrate, D., Lieshout, L. van, Bisoffi, Z., & Bottieau, E. (2020). New Insights on Acute and Chronic Schistosomiasis: Do We Need a Redefinition? *Trends in Parasitology*, *36*(8), 660–667. https://doi.org/10.1016/j.pt.2020.05.009

Goebel, C. (1905). Ueber die bei Bilharziakrankheit vorkommenden Blasentumoren mit besonderer Berücksichtigung des Carcinoms. *Zeitschrift für Krebsforschung*, *3*(3), 369–513. https://doi.org/10.1007/BF02215122

Gould, H. J., & Sutton, B. J. (2008). IgE in allergy and asthma today. *Nature Reviews Immunology*, *8*(3), 205–217. https://doi.org/10.1038/nri2273

Gould, H. J., Sutton, B. J., Beavil, A. J., Beavil, R. L., McCloskey, N., Coker, H. A., Fear, D., & Smurthwaite, L. (2003). The Biology of IgE and the Basis of Allergic Disease. *Annual Review of Immunology*, *21*(Volume 21, 2003), 579–628. https://doi.org/10.1146/annurev.immunol.21.120601.141103

Grevelding, C. G. (2004). Schistosoma. *Current Biology*, *14*(14), R545. https://doi.org/10.1016/j.cub.2004.07.006

Griffin, B. A., Adams, S. R., & Tsien, R. Y. (1998). Specific Covalent Labeling of Recombinant Protein Molecules Inside Live Cells. *Science*, *281*(5374), 269–272. https://doi.org/10.1126/science.281.5374.269

Gu, Z. (2022). Complex heatmap visualization. *iMeta*, *1*(3), e43. https://doi.org/10.1002/imt2.43

Haas, H., Falcone, F. H., Schramm, G., Haisch, K., Gibbs, B. F., Klaucke, J., Pöppelmann, M., Becker, W.-M., Gabius, H.-J., & Schlaak, M. (1999). Dietary lectins can induce in vitro release of IL-4 and IL-13 from human basophils. *European Journal of Immunology*, *29*(3), 918–927. https://doi.org/10.1002/(SICI)1521-4141(199903)29:03<918::AID-IMMU918>3.0.CO;2-T

Haeberlein, S., Obieglo, K., Ozir-Fazalalikhan, A., Chayé, M. A. M., Veninga, H., van der Vlugt, L. E. P. M., Voskamp, A., Boon, L., den Haan, J. M. M., Westerhof, L. B., Wilbers, R. H. P., Schots, A., Schramm, G., Hokke, C. H., & Smits, H. H. (2017). Schistosome egg antigens, including the glycoprotein IPSE/alpha-1, trigger the development of regulatory B cells. *PLoS Pathogens*, *13*(7), e1006539. https://doi.org/10.1371/journal.ppat.1006539

Harwood, N. E., & McDonnell, J. M. (2007). The intrinsic flexibility of IgE and its role in binding FcεRI. *Biomedicine & Pharmacotherapy*, *61*(1), 61–67. https://doi.org/10.1016/j.biopha.2006.11.004

He, L., Vasiliou, K., & Nebert, D. W. (2009). Analysis and update of the human solute carrier (SLC) gene superfamily. *Human Genomics*, *3*(2), 195–205. https://doi.org/10.1186/1479-7364-3-2-195

Heldin, C.-H., & Moustakas, A. (2016). Signaling Receptors for TGF-β Family Members. *Cold Spring Harbor Perspectives in Biology*, *8*(8), a022053. https://doi.org/10.1101/cshperspect.a022053

Herbert, D. R., Orekov, T., Perkins, C., Rothenberg, M. E., & Finkelman, F. D. (2008). IL-4R alpha expression by bone marrow-derived cells is necessary and sufficient for host protection against acute schistosomiasis. *Journal of Immunology (Baltimore, Md.: 1950)*, *180*(7), 4948–4955. https://doi.org/10.4049/jimmunol.180.7.4948

Hoffmann, C., Gaietta, G., Zürn, A., Adams, S. R., Terrillon, S., Ellisman, M. H., Tsien, R. Y., & Lohse, M. J. (2010). Fluorescent labeling of tetracysteine-tagged proteins in intact cells. *Nature protocols*, *5*(10), 1666–1677. https://doi.org/10.1038/nprot.2010.129

Hogan, P. G., Chen, L., Nardone, J., & Rao, A. (2003). Transcriptional regulation by calcium, calcineurin, and NFAT. *Genes & Development*, *17*(18), 2205–2232. https://doi.org/10.1101/gad.1102703

Hokke, C. H., & Yazdanbakhsh, M. (2005). Schistosome glycans and innate immunity. *Parasite Immunology*, *27*(7–8), 257–264. https://doi.org/10.1111/j.1365-3024.2005.00781.x

Holder, M. J., & Cooper, P. R. (2011). Species identification and authentification of human and rodent cell cultures using polymerase chain reaction analysis of vomeronasal receptor genes. *Cytotechnology*, *63*(6), 553–558. https://doi.org/10.1007/s10616-011-9394-1

Hutchinson, L. E., & McCloskey, M. A. (1995). FcεRI-mediated Induction of Nuclear Factor of Activated T-cells *. *Journal of Biological Chemistry*, *270*(27), 16333–16338. https://doi.org/10.1074/jbc.270.27.16333

Huynh, K., & Partch, C. L. (2015). Analysis of protein stability and ligand interactions by thermal shift assay. *Current Protocols in Protein Science*, *79*, 28.9.1-28.9.14. https://doi.org/10.1002/0471140864.ps2809s79

Ishida, K., Mbanefo, E. C., Le, L., Lamanna, O., Pennington, L. F., Finkel, J. C., Jardetzky, T. S., Falcone, F. H., & Hsieh, M. H. (2020). IPSE, a parasite-derived, host immunomodulatory infiltrin protein, alleviates resiniferatoxin-induced bladder pain. *Molecular Pain*, *16*, 1744806920970099. https://doi.org/10.1177/1744806920970099

Ittisoponpisan, S., Islam, S. A., Khanna, T., Alhuzimi, E., David, A., & Sternberg, M. J. E. (2019). Can Predicted Protein 3D Structures Provide Reliable Insights into whether Missense Variants Are Disease Associated? *Journal of Molecular Biology*, *431*(11), 2197–2212. https://doi.org/10.1016/j.jmb.2019.04.009

Jauréguiberry, S., Paris, L., & Caumes, E. (2010). Acute schistosomiasis, a diagnostic and therapeutic challenge. *Clinical Microbiology and Infection*, *16*(3), 225–231. https://doi.org/10.1111/j.1469-0691.2009.03131.x

Jiao, C.-Y., Delaroche, D., Burlina, F., Alves, I. D., Chassaing, G., & Sagan, S. (2009). Translocation and Endocytosis for Cell-penetrating Peptide Internalization. *Journal of Biological Chemistry*, *284*(49), 33957–33965. https://doi.org/10.1074/jbc.M109.056309

Johnston, C. J. C., Smyth, D. J., Kodali, R. B., White, M. P. J., Harcus, Y., Filbey, K. J., Hewitson, J. P., Hinck, C. S., Ivens, A., Kemter, A. M., Kildemoes, A. O., Le Bihan, T., Soares, D. C., Anderton, S. M., Brenn, T., Wigmore, S. J., Woodcock, H. V., Chambers, R. C., Hinck, A. P., … Maizels, R. M. (2017). A structurally distinct TGF-β mimic from an intestinal helminth parasite potently induces regulatory T cells. *Nature Communications*, *8*(1), 1741. https://doi.org/10.1038/s41467-017-01886-6

Joseph, J. V., Magaut, C. R., Storevik, S., Geraldo, L. H., Mathivet, T., Latif, M. A., Rudewicz, J., Guyon, J., Gambaretti, M., Haukas, F., Trones, A., Rømo Ystaas, L. A., Hossain, J. A., Ninzima, S., Cuvellier, S., Zhou, W., Tomar, T., Klink, B., Rane, L., … Miletic, H. (2022). TGF-β promotes microtube formation in glioblastoma through thrombospondin 1. *Neuro-Oncology*, *24*(4), 541–553. https://doi.org/10.1093/neuonc/noab212

Jurberg, A. D., Gonçalves, T., Costa, T. A., de Mattos, A. C. A., Pascarelli, B. M., de Manso, P. P. A., Ribeiro-Alves, M., Pelajo-Machado, M., Peralta, J. M., Coelho, P. M. Z., & Lenzi, H. L. (2009). The embryonic development of Schistosoma mansoni eggs: Proposal for a new staging system. *Development Genes and Evolution*, *219*(5), 219–234. https://doi.org/10.1007/s00427-009-0285-9

Kabat, E. A. (1978). The Structural Basis for Antibody Complementary1. In C. B. Anfinsen, J. T. Edsall, & F. M. Richards (Hrsg.), *Advances in Protein Chemistry* (Bd. 32, S. 1–75). Academic Press. https://doi.org/10.1016/S0065-3233(08)60574-4

Karanja, D. M., Colley, D. G., Nahlen, B. L., Ouma, J. H., & Secor, W. E. (1997). Studies on schistosomiasis in western Kenya: I. Evidence for immune-facilitated excretion of schistosome eggs from patients with Schistosoma mansoni and human immunodeficiency virus coinfections. *The American Journal of Tropical Medicine and Hygiene*, *56*(5), 515–521. https://doi.org/10.4269/ajtmh.1997.56.515

Kaur, I., Schramm, G., Everts, B., Scholzen, T., Kindle, K. B., Beetz, C., Montiel-Duarte, C., Blindow, S., Jones, A. T., Haas, H., Stolnik, S., Heery, D. M., & Falcone, F. H. (2011). Interleukin-4-inducing principle from Schistosoma mansoni eggs contains a functional C-terminal nuclear localization signal necessary for nuclear translocation in mammalian cells but not for its uptake.

Infection and Immunity, *79*(4), 1779–1788. https://doi.org/10.1128/IAI.01048-10

Kellermeyer, R. W., Warren, K. S., Waldmann, T. S., Cook, J. A., & Jordon, P. (1973). Concentration of Serum Immunoglobulins in St. Lucians with Schistosomiasis Mansoni Compared with Matched Uninfected St. Vincentians. *The Journal of Infectious Diseases*, *127*(5), 557–562. https://doi.org/10.1093/infdis/127.5.557

Kim, D., Paggi, J. M., Park, C., Bennett, C., & Salzberg, S. L. (2019). Graph-based genome alignment and genotyping with HISAT2 and HISAT-genotype. *Nature Biotechnology*, *37*(8), 907–915. https://doi.org/10.1038/s41587-019-0201-4

Kim, S. I., Kim, H. J., Lee, H.-J., Lee, K., Hong, D., Lim, H., Cho, K., Jung, N., & Yi, Y. W. (2016). Application of a non-hazardous vital dye for cell counting with automated cell counters. *Analytical Biochemistry*, *492*, 8–12. https://doi.org/10.1016/j.ab.2015.09.010

Kim, V. N. (2005). MicroRNA biogenesis: Coordinated cropping and dicing. *Nature Reviews. Molecular Cell Biology*, *6*(5), 376–385. https://doi.org/10.1038/nrm1644

Kinet, J.-P. (1999). The high-affinity IgE receptor (Fc??RI): From physiology to pathology. *Annual review of immunology*, *17*, 931–972. https://doi.org/10.1146/annurev.immunol.17.1.931

Klausner, R. D., Van Renswoude, J., Ashwell, G., Kempf, C., Schechter, A. N., Dean, A., & Bridges, K. R. (1983). Receptor-mediated endocytosis of transferrin in K562 cells. *The Journal of Biological Chemistry*, *258*(8), 4715–4724.

Knuhr, K., Langhans, K., Nyenhuis, S., Viertmann, K., Kildemoes, A. M. O., Doenhoff, M. J., Haas, H., & Schramm, G. (2018). Schistosoma mansoni Egg-Released IPSE/alpha-1 Dampens Inflammatory Cytokine Responses

via Basophil Interleukin (IL)-4 and IL-13. *Frontiers in Immunology*, *9*, 2293. https://doi.org/10.3389/fimmu.2018.02293

Kosugi, S., Hasebe, M., Matsumura, N., Takashima, H., Miyamoto-Sato, E., Tomita, M., & Yanagawa, H. (2009). Six classes of nuclear localization signals specific to different binding grooves of importin alpha. *The Journal of Biological Chemistry*, *284*(1), 478–485. https://doi.org/10.1074/jbc.M807017200

Krueger, F. (2019). *Trim Galore! Available online at http://www.bioinformatics.babraham.ac.uk/projects/trim_galore/. Te*.

Lallès, J. P., & Peltre, G. (2009). Lead Review Article Biochemical Features of Grain Legume Allergens in Humans and Animals. *Nutrition Reviews*, *54*(4), 101–107. https://doi.org/10.1111/j.1753-4887.1996.tb03883.x

Lawrence, M., Huber, W., Pagès, H., Aboyoun, P., Carlson, M., Gentleman, R., Morgan, M. T., & Carey, V. J. (2013). Software for Computing and Annotating Genomic Ranges. *PLoS Computational Biology*, *9*(8), e1003118. https://doi.org/10.1371/journal.pcbi.1003118

Lee, Y., Kim, M., Han, J., Yeom, K.-H., Lee, S., Baek, S. H., & Kim, V. N. (2004). MicroRNA genes are transcribed by RNA polymerase II. *The EMBO Journal*, *23*(20), 4051–4060. https://doi.org/10.1038/sj.emboj.7600385

Li, H., Sim, T. C., & Alam, R. (1996). IL-13 released by and localized in human basophils. *The Journal of Immunology*, *156*(12), 4833–4838. https://doi.org/10.4049/jimmunol.156.12.4833

Liu, J., Zhu, L., Wang, J., Qiu, L., Chen, Y., Davis, R. E., & Cheng, G. (2019). Schistosoma japonicum extracellular vesicle miRNA cargo regulates host macrophage functions facilitating parasitism. *PLoS Pathogens*, *15*(6), e1007817. https://doi.org/10.1371/journal.ppat.1007817

Liu, Z., Ye, Q., Wu, L., Gao, F., Xie, H., Zhou, L., Zheng, S., & Xu, X. (2018). Metallothionein 1 family profiling identifies MT1X as a tumor suppressor

involved in the progression and metastastatic capacity of hepatocellular carcinoma. *Molecular Carcinogenesis*, *57*(11), 1435–1444. https://doi.org/10.1002/mc.22846

Love, M. I., Huber, W., & Anders, S. (2014). Moderated estimation of fold change and dispersion for RNA-seq data with DESeq2. *Genome Biology*, *15*(12), 550. https://doi.org/10.1186/s13059-014-0550-8

Loverde, P., Niles, E., Osman, A., & Wu, W. (2011). Schistosoma mansoni male–female interactions. *Canadian Journal of Zoology*, *82*, 357–374. https://doi.org/10.1139/z03-217

Lu, Z., Sessler, F., Holroyd, N., Hahnel, S., Quack, T., Berriman, M., & Grevelding, C. G. (2017). A gene expression atlas of adult Schistosoma mansoni and their gonads. *Scientific Data*, *4*, 170118. https://doi.org/10.1038/sdata.2017.118

Lucius, R., Loos-Frank, B., & Lane, R. P. (2018). Parasitische Würmer (Helminthen) und Myxozoa. In R. Lucius, B. Loos-Frank, & R. P. Lane (Hrsg.), *Biologie von Parasiten* (S. 249–412). Springer. https://doi.org/10.1007/978-3-662-54862-2_3

Maizels, R. M., Pearce, E. J., Artis, D., Yazdanbakhsh, M., & Wynn, T. A. (2009). Regulation of pathogenesis and immunity in helminth infections. *Journal of Experimental Medicine*, *206*(10), 2059–2066. https://doi.org/10.1084/jem.20091903

Malleret, B., El Sahili, A., Tay, M. Z., Carissimo, G., Ong, A. S. M., Novera, W., Lin, J., Suwanarusk, R., Kosaisavee, V., Chu, T. T. T., Sinha, A., Howland, S. W., Fan, Y., Gruszczyk, J., Tham, W.-H., Colin, Y., Maurer-Stroh, S., Snounou, G., Ng, L. F. P., … Rénia, L. (2021). Plasmodium vivax binds host CD98hc (SLC3A2) to enter immature red blood cells. *Nature Microbiology*, *6*(8), 991–999. https://doi.org/10.1038/s41564-021-00939-3

Mason, P. R., & Fripp, P. J. (1977). The Reactions of Schistosoma mansoni Miracidia to Light. *The Journal of Parasitology*, *63*(2), 240. https://doi.org/10.2307/3280051

Mathieson, W., & Wilson, R. A. (2010). A comparative proteomic study of the undeveloped and developed Schistosoma mansoni egg and its contents: The miracidium, hatch fluid and secretions. *International Journal for Parasitology*, *40*(5), 617–628. https://doi.org/10.1016/j.ijpara.2009.10.014

Mbanefo, E. C., Agbo, C. T., Zhao, Y., Lamanna, O. K., Thai, K. H., Karinshak, S. E., Khan, M. A., Fu, C.-L., Odegaard, J. I., Saltikova, I. V., Smout, M. J., Pennington, L. F., Nicolls, M. R., Jardetzky, T. S., Loukas, A., Brindley, P. J., Falcone, F. H., & Hsieh, M. H. (2020). IPSE, an abundant egg-secreted protein of the carcinogenic helminth Schistosoma haematobium, promotes proliferation of bladder cancer cells and angiogenesis. *Infectious Agents and Cancer*, *15*(1), 63. https://doi.org/10.1186/s13027-020-00331-6

McDonnell, J. M., Dhaliwal, B., Sutton, B. J., & Gould, H. J. (2023). IgE, IgE Receptors and Anti-IgE Biologics: Protein Structures and Mechanisms of Action. *Annual Review of Immunology*, *41*(1), 255–275. https://doi.org/10.1146/annurev-immunol-061020-053712

McGraw, T. E., Greenfield, L., & Maxfield, F. R. (1987). Functional expression of the human transferrin receptor cDNA in Chinese hamster ovary cells deficient in endogenous transferrin receptor. *The Journal of Cell Biology*, *105*(1), 207–214. https://doi.org/10.1083/jcb.105.1.207

Meevissen, M. H. J., Driessen, N. N., Smits, H. H., Versteegh, R., van Vliet, S. J., van Kooyk, Y., Schramm, G., Deelder, A. M., Haas, H., Yazdanbakhsh, M., & Hokke, C. H. (2012). Specific glycan elements determine differential binding of individual egg glycoproteins of the human parasite *Schistosoma mansoni* by host C-type lectin receptors. *International Journal for Parasitology*, *42*(3), 269–277. https://doi.org/10.1016/j.ijpara.2012.01.004

Meningher, T., Barsheshet, Y., Ofir-Birin, Y., Gold, D., Brant, B., Dekel, E., Sidi, Y., Schwartz, E., Regev-Rudzki, N., Avni, O., & Avni, D. (2020). Schistosomal extracellular vesicle-enclosed miRNAs modulate host T helper cell differentiation. *EMBO Reports*, *21*(1), e47882. https://doi.org/10.15252/embr.201947882

Meyer, N. H., Mayerhofer, H., Tripsianes, K., Blindow, S., Barths, D., Mewes, A., Weimar, T., Köhli, T., Bade, S., Madl, T., Frey, A., Haas, H., Mueller-Dieckmann, J., Sattler, M., & Schramm, G. (2015). A Crystallin Fold in the Interleukin-4-inducing Principle of Schistosoma mansoni Eggs (IPSE/α-1) Mediates IgE Binding for Antigen-independent Basophil Activation. *The Journal of Biological Chemistry*, *290*(36), 22111–22126. https://doi.org/10.1074/jbc.M115.675066

Meyer, S., Tefsen, B., Imberty, A., Geyer, R., & van Die, I. (2007). The C-type lectin L-SIGN differentially recognizes glycan antigens on egg glycosphingolipids and soluble egg glycoproteins from Schistosoma mansoni. *Glycobiology*, *17*(10), 1104–1119. https://doi.org/10.1093/glycob/cwm073

Miller, T. W., Soto-Pantoja, D. R., Schwartz, A. L., Sipes, J. M., DeGraff, W. G., Ridnour, L. A., Wink, D. A., & Roberts, D. D. (2015). CD47 Receptor Globally Regulates Metabolic Pathways That Control Resistance to Ionizing Radiation. *The Journal of Biological Chemistry*, *290*(41), 24858–24874. https://doi.org/10.1074/jbc.M115.665752

Mirdita, M., Schütze, K., Moriwaki, Y., Heo, L., Ovchinnikov, S., & Steinegger, M. (2022). ColabFold: Making protein folding accessible to all. *Nature Methods*, *19*(6), 679–682. https://doi.org/10.1038/s41592-022-01488-1

Miyamoto, Y., Yamada, K., & Yoneda, Y. (2016). Importin α: A key molecule in nuclear transport and non-transport functions. *Journal of Biochemistry*, *160*(2), 69–75. https://doi.org/10.1093/jb/mvw036

Molé, C. M., Béne, M. C., Montagne, P. M., Seilles, E., & Faure, G. C. (1994). Light chains of immunoglobulins in human secretions. *Clinica Chimica Acta; International Journal of Clinical Chemistry*, *224*(2), 191–197. https://doi.org/10.1016/0009-8981(94)90185-6

Montaño, R. F., & Morrison, S. L. (2002a). Influence of the isotype of the light chain on the properties of IgG. *Journal of Immunology (Baltimore, Md.: 1950)*, *168*(1), 224–231. https://doi.org/10.4049/jimmunol.168.1.224

Montaño, R. F., & Morrison, S. L. (2002b). Influence of the isotype of the light chain on the properties of IgG. *Journal of Immunology (Baltimore, Md.: 1950)*, *168*(1), 224–231. https://doi.org/10.4049/jimmunol.168.1.224

Moore, D. V., & Sandground, J. H. (1956). The relative egg producing capacity of Schistosoma mansoni and Schistosoma japonicum. *The American Journal of Tropical Medicine and Hygiene*, *5*(5), 831–840. https://doi.org/10.4269/ajtmh.1956.5.831

Morales-Vicente, D. A., Zhao, L., Silveira, G. O., Tahira, A. C., Amaral, M. S., Collins, J. J., & Verjovski-Almeida, S. (2022). Single-cell RNA-seq analyses show that long non-coding RNAs are conspicuously expressed in Schistosoma mansoni gamete and tegument progenitor cell populations. *Frontiers in Genetics*, *13*, 924877. https://doi.org/10.3389/fgene.2022.924877

Morgan, M., Pagès, H., Obenchain, V., & Hayden, N. (2017). *Rsamtools: Bioconductor.*

Müller-Esparza, H., Osorio-Valeriano, M., Steube, N., Thanbichler, M., & Randau, L. (2020). Bio-Layer Interferometry Analysis of the Target Binding Activity of CRISPR-Cas Effector Complexes. *Frontiers in Molecular Biosciences*, *7*. https://doi.org/10.3389/fmolb.2020.00098

Nakamura, R., Ishiwatari, A., Higuchi, M., Uchida, Y., Nakamura, R., Kawakami, H., Urisu, A., & Teshima, R. (2012). Evaluation of the Luciferase Assay-Based In

Vitro Elicitation Test for Serum IgE. *Allergology International*, *61*(3), 431–437. https://doi.org/10.2332/allergolint.11-OA-0407

Nakamura, R., Uchida, Y., Higuchi, M., Nakamura, R., Tsuge, I., Urisu, A., & Teshima, R. (2010). A convenient and sensitive allergy test: IgE crosslinking-induced luciferase expression in cultured mast cells. *Allergy*, *65*(10), 1266–1273. https://doi.org/10.1111/j.1398-9995.2010.02363.x

Neill, P. J. G., Smith, J. H., Doughty, B. L., & Kemp, M. (1988). The Ultrastructure of the Schistosoma mansoni Egg. *The American Journal of Tropical Medicine and Hygiene*, *39*(1), 52–65. https://doi.org/10.4269/ajtmh.1988.39.52

Ochensberger, B., Rihs, S., Brunner, T., & Dahinden, C. A. (1995). IgE-independent interleukin-4 expression and induction of a late phase of leukotriene C4 formation in human blood basophils. *Blood*, *86*(11), 4039–4049.

Okano, M., Nishizaki, K., Abe, M., Wang, M. M., Yoshino, T., Satoskar, A. R., Masuda, Y., & Harn, D. A. (1999). Strain-dependent induction of allergic rhinitis without adjuvant in mice. *Allergy*, *54*(6), 593–601. https://doi.org/10.1034/j.1398-9995.1999.00063.x

Patella, V., Florio, G., Petraroli, A., & Marone, G. (2000). HIV-1 gp120 Induces IL-4 and IL-13 Release from Human FcεRI+ Cells Through Interaction with the VH3 Region of IgE1. *The Journal of Immunology*, *164*(2), 589–595. https://doi.org/10.4049/jimmunol.164.2.589

Pearce, E. J., Caspar, P., Grzych, J. M., Lewis, F. A., & Sher, A. (1991). Downregulation of Th1 cytokine production accompanies induction of Th2 responses by a parasitic helminth, Schistosoma mansoni. *The Journal of Experimental Medicine*, *173*(1), 159–166. https://doi.org/10.1084/jem.173.1.159

Pearce, E. J., & MacDonald, A. S. (2002). The immunobiology of schistosomiasis. *Nature Reviews. Immunology*, *2*(7), 499–511. https://doi.org/10.1038/nri843

Pennington, L. F., Alouffi, A., Mbanefo, E. C., Ray, D., Heery, D. M., Jardetzky, T. S., Hsieh, M. H., & Falcone, F. H. (2017). H-IPSE Is a Pathogen-Secreted Host Nucleus-Infiltrating Protein (Infiltrin) Expressed Exclusively by the Schistosoma haematobium Egg Stage. *Infection and Immunity*, *85*(12), e00301-17. https://doi.org/10.1128/IAI.00301-17

Peterková, K., Konečný, L., Macháček, T., Jedličková, L., Winkelmann, F., Sombetzki, M., & Dvořák, J. (2024). Winners vs. losers: Schistosoma mansoni intestinal and liver eggs exhibit striking differences in gene expression and immunogenicity. *PLOS Pathogens*, *20*(5), e1012268. https://doi.org/10.1371/journal.ppat.1012268

Pettersen, E. F., Goddard, T. D., Huang, C. C., Meng, E. C., Couch, G. S., Croll, T. I., Morris, J. H., & Ferrin, T. E. (2021). UCSF ChimeraX: Structure visualization for researchers, educators, and developers. *Protein Science: A Publication of the Protein Society*, *30*(1), 70–82. https://doi.org/10.1002/pro.3943

Pezzutto, A., Ulrichs, T., & Burmester, G.-R. (2007). *Taschenatlas der Immunologie: Grundlagen - Labor - Klinik* (2., vollständig überarbeitete und aktualisierte Auflage). Thieme.

Popiel, I., & Basch, P. F. (1984). Reproductive development of female Schistosoma mansoni (Digenea: Schistosomatidae) following bisexual pairing of worms and worm segments. *The Journal of Experimental Zoology*, *232*(1), 141–150. https://doi.org/10.1002/jez.1402320117

Prussin, C., & Metcalfe, D. D. (2006). 5. IgE, mast cells, basophils, and eosinophils. *Journal of Allergy and Clinical Immunology*, *117*(2), S450–S456. https://doi.org/10.1016/j.jaci.2005.11.016

Pumroy, R. A., & Cingolani, G. (2015). Diversification of importin-α isoforms in cellular trafficking and disease states. *The Biochemical Journal*, *466*(1), 13–28. https://doi.org/10.1042/BJ20141186

Richardson, D. R., & Ponka, P. (1997). The molecular mechanisms of the metabolism and transport of iron in normal and neoplastic cells. *Biochimica Et Biophysica Acta*, *1331*(1), 1–40. https://doi.org/10.1016/s0304-4157(96)00014-7

Riedlinger, T., Bartkuhn, M., Zimmermann, T., Hake, S. B., Nist, A., Stiewe, T., Kracht, M., & Schmitz, M. L. (2019). Chemotherapeutic Drugs Inhibiting Topoisomerase 1 Activity Impede Cytokine-Induced and NF-κB p65-Regulated Gene Expression. *Cancers*, *11*(6), Article 6. https://doi.org/10.3390/cancers11060883

Ross, A. G., Vickers, D., Olds, G. R., Shah, S. M., & McManus, D. P. (2007). Katayama syndrome. *The Lancet Infectious Diseases*, *7*(3), 218–224. https://doi.org/10.1016/S1473-3099(07)70053-1

Santos, L. L., Santos, J., Gouveia, M. J., Bernardo, C., Lopes, C., Rinaldi, G., Brindley, P. J., & Costa, J. M. C. da. (2021). Urogenital Schistosomiasis—History, Pathogenesis, and Bladder Cancer. *Journal of Clinical Medicine*, *10*(2), Article 2. https://doi.org/10.3390/jcm10020205

Schade, A. L., & Caroline, L. (1946). An iron-binding component in human blood plasma. *Science (New York, N.Y.)*, *104*(2702), 340.

Schade, A. L., Reinhart, R. W., & Levy, H. (1949). Carbon dioxide and oxygen in complex formation with iron and siderophilin, the iron-binding component of human plasma. *Archives of Biochemistry*, *20*(1), 170–172.

Schasfoort, R. B. M. (2017). *Handbook of Surface Plasmon Resonance: 2nd Edition*. Royal Society of Chemistry.

Schiffer, M., Girling, R. L., Ely, K. R., & Edmundson, A. B. (1973). Structure of a λ-type Bence-Jones protein at 3.5-Å resolution. *Biochemistry*, *12*(23), 4620–4631. https://doi.org/10.1021/bi00747a013

Schramm, G., Falcone, F. H., Gronow, A., Haisch, K., Mamat, U., Doenhoff, M. J., Oliveira, G., Galle, J., Dahinden, C. A., & Haas, H. (2003). Molecular

characterization of an interleukin-4-inducing factor from Schistosoma mansoni eggs. *The Journal of Biological Chemistry*, *278*(20), 18384–18392. https://doi.org/10.1074/jbc.M300497200

Schramm, G., Gronow, A., Knobloch, J., Wippersteg, V., Grevelding, C. G., Galle, J., Fuller, H., Stanley, R. G., Chiodini, P. L., Haas, H., & Doenhoff, M. J. (2006). IPSE/alpha-1: A major immunogenic component secreted from Schistosoma mansoni eggs. *Molecular and Biochemical Parasitology*, *147*(1), 9–19. https://doi.org/10.1016/j.molbiopara.2006.01.003

Schramm, G., & Haas, H. (2010). Th2 immune response against Schistosoma mansoni infection. *Microbes and Infection*, *12*(12–13), 881–888. https://doi.org/10.1016/j.micinf.2010.06.001

Schramm, G., Hamilton, J. V., Balog, C. I. A., Wuhrer, M., Gronow, A., Beckmann, S., Wippersteg, V., Grevelding, C. G., Goldmann, T., Weber, E., Brattig, N. W., Deelder, A. M., Dunne, D. W., Hokke, C. H., Haas, H., & Doenhoff, M. J. (2009). Molecular characterisation of kappa-5, a major antigenic glycoprotein from *Schistosoma mansoni* eggs. *Molecular and Biochemical Parasitology*, *166*(1), 4–14. https://doi.org/10.1016/j.molbiopara.2009.02.003

Schramm, G., Mohrs, K., Wodrich, M., Doenhoff, M. J., Pearce, E. J., Haas, H., & Mohrs, M. (2007). Cutting Edge: IPSE/alpha-1, a Glycoprotein from Schistosoma mansoni Eggs, Induces IgE-Dependent, Antigen-Independent IL-4 Production by Murine Basophils In Vivo1. *The Journal of Immunology*, *178*(10), 6023–6027. https://doi.org/10.4049/jimmunol.178.10.6023

Schwartz, C., & Fallon, P. G. (2018). Schistosoma “Eggs-Iting” the Host: Granuloma Formation and Egg Excretion. *Frontiers in Immunology*, *9*, 2492. https://doi.org/10.3389/fimmu.2018.02492

Schwartz, C., Oeser, K., Prazeres da Costa, C., Layland, L. E., & Voehringer, D. (2014). T cell-derived IL-4/IL-13 protects mice against fatal Schistosoma mansoni infection independently of basophils. *Journal of Immunology*

(Baltimore, Md.: 1950), *193*(7), 3590–3599. https://doi.org/10.4049/jimmunol.1401155

Schwartz, C., Turqueti-Neves, A., Hartmann, S., Yu, P., Nimmerjahn, F., & Voehringer, D. (2014). Basophil-mediated protection against gastrointestinal helminths requires IgE-induced cytokine secretion. *Proceedings of the National Academy of Sciences of the United States of America*, *111*(48), E5169–E5177. https://doi.org/10.1073/pnas.1412663111

Seder, R. A., Paul, W. E., Davis, M. M., & Fazekas de St Groth, B. (1992). The presence of interleukin 4 during in vitro priming determines the lymphokine-producing potential of CD4+ T cells from T cell receptor transgenic mice. *The Journal of Experimental Medicine*, *176*(4), 1091–1098. https://doi.org/10.1084/jem.176.4.1091

Serebryany, E., & King, J. A. (2014). The βγ-crystallins: Native state stability and pathways to aggregation. *Progress in biophysics and molecular biology*, *115*(1), 32–41. https://doi.org/10.1016/j.pbiomolbio.2014.05.002

Shamji, M. H., Valenta, R., Jardetzky, T., Verhasselt, V., Durham, S. R., Würtzen, P. A., & van Neerven, R. J. J. (2021). The role of allergen-specific IgE, IgG and IgA in allergic disease. *Allergy*, *76*(12), 3627–3641. https://doi.org/10.1111/all.14908

Shen, J., Cao, B., Wang, Y., Ma, C., Zeng, Z., Liu, L., Li, X., Tao, D., Gong, J., & Xie, D. (2018). Hippo component YAP promotes focal adhesion and tumour aggressiveness via transcriptionally activating THBS1/FAK signalling in breast cancer. *Journal of Experimental & Clinical Cancer Research: CR*, *37*(1), 175. https://doi.org/10.1186/s13046-018-0850-z

Smith, P., Fallon, R. E., Mangan, N. E., Walsh, C. M., Saraiva, M., Sayers, J. R., McKenzie, A. N. J., Alcami, A., & Fallon, P. G. (2005). Schistosoma mansoni secretes a chemokine binding protein with antiinflammatory activity. *Journal*

of Experimental Medicine, *202*(10), 1319–1325. https://doi.org/10.1084/jem.20050955

Snow, D. M., & Hart, G. W. (1998). Nuclear and Cytoplasmic Glycosylation. In K. W. Jeon (Hrsg.), *International Review of Cytology* (Bd. 181, S. 43–74). Academic Press. https://doi.org/10.1016/S0074-7696(08)60416-7

Sporn, M. B., Roberts, A. B., Wakefield, L. M., & Assoian, R. K. (1986). Transforming growth factor-beta: Biological function and chemical structure. *Science (New York, N.Y.)*, *233*(4763), 532–534. https://doi.org/10.1126/science.3487831

Stanfield, R. L., Zemla, A., Wilson, I. A., & Rupp, B. (2006). Antibody elbow angles are influenced by their light chain class. *Journal of Molecular Biology*, *357*(5), 1566–1574. https://doi.org/10.1016/j.jmb.2006.01.023

Stewart, M. (2007). Molecular mechanism of the nuclear protein import cycle. *Nature Reviews Molecular Cell Biology*, *8*(3), 195–208. https://doi.org/10.1038/nrm2114

Sugimoto, K., Urano, T., Zushi, H., Inoue, K., Tasaka, H., Tachibana, M., & Dotsu, M. (2002). Molecular dynamics of Aurora-A kinase in living mitotic cells simultaneously visualized with histone H3 and nuclear membrane protein importinalpha. *Cell Structure and Function*, *27*(6), 457–467. https://doi.org/10.1247/csf.27.457

Sullivan, B. M., Liang, H.-E., Bando, J. K., Wu, D., Cheng, L. E., McKerrow, J. K., Allen, C. D. C., & Locksley, R. M. (2011). Genetic analysis of basophil function in vivo. *Nature Immunology*, *12*(6), 527–535. https://doi.org/10.1038/ni.2036

Sutherland, D. E. K., Willans, M. J., & Stillman, M. J. (2010). Supermetalation of the beta domain of human metallothionein 1a. *Biochemistry*, *49*(17), 3593–3601. https://doi.org/10.1021/bi1003537

Sutton, B. J., & Gould, H. J. (1993). The human IgE network. *Nature*, *366*(6454), 421–428. https://doi.org/10.1038/366421a0

Taudou, G., Varin-Blank, N., Jouin, H., Marchand, F., Weyer, A., & Blank, U. (2009). Expression of the Alpha Chain of Human FcεRI in Transfected Rat Basophilic Leukemia Cells: Functional Activation after Sensitization with Human Mite-Specific IgE. *International Archives of Allergy and Immunology*, *100*(4), 344–350. https://doi.org/10.1159/000236436

Townsend, C. L., Laffy, J. M. J., Wu, Y.-C. B., Silva O'Hare, J., Martin, V., Kipling, D., Fraternali, F., & Dunn-Walters, D. K. (2016). Significant Differences in Physicochemical Properties of Human Immunoglobulin Kappa and Lambda CDR3 Regions. *Frontiers in Immunology*, *7*, 388. https://doi.org/10.3389/fimmu.2016.00388

Tsuchiya, Y., & Mizuguchi, K. (2016). The diversity of H3 loops determines the antigen-binding tendencies of antibody CDR loops. *Protein Science*, *25*(4), 815–825. https://doi.org/10.1002/pro.2874

van Panhuys, N., Prout, M., Forbes, E., Min, B., Paul, W. E., & Le Gros, G. (2011). Basophils are the major producers of IL-4 during primary helminth infection. *Journal of Immunology (Baltimore, Md.: 1950)*, *186*(5), 2719–2728. https://doi.org/10.4049/jimmunol.1000940

Vella, A. T., & Pearce, E. J. (1992). CD4+ Th2 response induced by Schistosoma mansoni eggs develops rapidly, through an early, transient, Th0-like stage. *Journal of Immunology (Baltimore, Md.: 1950)*, *148*(7), 2283–2290.

Vizcaíno, C., Mansilla, S., & Portugal, J. (2015). Sp1 transcription factor: A long-standing target in cancer chemotherapy. *Pharmacology & Therapeutics*, *152*, 111–124. https://doi.org/10.1016/j.pharmthera.2015.05.008

Voehringer, D. (2017). Recent advances in understanding basophil functions in vivo. *F1000Research*, *6*, 1464. https://doi.org/10.12688/f1000research.11697.1

von Bülow, V., Lichtenberger, J., Grevelding, C. G., Falcone, F. H., Roeb, E., & Roderfeld, M. (2021). Does Schistosoma Mansoni Facilitate Carcinogenesis? *Cells*, *10*(8), Article 8. https://doi.org/10.3390/cells10081982

Wahl, S. M., Hunt, D. A., Wakefield, L. M., McCartney-Francis, N., Wahl, L. M., Roberts, A. B., & Sporn, M. B. (1987). Transforming growth factor type beta induces monocyte chemotaxis and growth factor production. *Proceedings of the National Academy of Sciences of the United States of America*, *84*(16), 5788–5792. https://doi.org/10.1073/pnas.84.16.5788

Wan, D., Wang, X., Nakamura, R., Alcocer, M. J. C., & Falcone, F. H. (2014). Use of Humanized Rat Basophil Leukemia (RBL) Reporter Systems for Detection of Allergen-Specific IgE Sensitization in Human Serum. In B. F. Gibbs & F. H. Falcone (Hrsg.), *Basophils and Mast Cells: Methods and Protocols* (S. 177–184). Springer. https://doi.org/10.1007/978-1-4939-1173-8_13

Wan, D., Wang, X., Nakamura, R., Alcocer, M. J. C., & Falcone, F. H. (2020). Use of Humanized RBL Reporter Systems for the Detection of Allergen-Specific IgE Sensitization in Human Serum. *Methods in Molecular Biology (Clifton, N.J.)*, *2163*, 145–153. https://doi.org/10.1007/978-1-0716-0696-4_11

Weinstock, J. V., & Boros, D. L. (1983). Organ-dependent differences in composition and function observed in hepatic and intestinal granulomas isolated from mice with Schistosomiasis mansoni. *Journal of Immunology (Baltimore, Md.: 1950)*, *130*(1), 418–422.

Wendt, G., Zhao, L., Chen, R., Liu, C., O'Donoghue, A. J., Caffrey, C. R., Reese, M. L., & Collins, J. J. (2020). A single-cell RNA-seq atlas of Schistosoma mansoni identifies a key regulator of blood feeding. *Science (New York, N.Y.)*, *369*(6511), 1644–1649. https://doi.org/10.1126/science.abb7709

Wickham, H. (2016). *ggplot2: Elegant Graphics for Data Analysis* (2nd ed. 2016). Springer International Publishing : Imprint: Springer. https://doi.org/10.1007/978-3-319-24277-4

Wiedemann, M., & Voehringer, D. (2020). Immunomodulation and Immune Escape Strategies of Gastrointestinal Helminths and Schistosomes. *Frontiers in Immunology*, *11*. https://doi.org/10.3389/fimmu.2020.572865

Wong, W. K., Leem, J., & Deane, C. M. (2019). Comparative Analysis of the CDR Loops of Antigen Receptors. *Frontiers in Immunology*, *10*. https://doi.org/10.3389/fimmu.2019.02454

Wuhrer, M., Balog, C. I. A., Catalina, M. I., Jones, F. M., Schramm, G., Haas, H., Doenhoff, M. J., Dunne, D. W., Deelder, A. M., & Hokke, C. H. (2006). IPSE/alpha-1, a major secretory glycoprotein antigen from schistosome eggs, expresses the Lewis X motif on core-difucosylated N-glycans. *The FEBS Journal*, *273*(10), 2276–2292. https://doi.org/10.1111/j.1742-4658.2006.05242.x

Xu, Y.-Z., & Dresden, M. H. (1990). The hatching of schistosome eggs. *Experimental Parasitology*, *70*(2), 236–240. https://doi.org/10.1016/0014-4894(90)90104-K

Yang, J., Okabe, H., & Monga, S. P. (2014). Liver Development, Regeneration, and Stem Cells. In L. M. McManus & R. N. Mitchell (Hrsg.), *Pathobiology of Human Disease* (S. 1783–1799). Academic Press. https://doi.org/10.1016/B978-0-12-386456-7.04203-9

Yoneda, Y. (2000). Nucleocytoplasmic protein traffic and its significance to cell function. *Genes to Cells*, *5*(10), 777–787. https://doi.org/10.1046/j.1365-2443.2000.00366.x

Yu, G., Wang, L.-G., Han, Y., & He, Q.-Y. (2012). clusterProfiler: An R Package for Comparing Biological Themes Among Gene Clusters. *OMICS: A Journal of Integrative Biology*, *16*(5), 284–287. https://doi.org/10.1089/omi.2011.0118

6. APPENDIX

Plasmid Maps

pTT5 vectors are mammalian expression vectors that confer ampicillin for bacterial selection. These expression vectors in general contain a hVGEF Signal Peptide, an N-terminal 8x His-tag, TEV-cleavage site, β- globin polyadenylation site and Ori. The pTT expression systems are licensed by the Canadian National Research Council, Cananda.

Sm IPSE pTT5

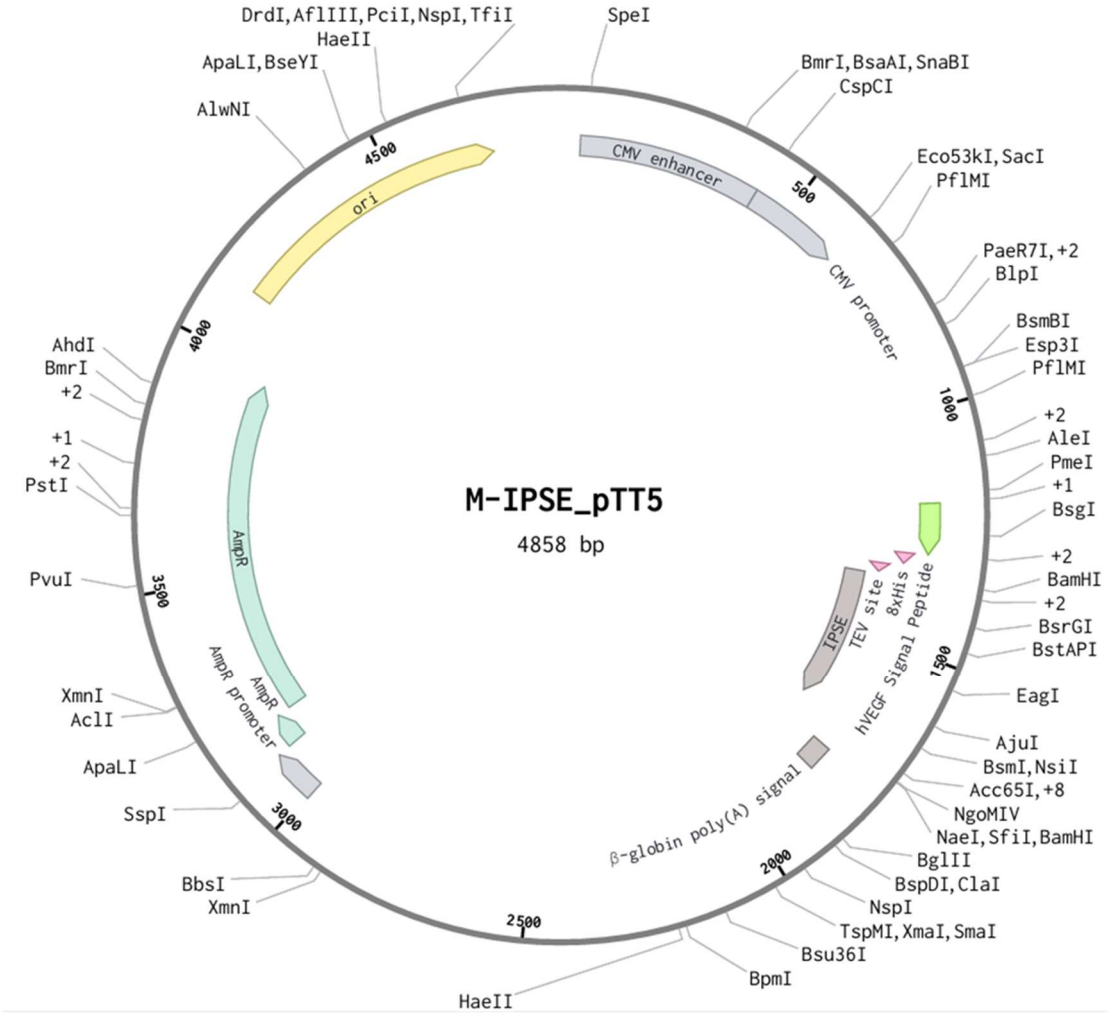

N TC-Sm IPSE pTT5 (pTT5-SmTC-A1N)

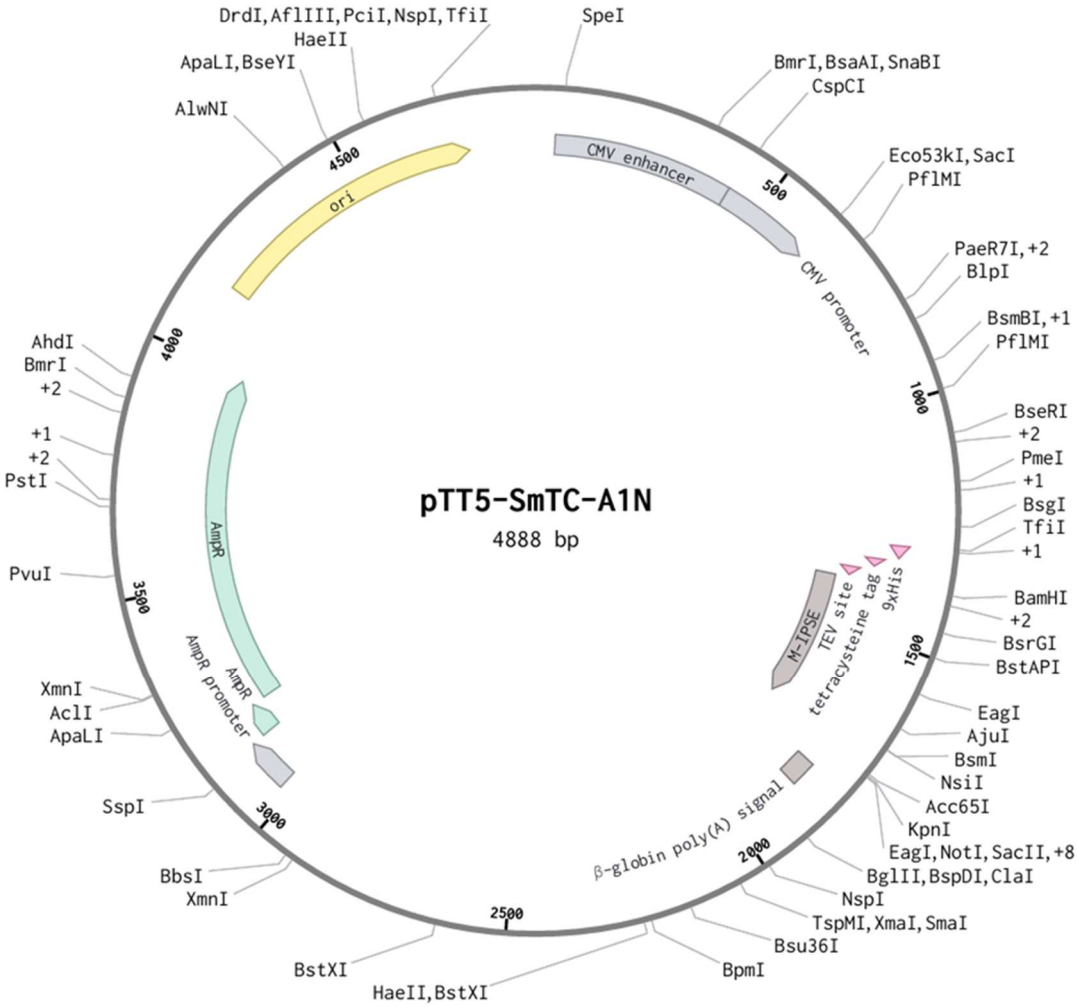

C TC-Sm IPSE pTT5 (pTT5-SmTC-A1C)

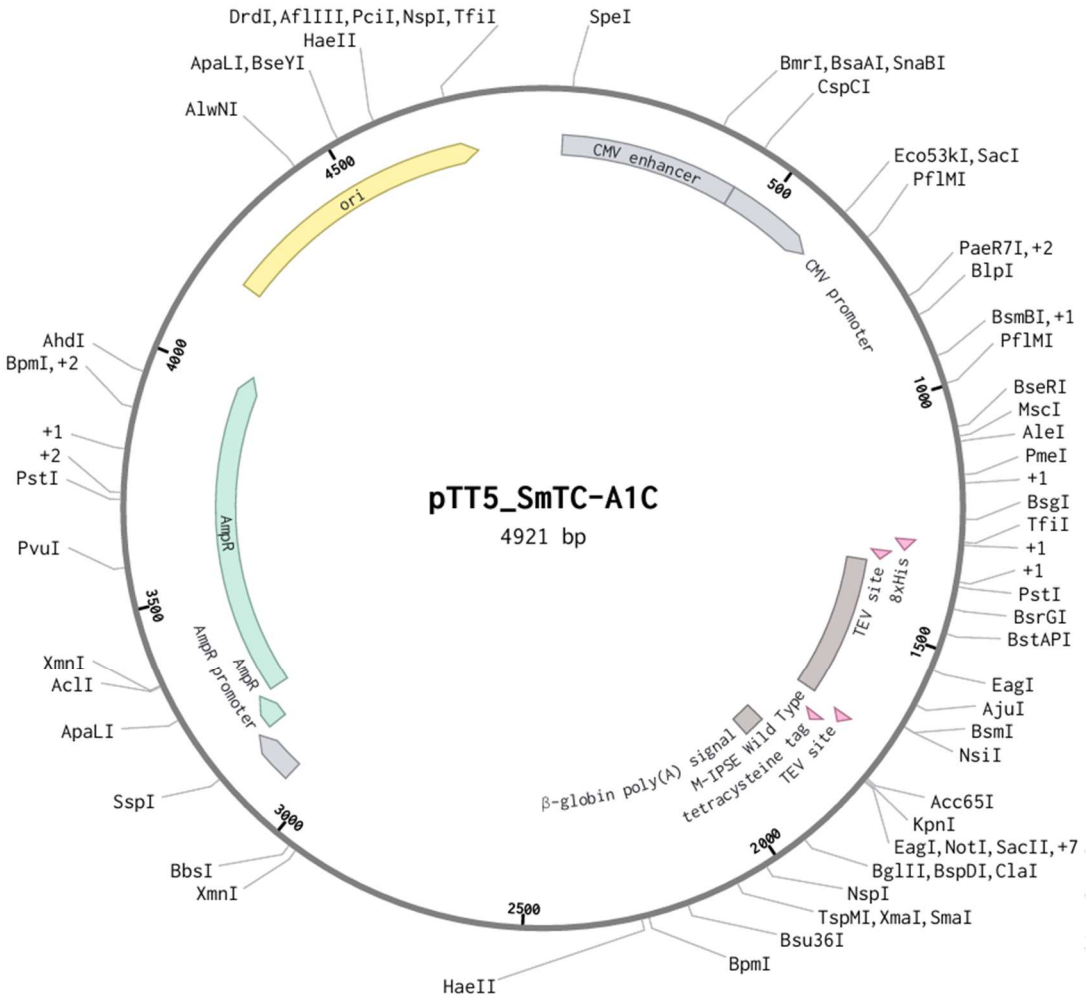

Sh03 IPSE pTT5

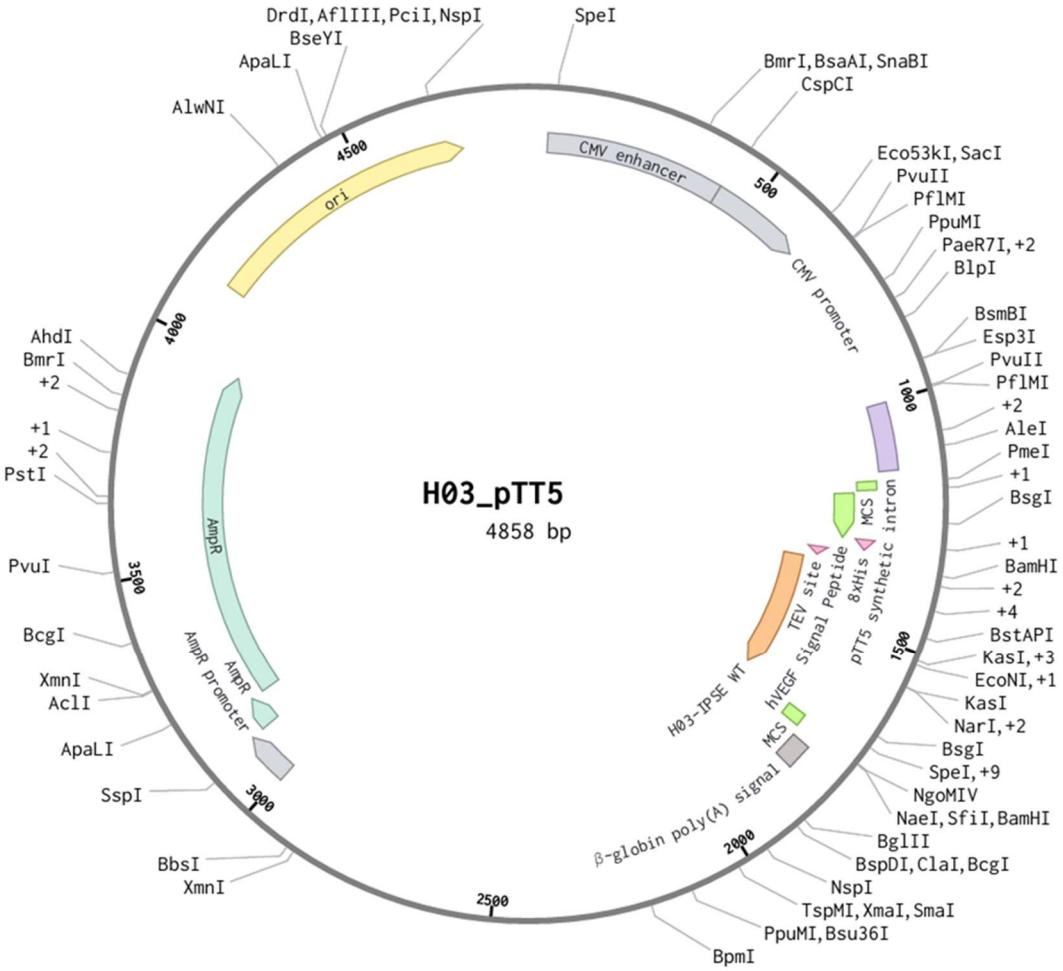

Sh06 IPSE pTT5

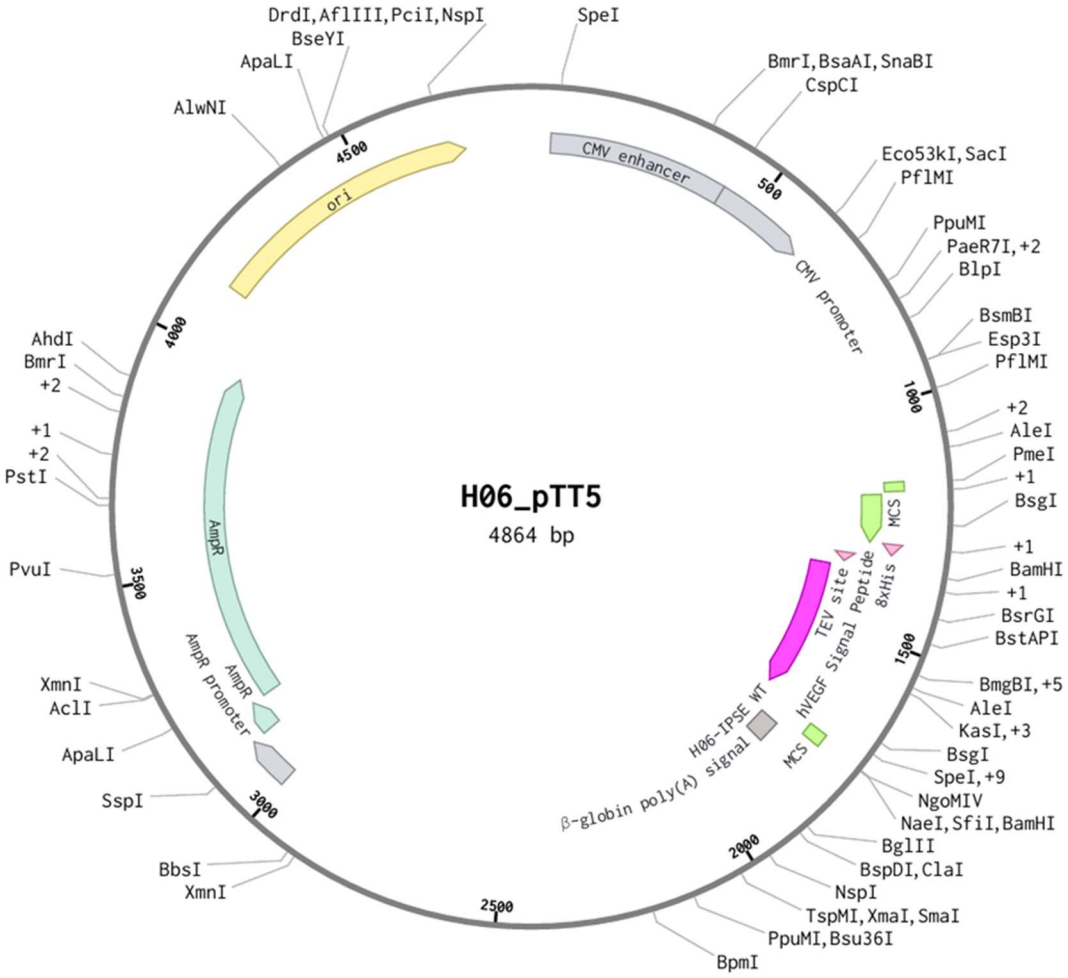

pVITRO-102.1F10-IgEλ

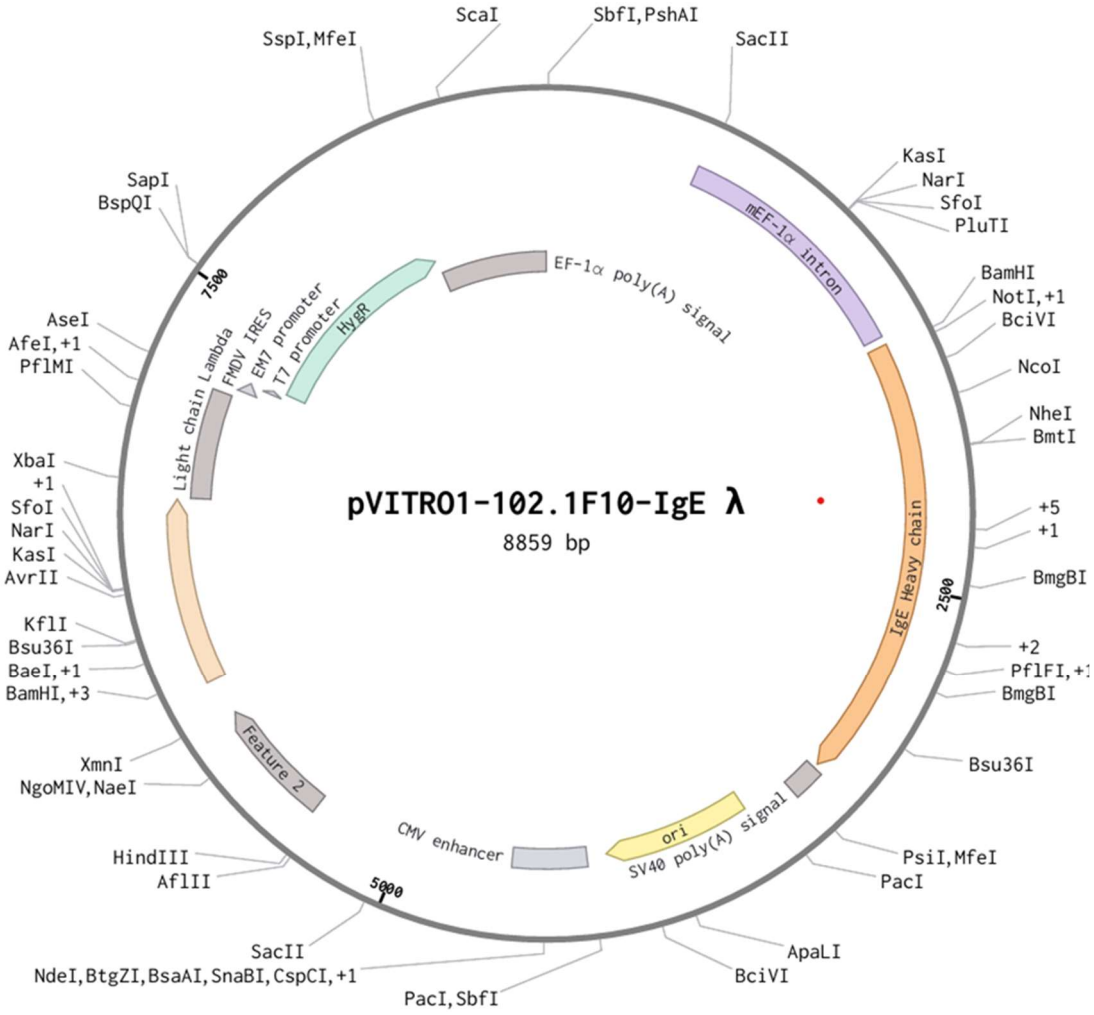

huFcεRIα$_{Val26-Gln295}$ pTT28

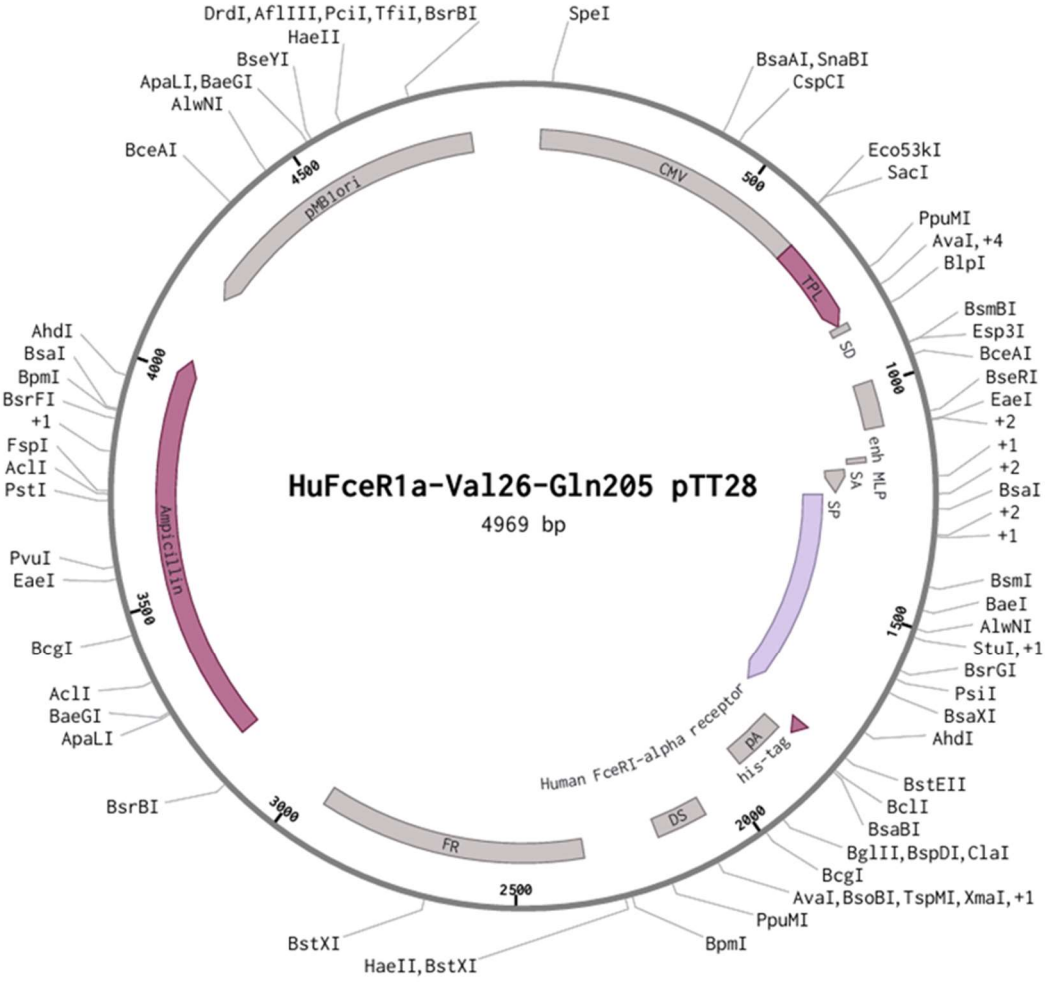

IgE Motavizumab pTT5

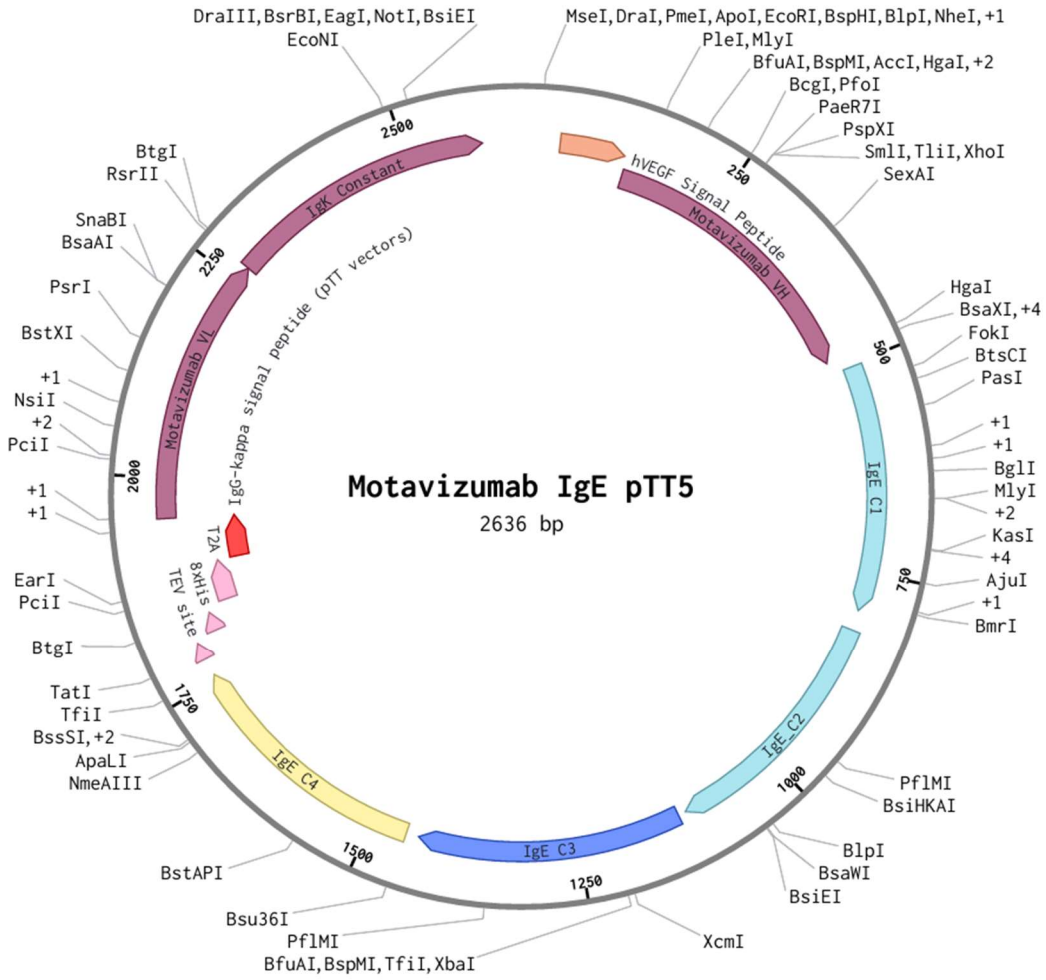

IgE Cε2-4 pTT5

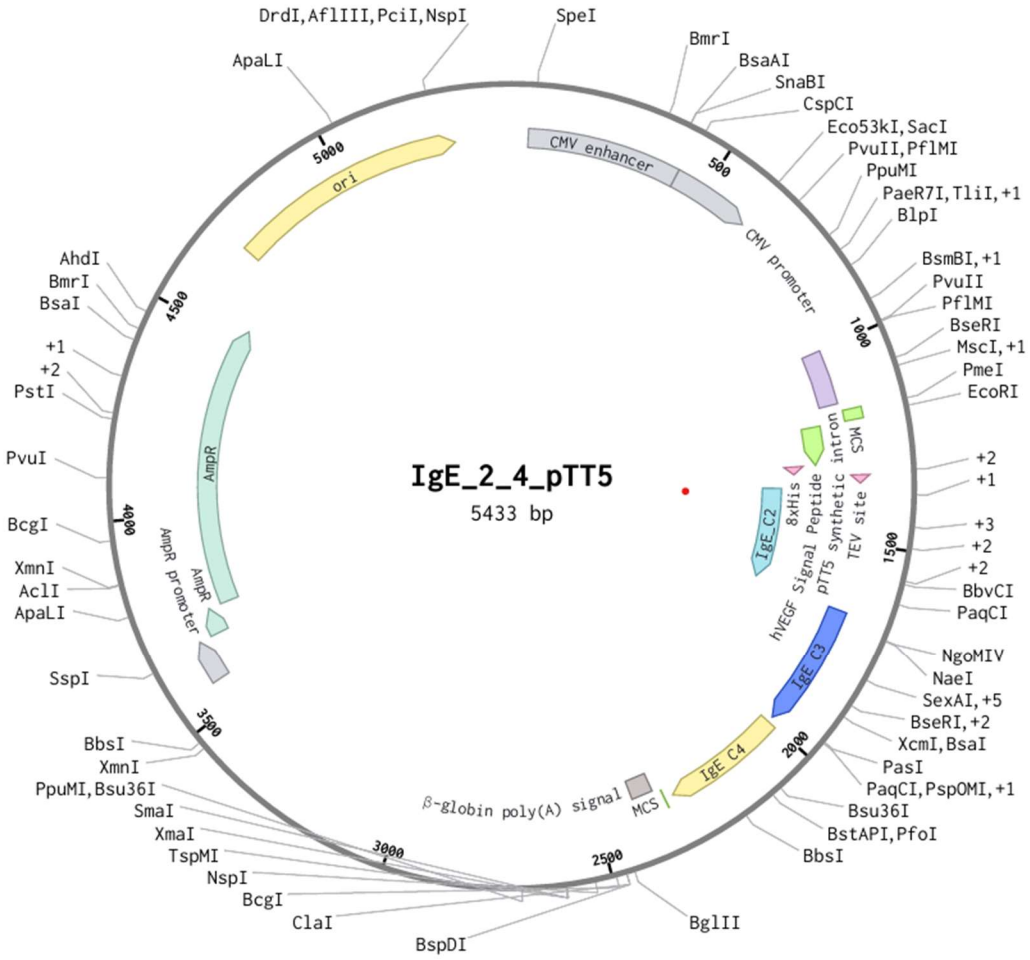

IgE Cε3-4 pTT5

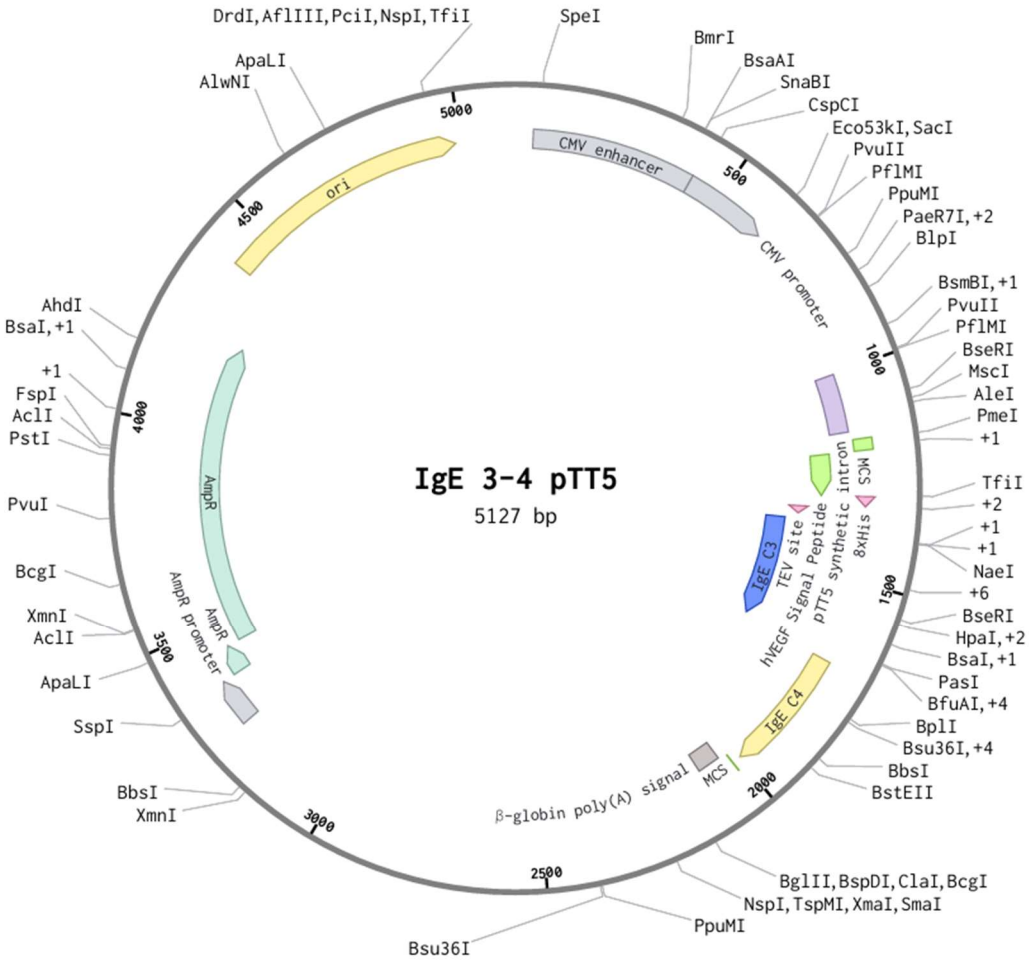

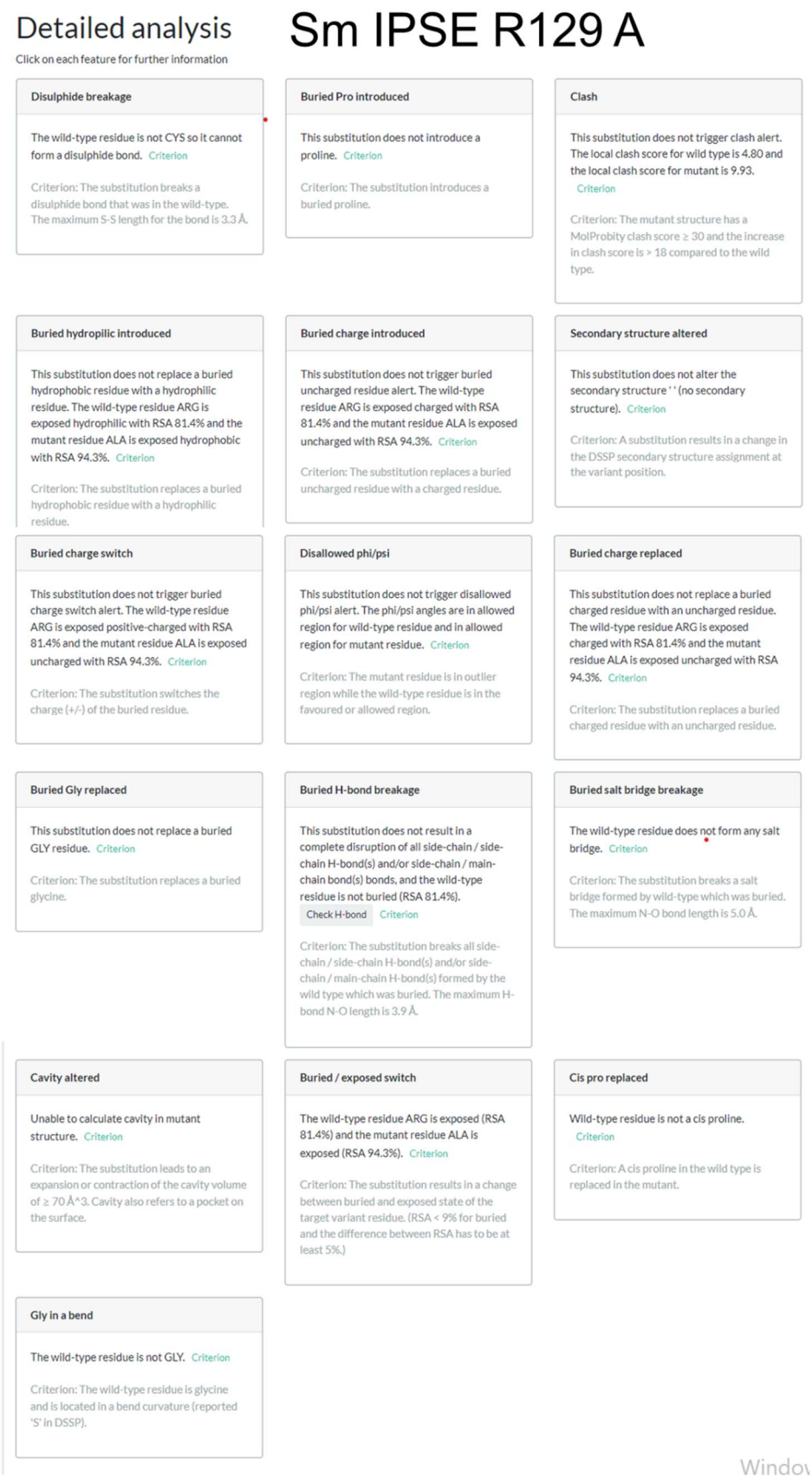

Missense3D analysis of Sm IPSE R127A

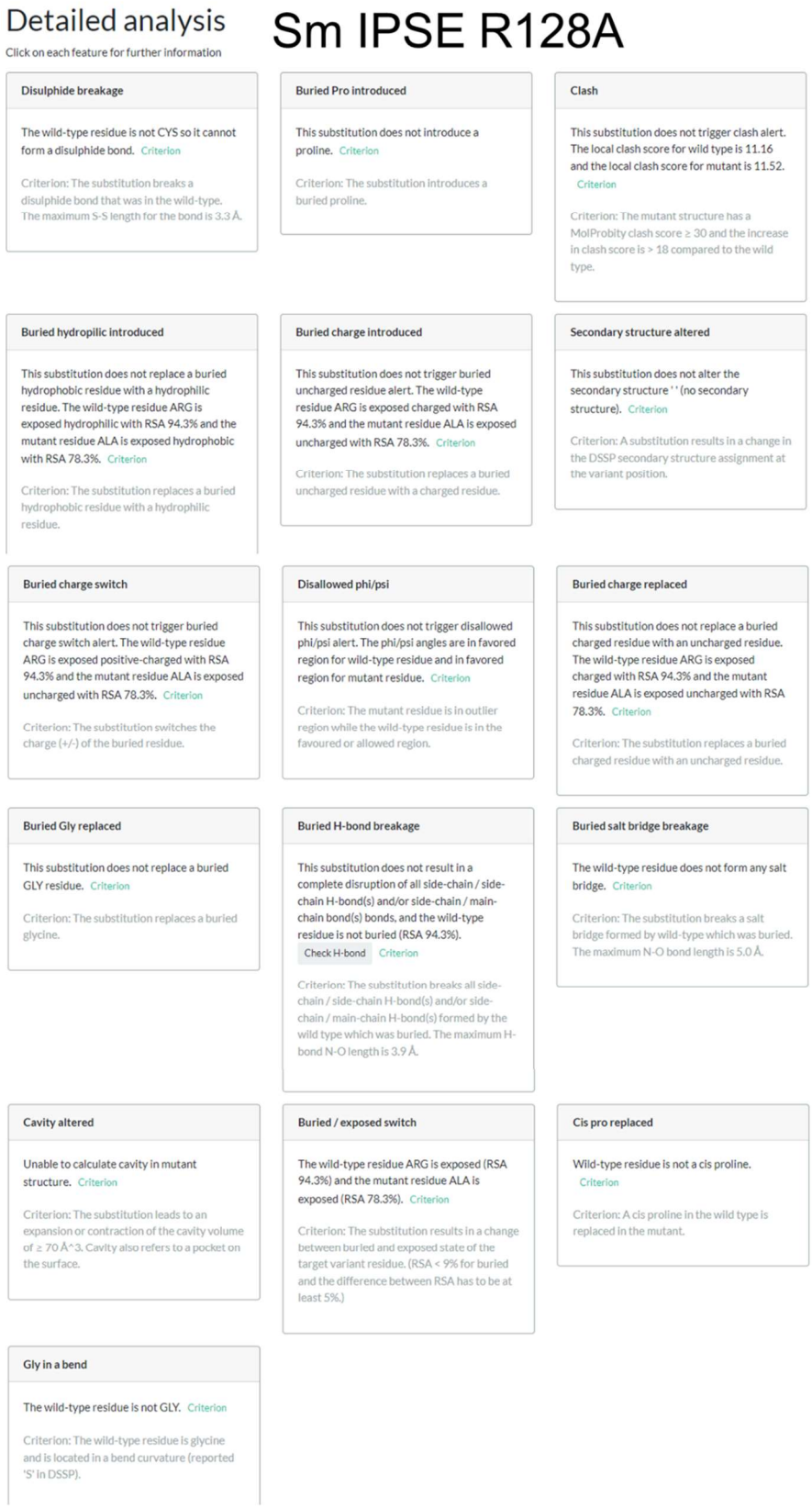

Missense3D analysis of Sm IPSE R128A

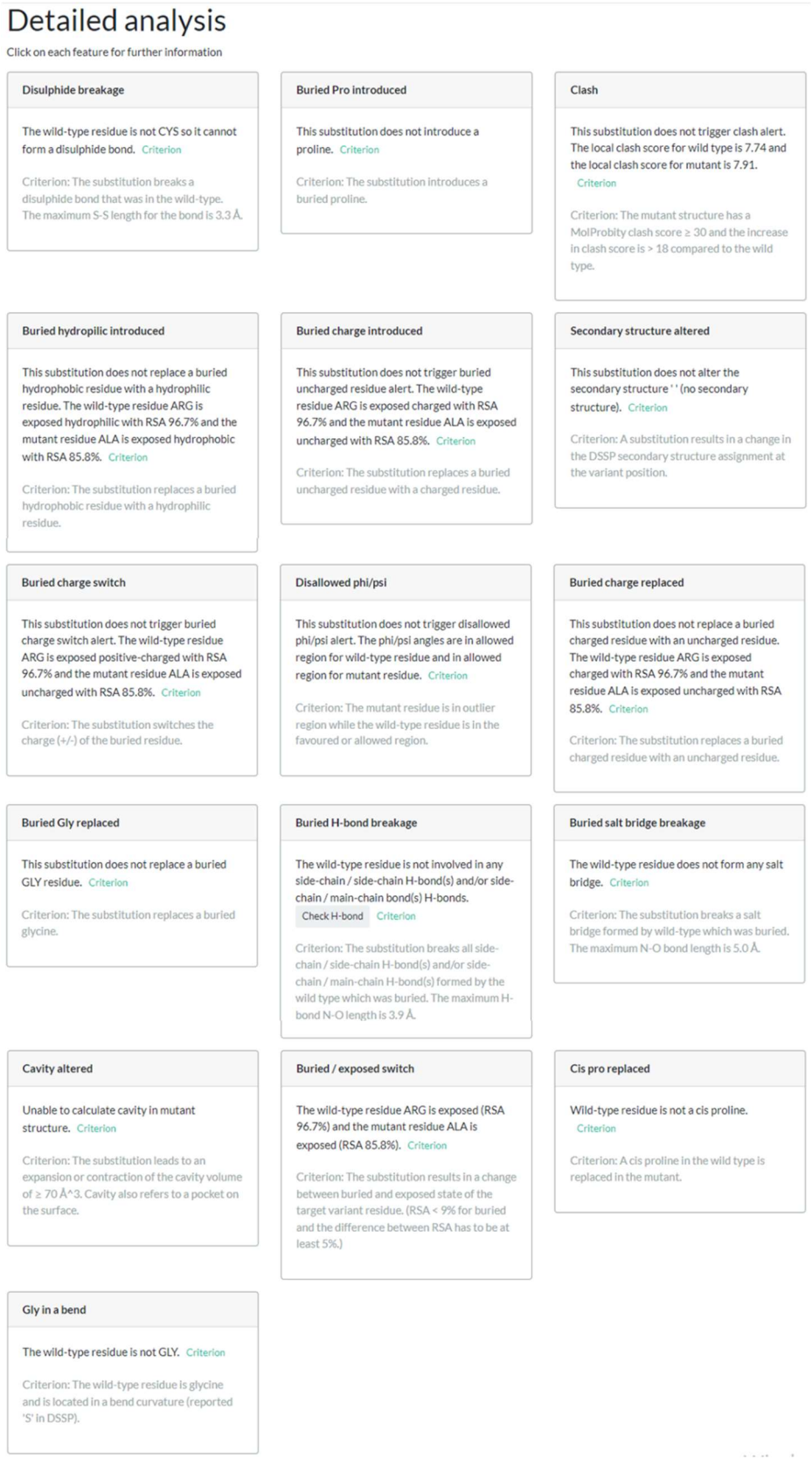

Missense3D analysis of Sm IPSE R127A

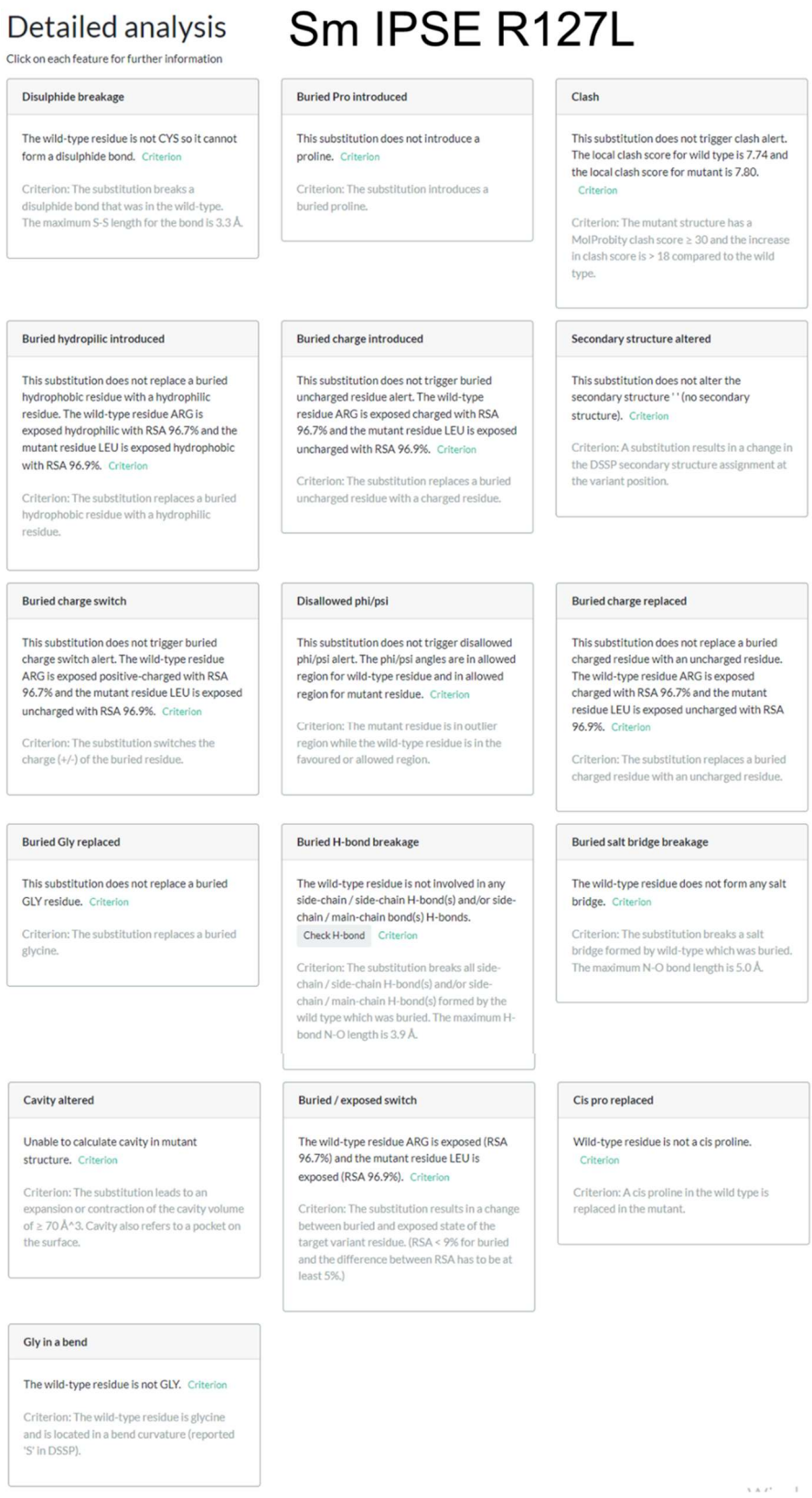

Missense3D analysis of Sm IPSE R127L

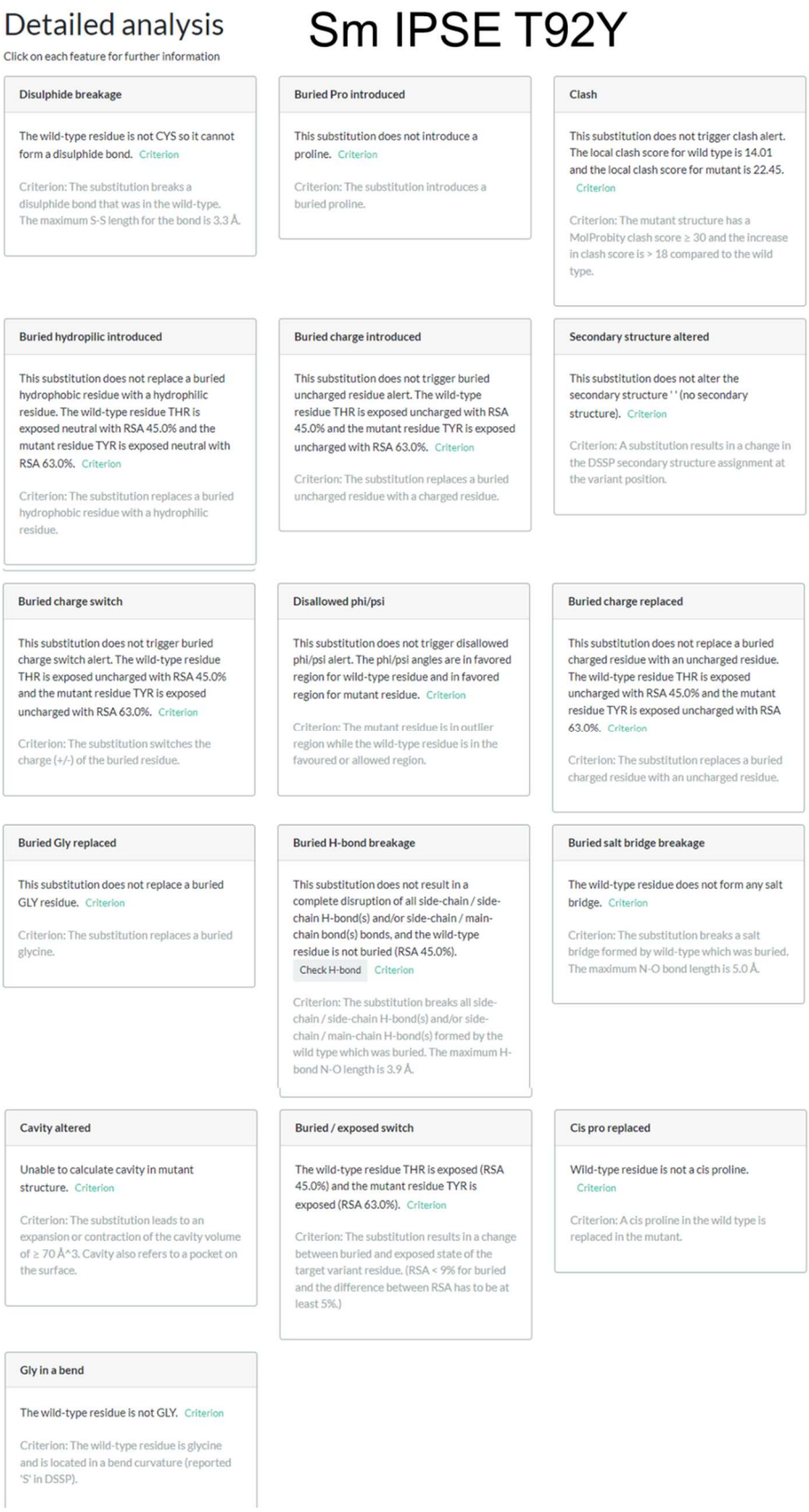

Missense3D analysis of Sm IPSE T92Y

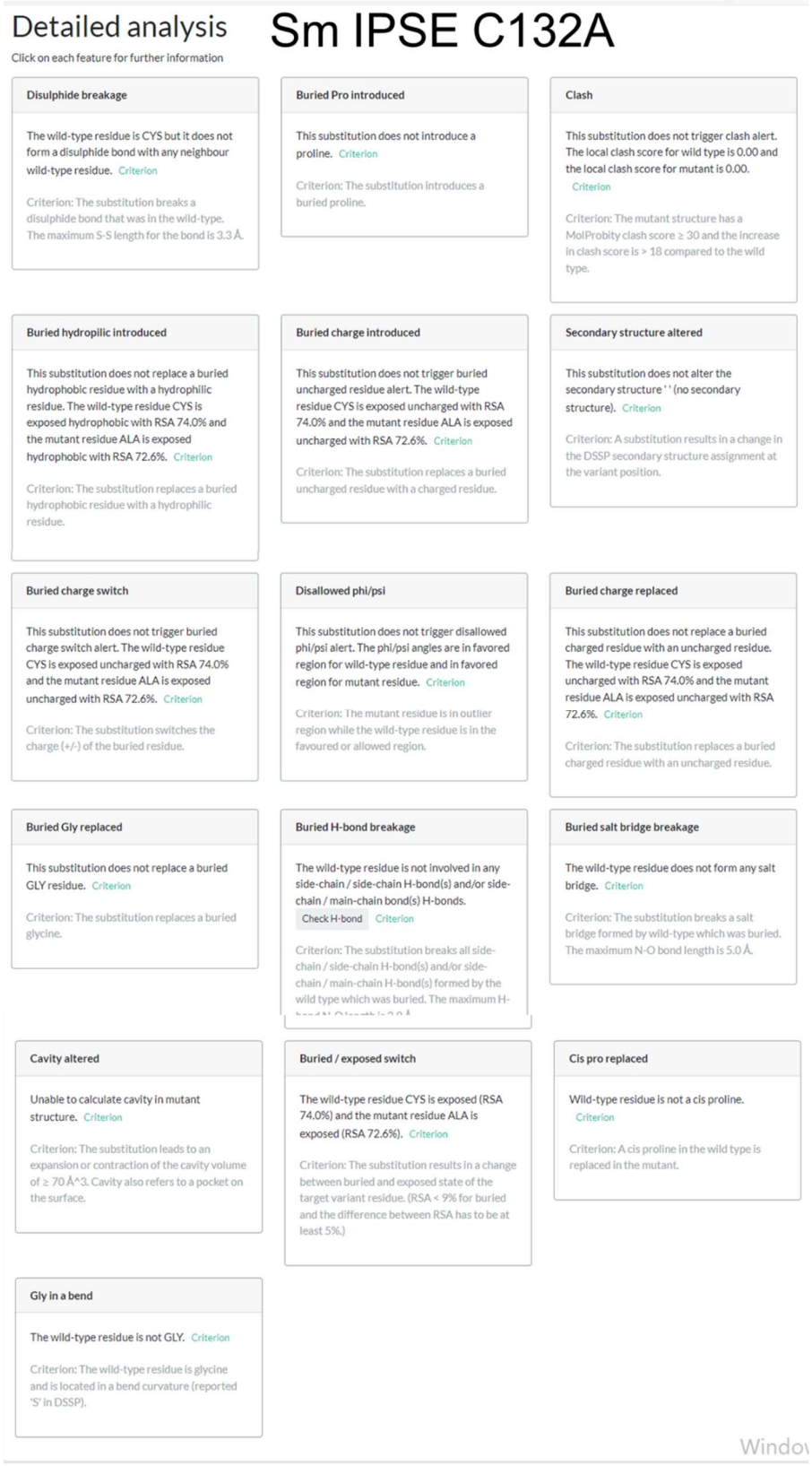

Missense3D analysis of Sm IPSE C132A

IgE motavizumab (2) Reporter Assay evaluation after IPSE-stimulation of IgE-mota -sensitized RS-ATL8 cells. Statistics data analyses was performed using Ordinary one-way ANOVA (Dunnett's multiple comparisons test); significance was tested against negative control (non-stimulated cells).

Dunnett's multiple comparisons test	95,00% CI of diff.	Significance	Adjusted P Value
Neg.(only sens.) vs. ConA I 10 µg/mL	-6787 to -5709	Yes	<0,0001
Neg.(only sens.) vs. a-IgE 0.01 µg/mL	-580,1 to 497,1	No	0,9997
Neg.(only sens.) vs. a-IgE 0.1 µg/mL	-1101 to -23,87	Yes	0,0374
Neg.(only sens.) vs. a-IgE 1 µg/mL	-4741 to -3663	Yes	<0,0001
Neg.(only sens.) vs. a-IgE 10 µg/mL	-1681 to -603,9	Yes	<0,0001
Neg.(only sens.) vs. Sm IPSE 0.01 µg/mL	-392,6 to 684,6	No	0,9748
Neg.(only sens.) vs. Sm IPSE 0.1 µg/mL	-437,6 to 639,6	No	0,9968
Neg.(only sens.) vs. Sm IPSE 1 µg/mL	-422,4 to 654,9	No	0,9930
Neg.(only sens.) vs. Sm IPSE 10 µg/mL	-455,6 to 621,6	No	0,9993

IgEλ (2) Reporter Assay evaluation after IPSE-stimulation of IgEλ (Bio-Rad)-sensitized RS-ATL8 cells. Statistics data analyses was performed using Ordinary one-way ANOVA (Dunnett's multiple comparisons test); significance was tested against negative control (non-stimulated cells).

Dunnett's multiple comparisons test	95,00% CI of diff.	Significance	Adjusted P Value
Neg.(only sens.) vs. ConA I 10 µg/mL	-5817 to -4174	Yes	<0,0001
Neg.(only sens.) vs. a-IgE 0.01 µg/mL	-841,1 to 801,6	No	>0,9999
Neg.(only sens.) vs. a-IgE 0.1 µg/mL	-1401 to 241,8	No	0,2710
Neg.(only sens.) vs. a-IgE 1 µg/mL	-5821 to -4178	Yes	<0,0001
Neg.(only sens.) vs. a-IgE 10 µg/mL	-2081 to -438,4	Yes	0,0010
Neg.(only sens.) vs. Sm IPSE 0.01 µg/mL	-2955 to -1312	Yes	<0,0001
Neg.(only sens.) vs. Sm IPSE 0.1 µg/mL	-5952 to -4309	Yes	<0,0001
Neg.(only sens.) vs. Sm IPSE 1 µg/mL	-2131 to -487,9	Yes	0,0007
Neg.(only sens.) vs. Sm IPSE 10 µg/mL	-2735 to -1092	Yes	<0,0001

IgE Cε2-4 (2) Reporter Assay evaluation after IPSE-stimulation of IgE Cε2-4-sensitized RS-ATL8 cells. Statistics data analyses was performed using Ordinary one-way ANOVA (Dunnett's multiple comparisons test); significance was tested against negative control (non-stimulated cells).

Dunnett's multiple comparisons test	95,00% CI of diff.	Significance	Adjusted P Value
Neg.(only sens.) vs. ConA I 10 µg/mL	-7846 to -6380	Yes	<0,0001
Neg.(only sens.) vs. a-IgE 0.01 µg/mL	-832,0 to 634,0	No	0,9994
Neg.(only sens.) vs. a-IgE 0.1 µg/mL	-2879 to -1413	Yes	<0,0001
Neg.(only sens.) vs. a-IgE 1 µg/mL	-7952 to -6486	Yes	<0,0001
Neg.(only sens.) vs. a-IgE 10 µg/mL	-2231 to -765,2	Yes	<0,0001
Neg.(only sens.) vs. Sm IPSE 0.01 µg/mL	-768,5 to 697,5	No	0,9998
Neg.(only sens.) vs. Sm IPSE 0.1 µg/mL	-720,5 to 745,5	No	>0,9999
Neg.(only sens.) vs. Sm IPSE 1 µg/mL	-772,5 to 693,5	No	0,9998
Neg.(only sens.) vs. Sm IPSE 10 µg/mL	-823,5 to 642,5	No	0,9995

IgE Cε3-4 (2) Reporter Assay evaluation after IPSE-stimulation of IgE Cε3-4-sensitized RS-ATL8 cells. Statistics data analyses was performed using Ordinary one-way ANOVA (Dunnett's multiple comparisons test); significance was tested against negative control (non-stimulated cells).

Dunnett's multiple comparisons test	95,00% CI of diff.	Significance	Adjusted P Value
Neg.(only sens.) vs. ConA I 10 µg/mL	-5647 to -4076	Yes	<0,0001
Neg.(only sens.) vs. a-IgE 0.01 µg/mL	-846,7 to 724,2	No	0,9997
Neg.(only sens.) vs. a-IgE 0.1 µg/mL	-1698 to -126,8	Yes	0,0168
Neg.(only sens.) vs. a-IgE 1 µg/mL	-5211 to -3640	Yes	<0,0001
Neg.(only sens.) vs. a-IgE 10 µg/mL	-2119 to -548,5	Yes	0,0003
Neg.(only sens.) vs. Sm IPSE 0.01 µg/mL	-781,0 to 790,0	No	>0,9999
Neg.(only sens.) vs. Sm IPSE 0.1 µg/mL	-794,2 to 776,7	No	>0,9999
Neg.(only sens.) vs. Sm IPSE 1 µg/mL	-773,2 to 797,7	No	>0,9999
Neg.(only sens.) vs. Sm IPSE 10 µg/mL	-797,0 to 774,0	No	>0,9999

IgE motavizumab (3) Reporter Assay evaluation after IPSE-stimulation of IgE motavizumab-sensitized RS-ATL8 cells. Statistics data analyses was performed using Ordinary one-way ANOVA (Dunnett's multiple comparisons test); significance was tested against negative control (non-stimulated cells).

Dunnett's multiple comparisons test	95,00% CI of diff.	Significance	Adjusted P Value
Neg.(only sens.) vs. ConA I 10 µg/mL	-1595 to -1272	Yes	<0,0001
Neg.(only sens.) vs. a-IgE 0.01 µg/mL	-154,1 to 168,6	No	0,9998
Neg.(only sens.) vs. a-IgE 0.1 µg/mL	-476,6 to -153,9	Yes	<0,0001
Neg.(only sens.) vs. a-IgE 1 µg/mL	-1322 to -999,4	Yes	<0,0001
Neg.(only sens.) vs. a-IgE 10 µg/mL	-737,3 to -414,7	Yes	<0,0001
Neg.(only sens.) vs. Sm IPSE 0.01 µg/mL	-137,6 to 185,1	No	0,9994
Neg.(only sens.) vs. Sm IPSE 0.1 µg/mL	-136,1 to 186,6	No	0,9993
Neg.(only sens.) vs. Sm IPSE 1 µg/mL	-86,56 to 236,1	No	0,7076
Neg.(only sens.) vs. Sm IPSE 10 µg/mL	-166,3 to 156,3	No	0,9999

IgEλ (3) Reporter Assay evaluation after IPSE-stimulation of IgEλ-sensitized RS-ATL8 cells. Statistics data analyses was performed using Ordinary one-way ANOVA (Dunnett's multiple comparisons test); significance was tested against negative control (non-stimulated cells).

Dunnett's multiple comparisons test	95,00% CI of diff.	Significance	Adjusted P Value
Neg.(only sens.) vs. ConA I 10 µg/mL	-1736 to -911,3	Yes	<0,0001
Neg.(only sens.) vs. a-IgE 0.01 µg/mL	-460,4 to 364,4	No	0,9995
Neg.(only sens.) vs. a-IgE 0.1 µg/mL	-680,4 to 144,4	No	0,3526
Neg.(only sens.) vs. a-IgE 1 µg/mL	-1917 to -1092	Yes	<0,0001
Neg.(only sens.) vs. a-IgE 10 µg/mL	-990,4 to -165,6	Yes	0,0029
Neg.(only sens.) vs. Sm IPSE 0.01 µg/mL	-1156 to -330,8	Yes	0,0001
Neg.(only sens.) vs. Sm IPSE 0.1 µg/mL	-1879 to -1054	Yes	<0,0001
Neg.(only sens.) vs. Sm IPSE 1 µg/mL	-1264 to -439,6	Yes	<0,0001
Neg.(only sens.) vs. Sm IPSE 10 µg/mL	-1234 to -409,6	Yes	<0,0001

IgE Cε2-4 (3) Reporter Assay evaluation after IPSE-stimulation of IgE Cε2-4-sensitized RS-ATL8 cells. Statistics data analyses was performed using Ordinary one-way ANOVA (Dunnett's multiple comparisons test); significance was tested against negative control (non-stimulated cells).

Dunnett's multiple comparisons test	95,00% CI of diff.	Significance	Adjusted P Value
Neg.(only sens.) vs. ConA I 10 µg/mL	-2423 to -1950	Yes	<0,0001
Neg.(only sens.) vs. a-IgE 0.01 µg/mL	-336,4 to 136,4	No	0,7857
Neg.(only sens.) vs. a-IgE 0.1 µg/mL	-1125 to -652,1	Yes	<0,0001
Neg.(only sens.) vs. a-IgE 1 µg/mL	-2842 to -2369	Yes	<0,0001
Neg.(only sens.) vs. a-IgE 10 µg/mL	-907,9 to -435,1	Yes	<0,0001
Neg.(only sens.) vs. Sm IPSE 0.01 µg/mL	-205,4 to 267,4	No	0,9994
Neg.(only sens.) vs. Sm IPSE 0.1 µg/mL	-213,1 to 259,6	No	0,9996
Neg.(only sens.) vs. Sm IPSE 1 µg/mL	-221,9 to 250,9	No	0,9997
Neg.(only sens.) vs. Sm IPSE 10 µg/mL	-241,1 to 231,6	No	>0,9999

IgE Cε3-4 (3) Reporter Assay evaluation after IPSE-stimulation of IgE Cε3-4-sensitized RS-ATL8 cells. Statistics data analyses was performed using Ordinary one-way ANOVA (Dunnett's multiple comparisons test); significance was tested against negative control (non-stimulated cells).

Dunnett's multiple comparisons test	95,00% CI of diff.	Significance	Adjusted P Value
Neg.(only sens.) vs. ConA I 10 µg/mL	-1577 to -1179	Yes	<0,0001
Neg.(only sens.) vs. a-IgE 0.01 µg/mL	-233,7 to 165,2	No	0,9973
Neg.(only sens.) vs. a-IgE 0.1 µg/mL	-531,2 to -132,3	Yes	0,0004
Neg.(only sens.) vs. a-IgE 1 µg/mL	-1579 to -1181	Yes	<0,0001
Neg.(only sens.) vs. a-IgE 10 µg/mL	-771,9 to -373,1	Yes	<0,0001
Neg.(only sens.) vs. Sm IPSE 0.01 µg/mL	-229,2 to 169,7	No	0,9994
Neg.(only sens.) vs. Sm IPSE 0.1 µg/mL	-247,7 to 151,2	No	0,9881
Neg.(only sens.) vs. Sm IPSE 1 µg/mL	-219,9 to 178,9	No	0,9996
Neg.(only sens.) vs. Sm IPSE 10 µg/mL	-269,4 to 129,4	No	0,9013

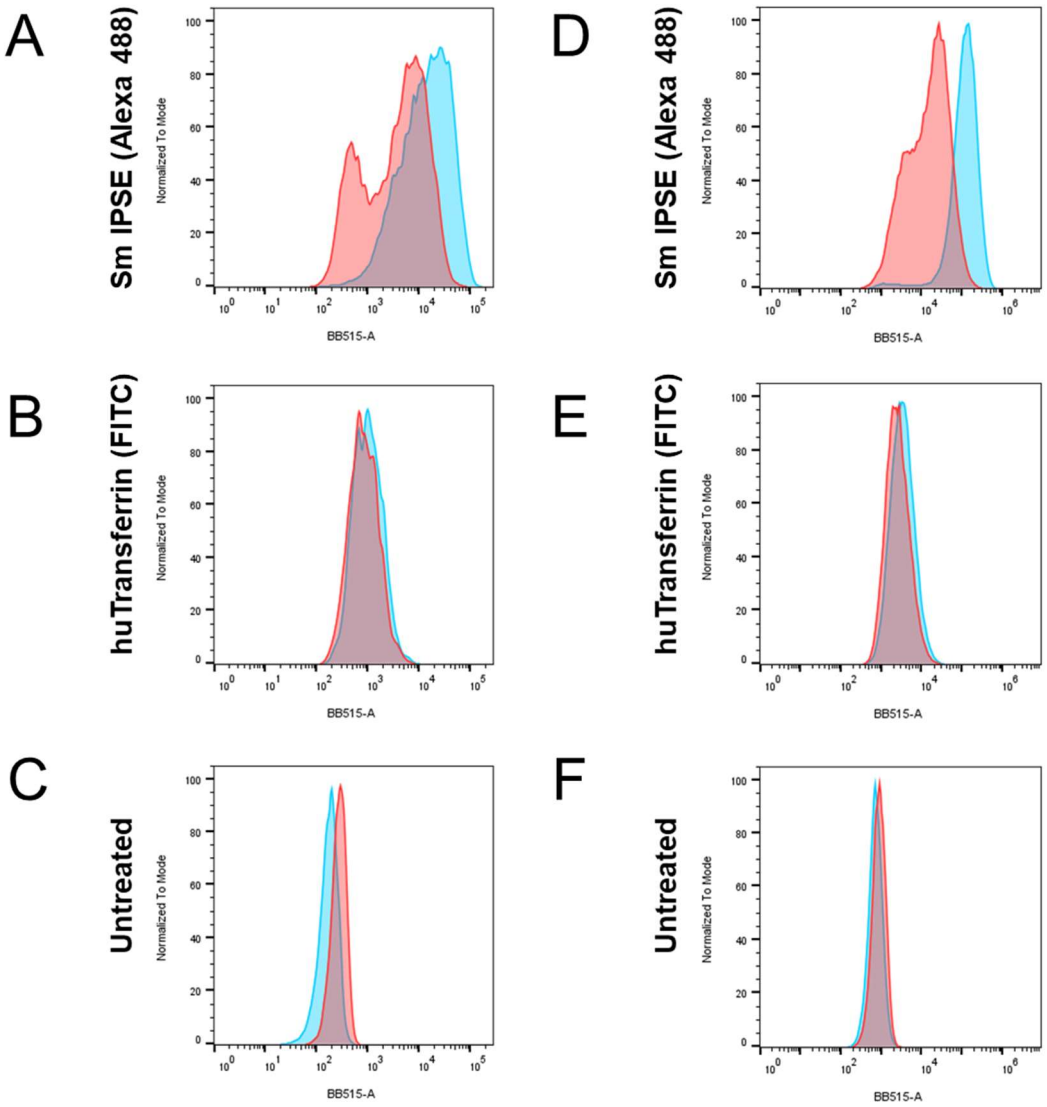

HCT 116 cells (37°C) treated with either Sm IPSE or hTrf. Cells were resupended in PBS or Trypanblue. Analyses of HCT-116 pre-incubated with either Sm IPSE DyLight488 or human Transferrin-FITC at 37°C with FACS measuring BB515-A (channel designed for exciting with blue laser at 488 nm).

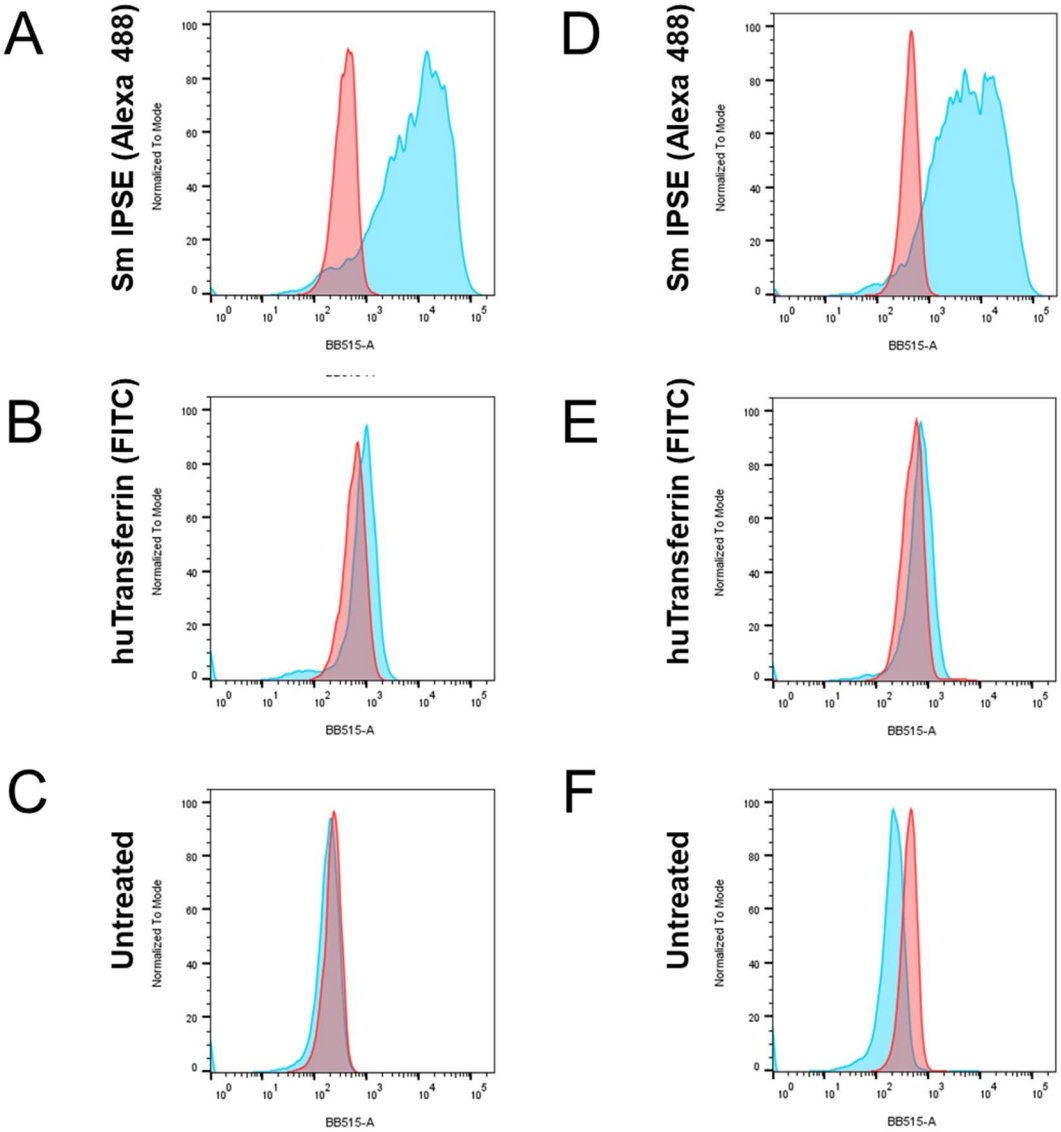

HCT 116 cells (4°C) treated with either Sm IPSE or hTrf. Cells were resupended in PBS or Trypanblue. Analyses of HCT-116 pre-incubated with either Sm IPSE DyLight488 or human Transferrin-FITC at 4°C with FACS measuring BB515-A (channel designed for exciting with blue laser at 488 nm).

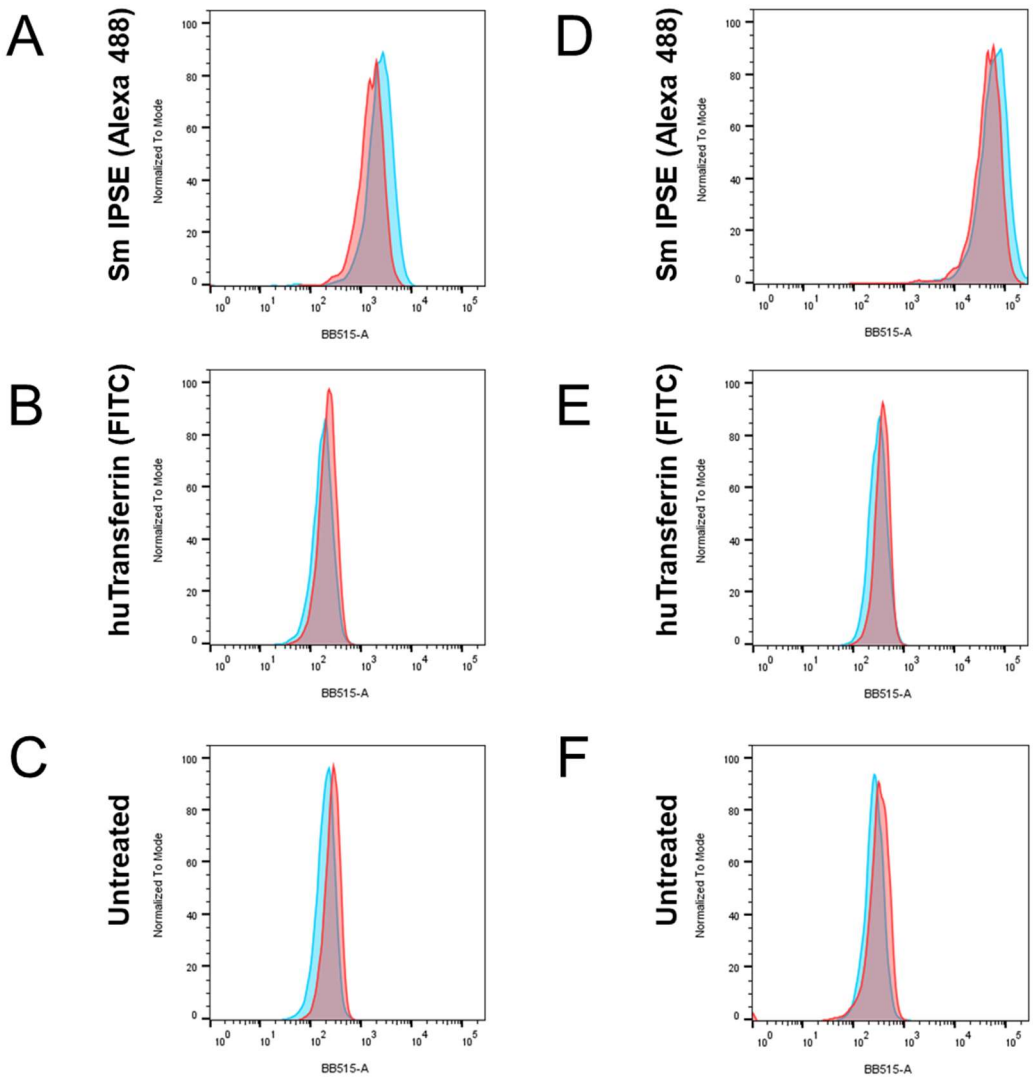

CHO-Trvb (37°C) treteated with either h TRF oder Sm IPSE. Cells were resuspended in PBS or Trypan Blue. Analyses of CHO-Trvb pre-incubated with either Sm IPSE DyLight488 or human Transferrin-FITC at 37°C with FACS measuring BB515-A (channel designed for exciting with blue laser at 488 nm).

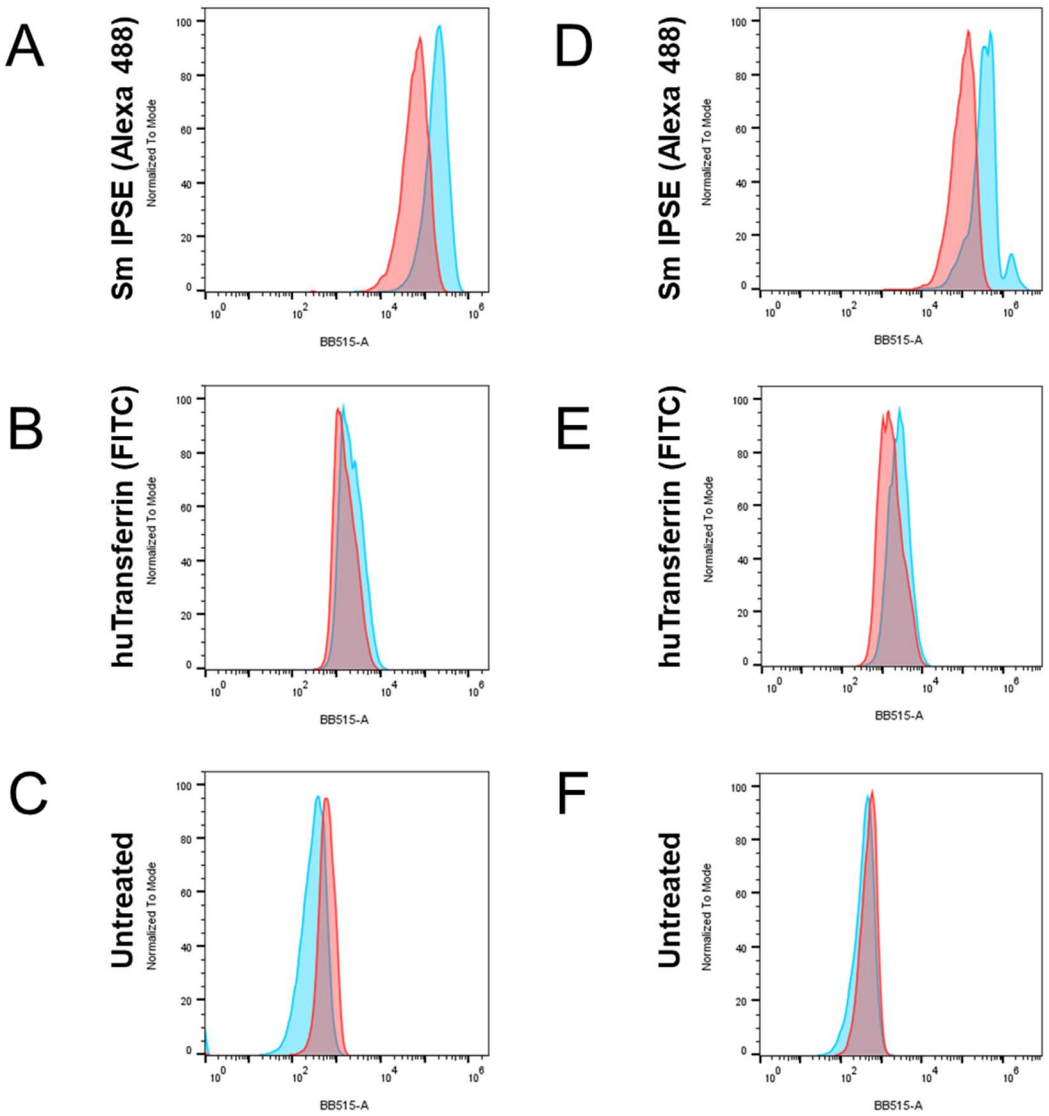

HepG2 (37°C) treteated with either h TRF oder Sm IPSE. Cells were resuspended in PBS or Trypan Blue. Analyses of HepG2 cells pre-incubated with either Sm IPSE DyLight488 or human Transferrin-FITC at 37°C with FACS measuring BB515-A (channel designed for exciting with blue laser at 488 nm).

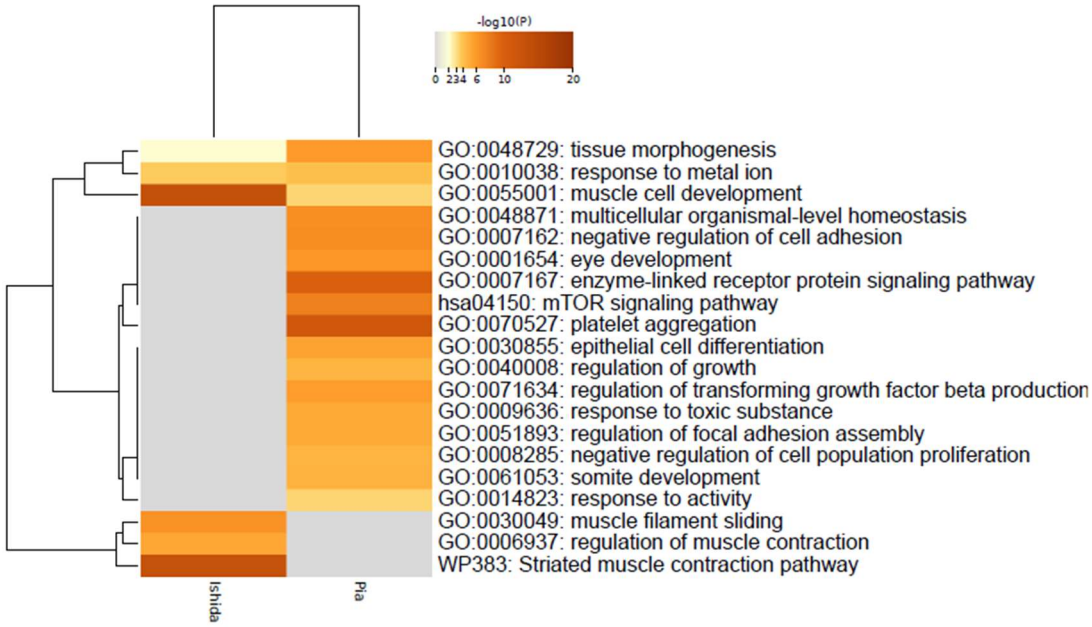

Comparison of deregulated pathways between this study and Ishida et al., 2020 using GO data base